

Controlling cellular structure in thermoplastic foam injection molding – influence of processing and mold technologies

von der Fakultät für Maschinenbau
der Universität Kassel
genehmigte Dissertation
zur Erlangung des Grades

Doktor-Ingenieur

vorgelegt von:

Mike Tromm

Fachgutachter:

Professor Dr.-Ing. Hans-Peter Heim
Professor Dr.-Ing. Georg Steinbichler

Für die Nutzung dieser Dissertation gelten folgende rechtliche Bestimmungen

- Die vorliegende Dissertation darf von der Universität Kassel frei im Internet angeboten werden. Eine weitere Verbreitung oder öffentliche Wiedergabe ist nicht gestattet und kann nur mit ausdrücklicher Genehmigung des Autors (Promovierten) geschehen.
- Die Vervielfältigung ist nur im Rahmen des privaten und eigenen wissenschaftlichen Gebrauchs (§ 53 UrhG) erlaubt.
- Die Publikation darf nicht bearbeitet oder in anderer Weise verändert werden.
- Der Autor hat das Recht, sein Werk, auch auszugsweise, anderweitig verfügbar zu machen und zu verbreiten.
- Für den Inhalt des Dokuments ist allein der Autor verantwortlich.

This publication (dissertation) is subject to the following terms of use:

- The University of Kassel is entitled to give open access to this publication. Further publication or public broadcasting needs explicit authorization of the copyright owner (doctor).
- Copying is permitted only for private or the own scientific purposes of the person who performs copying (according to § 53 of the German Copyright Act). The copyright owner grants production of complete single copies of this publication by means of a print on demand service.
- This publication may not be edited or changed otherwise.
- The copyright owner has got the right to publish or broadcast this publication as a whole or parts thereof elsewhere.
- The author is exclusively responsible for the content of this publication.

***“You need to try to go to the limit of the inside.
The enemy of human being is the surface.”***

SAMUEL BECKETT

Preface and acknowledgement

The procedure of foam injection molding is mentioned to be established since years. However, despite the light-weight trend, in industry the technology is only recognized slowly. A lack of knowledge about this technology as well unclear definitions and demarcation of process variants still exist. Especially the potential for applications given by special mold technologies is typically unknown or the distinction of process variants is not clear. The author's impression is to explain the process and clarify the differences of foam injection molding and its process variants to exploit the light-weight potential of the technology in more applications.

This thesis consists in principle of two parts connected one with another. The first part is textbook-like. Here, state of the art in technology and research is worked out and extended by own supplementations to clearly show and separate the foam injection molding procedures, their restrictions and potentials. In the second part, foam injection molding with mold volume expansion is in focus. The new procedure of local core-back is introduced, differentiated and its tremendous potential for lightweight applications is shown. The influence of processing on structure formation in foam injection molding is worked out for the different procedures. Here, also foam injection molding with mold volume expansion and the major influence of packing phase, which is an unusual and typically not respected process parameter in foam injection molding, is in focus.

I want to thank the German Federal Ministry of Economics and Technology for financial support of project costs. A special thanks to the board of examiners: Prof. Dr.-Ing. H.-P. Heim, Institute of Materials Engineering, Polymer Technology, University of Kassel (Germany); Prof. Dr.-Ing. G. Steinbichler, Institute for Polymer Injection Molding and Process Automation, Johannes Kepler University Linz (Austria); Prof. Dr.-Ing. A. Ries, Institute of Materials Engineering, Heterogeneous Materials, University of Kassel and Prof. Dr.-Ing. O. Wünsch, Institute of Mechanics, Fluid Mechanics, University of Kassel for discussions, expert advice and time.

Many thanks to my former colleagues from the institute, all my office mates and all the student workers and thesis students for good conversations, help with sample production, preparation, analysis etc. during my time at the institute (2011 – 2018).

Furthermore, many thanks to Prof. Dr. Chul B Park, Microcellular Plastics Manufacturing Laboratory, University of Toronto (Canada) and his team, who gave me the possibility to work with them. The output of my short research stay in Toronto clarified, confirmed and contributed to the results of this thesis.

A very special thanks to my wife Sarah and my daughter Ella, who gave me the power and shared my time with *“the thesis”* between job and family life.

Kurzfassung

Schaumspritzgießen ist ein Verarbeitungsverfahren zur Serienproduktion von geschäumten Kunststoffteilen, welches ein zunehmendes Interesse und Verwendung in der Industrie erlangt. Jedoch sind die Anwendungen aufgrund unzureichender Kenntnisse der Prozessführung und der mechanischen Eigenschaften, der begrenzten Nutzung des Leichtbaupotentials sowie eingeschränkter Oberflächenqualitäten begrenzt. Alle diese Nachteile sind mit der Zellstruktur verbunden. Die Strukturmerkmale wie Randschichtdicke, Zellgröße, Dichte und Homogenität werden während des Verfahrens ausgebildet. Daher ist die Kontrolle der Zellbildungsmechanismen der Schlüssel, um den Einschränkungen entgegenzuwirken und die mechanischen Eigenschaften zu optimieren.

Beim konventionellen bzw. Niederdruckschaumspritzgussverfahren finden die Füllung der Kavität und die Zellbildung simultan statt. Die Zellstruktur kann nur in einem sehr begrenzten Bereich kontrolliert werden und ist häufig ungleichmäßig über Fließweglänge und Bauteilquerschnitt, wodurch keine genaue Vorhersage der mechanischen Eigenschaften möglich sind. Diesen Einschränkungen kann durch Hochdruckschaumspritzgießen mit volumen-expandierbaren Werkzeugen entgegengewirkt werden. Diese spezielle Prozessvariante kann die Füll- und Aufschäumphase voneinander entkoppeln und eine aktive Kontrolle der Zellstruktur ermöglichen. Die Zellbildungsmechanismen können aktiv vom Zellwachstum zur Nukleierung verschoben werden. Somit können feinzelligere, homogenere, weniger fließwegabhängige Strukturen mit Dichtereduktionen $> 50\%$ erreicht und die mechanischen Eigenschaften aktiv beeinflusst werden. Dieses Potenzial ist häufig unbekannt aufgrund unzureichender Kenntnis über Prozessparameter und deren Auswirkung auf die Strukturbildung. Während das konventionelle bzw. Niederdruckverfahren in industriellen Anwendungen durchgesetzt hat und verwendet wird, ist das Hochdruckverfahren mit volumen-expandierbaren Werkzeugen oft unbekannt oder wird nur in einem sehr begrenzten Bereich verwendet.

Diese Arbeit befasst sich mit der Bildung der Zellstruktur im Thermoplast-Schaumspritzguss und konzentriert sich auf die Einflüsse von Prozessführung und Werkzeugtechnologie. Im Fokus steht das Hochdruckschaumspritzgießverfahren in Kombination mit volumen-expandierbaren Werkzeugen; Werkzeugöffnung oder Kernzugverfahren. Als neue Prozessvariante wird das lokale Kernzugverfahren (lokale Volumenexpansion) eingeführt, welches eine lokale Beeinflussung der Schaumstrukturen ermöglicht. Die Unterschiede in den Verfahrensvarianten und der Einfluss der zusätzlichen Prozessparameter wurde herausgearbeitet. Hier wird insbesondere die Rolle des Nachdrucks als Schlüsselfaktor für die Strukturbildung diskutiert. Um mehr Informationen über die Randbedingungen innerhalb des Werkzeuges während des Verfahrens zu erhalten und den Prozess transparenter zu machen, wurden Füllsimulationen und Visualisierungsversuche mit einem Sichtfensterwerkzeug durchgeführt. Weiterhin wurde ein neues Spritzgusswerkzeug gebaut und verwendet, welches u.A. eine aktive Kontrolle der Druckabfallrate erlaubt. Zur Analyse der Struktur und zur Quantifizierung der Strukturparameter wurde neben Lichtmikroskopie und REM auch die Computertomografie (μ CT) eingesetzt, um eine dreidimensionale Charakterisierung von Strukturen zu ermöglichen.

Abstract

Foam injection molding is a processing technology to produce foamed plastic parts in serial production, attaining an increasing interest and use in industry. However, the applications are limited due to insufficient knowledge of processing and mechanical properties, limited use of light-weight potential as well as restricted surface qualities. All these drawbacks are associated with the cellular structure. The structure characteristics like skin layer thickness, cell size, density and uniformity are developed during the procedure. Thus, controlling the cell formation process is the key to work against the restrictions and optimize mechanical properties.

In conventional or low-pressure foam injection molding procedure, mold filling and foaming occur simultaneously. The cellular characteristics can only be controlled in a very limited range and are often non-uniform by flow length and cross-section, not allowing a precise prediction of the mechanical performance. These limitations can be counteracted by high-pressure foam injection molding with volume-expandable molds. This special process variant may decouple filling and foaming phase and allow an active control of cellular characteristics. Cell formation mechanism may actively be shifted from cell growth to nucleation. Thus, finer-celled, homogeneous, less flowpath dependent structures with density reductions > 50 % can be achieved, and the mechanical properties can actively be influenced. This potential is often unknown due to insufficient knowledge about the process parameters and its effects on structure formation. While the conventional or low-pressure procedure has been asserted and is used in industrial applications, high-pressure procedure with volume-expandable molds is often unknown or used in a very limited range.

This thesis deals with the formation of cellular structure in thermoplastic foam injection molding process. The work focuses on influences by processing and mold technologies. High-pressure procedure in combination with volume-expandable molds – mold opening or core-back - is in focus. As a new process variant, the local core-back procedure (local mold volume expansion) is introduced, enabling a local customization of foam structures. The differences in procedures and the influence of additional process parameters are worked out. Here, especially the role of packing pressure as a key factor for structure development is discussed. To get more information on boundary conditions inside the mold during the procedure and make the process more transparent, numerical simulation has been used and visualization molding trials were conducted to monitor the cell development inside the mold during processing. Furthermore, a new mold, i.e. allowing an active control of pressure drop rate, was built and used. To analyze the structure and quantify the structural parameters, besides light microscopy and SEM, also x-ray tomography (μ CT) was used to allow a three-dimensional characterization of structures.

Index

Index	I
Symbols and abbreviations	V
Abstract	VIII
1 Motivation and hypothesis	1
2 Introduction and focus of thesis	5
3 Foam injection molding	10
3.1 Classification	10
3.2 Basics of structure formation	12
3.2.1 Solubility of gasses in molten polymers.....	14
3.2.2 Diffusion of gasses in molten polymers	16
3.2.3 Nucleation phenomena.....	18
3.2.4 Cell growth mechanism.....	20
3.2.5 Modelling.....	25
3.2.6 Influence of material and blowing agents	27
3.3 Characteristics of foam structures.....	29
3.3.1 Methods of characterisation.....	35
3.3.2 Challenges in evaluation of foam structures	41
3.4 Observation of cell formation.....	44
3.4.1 Visualization experiments	44
3.4.2 Simulation of procedure	45
4 General mechanism of cell formation in foam injection molding	48
4.1 Plasticizing process	48
4.2 Filling phase	52
5 Low-pressure / conventional foam injection molding procedure	55
5.1 Phases of cell formation in low-pressure procedure	56

5.2	Evolution of cells in low-pressure procedure.....	59
5.3	Final cell structure in low-pressure procedure	65
5.4	Potential and restrictions of low-pressure procedure.....	70
6	High-pressure foam injection molding procedure with mold volume expansion	73
6.1	Phases of cell formation in high-pressure procedure with mold volume expansion.....	76
6.2	Evolution of cells in high-pressure procedure with mold volume expansion	79
6.2.1	Re-diffusion of early nucleated cells.....	84
6.2.2	Pressure drop rate / Comparison with batch foaming.....	86
6.3	Final cell structure in high-pressure procedure with mold volume expansion	88
6.4	Mold concepts for mold opening.....	92
6.5	Mold concepts for core-back	93
7	Local core-back procedure	96
7.1	Mold concepts for local volume expansion	100
7.1.1	First simple mold.....	101
7.1.2	Improved mold.....	101
7.2	Density distribution	105
7.3	Focusing temperature conditions	109
7.4	Geometrical boundary conditions.....	114
7.5	Freedom of design and geometrical transferability.....	117
8	Process – structure relationship	120
8.1	Process parameter independent of process variant.....	120
8.1.1	Blowing agent content.....	120
8.1.2	Melt and mold temperature.....	121
8.2	Process parameter influences for low-pressure procedure	122

8.2.1 Injection volume (switch over point)	124
8.2.2 Injection speed	126
8.3 Process parameter influences for high-pressure procedure with mold volume expansion	132
8.3.1 Procedure specific parameters	133
8.3.2 Significance and effective direction of process parameters.....	141
8.3.3 Significance of injection speed.....	146
8.4 The role of packing phase in high pressure procedure with mold volume expansion.....	152
8.4.1 Evolution of cells during filling and packing phase	153
8.4.2 Effect of packing pressure on final cell structure	159
8.4.3 The effect of pressure level.....	165
8.4.4 Repeated compression and decompression of melt	175
9 Conclusion.....	178
10 References	187
List of author's publications / contributions	205
11 Appendix.....	209
11.1 General information.....	209
11.2 Light-weight potential of High-pressure foam injection molding	210
11.3 Parameter settings.....	212
11.4 Details on μ CT analysis.....	214
11.5 Simulation	216
11.5.1 Definition of foam injection molding process in Moldex3D	216
11.5.2 Results for cell density.....	217
11.5.3 Simulation of local core-back procedure	220
11.6 Mold concepts for mold opening.....	221
11.7 Mold concepts for core-back	223

11.8	Details on improved mold	225
11.9	Rapid heat cooling process	229
11.10	Picture Credits	232

Symbols and abbreviations

afg	Away from gate (position of flow path)
ba	Blowing agent
c	Core layer (position in thickness of specimen)
cba	Chemical blowing agent
CB	Core-back - mold volume expansion via moving elements inside closed mold
CD	Cell density [$1/\text{cm}^3$]
CNT	Classical nucleation theory
CO ₂	Carbon dioxide
CS	Cell size [μm]
DoE	Design of Experiments
EOC	End of cooling
EOF	End of filling
EOP	End of packing
ER	Expansion ratio: volume after expansion in relation to volume before expansion [-]
FIM	Foam injection molding
GCP	Gas counter pressure
HDPE	High-density polyethylene
HP-CB-FIM	High-pressure core-back foam injection molding
HP-FIM	High-pressure foam injection molding

HP-MO-FIM	High-pressure mold opening foam injection molding
HP-VE-FIM	High-pressure volume expansion foam injection molding
η	Dynamic viscosity [Pas]
im	Intermediate layer (position in thickness)
IMM	Injection molding machine
LP-FIM	Low-pressure foam injection molding (conventional procedure)
m	Middle (position of flow path)
MO	Mold opening – mold volume expansion by opening stroke via injection molding machine
μ CT	X-ray microtomography
ng	Near gate (position of flow path)
N ₂	Nitrogen
PA6-GF15	Polyamide 6 with 15wt% glass fibers
PA6-GF30	Polyamide 6 with 30wt% glass fibers
pba	Physical blowing agent
PE	Polyethylene
PC	Polycarbonate
PC-ABS	Polycarbonate acrylonitrile-butadiene-styrene blend
p_{pack}	Packing pressure [bar]
PDR	Pressure drop rate [MPa/s]
PP	Polypropylene
PS	Polystyrene

PVC	Polyvinylchloride
ρ	Density [g/cm ³]
ρ_{foam}	Density of foamed material [g/cm ³]
ρ_{solid}	Density of solid material [g/cm ³]
RLM	Reflected light microscopy
s	Skin layer (position in thickness)
SCF	Super critical fluid / blowing agent content [wt%]
SEM	Scanning Electron Microscopy
SOP	Switch over point (end of filling phase)
T_C	Crystallization temperature [°C]
t_D	Delay time [s] - time between volumetrically injection and volume expansion
T_{freeze}	Freezing temperature
T_G	Glass transition temperature [°C]
t_{pack}	Packing time [s]
T_{melt}	Melt temperature [°C]
T_{mold}	Mold temperature [°C]
v_{inj}	Injection speed [mm/s]
v_O	Opening / expansion speed [mm/s]

Abstract

Foam injection molding is a processing technology to produce foamed plastic parts in serials production, attaining an increasing interest and use in industry. However, the applications are limited due to insufficient knowledge of processing and mechanical properties, limited use of light-weight potential as well restricted surface qualities. All these drawbacks are associated with the cellular structure. The structure characteristics like skin layer thickness, cell size, density and uniformity are developed during procedure. Thus, controlling the cell formation process is the key to work against the restrictions and optimize mechanical properties.

In conventional or low-pressure foam injection molding procedure, mold filling and foaming occur simultaneously. The cellular characteristics can only be controlled in a very limited range and are often non-uniform by flow length and cross-section, not allowing a precise prediction of the mechanical performance. These limitations can be counteracted by high-pressure foam injection molding with volume-expandable molds. This special process variant may decouple filling and foaming phase and allow an active control of cellular characteristics. Cell formation mechanism may actively be shifted from cell growth to nucleation. Thus, finer-celled, homogeneous, less flowpath dependent structures with density reductions > 50 % can be achieved, and the mechanical properties can actively be influenced. This potential is often unknown due to insufficient knowledge about the process parameters and its effects on structure formation. While the conventional or low-pressure procedure has been asserted and is used in industrial applications, high-pressure procedure with volume-expandable molds is often unknown or used in a very limited range.

This thesis deals with formation of cellular structure in thermoplastic foam injection molding process. The work focusses on influences by processing and mold technologies. High-pressure procedure in combination with volume-expandable molds – mold opening or core-back - is in focus. As a new process variant, the local core-back procedure (local mold volume expansion) is introduced, enabling a local customization of foam structures. The differences in procedures and the influence of additional process parameters are worked out. Here, especially the role of packing pressure as a key factor for structure development is discussed. To get more information on boundary conditions inside the mold during procedure and make the process more transparent, numerical simulation has been used and visualization

molding trials were conducted to monitor the cell development inside the mold during processing. Furthermore, a new mold, i.a. allowing an active control of pressure drop rate was built and used. To analyze the structure and quantify the structural parameters, besides light microscopy and SEM, also x-ray tomography (μ CT) was used to allow a three-dimensional characterization of structures.

1 Motivation and hypothesis

Motivation

The importance of foam injection molding as a method to produce light weight parts has increased within the last years. Due to several advantages in processing and a better process controllability, applications in packaging, consumer goods and automotive parts are realized with this processing technology. However, the acceptance of this technology took a long time and although a lot of research has been done, the light-weight potential has not been fully exploited in applications up to now.

For most technical products, a reliable and predictable cellular structure, defining the mechanical properties, is the key factor. Studies have shown that structures with same density reductions, but different foam characteristics can exhibit a variation of mechanical properties in a wide range. In foam injection molding, typically an integral foam structure with a cellular core and a compact skin layer is created. Structural parameters like skin layer thickness, cell size, cell density, shape of cells and uniformity are strongly affected by material, blowing agent and process parameters. The formation of structure is a complex process, depending on these factors and their interaction. Previous and ongoing investigations aim to describe these interactions and try to optimize the structure.

By using conventional molds, the achievable density reduction is restricted. The process cannot be controlled adequately to exploit the theoretical possibilities for light-weight potential. Expandable mold technologies like core-back can have a huge influence on structure formation. High density reductions (> 50 %), uniform, flow-path independent structures and even open-celled or nanofoams can be achieved. To clarify how the process parameters interact with the structure, it is important to know, how the parameters influence the boundary conditions (pressure, temperature, time, etc.) and thus the cell formation process during processing. Currently, these interactions are not completely clarified. Especially the influences defined by differences in process sequence on structure formation and in regard to the final foam structures – especially for highly foamed structures - are not completely understood. Published investigations mainly focused on single parameter variations, do not include all procedure-specific process parameters or were restricted by their experimental molds used. Thus, interactions of “standard injection

parameter“ and „procedure-specific parameter“ have only been worked out with restrictions. Using the process variant of high-pressure foam injection molding with mold volume expansion, additional parameters and differences in process sequence are on hand. Here, especially the influence of packing pressure is discussed rarely in literature and the effect of duration and level has not been worked out clearly.

The foam structure inside a part can actively be influenced and optimized by process parameter variation. This makes the process more complex. But, once the influences and the interactions of the involved factors are understood, the possibility to precisely tailor the structural parameter is on hand. To clearly find out which processing parameter affected the final foam structure in the product, the whole structure formation process must be considered. Thus, it is necessary to have a closer look on the development of structure inside the mold. The thesis should clarify the influences of the process parameters in foam injection molding on structure formation during procedure as well on the final foam structure. Once the whole process is understood and it is known how to specifically affect the structure, it can be tailored, and the resulting properties can be estimated by the correlations which are already worked out by other authors.

The first aim of this thesis is to work out and clarify the differences of both process routes and contribute to make the structure formation within the mold during procedure more transparent and comprehensible. This should be a contribution to better understand the complex procedure to establish the enormous light-weight potential of high-pressure foam injection molding with volume-expandable molds to more industrial applications and help to bring this innovative technology to industrial acceptance. The knowledge of processing and the influence of boundary conditions on the cellular structure and geometrical restrictions are essential for applications and part design.

The second aim of this thesis is to work out process-structure relationships for high-pressure foam injection molding with volume-expandable molds. Thus, within the thesis, a new unique injection mold was designed and built which allows to use high packing pressures and precisely define the parameters for volume expansion. Expansion ratio, expansion speed (thus pressure drop rate) as well variotherm temperature control to achieve high surface qualities can be set independently of injection molding machine cycle. The mold volume is expanded locally (local core-

back operation), conducted by a changeable geometry mounted on the movable core. Thus, the foam structure inside the parts can be influenced locally. These features extend the possibilities of existing molds. The investigations deal with the influences of process parameters on structure formation in core-back and local core-back procedure. Here, influences of injection-related parameters and parameters given by the special procedures are considered. Design of experiments was used to plan and analyze the experiments and ensure the statistical significance. Correlations of process and structure are worked out. The role of an active packing pressure and its effect on re-diffusion of cells during procedure as well on uniformity of structure is discussed deeply.

Hypothesis

High-pressure procedure with mold volume expansion can have a huge influence on pressure and temperature conditions inside the cavity. Besides the standard process parameters, also additional procedure-specific parameters are on hand able to influence structure formation. In this context the following hypothesis should be clarified:

Hypothesis 1: “The influence of machine-defined injection parameter as they are found for low-pressure procedure may be overlaid by specifics of high-pressure procedure with mold volume expansion (difference in process sequence and additional process parameters).”

The additional process parameters, defined by the difference in process sequence (packing phase – pressure and time) and the additional process specific parameters (expansion specific parameters – speed, distance, delay) affect the structure formation. It is expected, that the effect of injection related parameters (machine defined) can be overlaid, maybe increased or decreased by specifics of procedure. Especially the influence of injection speed on structure is expected to be negligible in high-pressure procedure executed by applying an active packing phase.

Hypothesis 2: “An active packing phase may decouple filling and foaming resulting in significantly different cellular structures for high-pressure foam injection molding with mold volume expansion compared to low-pressure foam injection molding.”

In conventional or low-pressure foam injection molding, packing phase is omitted. In high-pressure foam injection molding with mold volume expansion, an active packing phase defines, if cells nucleated during filling may be re-dissolved or if these cells still exist before mold volume expansion. If packing pressure and time is used, cells may be forced back into solution, decoupling filling phase and foam formation. It is assumed that cellular structures achieved by conventional foam injection molding / low-pressure procedure are significantly different from the ones using core-back procedure with an active packing phase.

Hypothesis 3: "Increased packing conditions support fine-celled structures and overall uniformity in high-pressure foam injection molding with mold volume expansion."

Applying sufficient packing pressure and time before expanding the mold volume is proposed to get the cells back in solution and to achieve a more homogeneous, fine-celled final foam structure. It is known that the pressure drop rate, induced by core-back operation significantly influences the cell formation. But, currently the influence of packing phase is not completely clear. It is assumed that the level of pressure inside the cavity before core-back also affects the structure formation. A higher level is expected to increase pressure drop rate, thus lead to finer-celled structures and supports overall uniformity of structure.

2 Introduction and focus of thesis

The mechanical properties of an injection molded foam are mainly defined by its cellular structure. Cellular characteristics like skin layer thickness, cell size, cell size distribution as well shape of cells are highly relevant to the mechanical properties. First approaches to describe the mechanical properties of foam injection molded structures in correlation to their density were made in 1960 - 1980's. Here, sometimes skin layer thickness was included, but in general structural parameters were not considered. In the 1980 - 1990's some researcher also included these important factors. An overview of the investigations and more detailed information can be found in [1].

In never literature, a lot of paper deal with correlations of morphology and properties respective to different process settings: [2–13]. Also, several PhD thesis published in Germany dealt with this topic, some of them at the same time: [1, 14–18]. They also included the influence of process on the resulting morphology. Investigations of Cramer [19] have shown that injection molded foams with same density but variations in structure can exhibit variations in mechanical properties up to 40 % [19]. The same observation is shown by Flórez Sastre [1]. Here, bending modulus variation of 35 – 45 % for foams with similar densities, but differences in skin layer thickness and density distribution could be observed [1]. Kirschling [16, 20] recapped the main structure characteristics and grouped the overall structures into different morphological models. He stated that these models exhibit optimized mechanical performances for different load cases.

At the Institute of Materials Engineering at the University of Kassel in the past, several experimental investigations also concerning core-back mold technology [16–18] have been conducted. The influences of the process parameters on final foam structure were worked out as well a huge amount of different mechanical testing was done. The correlations of process-structure and properties were described including optimized parameter settings to create structures for different loads. However, these investigations mostly focused on Polycarbonate with low expansion ratios of 20 – 25 %. Furthermore, here [16–18] as well in similar investigations [1] and investigations for highly expanded structures with density reduction > 50 % produced by core-back procedure [14, 15], structure formation during procedure affected by core-back parameters is not in focus. Thus, core-back parameters were not varied intensively,

process definition (especially the definition of packing phase) is not always clear and in parts parameters were varied individually, not allowing to detect interactions of process parameters. These restrictions occurred in parts by the restrictions of the experimental molds used within these experiments.

In the aforementioned investigations, in general final foam structures were analyzed, not considering cell evolution mechanism during processing. Evolution of cells in foam injection molding, especially in high-pressure procedure is still less understood [21]. To observe the cell formation mechanism during procedure, researchers build visualization molds including glass windows to in-situ visualize the foam formation process. In regards to conventional foam injection molding [22–29] and in the last years also in regards to high-pressure foam injection molding without cavity expansion [21, 30–32] as well in combination with mold opening or core-back [24, 33–36] general results and in-depth investigations were published. However, these investigations mostly focused on single parameter variation and considered the complete process and possible interactions of processing parameters only in parts.

Apart from experiments, numerical simulation is a method to predict the characteristics of the final cellular structure as well to provide a better understanding on the conditions and mechanism inside the mold during procedure. Commercially available simulation software just started to implement the option to simulate these special processes. The conventional foam injection molding process (low-pressure foaming) has successfully been simulated by institutes and the software developers [37–39]. New software developments now enable a simulation including the core-back procedure, presented in [40]. In an own publication, firstly the simulation of “local core-back procedure” as well the qualitative verification was shown [41].

Scope of thesis

A lot of interesting and intensive investigations in field of foam injection molding exist. However, many published investigations refer to specific materials, blowing agents, combinations of both or specific aspects limiting the transferability of results. No comprehensive investigation to clarify the differences of processing variants and the specifics of mold technologies like core-back procedure considering the effect of cell formation mechanism inside mold during filling is known. This aim of the thesis is to clarify the differences in foam injection molding procedures – conventional /

low-pressure and high-pressure procedure with mold volume expansion - and to show the potential to active influence the cellular structure by new mold technologies. The thesis should not workout extensive correlations to mechanical properties. This was done in many investigations before. Material's influence and plasticization process are also not considered in this thesis. Physical blowing agents were used because structure is more influenced by processing here, compared to chemical blowing agents, which often include nucleation additives.

Figure 1 highlights the scope of this thesis and the methods used for investigation of process and characteristics of structure. The general relationships and possibility of controlling cellular structure by processing and in combination with special mold technologies should be in focus. A systematical analysis of process parameters and their occurrences on the conditions inside the mold (pressure, temperature, etc.) should be given.

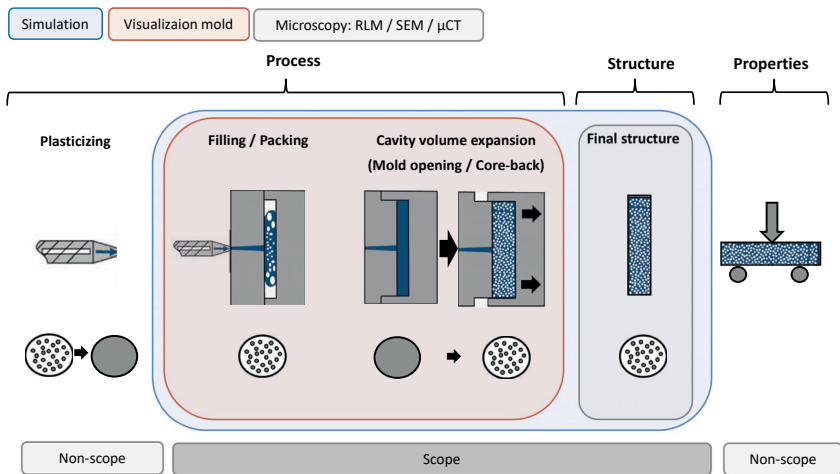


Figure 1: Scope and non-scope of thesis and methods used for investigation and characterization

Filling phase

At the moment the gas-melt mixture is leaving the nozzle of the plasticization unit and entering the mold, a huge pressure drop occurs, initiating nucleation and cell growth during filling process. Cell formation and evolution is a function of geometrical boundary conditions, defined by mold geometry and injection parameters,

defined by the process. A pressure and temperature gradient between gate and flow front exists, affecting the cell formation locally.

In conventional procedure, injection is stopped before volumetrically filling of cavity volume. No packing pressure is applied, enabling the foam to expand. The process sequence is continued by cooling phase to solidify the foam structure. In high-pressure procedure in combination with expandable molds, the mold is filled volumetrically. Afterwards, packing pressure is applied as it is done in conventional injection molding process, trying to get the cells back into solution and again achieve a single-phase polymer gas mixture before cavity expansion.

Cavity volume expansion - mold opening (MO) / core-back (CB)

By applying packing pressure in high-pressure process, presupposed the polymer is still molten, the cells developed in filling process may be forced back into solution and again a single-phase mixture may be achieved. Thus, filling and foaming may be decoupled. The active cavity expansion again initiates a huge pressure drop, resulting again in nucleation and cell growth. The pressure drop in the expanded volume is initiated at every position of the part at the same time, thus a more uniform cell structure independent of flow path may be achieved. By controlling expansion speed, cell formation mechanism can be controlled actively and for high speeds mechanisms can be shifted to nucleation instead of cell growth.

Final foam structure

Cell formation and growth is a consequence of boundary conditions affected by the mold geometry, the procedure as well process parameter settings. Cells are nucleated and grow until an equilibrium of forces inside cells and forces in the surrounding melt are on hand, the available gas is consumed, or the expandability is limited by the geometry. Besides type and amount of blowing agent, also geometry and processing defines the final structures. Several structure characteristics pointed out in chapter 3.3 are analyzed at different locations to point out the differences in procedures and to judge the influence of process parameters. Final structures are analyzed by 2D and 3D methods.

Within this thesis, structure formation and evolution of cells during process are investigated by simulation, visualization molding trials and by using an innovative core-back mold, designed and built within the work on this thesis. The cell formation during filling phase is discussed in detail in chapter 4. The differences to conventional foam injection molding, as well the evolution of cells during procedures and process parameter influences are discussed in chapters 5 to 8.

3 Foam injection molding

3.1 Classification

Besides foam extrusion and bead foaming, foam injection molding is one of the dominant industrially relevant foaming technologies for thermoplastic polymers [42]. All these methods have in common that first a polymer-gas solution is created by the use of high pressure followed by pressure drop or temperature increase, initiating nucleation and cell growth [42].

While thermoset and thermoplastic foams were produced earlier via an autoclave-like procedure, thermoplastic foam injection molding started in the 1950's. In manufacturing, some baking powder was added to the polymer to counteract sink marks in thick-walled parts. In 1979 Meyer reports that foam injection molding is "*a well-recognized technology in the USA and Europe since the late 1960s*" [43]. In the 1960's economical production of foam injection molded components started, first technologies to introduce physical blowing agents were invented [44] and first patents are reported (e.g. by Dow Chemical Co. and Union Carbide Co.) [22, 45]. An overview of the first patented solutions in this field is given by Throne [46]. While in the 1970's in the US most applications were in the field of building industry and materials handling products, in Europe manufacturers of consumer electronics as well manufacturers of furniture used this technology [47]. Applications mentioned in [43] are a TV front panel, a shelf system, a file cabinet, drawer fronts of an office desk and outdoor lawn chairs. Also, housings of refrigerators, flowerpots and even a telephone booth were produced by foam injection molding [44]. The early applications mostly were produced by using low-pressure foaming in combination with chemical blowing agents [44]. Another overview of first applications and procedures used is given in [48]. In the 1970's and 1980's the use of physical foaming agents started. It was quite challenging due to the dynamic and discontinuity of the process [19]. In the 1990's the process got more controllable by better valve and regulating technology.

Despite integral foams produced by high pressure foam injection molding with cavity expansion are firstly mentioned in 1979 by MacMillan [49] and in 1981 by Eckardt [48] up to now only a few products are produced using this special process variant.

Foam injection molding offers several advantages for process and product. In terms of processing, for example a lower viscosity of the melt containing blowing agent is on hand. Also, the expansion of the gas can be used to compensate material shrinkage during cooling phase. In regard to the conventional procedure, these effects can lead to a reduction of cycle time and may allow the usage of smaller clamping forces, e.g. smaller machines. About the product, weight and material savings, as well a reduction of shrinkage and warpage are the main reasons to use the foam injection molding procedure. Nowadays, a lot of different applications are realized in foam injection molding (printer chassis, packaging goods, automobile parts) due to different motivations. However, the foamed structure affects the mechanical properties, generally in a negative way compared to compact non-foamed products of same geometry. Thus, the specific mechanical properties can be higher and by changing geometry (sandwich effect) and components of higher flexural modulus at equal component weight can be achieved.

The surface quality already has been an important aspect for the early applications mentioned in the introduction. Process-related, foam injection molded products are characterized by visible effects like silver streaks as well a lightly rougher surface avoiding the use in visible components. When melt leaves the nozzle and enters the mold, a huge pressure drop is on hand which leads to cell nucleation and cell growth. By the frontal flow of the melt, cells are sheared, can break open and are transported to the cavity wall. Also, leaked gas can move between the cavity and product surface. Due to the difference in temperature, solidification starts quickly in the moment of contact. As a result, flow marks and roughness can occur. The insufficient surface quality is unacceptable in many applications, especially for visible components. To improve, new technologies like machines allowing a high injection speed (machine constructions with a 2-stage screw injection system with a separate plunger) as well gas counter-pressure and co-injection molding technologies were developed [43, 44].

However, there is an increasing interest of industry in this technology due to light-weight constructions. Within the last years several attempts were made to affect foam structure and surface quality via mold technologies. For example, molds with expandable cavity volumes (see chapter 6), as well gas-counter pressure technology and variotherm molds are used to improve surface quality. Thus, meanwhile all drawbacks of processing can be waived, and the light-weight potential of foam injection molding could be exploited.

3.2 Basics of structure formation

The basic mechanism in thermoplastic foaming processes are sorption and dissolution of gas, nucleation, cell growth and stabilization [42, 50]. The same applies for the foam injection molding process, the relevant phases are shortly introduced in the following:



Figure 2: Mechanism in thermoplastic foaming process

1. Sorption and diffusion

The mass transport phenomena start with adsorption of a fluid on the polymer surface [44]. Using gasses in supercritical states increases the solubility and diffusion rates [51]. The ability of a polymer to uptake gas is described by its solubility, depending on several factors, e.g. the type of polymer and the pressure. The gas molecules are transported by diffusion mechanism driven by concentration and partial pressure differences [44], ideally resulting in a homogeneous single-phase mixture to be provided prior to injection.

2. Nucleation

The formation of cell nucleus is driven by thermodynamic instability. A pressure drop or an increase in temperature, usually occurring during injection phase (melt-gas mixture leaves the nozzle and enters the mold), changes the solubility. Nucleation starts by desorption of gas in the polymer which is a non-steady process.

In nucleation phase, nucleation and cell growth compete for the available gas [51]. When cells are nucleated at different times gas may prefer to diffuse into existing cells due to a lower free energy [51]. A quickly induced thermodynamic instability promotes nucleation before diffusion phenomena take place within the growing phase and supports fine-celled structures. Thus, by controlling the thermodynamic instability, the mechanism may be shifted between nucleation and diffusion. A sudden pressure drop results in smaller cells and a more uniform structure [51]. A

higher level of supersaturation results in a higher number of nucleated cells [51]. For slow pressure drop rates, nucleation and cell growth may happen simultaneously followed by pure cell growth [51].

As a consequence, cell density is a function of pressure drop rate and pressure level [51].

3. Desorption and cell growth

The gas starts to desorb and the single-phase mixture changes into a two-phase mixture of polymer and gas. The gas is consumed by the growing cells, diffusing into the existing ones promoting their growth. Besides a gradient in concentration also a gradient in pressure is on hand influencing transport processes.

4. Stabilization

The cells grow until the gas is consumed or the viscosity or resistance of the melt is too high for further growth. Coalescence phenomena, which is the conclusion of individual cells may occur. The final structure depends on concentration and diffusivity on gas in polymer, interfacial tension of polymer and gas and rheological properties during sorption and decompression [42]. Furthermore, the total amount of gas and the flow characteristics at nucleation temperature play an essential role [51].

The mentioned mechanism depend on materials properties, especially extensional viscosity of the polymer melt [52]. Moreover, they may actively be influenced by process parameter influences e.g. pressure gradient, shear rate and blowing agent concentration [52]. An active control of process parameters, thus an active influence on structure formation mechanism is possible especially for high-pressure procedure with mold volume expansion. The mechanism and boundary conditions are described more in detail in the following subchapters. For more information please refer to basic literature or in-depth investigations: e.g.[53, 54].

3.2.1 Solubility of gasses in molten polymers

Mass transport phenomena start with adsorption of gas fluid molecules on the surface of the polymer. The gasses can be generated within the polymer synthesis (e.g. PU foam) or by addition of physical or chemical blowing agents. Latter ones can be added in synthesis (e.g. PS particle foams), being dissolved in solid-state by high pressure (batch foaming process) or being added into the molten polymer under high-pressure conditions (foam injection molding or foam extrusion) [55].

Solubility defines the amount of gas which can be dissolved in a polymer by a given temperature and pressure [15], depending on the affinity of polymer to gas and mostly increases by increasing molecular weight or chemical similarity of gas to polymer [15]. Most polymers are hydrocarbon-based, thus exhibit high affinity for hydrocarbon-based gasses or volatile blowing agents. Non-hydrocarbon-based gasses like nitrogen generally exhibit low solubilities in polymers [56]. During processing, solubility is favored by high pressure, a good mixing process and longer dwelling times [52].

For calculation of saturation concentration, several complex models exist which are based on different assumptions (as reported by and cross-referenced in [55]). A simplified model which can describe simple sorption processes including the dependency of pressure on solubility in an adequate way, is the law of Henry [55]. This model describes a linear correlation of saturation concentration C to the hydrostatic pressure p , while C is the proportion of the mass of gas to the mass of polymer in saturation state. In general, for all gasses at moderate levels, solubility increases linear with increasing pressure [56, 57]. But, the constant of Henry can also be used to predict the solubility at high pressures [57].

$$C = S * p \text{ (Equation 1) [55, 56]}$$

$$\text{with } S = S_0 * e^{-\frac{E_s}{R*T}} \text{ (Equation 2) [55, 56]}$$

with C = saturation concentration, p = hydrostatic pressure, S_0 = coefficient (solubility coefficient extrapolated on endless temperature (experimental measurement e.g. by magnetic balance), E_s = heat of solution, R =general gas constant and T = absolute temperature.

The solubility coefficient also changes by temperature. However, the effect of temperature on solubility depends on the type of gas. The typical gasses CO_2 and N_2

used in foam injection molding may exhibit an opposite trend. While for CO₂ an increase in temperature results in a decreasing solubility, reported for PE and PP [57], for N₂ an increase in temperature for PP and PE is reported to decrease the solubility [56, 57].

The solubility and the necessary pressure to force the gas into solution depends on the type of gas as well its concentration. By the example of PP, solubility of CO₂ is ~ 5 times higher than solubility of N₂. The higher the gas concentration, the more pressure is needed to achieve complete solubility. Exemplarily solubility pressures for typical polymer-gas combinations are:

- PP/0.5wt%N₂ at 200 °C: 3.5 MPa [15].
- PP/1wt%N₂ at 200°C: 7.0 MPa [15]
- PP/1wt%CO₂ at 200°C: 1.5 MPa [15]
- PS/3wt%CO₂ at 220°C: ~ 7.8 MPa [58]
- PS/5wt%CO₂ at 220°C: ~ 13.2 MPa [58, 59]

It needs to be noted, that solubility values are usually measured under static conditions. However, in processing conditions are dynamic. Thus, solubility values may be used as a guideline but are not valid for foam injection molding process [60]. An approach to develop a measurement method to determine dynamic solubility limits in foam injection molding is described in [60]. By applying shear stress, solubility has been observed to increase, indicating that it is more process related than a material constant [60].

A blowing agent in solution acts like a lubricant and leads to an increase of movability of polymer chains. This plasticizing effect is especially significant for CO₂ [42] and is not that pronounced for N₂. Dissolved gas in polymer leads to a viscosity decrease due to gas molecules being located between molecular chains of the polymer resulting in an increasing mobility of molecular chains [44]. The viscosity is lowered with sorption and increased with desorption of gas [42]. The pressure drop during processing leads to a desorption of blowing agent and a loss of plasticization effect. This helps to stabilize cells, equivalent to a temperature decrease [42]. This plasticizing effect results in a decrease of glass transition temperature (T_G) (as reported and cross-referenced in [15]). As an example, by [61] reported in [15], it is claimed that 1wt% of CO₂ lowers T_G by 8 K, thus a polymer-gas mixture containing

5wt% CO₂ at 200°C would exhibit the same viscosity as a neat polymer at 240 °C. For PE, PP, PA it became evident that viscosity lowering effect of blowing agent is in a similar range (as reported in [15]). Di Maio and Kiran [42] mentions a reduction of T_G by 50°C for a PS exposed to CO₂ at ~ 5 MPa and a reduction of T_{melt} of ~ 25 °C for 10 MPa [42]. The crystallization temperature (T_C) is not affected for N₂. For CO₂, T_C is lowered for some Kelvin (as reported in [15]).

The effect of a decreasing melt viscosity can be used to reduce melt temperature in processing and support faster cycle times by faster cooling. Furthermore, during cell growth, the blowing agent exhibits an inner cooling effect by adiabatic gas expansion. This effect in combination with material savings in foaming (less material which needs to be cooled down) can also support faster cycle times.

3.2.2 Diffusion of gasses in molten polymers

After the gas is dissolved in the polymer melt, diffusion processes take place leading to an equal distribution of gas [55]. Diffusion enables the transport of the gas molecules through the polymer into the free space between the polymer molecules [56, 62]. It is mainly driven by differences in gas concentration, pressure and temperature [56]. The sorption of gas leads to a swelling of the polymer [63]. Gasses with small molecules like hydrogen, helium or carbon monoxide exhibit faster diffusion speeds than gasses with big molecules [56].

The speed of diffusion strongly depends on temperature. Heat supports flexibility of polymer chain movement [55]. For amorphous polymers the diffusion rate decreases significantly at T_G, for crystallizing polymers a drastic decrease is reported by passing T_C [56]. The diffusion speed decreases the closer the solubility level is to saturation point [44]. The time for gas diffusion is proportional to the diffusion path. Thus, to increase diffusion rate and time, besides a temperature increase, also the diffusion path has to be shortened [51]. In processing, this may be achieved by initiating shear distortion [51]. Thus, within the plasticization unit, shear elements mounted on the screw are usually used to stretch the gas cells and break them open.

Besides temperature, the speed of diffusion also depends on the type and structure of polymer and concentration of the gas in solution. For one-dimensional transport

phenomena, diffusion speed of a fluid molecule through the polymer can be described by 1. Fick's law:

$$\frac{dm}{dt} = -D * A * \rho * \frac{dc}{dx} \quad (\text{Equation 3}) [44]$$

$$\text{with } D = D_0 * e^{-\frac{\Delta E_D}{R*T}} \quad (\text{Equation 4}) [44]$$

where D_0 = constant for polymer-gas system, E_D = activation energy for diffusion, A = area, ρ = density, dc/dx = concentration gradient contrary to diffusion direction

These equations state that diffusion coefficient and thus diffusion speed increases by increasing temperature. If the amount of gas is close to saturation level, diffusion speed is lowered by decreasing local concentration differences. The saturation level is described by the law of Henry (see Equation 1 and 2) [44].

In practice, the diffusion coefficient may be measured by recording pressure versus time during gas dissolution experiments at different temperatures [64]. More details on solubility and diffusion coefficients of CO_2 and N_2 for Polyolefins and for Polystyrene can be found in [57]. Exemplarily diffusion coefficients for typical polymer-gas combinations are:

- For ambient temperature (24.85 °C) (as reported and cross-referenced in [19]):
 - PE-LD/ N_2 : $0,35 \times 10^{-6} \text{ cm}^2/\text{s}$
 - PE-LD/ CO_2 : $0.37 \times 10^{-6} \text{ cm}^2/\text{s}$
 - PC/ N_2 : $0.015 \times 10^{-6} \text{ cm}^2/\text{s}$
 - PC/ CO_2 : $0.005 \times 10^{-6} \text{ cm}^2/\text{s}$
- For processing temperatures (230°C):
 - PP/ CO_2 : $0.807 \times 10^{-4} \text{ cm}^2/\text{s}$ [34]

For thermoplastic foam processes, the diffusion coefficient of gasses should be in a range to allow a fast diffusion into the polymer. Suh [51] mentions estimated diffusion and solution times in plasticizing processes (in an extruder for typical processing temperatures) to be in the range of 60 - 100 s for PET and 10 – 20 s for PS, PVC and HDPE and a few seconds for LDPE.

3.2.3 Nucleation phenomena

Nucleation phenomenon is a thermodynamic process, controlled by phase separation [65]. It is the initial process in spontaneous formation of a new thermodynamic phase or a new structure within a metastable system and is affected by the level of supersaturation as well the temperature. As an example of temperature influence, boiling of liquids may be mentioned. Here, the change in temperature leads to a local change in pressure promoting formation of vapor nuclei [65]. For supersaturated systems at a constant temperature, nucleation is initiated due to the pursuit of re-establish an equilibrium status [65]. Nucleation reduces the local supersaturation levels (as it is observed by opening carbonated beverages). In general, four mechanisms of nucleation phenomena are used to describe nucleation of gasses in supersaturated systems as reported in [65]:

- Homogeneous nucleation: nucleation is initiated by thermodynamic instability of a single-phase mixture of gas and liquid for high levels of supersaturation
- Heterogeneous nucleation: nucleation is based on the presence of multiple phases and starts at the interfaces, particles or surfaces for lower levels of supersaturation compared to homogeneous nucleation
- Pseudo-classical nucleation: nucleation starts at pre-existing gas inclusions exhibiting radii smaller than the critical radius as it is predicted by the classical nucleation theory
- Non-classical nucleation: nucleation starts at pre-existing gas inclusions exhibiting radii larger than the critical radius as it is predicted by the classical nucleation theory

Pre-existing gas inclusions as they are described to be the basis for pseudo and non-classical nucleation may be on hand due to previous nucleation, gas entrainment by the flow of liquid, gas or nanobubbles which may be trapped at solid surfaces [65].

Classical nucleation theory

The classical nucleation theory (CNT) and the concept of critical radius is a theoretical model to quantitatively study the kinetics of nucleation and predict the kinetic instability for cell nucleation, based on thermodynamic rules [66]. Here, the free

energy defines the required energy to create a void in an liquid [67]. A critical free energy barrier must be passed to start nucleation. The process depends on two competing factors which are the available energy of gas diffusing in a cell embryo and the surface energy needed to form a cell surface [51]. Here, a critical cell size exists, defining if a cell is stable and grows or the cell embryo collapses [51]. The critical cell radius is defined by the boundary conditions of the system (temperature, pressure, gas concentration etc.) [66]. Once, nucleation is started, the concentration of dissolved gas in the melt decreases, increasing the critical free energy barrier for further nucleation (reducing nucleation) [68].

In homogeneous nucleation, the critical free energy barrier decreases by an increasing pressure drop rate [69]. Consequently, for higher pressure drop rates the energy barrier is lower, and nucleation is enhanced. In polymer processing, homogeneous nucleation refers to the thermodynamic instability of the single-phase polymer-gas mixture. In processing, the instability is induced by pressure drop which initiates the supersaturation of the mixture. The desorption of gas leads to formation of metastable nucleus as a new phase. The homogeneous nucleation is governed by pressure drop rate. Thus, for same polymer-gas mixtures different structures are achieved for different processing techniques. Furthermore, the level of supersaturation needed for homogeneous nucleation is very high.

Heterogeneous nucleation occurs in systems including foreign phases. In comparison to homogeneous nucleation it is thermodynamically favored because the activation energy is lower by the existence of nucleating agents [15]. Nucleus are built at the interface of phases, which can be particles, contamination, surfaces, etc. [44]. Thus, in real processes it is more common and starts before homogeneous nucleation [44]. For heterogeneous nucleation on liquid-liquid or liquid-solid interfaces a lower level of supersaturation is required than for homogeneous nucleation [66].

Pure homogeneous nucleation would be based on a system without any contaminates which is not possible in real processing [66]. Thus, both, homogeneous and heterogeneous nucleation take place [44]. To achieve microcellular structures, according to [51] amongst others, homogeneous nucleation should be the dominant effect even for the presence of nucleation particles or fillers which support heterogeneous nucleation [51].

Nucleation in plastics foaming process

The classical nucleation theory (CNT) does not apply for plastics foaming process [67]. Here, CNT overestimates the degree of supersaturation necessary for nucleation. Consequently, observations for nucleation rates are higher than the ones predicted by the CNT [66]. Thus, a lot of adaptations of this theory have been worked out. These modifications inter alia include a modification of free energy, supersaturation of blowing agent, polymer-solvent interactions, or the reduction of surface tension by dissolved gasses or shear-induced nucleation to approximate nucleation phenomena to real processing conditions [67]. The pseudo-classical nucleation theory respects micro voids existing in the free volume between the polymer chains in a metastable state with a radius smaller than the critical radius. The micro voids can serve as nucleation sites and grow spontaneous to become a nucleated cell [66].

Potential activation sites for nucleation are e.g. (listed by increasing potential): solid/polymer interfaces, high-strain regions, free volume, crystalline-amorphous interfaces, interfaces between crystallites or polar groups of polymers [51]. The nucleation sites nearly increase exponentially by the amount of blowing agent [51].

As already mentioned, stress-induced nucleation, initiated e.g. by extensional and shear stress significant effect nucleation [66]. In processing, stress may be induced by melt flow phenomena like extensional strain, shear-strain or due to bubble growth [23, 50]. For the so-called bubble growth induced nucleation, the expansion of cells initiates tensile stresses within the surrounding melt, resulting in a decreased local system pressure. Consequently, the degree of supersaturation is higher here and secondary microbubbles nucleated around the initial bubble are created. Shaayegan et al. [21] observed this phenomenon of cells nucleated and growing around previously nucleated cells and called it "*satellite phenomenon*". More details can be found elsewhere: [21, 50, 54].

3.2.4 Cell growth mechanism

Cell growth describes the growth of stable nucleus, meaning cell nucleus which have achieved the critical size [55]. Cell growth may occur simultaneously to nucleation or afterwards, depending on location and boundary conditions. At the early stage, cell

growth is pressure dominated while from a distinct cell size the mechanism is shifted to a diffusion dominated mechanism. In processing, nucleation and cell growth are competing mechanism, both consuming the available gas. Depending on the boundary conditions, especially the pressure drop rate, mechanism may be shifted to nucleation (fast pressure drop) or cell growth (slow pressure drop).

The classical cell growth model is a simplified assumption. Here, an isolated single cell, surrounded by single-phase polymer-gas mixture growing in an endless viscoelastic medium, being representative for the growth of all cells is assumed [44, 55]. If supersaturation pressure is not high enough for further nucleation, pure cell growth is on hand by diffusion of the remaining gas into the existing cells [68]. The more gas has diffused into the cells, the less gas is available in the melt [44].

At the early beginning, growth is driven by pressure difference of internal gas pressure inside the cells and the surrounding polymer. At this stage, growth speed depends on surface tension and viscoelastic properties of the melt and is not controlled by diffusion (as reported and cross-referenced in [55]). Thus, the start of cell growth is also described as nucleation favored cell growth. Right after nucleation, the pressure inside the cells is equal to saturation pressure [51]. The concentration of gas in the melt is equal for all positions. In the cell's shell the gas concentration is zero and it is assumed to be surrounded by an endless amount of gas [44]. When all gas in the direct environment of the cell is moved into the cell, cell growth is shifted from a pressure dominated to a diffusion dominated process (as reported and cross-referenced in [55]). From this point in time, the gas needed for further cell growth has to move from regions outside the direct cell environment, driven by diffusion [55]. The single cells can still be regarded as an isolated system, however the area influenced by the cell is significantly bigger now. Figure 3 illustrates a growing cell and the influenced region within the polymer matrix. The cell is surrounded by a spherical shell of influenced polymer volume. The gas diffuses from this volume into the cell, resulting in less concentration of gas in the shell region. The concentration of gas is lowest in the transition zone of cell to shell and increases by distance away from the cell. At the boundary of the influenced zone, the gas concentration corresponds to the saturation concentration [55].

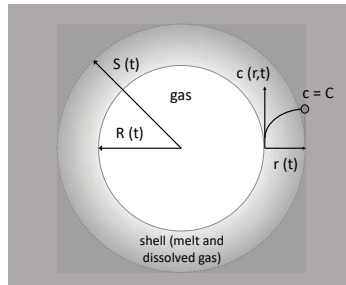


Figure 3: Scheme of cell growth of an isolated cell in the polymer matrix according to [70] and [44]; $R(t)$ = time dependent cell radius, $S(t)$ = time dependent radius of influenced area, $c(t)$ = time dependent gas concentration within the influenced area (shell)

By the growth of the cell also an increasing area is influenced. From now, mass transfer has to be considered for cell growth modeling. Therefore, the law of conservation of mass, the law of conservation of momentum and the law of conservation of energy have to be considered for cell growth of each cell [55]. Literature provides several models to describe the diffusion driven growth. For more information please refer to [55] and the cross references given here.

The continuing cell growth leads to a reduction of pressure inside the cells [69]. This correlation is depicted in Figure 4. The pressure inside a cell is plotted over its volume. By increasing cell size, the pressure decreases and the cell volume increases to a greater extent than the cell's surface [69].

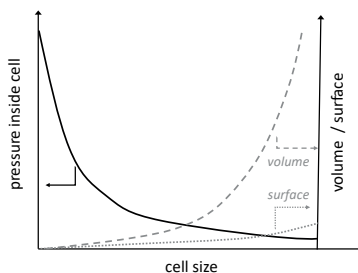


Figure 4: Correlation of cell volume, cell's surface and internal pressure for a growing cell according to [69]

Cell growth stretches the melt and may lead to a macromolecular orientation of polymer chains [69]. If melt strength is too low, cell walls can rip open in this stage [69].

Cells can in principle expand until the viscosity of the matrix allows a viscoelastic-plastic deformation. However, the role of viscoelasticity in cell growth is still not clear at all [67]. Viscosity decreases by an increasing temperature. Thus, gas molecules can move more easily, resulting in shorter diffusion times. Consequently, cells can grow faster. During procedure, cell growth decreases the available amount of gas in the melt resulting in an increase of viscosity [44]. An increase in temperature leads to a reduction of tangential forces in the cell wall, resulting in faster cell growth. However, this effects can also support coalescence [69]. During cell growth the melt viscosity is locally different [71]. Through diffusion processes a viscosity profile around the growing cells is on hand and the viscosity is significantly higher in the interface region of cell and melt compared to the regions further from the cell [71]. The viscosity profile inhibits deformation by shear stresses and promotes the growth of spherical shapes [71].

In real, non-idealized systems the influenced regions or shells of multiple cells come into contact before cells directly interact with one another [55]. At this point in time, growth of the shell (influenced area) stops, and just the growth of the cell itself continues until the remaining gas within the shells is diffused into the cells [55]. If cells were nucleated at the same time, able to grow simultaneously by equal conditions and the distance between nucleus was equal, the same final cell size would occur [55]. This illustrates the main influence of high nucleation rate and nucleation sites necessary for homogeneous cell formation [55]. However, in real process, nucleation often takes place at different points in time and by different boundary conditions. Pressure and temperature are not the same at every location, thus small cells and big cells exist growing simultaneously. By contact of cells with different cell sizes, diffusion is favored from small to big cells.

Without further forces affecting the cell growth, circular cells would occur due to the attempt of establishing a minimum surface to volume ratio (energy reasons) [19]. Thus, for idealized conditions, cells are assumed to be spherical during growth [67]. However, in a real process, cells often grow by the presence of shear forces and stabilize in a non-spherical shape. Furthermore, not all cells are nucleated at the same time, thus, for the later nucleated cells less amount of dissolved gas is available and they do not grow to the same size [67]. Assuming constant surface tension, the initial pressure in small cells is higher compared big ones. Thus, by contact of different size

cells, the gas of small cells can diffuse into big ones and support their growth [44]. Due to this effect, coarse-celled and inhomogeneous structures may occur [44].

The larger the number density of cells, the less gas is available for each single cell, thus the gas consumption is smaller and cells grow less [34]. Cell growth ends by achieving an equilibrium of forces, which is the pressure inside the cell versus the forces needed for further cell growth defined by surface forces and stresses in the viscoelastic cell wall [51, 69]. The resulting forces are illustrated in Figure 5.

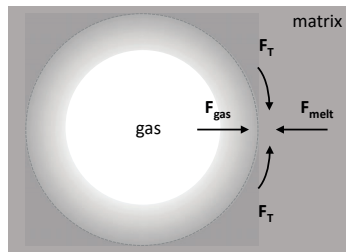


Figure 5: Scheme of forces during cell growth of an isolated cell according to [69] with F_{gas} = forces of gas, F_{melt} = forces of the melt and F_T = tangential forces by extensional viscosity, elasticity and surface tension

In terms of microcellular structures, cell growth starts at a high number of nucleation sites. In the diffusion-controlled growth period, the diffusion paths are very short. Due to this fact and because of the simultaneous diffusion of gas into the high number of cells, cell growth stops earlier compared to non-microcellular structures [51].

To achieve fine-celled and homogeneous structures, growing cells have to be stabilized [44]. Growth induces a bi-directional extensional flow, thus extensional material characteristics are important for stabilization [52]. Stabilization is mainly given by increasing viscosity, occurring during procedure by melt cooling, decreasing gas content in melt, elongation of cell walls by cell growth (increasing extensional viscosity by decrease of cell wall thickness) and by orientation of molecules. Destabilization like inhomogeneities or rupture of cell walls may occur due to high temperatures, slow cooling or locally different boundary conditions for cell growth (as discussed before) [52].

In processing, stabilizing and destabilizing effects occur simultaneously and are mainly defined by temperature of melt and mold, wall thickness of the part [44] as

well the available expansion volume. In foam injection molding, the mold and the part design affect the boundary conditions for stabilization in a significant manner.

3.2.5 Modelling

In real processes, mechanisms are different from idealized assumptions, they in parts happen simultaneously or interact one with another. Thus, in parts complex models on nucleation and cell growth have been worked out. A lot of literature exists, dealing with these models or modification / shortcomings of them. In the following only a short excerpt is mentioned.

An overview on mathematical models for cell growth is given in [72]. Here, the historical development of models (not all referred to plastics) from 1917 to 2009, classified in several categories is given for 30 models. Besides single bubble growth models (1917 – 1984), also cell models including simultaneous growth without interaction and recent bubble growth models are described. Another deep review on studies on cell nucleation and growth in polymeric foams is given in [68]. Here, details on several studies and models from 1969 to 2004 are described, including models considering simultaneous nucleation and growth [68]. In Tammaro et. al [73] a type of timeline of publications and their classification to the foam evolution steps (polymer-gas solution, nucleation, growth, impingement as well cell wall rupture), from the years 1990 up to 2012 is given.

Many of these models are based on experimental observations and visualization experiments as they are described in chapter 3.4.1. Taki [68] did visual observation of batch-foaming experiments and investigated the effect of pressure drop rate on the cell density and the cell growth. The cell growth models of Han and Yoo, Payvar and Shafi et al. were compared with experimental results. It was found that for a PP/CO₂ mixture Han and Yoo model was the closest while for a PS/CO₂ mixture Payvar's model was closest to experiments [68].

Feng and Bertelo [67] introduced a model which employs effects of neighboring cell growth as well decreasing blowing agents. Thus, different nucleation rates for earlier and later nucleated cells are considered, allowing the model to describe cell size distribution [67]. However, they state that cell size distribution is affected by many

other factors like melt rheology, solubility, temperature, pressure and nucleating agents [67].

A cell growth model consisting of Newtonian constitutive equation for cell radius, Han and Yoo mass transfer model for cell pressure and a modified classical nucleation rate equation is presented in [68]. By the help of this model, the author was able to describe simultaneous nucleation and cell growth and identified 3 phases (which are in parts already mentioned in chapter 3.2.4), listed in following and qualitatively described in Figure 6:

- 1. Viscosity controlled period (short): At start of nucleation phase, the pressure inside the cell is equal to saturation pressure [68]. The higher the viscosity, the longer this period is. The driving force here is the pressure difference [68].
- 2. Transient period: The period between nucleation and diffusion is driven by the driving forces of both, the pressure difference and the diffusion of the blowing agent [68]. The pressure inside the cells decreases significantly by a simultaneously increase of its radius [68].
- 3. Diffusion controlled period (longest period): The gas diffuses into the cells. The rate is proportional to the product of diffusion coefficient and concentration gradient. Diffusion controlled cell growth consumes the main amount of gas and gas concentration decreases [68].

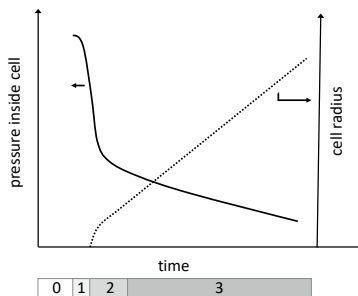


Figure 6: Qualitative description of cell growth according to [68]: cell radius and pressure inside the cell plotted over time; 0 = onset of nucleation, 1 = viscosity controlled period, 2 = transient period and 3 = diffusion controlled period

Nowadays in several commercially available software tools for numerical flow simulation of polymers (Moldflow® (Autodesk), Moldex3D® (Coretech Systems),

CADMOULD® (Simcon)), also cell growth models are implemented to allow the simulation of foam injection molding. The most important physical properties for numerical simulation are solubility parameter, diffusion coefficient, surface tension and viscosity [68]. However, these parameters depend on the polymer-blowing agent system and need to be adapted for each system. Within this thesis Moldex3D was used for simulation of foam injection molding procedures. Here, three models for calculation of cell growth are implemented: Han and Yoo, Payvar and Shafi and the aforementioned parameters are editable by the user. Details on definition of process and calculation are given in chapter 3.4.2 and in the appendix (chapter 11.5.1).

3.2.6 Influence of material and blowing agents

Material

The extensional rheology of a material is an indicator for the material's ability for foaming processes [52]. Materials exhibiting a good solubility of blowing agents and sufficient melt strength are advantageous here [42, 52]. During nucleation and growth, materials' viscosity should be high enough to prevent gas from escaping out of the melt or to undergo cell collapse, but low enough to allow expansion. The solubility of gas as well the formation of cells depends, among others, on the crystallinity of the material. An increasing crystallinity leads to a decreasing solubility of gases. Diffusion and absorption processes take place in the amorphous regions. Solubility and cell density decrease by increasing crystallinity. Thus, materials with less crystallinity are feasible to uptake more gas. This leads to higher thermodynamic instability, thus to an increase in cell density as well a more homogeneous structure.

While in amorphous polymers mostly homogeneous nucleation takes place, in semi-crystalline polymers crystals act as heterogeneous nucleation sites. The effect of crystallization affects the rheology and thus the foaming process. Semi-crystalline polymers exhibit a very narrow process window for foaming, defined by insufficient melt-strength for high temperatures and crystallization effects for low temperatures [42]. However, for semi-crystalline polymers, the crystallization process initiates a dramatic increase in viscosity, promoting the stabilization of structure [55]. Furthermore, semi-crystalline polymers distinguish a faster freezing of the melt front. Hereby, as a tendency, the compact skin layer thickness is thinner [17, 74–76]. In

regard to processing, as a result of the aforementioned facts, amorphous polymers exhibit a wider temperature window for foaming compared to semi-crystalline polymers.

It should also be mentioned that semi-crystalline polymers exhibit more free volume for foam expansion due to a higher material's shrinkage. Thus, especially for low-pressure foam injection molding or low-expanded foams the lightweight potential by materials reduction may be higher for semi-crystalline materials.

The influence of material properties or the influence of different material types are not in focus of this thesis. For more information please refer to the investigations of: [15, 52, 55, 77, 78]. Their investigations focused on different types of PP and showed that long chain branched types (LCB-PP) exhibits a good melt stretchability and melt strength, being advantageous for high expansion ratios [52, 77, 78]. PP types with high viscosities (HMW-PP) resulted in inhomogeneous structures with big voids [15]. The positive effect of branched PP types is also reported in [79]. Rheological aspects in terms of foaming processes are discussed elsewhere: [15, 52, 55, 77].

Heterogeneous nucleation may be supported by additives, like Talcum [80]. Spörrer [15] did investigations with various types of PP and also used nucleation additives. In his investigations it became evident that expansion ratio and melt temperature exhibit a more significant influence on the foam structure than the nucleation effect of additives. However, the presence of Talcum as nucleation agent lead to smaller cells and enabled a wider process window.

Blowing agents

Chemical blowing agents (cba) decompose by temperature influence and release CO₂ or N₂. Depending of the type of blowing agent (ba) used, an endothermic or an exothermic reaction is initiated. Cba are usually processed as masterbatches, consisting of a carrier polymer, an active substance, fillers, nucleation and processing additives. Thus, several substances come along with the ba delivery, affecting the structure formation. For physical blowing agents (pba) only the gas itself is added to the polymer; no by-substances are on hand during cell formation. In processing of physical blowing agents, also usually CO₂ or N₂ are used. Both gasses were compared in experiments of [34]. In high-pressure foam injection molding with core-back

experiments, the number density of cells by using N₂ (at lower concentrations than CO₂) was 30 times higher and cell size was 1/3rd smaller compared to CO₂ [35]. It is constituted by the lower solubility and higher degree of supersaturation for N₂ [35]. The classical nucleation and cell growth models for batch foaming can be used to explain these differences [35]. Simulations also confirmed this result [35]. The concentration of the used gas is in general several times higher for CO₂ than for N₂. In own experiments as well in results shown in chapter 8.4.2, PS/ 0.5wt%N₂ resulted in much finer cell structures compared to PS/3wt%CO₂.

Independent of the used gas, an increasing gas concentration decreases viscosity and glass transition temperature [51].

3.3 Characteristics of foam structures

General aspects

A cellular structure is defined by several characteristics which are used for general classification in terms of their typical application field.

A foam may be characterized by its type of cells which can be an open, a closed or for some cases also a mixed-celled structure [79]. Also, the homogeneity or distribution of cell sizes is often used for classification. A repetitive uniform cell structure may be described as a syntactic foam. Here, also cell sizes may differ but no cluster of big or small cells can be assigned to special positions. A foam structure which's cells' characteristics change by position, i.e. from small cells in the outer layers to big cells in the foams center, may be described as an integral cell structure. Besides this definition, foams are also often distinct into their overall density. Low-density foams (with a relative density < 0.1) are mainly characterized by edges, struts and membrane-like thin faces defining the individual polygonal cells connecting each other [79]. This is for example the case for low-density PU foams, created out of liquid phases. In structural foams (with a relative density ~ 0.4 - 0.8) mainly individual cells embedded in a polymer matrix are on hand and the properties are described to be close to them of bulk polymers [79]. The structural characteristics are affected by the materials, procedures and boundary conditions used for manufacturing.

In foam injection molding of thermoplastics, typically integral, closed-cell structures occur, not allowing a movement or flow of media through the structure. In general, the structure may be described as an integral structure with non-foamed skin layers and a graded cell structure in the inside. Typically, the cell size distribution by cross-section is observed with increasing cell size towards the core of the sample. This is a result of the temperature gradient inside the sample and the outer cooling by the mold. Temperature and viscosity are highest in the center, resulting in a faster cell growth and bigger cells here [36]. The individual characteristic of the cell structure and the specificity of the integrality depend on the type of procedure and mold technology used. While in conventional / low-pressure procedure the characteristics can only be influenced in a limited way, in high-pressure procedure with expandable molds a huge influence can be performed.

As mentioned later, in foam injection molding often the creation of a microcellular structure is aimed to affect the mechanical properties just in a minor way. However, the definition of microcellular structure is very diverse in literature. While in some literature a cell diameter of around 10 μm is given [80], Cramer [19] lists several definitions of mean cell sizes ranging from < 10 μm up to 100 μm . Some literature mentioned here also qualifies the cell density ranging from 10^9 to 10^{12} $1/\text{cm}^3$ or even defining typical cell wall thicknesses of 1- 5 μm [19].

Characteristics of structure

In general, the measurement of cells' characteristics is diverse in literature and the exact procedure is often not described in detail. Several challenges exist, e.g. the question how to deal with merged or connected cells and cells which are not completely included in the chosen observation area. Merged cells may be rated as one cell or split and rated as individual cells. Cells which are not completely included in the observation area may be excluded or not. The smaller the observation area is, the more cells are affected and the bigger the resulting differences in interpretations are. These difficulties are on hand for all characterization methods – 2D and 3D. Thus, the results are very individual and user sensitive. In the following, diverse characteristics are described and highlighted in Figure 7.

Two parameters often used to describe or compare the structure characteristics of foam injection molded structures are:

- **Cell size / Cell diameter:** This parameter is often measured in Scanning Electron Microscopy (SEM) pictures, using cryo- broken samples or in Reflected Light Microscopy (RLM) samples. The diameter or the circumference of the cell is measured in a 2D observation level. Thus, the measurement depicts just a cut-out of the cells' shape and mean diameter and 3D shape may be different. In general, a 2D measurement does not reproduce the widest diameter of a cell which leads to smaller cell size values. This point is discussed in chapter 3.3.2.
- **Cell density:** This parameter is a measure for number of cells per volume unit (cells per cm^3). For 2D measurements this parameter may be less sensitive in terms of the influence of the observation level compared to the cell size. While cell size value may change a lot in dependency of the observation level, the number of cells may be comparable (assuming the cells are individual and structure does not change significantly by observation level). Cell density refers to a volume, however its calculation is based on 2D data and the assumption of isotropic spherical cells without coalescence phenomena [81] and a uniform distribution in all directions [82]. The cell density of the foamed material (N) measured in 2D is determined as follows [31, 33, 83]:

$$N = \left(\frac{n}{A}\right)^{3/2} \times \frac{1}{1-v_f} [1/\text{cm}^3] \quad (\text{Equation 5})$$

where n is the number of cells counted in an area of A in the image; v_f is the foams' local void fraction obtained as follows:

$$v_f = 1 - \frac{\rho_{foam}}{\rho_{solid}} \quad (\text{Equation 6})$$

in which ρ_{solid} is the density of the solid sample and ρ_{foam} is the density of the foamed one.

In literature (e.g. [10, 81, 84]) also another definition of cell density is often used based on a theoretical approximation by Kumar:

$$N = \left(\frac{nM^2}{A}\right)^{3/2} * \frac{\rho_{foam}}{\rho_{solid}} [1/\text{cm}^3] \quad (\text{Equation 7})$$

where M is the magnification of the analyzed picture and A the image area.

For the calculation of the cell density within this thesis Equation 5 was used. A discussion on methods for cell density calculation of polymeric foams can be found elsewhere: [82].

Based on the assumption of an ideal cell structure with spherical cells in a closely packed cubic structure, 74 % of volume is omitted by cells and 26 % by bulk material [51]. For the ideal cell structure, cell size corresponds directly to cell density [51] and the number of cells is inverse proportional to the cube of the cell diameter and may be calculated the following [51]:

$$N_{0,ideal} = \left(\frac{1}{cellsize}\right)^3 * \left(\frac{1}{0,26}\right) [1/cm^3] \text{ (Equation 8)}$$

Thus, a cell size of 0.1 μm corresponds to a cell density of $3,85 \times 10^{15} \text{ 1/cm}^3$, a cell size of 1 μm to $3,85 \times 10^{12} \text{ 1/cm}^3$ and a cell size of 10 μm to $3,85 \times 10^9 \text{ 1/cm}^3$ [51]. However, the real number of cells can increase if cells expand and cell walls are thinned [51]. Foam injection structures are typically not ideal structures with closely packed cells. Thus, the direct correlation of cell size and cell density is not valid here and should be judged as a general trend.

Furthermore, in literature (e.g. [1, 16, 18, 19, 81, 85]) also other characteristics are used for characterization, some of them are highlighted in Figure 7:

- *Cell aspect ratio / anisotropy*: Proportion of widest to smallest diameter
- *Orientation angle*: Angle between main axle of cell (widest diameter) to reference axis (e.g. cross section or main flow direction of sample)
- *Thickness of compact skin layer*: Distance from outer cells to surface of sample
- *Cell distance*: Distance between center of cells'
- Cell wall thickness: Thickness of struts between cell walls
- Circularity: Deviation from ideal circular shape; max. value = 1

$$\left(\text{Circularity} = \frac{4 * \pi * \text{Cell Area}}{(\text{Cell Perimeter})^2}\right)$$

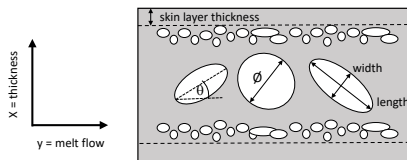


Figure 7: Diverse characteristics of cellular structures used for quantification of foam injection molded structures: skin layer thickness, θ = orientation angle ; ϕ = diameter; aspect ratio = proportion of widest to smallest diameter

Characterization of integral structures

Despite foam injection molded structures are characterized by an integral cell size changing by cross sectional position, often only one value is used to describe or compare the structures. Here, often mean cell size, cell density or mean density in the center of the part is used for evaluation and comparison of structures. This method is widely accepted, but it just gives an information about the characteristics in the core area and does not provide any information on the characteristics change in thickness [1]. Figure 8 depicts cross-sectional cuts of foam injection molded structures with different cell size and density distributions. As obvious here, one single value measured in the core area is not appropriate to specify these structures or compare them one with another.

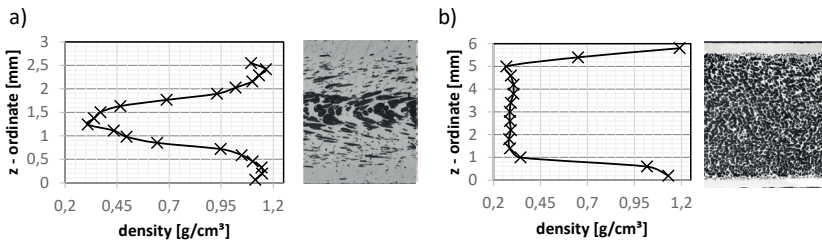


Figure 8: Cross-sectional cuts of foam injection molded structures with different cell size and density distribution: a) low pressure foam injection molded structure, b) high-pressure foam injection volume-expanded structure [86]

To consider the change in structure, often layer models are used to describe individual cell characteristics at different positions in the cross section of the parts as it is done e.g. in [16, 18, 87]. Usually, the cross section is divided in several layers (e.g. core layer, transition layer, skin layer) and structure characteristics for each layer are measured or a qualitatively description is made.

Qualitative characterization of integral structure

In his PhD thesis, Kirschling [16] intensively worked out process-structure-property relationships of foam injection molded structures. Within this context he found different structures and analyzed its variation in cross-section. Based on layer models he qualitatively classified the structures into different models and found structures

to be advantageous for different load cases. Figure 9 summarizes some of his results and shows the general characteristics of three different structures he identified and their trends in density profile. These classifications were found by analyzing foams with low expansion ratios. For high expanded foams produced within this thesis these differences in structure have not been observed.

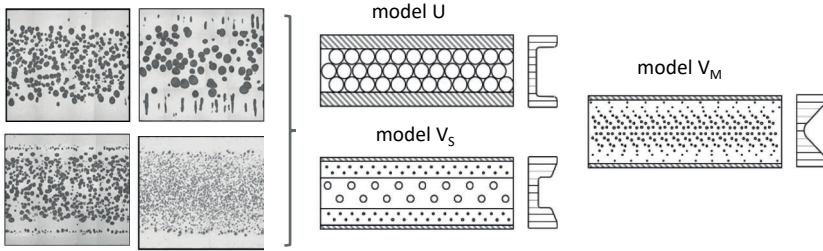


Figure 9: Abstraction and modelling of foam injection molded structures by Kirschling [13, 16] (with kind permission of the author)

Quantitative / functional characterization of integral structures

In Rizvi et. al. [88] a “Cell Distribution Index (CDI)” has been defined to be a quantitative parameter for characterization of injection molded foams. This index should describe to deviation in cell size as a measure for uniformity and is defined as follows [88]:

$$CDI = \frac{\bar{\Phi}_D}{\bar{\Phi}_N} \quad (\text{Equation 9})$$

$$\bar{\Phi}_N = \frac{\sum_i N_i \Phi_i}{\sum_i N_i} \quad (\text{Equation 10})$$

$$\bar{\Phi}_D = \frac{\sum_i N_i \Phi_i^2}{\sum_i N_i \Phi_i} \quad (\text{Equation 11})$$

with Φ_i = cell diameter in μm and N_i = number of cells with diameter Φ_i

A value of 1 indicates a perfect uniformity and deviations lead to an increase in value. This method seems to be a good way to describe and compare the uniformity for a selected area, e.g. core area. However, it may not be a suitable method for characterization of an overall structure including compact skin layers or huge deviations in structure.

Several approaches to describe the density profile of integral foams by mathematical functions are mentioned in [89] and cross-referenced in [1, 89]. In Flórez Sastre [1] and Cramer [19], 2D microscopic images depicting the cross section of a foamed specimen were analyzed by image editing software. The images have been transformed into a high-contrast black / white color scheme. Cells appeared in black while the neat polymer appeared in white. They converted the grey values with the neat polymers' density. Thus, they were able to depict the density profiles over the cross section. For low expanded or low density reduction foams in general a pronounced integral structure was observed. This approach is also used within this thesis to characterize the density by specimens' thickness. For a systematical comparison of structures, it was found that cell size distribution by part's cross section may be approximated by a Gauss function and density profile via a Boltzmann function [1, 19]. The equations can be used to mathematically describe the distribution of cell size (small to big from outer layers to core) and density (high to low from outer layers to core) for low-pressure foam injection molding in a good approximation. For high expanded or high density reduction structures often an abrupt change in density could be seen. Thus, approximations via Gauss or Boltzmann function are stated not to be suitable for description [1]. Instead, mean cell size may be a sufficient characteristic to be used to describe the structure in the core area. Furthermore, aspect ratio and cell orientation are also stated to be less important parameters for description [1]. The effect of density profiles on flexural properties was investigated in [89] and [90]. Here, a direct measurement of the density profile of the used specimen has been done by the help of an x-ray density profiler device.

The general difference in density profiles for low and high expanded foam structures is also mentioned by [44]. Here for low density reduction foams a smooth transition could be investigated while for density reduction $> 30\%$ an abrupt rise in transition is reported.

3.3.1 Methods of characterisation

In the following, several characterization methods, used within this thesis are described, omitting technical details or physical basics. The Reflected Light-Microscopy (RLM) and Scanning Electron Microscopy (SEM) are 2D characterization

methods which may be judged as established methods for structure characterization. The users do not have to be specially trained. However, the preparation of the samples may be time consuming and its quality is user sensitive which may affect the analysis result. For 3D analysis, the X-ray micro-Computer Tomography (μ CT) method may be used for characterization. However, this method is relatively new and users have to be appropriately trained. Thus, it is rarely used to characterize structures of cellular polymers.

In 2D analysis methods, the result is a sectional plane which represents a cut-out of the structure and may not be representative for other layers. For example, cells not being connected in 2D analysis found to be connected by 3D analysis [91]. Based on theoretical calculations 3D characteristics may be obtained from 2D data [81, 85]. For both, 2D and 3D methods, the analysis of coarse structures may be quite challenging, and the result is user dependent. Judging of merged cells to be individuals or one big cell is, independent if user or software decided, a challenge which may significantly influence the results. These points are discussed in chapter 3.3.2.

3.3.1.1 Conventional imaging techniques

Reflected light microscopy (RLM)

The sample needs to be prepared in several steps to achieve a planar surface with negligible differences in height. First, the sample needs to be cut / milled according to the investigation area, followed by embedding it in a resin. After curing of the resin, a stepwise grinding and polishing is needed to gain a planar and smooth surface for the light microscopic analysis. Grinding and polishing may be done by hand or by special machines. For the cutting or milling as well the grinding and polishing processes, usually water-assisted saws and plates are used to prevent the sample from frictional heating during preparation.

The microscope pictures can be taken in bright field or dark field method. In bright field method, the light source is from same direction as the objective lens, resulting in a bright impression of the sample. In dark field method, the light source is arranged sideways, resulting in a dark impression of the sample. For the reflected light-microscopic pictures depicted within this thesis, digital light-microscopes (Keyence VHX

series) with dark field method - resulting in dark cells and a bright matrix – were used (see Figure 10). The analysis of the pictures including measurement operations was done by the help of image editing software (Adobe Photoshop®). For larger investigation areas, several pictures were taken and merged to one big picture by the software.

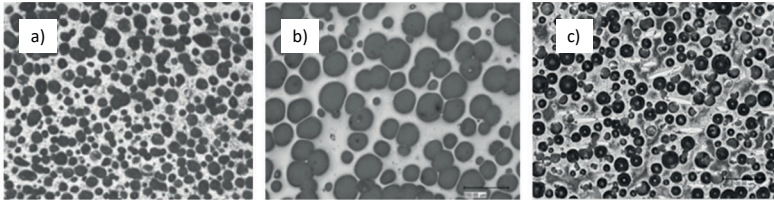


Figure 10: Examples for RLM images captured by dark field method - different foamed polymers: a) PC-ABS/N₂; b) PC/N₂; c) PA-GF15/N₂

Scanning Electron Microscopy (SEM)

The SEM may deal with uneven surfaces, thus a cryo-break (short storage in liquid nitrogen, followed by mechanical breaking) of the sample is usually done. Polymer samples need to be coated with a very thin layer of conductible material (usually gold). The sample is glued onto a sample holder, the coating is done in a sputter device and is typically finished within seconds or minutes. The samples are put into the vacuum chamber of the microscope and pictures can be taken. Microscopes may use different levels of vacuum and may require different demands on sample preparation (type of glue or type of coating needs to be respected).

The method does not need an excessive preparation and pictures may be taken quickly. However, by using brittle cellular materials (like PS), in some cases cell wall fragments have been found in neighboring cells, hindering the analysis.

The SEM pictures shown within this thesis were taken by a CAMSCAN MV2300 and a JEOL JSM-6060. Figure 11 shows an example of a uniform, spherical-celled structure (a) and a non-uniform coarse-celled structure (b).

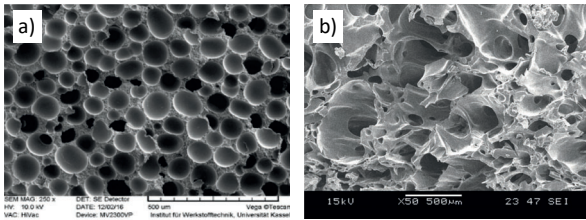


Figure 11: Example for SEM images – foamed polymers: a) PC-ABS/N₂; b) PS/N₂.

3.3.1.2 Micro-Computer Tomography (μ CT)

X-ray computer tomography is increasingly used in materials science to gain new insights into materials' structure [81, 91–94]. A high number of morphological data for all dimensions may be obtained. Hence, the morphological complexity of microstructures may be described more into detail, thus a better understanding of and conclusions on the process may be worked out more accurately. In Bacaicoa et al. [94] a comparative investigation of microstructure analysis by using 2D image analysis and μ CT has been conducted by using three different materials (metal, concrete, polymer). The results showed that a 2D characterization often is not suitable for complex shapes due to the lack of data for the 3rd dimension [94]. The 3D data provide a lot of information on structure characteristics which are hidden or only known in cut-offs by 2D analysis. Once the reconstruction is done, a lot of information can be analyzed quickly.

However, also for this method the results are highly user dependent. The user defines the algorithm to judge on merged cells to be rated individually or splits merged cells. Due to the three dimensions include here, the probability of cells' contact is higher compared to 2D analysis. Furthermore, specific expensive measurement equipment, usually a long data processing time and expensive software is needed [81]. Another challenge is to analyze structures with large differences in cell sizes and wall thicknesses, which is often not possible by scanning with a unique resolution [95].

The sample preparation is in principle non-destructive. Bigger samples may need to be cut into dimensions restricted by the μ CT device. In the first step the sample is scanned. Here, resolution and quality are defined by several parameters. In general, the more detailed and the higher density the material, the longer the scanning time.

Afterwards, the 3D volume reconstruction is done by a reconstruction software and the 3D structure characteristics may be analyzed for the investigated volume. Once the reconstruction is done, characteristics can be exported within a “.csv” file. For cellular materials, several characteristics may be analyzed:

- *“Volume3D”*: Information on cell volume
- *“Aspect Ratio 3D”* (proportion of max. width to max. length): Information on shape or elongation of cells
- *“Sphericity”*: Information on deviation of shape from a perfect sphere (max. value = 1)
- *“BaryCenter X, Y, Z”*: Information on position of cells’ barycenter (x, y, z – direction)
- *Number of cells*
- *etc.* (more characteristics available)

Besides the 3D evaluation, also 2D evaluation within the scanned volume is possible, providing the option to make slices at every desired position. These pictures are comparable with the 2D pictures taken by RLM (layer fixed by preparation).

For the investigation within this thesis, the (3D) X-ray micro tomography (μ CT) was done using a Zeiss XRadia 520 Versa microscope with a standard voltage setting of 80 kV and 6 - 7 W. In general, for each sample 1601 images were taken with a resolution of 5.7 to 6.1 $\mu\text{m}/\text{pixel}$ and an exposure time of 1 to 2 s. The tomographical data has been reconstructed by Zeiss TXM Re-structor software. Finally, the re-constructed data was analyzed using AVIZO (FEI) software. Cylindric samples of ~ 5 mm in length, ~ 5 mm in width and ~ 3 to 6 mm in height (~ 75 to 150 mm^3) have been scanned and analyzed. In AVIZO a non-local means filter was applied, and an automatic segmentation of cells was conducted. The segmentation is based on grayscale values and automatically judges if merged cells are split and counted individual or not. The greyscale thresholds can be set by the user and may differ for different structures. Due to its high significance on the results, the segmentation step will separately be discussed later.

Figure 12 depicts an exemplary sample reconstruction of a PS foam. Cell volumes were reconstructed in different ways: (i) reconstruction of the entire foamed volume

of the sample; that is, the region between the solid skin layers, and (ii) a reconstruction of an area in the center of the specimen (a sub-volume defined as 1/3 of the sample's thickness). A special filter named "border-voxel-count" (BVC) was used to eliminate cells which had been cut by the borders of the defined volumes. Thus, only fully shaped cells within the investigated volume are displayed and used for further analysis, and artefacts or cell fragments are excluded (this procedure is also reported in [95]). However, in the given example (ii) the limits of the sub-volume definition cut a lot of cells while in (ii-BVC), the BVC filter excludes these cells, resulting in a reconstruction of just a few cells. A typical scanning time was around 1.5 h, the reconstruction was about 1 – 1.5 h.

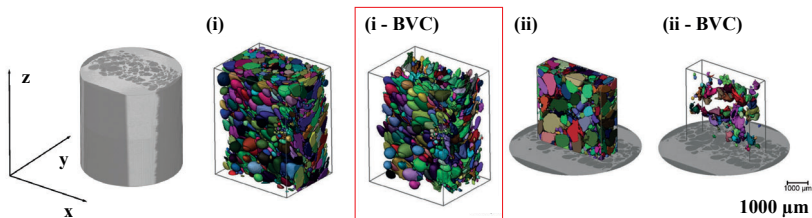


Figure 12: X-ray micro tomography of a foam injection molded sample (PS/CO₂) - Reconstruction of 3D Cell volumes: (i) segmentation of full-cell volume; (i -BVC) segmentation of full-cell volume with BVC; (ii) segmentation of a sub-volume in the core area; (ii - BVC) segmentation of a sub-volume in the core area with the BVC (Y: sample thickness direction; z: Melt-flow direction)

Based on the reconstruction, the following characteristics were calculated by the AVIZO software: max. length (*Length3D*), max. width (*Width3D*), volume (*Volume3D*), aspect ratio (*Aspect Ratio3D*), sphericity (*Sphericity*) and barycenter (*BaryCenterX*, *BaryCenterY*, *BaryCenterZ*) as a measure for cell's position for every direction.

In order to achieve a more adequate description of structures, the cell characteristics volume and sphericity have been analyzed in terms of their position, represented by the barycenter values. Thus, trends in cells size or shape of cells referred to the coordinate system (flow direction, thickness direction, and parallel to flow direction) can be analyzed. In the later chapters this analysis is done in terms of scatterplots. Figure 13 shows an exemplarily scatterplot of a FIM structure. Here, the volume of each individual cell is plotted over its barycenter position in the "y direction", representing the specimen's cross section. The barycenter refers to the set

coordinate system, including the unfoamed skin layers. Thus, the cell size distribution over the thickness of the specimen (here: 6 mm) can be investigated. A clear trend of increasing cell sizes from the outer layers to the core can be seen.

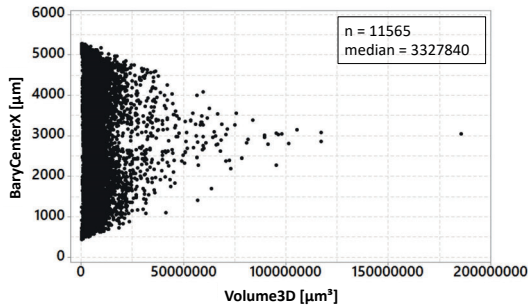


Figure 13: Distribution of cell size over the specimen's cross section: volume of cells (Volume3D) plotted over position of its barycenter in specimen's thickness direction (BaryCenterX)

3.3.2 Challenges in evaluation of foam structures

Measuring foams' characteristics is quite challenging. It depends a lot on sample preparation, the methods used for calculation and user's influence. Especially for 2D characterization methods a lack of information on the structure below the observation level may lead to erroneous interpretation. The following major problems are on hand by characterization of foams. However, in literature it is often not clearly described how the authors did handle with these points:

1.) Dealing with observation levels (2D analysis methods)

For 2D measurement methods only one layer is observed. It is not clear where exactly the cells are cut or broken (see Figure 14). It is assumed that cells are cut or broken in their center in the rarest cases. Thus, the evaluated cell size or diameter is not representative and is in general smaller than its maximum diameter due to an out-center cut [19, 96]. This effect is sometimes described as "Tomato slice effect" in literature. Another unknown aspect is the 3D shape of the cells which may lead to erroneous interpretation of characteristics. Cells are often not spherical and

characterized by a complex 3D shape. Thus, dimensions may be different in another observation layer.

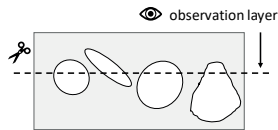


Figure 14: Sketch of a cell structure ; depiction of 2D observation area

2.) Dealing with incomplete cells within the area of investigation

Independent of the analysis method, 2D or 3D, usually incomplete cells at the limit of the observation area are on hand. These cells may be excluded from analysis (see “BVC” images in Figure 12) as it was done within this thesis and in is reported in [95] or counted in an individual way. Here, one option is to count them as halves as mentioned in [81]. The smaller the observation area and the larger the cells are, the bigger is the impact on the result.

3.) Dealing with merged cells (2D and 3D analysis methods)

Structures where cells are merged or connected one with another are often difficult to measure. There is no consistent method how to deal with it. Connected cells may be separated and counted as individual or they may be rated as one individual cell (see highlighted cells in Figure 15 a)). However, the definition of “*connection*” or “*merge*” (any overlapping / how much overlapping) is often not clear and is highly user and sample preparation dependent. While in 2D analysis only the observation level may be judged, in 3D also a connection of cells underneath the observation level may be on hand (see Figure 15 b). For example, the cells highlighted in the detail of Figure 15 b, are connected in an observation level underneath the cutting level. However, in 2D analysis they would be rated as individuals without any doubt.

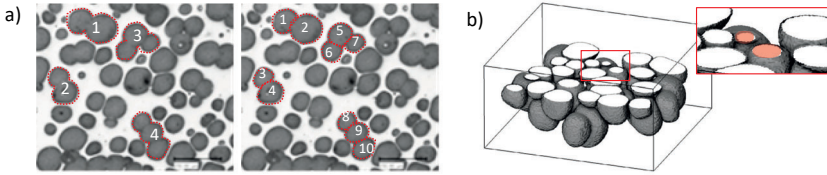


Figure 15: Analysis of cellular structures: a) 2D cut of a foam injection molded structure with connected /merged cells counted in different ways and b) sketch of a 3D foam structure with interconnection of cells underneath the observation level

For software-based evaluation, an algorithm, based on a user-defined threshold decides if a cell is rated as an individuuum or not. Thus, these evaluation methods are also highly user-sensitive by definition of the threshold, however the assessment of the structure is done a consistent manner.

To separate matrix and cells, in AVIZO software the operation “*Thresholding*” is used. Here, the differences in grey values (differences in density) provide a basis for distinction. If the contrast is too low, cell walls may not be calculated, and several cells may be rated as one cell instead of individuuum. The operation “*separate objects*” is used to separate connected cells. By an example of a PC foam the effect of different “*Separate objects*” settings is shown in Figure 16. No use of this operation resulted in almost one big cell (Figure 16 a) while a high separation level (Figure 16 c) results in a high amount of smaller cells. The results show the huge impact of this operation on reconstruction and evaluation of results. The choice of the threshold should be done very carefully to achieve an adequate reproduction of the real structure.

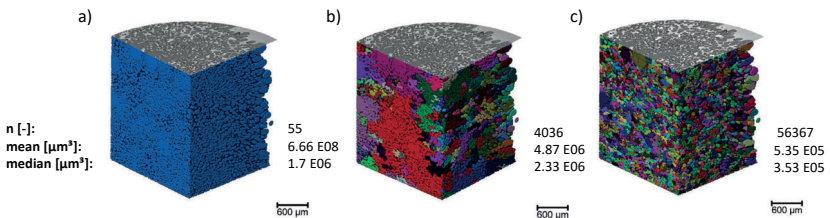


Figure 16: Influence of “*Separate objects*” setting on the evaluation of a PC foam structure (based on [97]): a) no use of separate objects, b) low separation level, c) high separation level (n = number of cells, mean = mean cell volume, median = median cell volume)

For the evaluations within this thesis “separate objects” operation was set individually and consistent to the different types of structures. Furthermore, another analysis filter was used which excluded artefacts and particles. For more information on the operations used for structure analysis in the reconstruction software (AVIZO) please refer to the appendix (Figure 131).

3.4 Observation of cell formation

3.4.1 Visualization experiments

To in-situ observe and analyze the filling behavior, several researcher groups built special molds and used visualization systems to monitor foam formation.

Analyzing the basic mechanism of foaming (independently of process), at Kyoto University, Japan a high-pressure autoclave with a sapphire windows and a high-speed camera was used [98]. Researchers from Toronto University, Canada used a high-pressure, high temperature chamber, additionally applying shear and extensional stress [54, 99, 100]. Also at University of Naples, Italy, a batch-foaming system (mini-batch) with visualization window was used for investigations [73, 93, 101].

To in-situ analyze the foaming behavior in foam injection molding process, even in 1978 investigations were conducted. Han and Villamizar [102] and Yoo et al. [103] did is-situ visualization investigations in extrusion foaming. First observations on cell formation and growth in foam injection molding were also done by them, using a mold with a glass window and recording movies of mold filling in an isothermal process [22, 23]. Their investigations lead to important basics of modelling of cell formation behavior. Nowadays, current visualization investigations on the foam formation in foam injection molding are known from University of Teheran, Iran [24, 29], University of Toronto, Canada [21, 30–32, 59], University of Kyoto, Japan [34–36] as well Zhengzhou University, China [84] and South China University of Technology, China [104].

3.4.2 Simulation of procedure

Using numerical simulation is mentioned to be an effective way to analyze and learn about injection molding and especially also about foam injection molding process [59, 84, 104]. Simulation software helps to get an insight in procedure and make the process more transparent. It is an approach to get knowledge on parameters which are hard to be obtained from experiments.

To determine the boundary conditions inside the cavity, simulation software also was used in several studies in terms of foam injection molding [15, 19, 105]. Software was used to determine the general boundary conditions like temperature profiles, pressure conditions and flow front profiles in dependency of process parameter settings.

Basics for accurate flow simulations have been worked out by different institutions, e.g.: [37, 38, 106–109]. Recently developed, several commercially available software tools for polymer flow simulation provide the possibility to simulate the foam injection molding procedure. Currently, two software tools, Moldflow (Autodesk) and Moldex3D (CoreTech Systems) furthermore provide the possibility to simulate the core-back procedure.

Within this thesis Moldex3D (R14/ R15) was used as a tool to explain differences in procedures and analyze boundary conditions in molding procedures. Moldex3D predicts cell size and cell density by considering both, cell nucleation and cell growth simultaneously. Interaction between cell formation and melt flow are considered by a dynamic cell growth model. The calculation can be conducted by using “*Han and Yoo*”, “*Payvar*” or “*Shafi*” cell growth model. For details concerning calculation definition options available in Moldex3D (R15) please see appendix (chapter 11.5.1). Details on the numerical models for simulation implemented in Moldex3D are given elsewhere: [37, 38, 106, 110].

The suitability of Moldex3D to simulate foam injection molding has been shown in several publications and a good agreement with experimental data has been observed. It was used to simulate the low-pressure foam injection molding process [38, 38, 39, 105, 106, 110]. An example in context of automotive applications is given in [105]. Here, cellular structures for a PP-GF were predicted by simulation and showed a close agreement to experiments. At Kyoto University, Japan, Moldex3D was also used to simulate the high-pressure foam injection molding process in combination with core back procedure. They used a simple rectangular part geometry

which was completely expanded by a mold with shearing edges. They validated their simulation with experimental results and found that simulation was able to predict the foaming behavior. Simulation showed the same trends and provided a close approximation to their experimental results [40].

In the author's own work, the special procedure of local core-back was simulated and qualitatively compared to experimental results. Thus, the boundary conditions have been made more transparent to explain phenomena observed in own experiments. Local foam formation as well the qualitative accordance of process parameter effects have been simulated [41, 111]. A quantitative comparison of simulation and experiment could not be done due to restricted possibilities of material and foaming parameter's definition and calculation issues for high expansion ratios. As a standard in Moldex3D, foaming parameter for a combination of PP/N₂ are used. The parameters may be edited by the user, but neither it is known on which type of Polypropylene they are based on nor which values must be put in here for other material-gas combinations. For information on pre-set values please see the attachment (chapter 11.5.1). However, simulation software has demonstrated the general suitability to simulate the foam injection molding processes qualitatively.

For all simulations shown within this thesis, Han and Yoo model was chosen for calculation of cell formation. For core-back procedure, the expanded volume area and all relevant parameter (core-back distance, core-back speed, delay time) can be defined. For mold opening or core-back procedure, two different part geometries, according to the experiments of this thesis were used for simulation. The parts have been meshed with tetrahedron elements. A boundary layer mesh (BLM) with an additional multi-layer prismatic mesh for the surface layers has been waived due to calculation issues. The areas for core-back or local core-back had to be defined as "*moving surfaces*" by using the final part volume (volume after core-back operation). Within the calculation, the mesh in the core-back area first was deformed to the initial cavity volume and expanded after calculation of filling and packing phase. To be able to monitor the process and to analyze individual results, several sensor nodes were attached to the parts' meshes, covering different locations and different layers over parts' thickness. Sensor nodes record all simulation results over the whole cycle. Thus, conditions for each sensor node position may be analyzed and results (e.g. pressure, temperature, cell size) can be plotted over time (xy-plots). Figure 17 and Figure 18 show the parts used for experiments and simulation within this thesis. The

core-back areas and the definition of the sensor nodes are highlighted here. Figure 17 shows a local-core back part where the mold existed before the start of this thesis. The cross-ribbed section at the backside of the part defines the expandable volume and can be set to different positions. The part geometry in Figure 18 and its injection mold was designed within the thesis. Here, either the whole rectangular area at the backside of the part may be expanded by mold-opening operation (Figure 18b)) or 4 ribs of different width may be expanded within the process by local core-back operation (Figure 18c)).

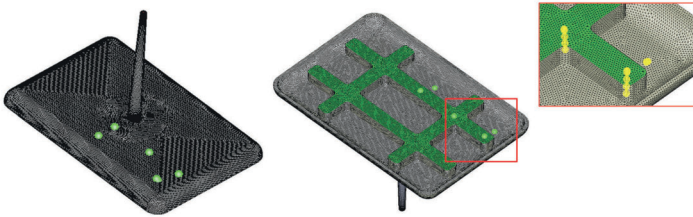


Figure 17: Finite element model used for numerical simulation: Part1 – Thin-walled plate; dimensions: 120 x 80 mm, wall thickness: 1.5mm, central cold runner on surface side and expandable cross-ribbed structure at backside (green); sensor nodes are defined over flow length and cross section of the part; total number of elements (parts and runner): 906.186

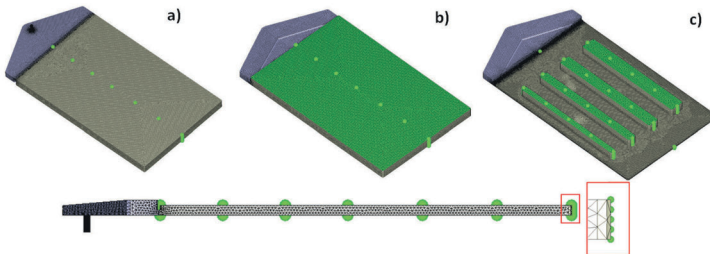


Figure 18: Finite element model used for numerical simulation: Part2 – Thin-walled plate; dimensions: 120 x 80 mm, variable wall thickness: 1.0 / 1.5 / 3 mm, hot-runner + fan gate; variants a): non-expanded part, b) mold opening - part with full volume expansion (green) and c) local core-back = local expanded ribs (green); sensor nodes are defined over flow length and cross section of the part; total number of elements (part and runners): ~ 640.000

It should be noted that the simulation results are idealized results based on theoretical models and may differ from experimental results. However, they point out the basic cell formation during procedure and help to make cell formation during procedure more transparent.

4 General mechanism of cell formation in foam injection molding

All mechanism associated with solubility of gasses and evolution of cells, which is nucleation, cell growth and fixation, mainly depend on pressure and temperature conditions. These conditions change during procedure. All main process parameters directly or indirectly affect pressure, temperature or viscosity. These physical sizes, named as process values in the following, also interact with another. For example, the higher the temperature, the lower the viscosity, consequently the pressure distribution or pressure transfer is affected. The process parameter define the boundary conditions for solution of gas and cell formation.

4.1 Plasticizing process

Cell formation or evolution starts within the plasticizing process. Here, different types of blowing agents and methods are used. At the beginning two phases exist, the polymer and the gas. Independently of the blowing agent (ba) or process used, by the help of increasing temperature and pressure, a uniform single-phase mixture with a molecular distribution of ba fluid in polymer melt is aimed for prior to injection, enabling an achievement of homogeneous cell nucleation and cell growth in the cavity [44]. In presence of undissolved gas pockets injected into the cavity, the gas molecules in solution tend to diffuse into these pockets instead of creating new cells (growth is thermodynamically favored instead of nucleation). Furthermore, small cells located around may collapse by diffusion into the large gas pockets. As a consequence, a non-uniform, coarse structure with low cell density results [66]. The gas is prevented to escape from the plasticization unit by a shut-off nozzle (alternatively in some cases the procedure can be also conducted by a fitted nozzle). The pressure to get the gas into solution is applied by back-pressure of the screw during plasticizing. However, in real processes still uncertainty of conditions and solubility processes within the plasticizing unit exists [60]. Here, apart from static solubility, also dynamic solubility is on hand [60]. Diffusion processes can be supported by shortening the diffusion paths by using mixing and shear elements. Shear deformation stretches and may divide cells, support their distribution in the melt and increase the contact area of melt and gas [51, 55]. It may shorten the diffusion path up to 100 μm (as reported and cross-referenced in [55]). In terms of

usual processing temperatures of around 200 °C, diffusion coefficients of both CO₂ and N₂ in Polystyrene, Polyethylene and Polypropylene are around 10⁻⁴ to 10⁻⁵ cm²/s (as reported and cross-referenced in [55]). Thus, diffusion times of mixing within a shear field (e.g. in extrusion) is mentioned to be less than 10 s.

In the following, methods to get the gas into the polymer before injection are basically classified. All these processes have their own specifics in terms of blowing agent's specifics (e.g. type, homogenization, concentration, etc.) as well processing specifics (e.g. shear effects, pressure, etc.) and thus on homogeneity of the melt-gas mixture. Moreover, also method independent processing parameters, like temperature profiles, back pressure, screw speed, type and amount of blowing agent can have a huge influence on the mixing result. A discussion on details and differences of the individual processes will be omitted here.

1) Adding blowing agent as solid additive before plasticizing process

The simplest way of adding a ba which does not require special equipment is to add a chemical blowing agent (cba) as an endothermic or exothermic substance in a solid phase mixed with the polymer granulate and feed the mixture via the hopper. Within the plasticizing process a chemical reaction is started, the gas is released by the increasing temperature and is mixed with the polymer melt. The injection molding machine does not have to fulfill special technical requirements. Just the control of the screw position and back pressure, as well already mentioned a shut-off nozzle is necessary to create a homogeneous polymer-gas mixture.

Another option is the use of thermoplastic expandable microspheres. A blowing agent is included within an elastic shell. An increase in temperature leads to an expansion of the gas, thus the microsphere expands. The shell is stretched and thinned during the expansion. As a result, typically spherical cells (expanded microspheres) are created. The cells still exhibit an own shell and the gas is still locked in. Thus, expandable microspheres may be used for polymer melts with a weak melt strength [112–114].

II) Adding blowing agent in gaseous / supercritical phase within plasticizing process

Another way, which requires additional technical equipment is the use of physical blowing agents (pba). Based on the observations for most properties of foam structures to improve by decreasing cell size, microcellular foams and technologies to process supercritical fluids as blowing agents were introduced [42, 51]. The idea behind microcellular structure was to create cell sizes which are smaller than existing defects in the polymer melt. Thus, mechanical properties should not or less be affected by foaming. Furthermore, it was assumed that small cells could damp the broadening of cracks and help to make the material tougher [51]. Inertial gases (usually N₂ or CO₂ in supercritical state) are injected directly into the molten polymer. When brought in supercritical state (above critical pressure and temperature: CO₂ = 73.8 bar (7.38 MPa) @ T = 31 °C; N₂ = 34 bar (3.4 Mpa) @ T=-146.75 °C [44]), the gas exhibits gas-like and liquid-like properties. It shows compressibility as a liquid while the diffusivity is gas-like. Thus, it shows a good diffusivity and good dissolution, supporting the formation of a single-phase solution in the plasticizing unit. Different procedures have established in the market and are in general available as additional equipment by the injection molding machine producers. In the 1990's the "*MuCell*" (Trexel Inc.) process was invented at the Massachusetts Institute of Technology and commercialized by Trexel Inc. as a patented technology. From 2000 several alternative process techniques for physical gas insertion arised in Europe [19, 92]. Machine producers and other companies invented similar technologies, e.g. "*Cellmould*" (Wittmann Battenfeld), "*Optifoam*" (Sulzer Chemtech AG), "*Smartfoam*" (Stieler Kunststoff Service GmbH), as well technologies were invented by research institutions, e.g. "*Advanced Structural Foam Molding*" (MPML, University of Toronto) [10]. Some of them are not commercially available anymore due to patent situations. However, in principal in most of these procedures physical blowing agents, typically nitrogen or carbon dioxide, are injected in the melt and well mixed; the difference is in technical details.

Another new approach has recently been presented by the Kyoto University [115]. They developed a simplified process technology, claiming that pressurizing physical blowing agents to high pressures is not necessarily required to produce fine-celled foam injection molded structures [115, 116]. They just supplied gas directly into the molten polymer without a pressurization system or an injector valve and produced

microcellular foams by low pressures [115, 116]. Furthermore, they were the first who used air as physical blowing agent and achieved microcellular foams of $\sim 7 \mu\text{m}$ ($1.63 \times 10^9 \text{ 1/cm}^3$) [115].

III) Adding gas-load granulate before plasticizing process

Besides the methods dealing with injection of supercritical fluids into the molten polymer, also “autoclave-like methods” are available. Here, blowing agents (usually CO_2) are forced to diffuse into the polymer granulate before processing within pressure chambers. Such technologies were invented by the IKV Aachen (now commercially available as “*ProFaom*®” by Arburg GmbH), the Kunststoffinstitut Lüdenschied in cooperation with Linde AG (“*Plastinum Process*”) [117] as well the “*IQ Foam*®” technology developed by Volkswagen AG [118]. In the “*ProFaom*®” process the plasticizing unit is equipped with a special sealed hopper using air locks. The diffusion process of CO_2 into the polymer granulate takes place inside the hopper as well in the first section of the screw. A similar equipment is used in the “*IQ Foam*®” setup. Here a two-chambered unit is installed between the hopper and the feeding zone and the gas is retoured from one chamber to the other to reduce leakage [118]. It is reported that N_2 , CO_2 or any other physical blowing agent may be used [118]. In the “*Plastinum Process*” also CO_2 is used as a blowing agent. Diffusion takes place in an external processing unit and pre-loaded granulates can centrally be feed to the machines.

A similar approach published by the University of Wisconsin-Madison is called “*Supercritical fluid laden pellet Injection molding Foaming Technology – SIFT*” [119]. Here, also a gas-loaded granulate is used, produced by an upstreamed foam extrusion step. In foam extrusion, CO_2 or N_2 loaded pellets are produced and finally feed individually or as a blend of both to the injection molding machine [119–121]. Another approach, also presented by the University of Wisconsin-Madison is the use of water vapor in combination with i.a. cubic sodium chloride (NaCl) as a nucleation agent [121]. By this, they also produced microcellular foam structures without a SCF generation and injection system [121].

4.2 Filling phase

In the following, the basic mechanism occurring during filling phase are described. These mechanisms are independent of process variant. Chapters 5.1 and 6.1 tie in with here and describe process specific structure formation for low-pressure and high-pressure procedure.

Inside the plasticizing unit the gas is in solution and a supersaturated state is maintained by the high pressure. Due to the pressure drop during filling phase, the supersaturated single-phase mixture separates, and nucleus are created during filling. This process starts at the point in time the pressure inside the melt is lower than the partial pressure of the blowing agent [19]. The shifting flow front also shifts pressure conditions inside the cavity. The pressure in the melt behind the flow front increases by increasing filling rate. Thus, melt pressure here exceeds again the partial pressure of the blowing agent [19] and cells may be forced back into solution. The melt directly behind the flow front instead, exhibits lower pressure levels than the partial pressure. Nucleus are built and dependent on the pressure drop rate new nucleus or cells are created or existing cells start to grow [19]. The pressure drop is highest at the flow front; thus, nucleation and cell growth mainly take place here. The initial time before cells start to grow depends on their initial radius. The bigger the cells are, the faster they grow (as reported and cross-referenced in [122]). Pressure level and gradient of pressure are important because they mainly define nucleation and balance of forces within the cavity [19]. The gas is consumed by two competitive effects: nucleation and cell growth [68]. Either the gas starts to build a cell at a nucleus or diffuses into an existing cell. Fast nucleation leads to less gas available for cell growth, thus more cells and smaller cells are created. In this case, diffusion rate is low and it is more beneficial to build new nucleus than to do a long diffusion way and support the cell growth of another cell. A slow nucleation instead, shifts the effect to cell growth. Less cells and bigger cells are created by diffusion of the available gas into the existing cells [19]. By stop of injection, cavity pressure drops and nucleation of new cells as well growth of existing cells continues. Especially the injection speed influences the resulting pressure and pressure drop inside the cavity [19]. The influence of this parameter on the final structure is discussed in chapter 8.2.2.

Figure 19 exemplarily shows simulation results for pressure and cell size during filling phase for a timestep during filling ($t = 0.4$ s) and the point in time filling is stopped

(switch over point; $t = 0.64$ s). The gradient of both, pressure and cell size over the flow path and the shift of cell size values due to the shifting pressure conditions can be seen.

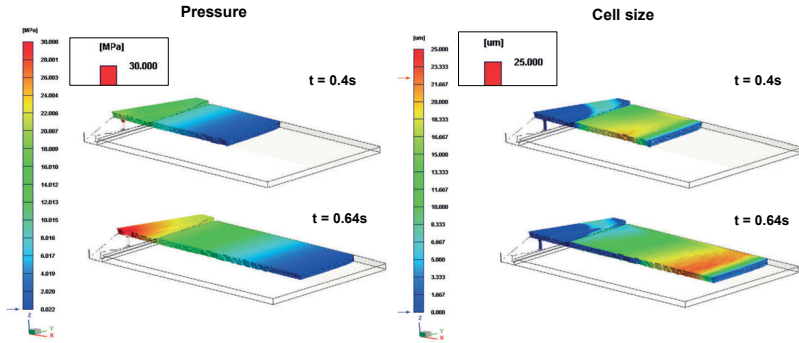


Figure 19: Cross sectional cut of a rectangular plate filled by a film gate – simulation result for cavity pressure (left) and resulting cell size (right) for different filling rates: $t = 0.4$ s and switch over point: $t = 0.64$ s (Material = PC, Makrolon 2405; $V_{inj} = 50$ cm³/s; SCF = 0.3wt% N₂)

Polymer is non-Newtonian fluid exhibiting a viscoelastic behavior. The melt flow is described by a laminar shear flow with a fountain flow at the flow front [28]. The fountain flow transports the melt front to the outer layer and cavity filling is conducted through the center [28]. The velocity in the center is higher compared to the outer layers. Thus, in general a huge gradient in velocity, resulting in a gradient in shear stress is on hand across cavity thickness [28]. Usually, an almost non-slip condition at the cavity wall exists [28]. Thus, an increase in injection speed results in a higher velocity gradient and a higher shear rate [28]. In the center, shear rate is zero and cells exhibit a circular shape [28]. The shear rate increases from the center to the cavity wall. However, the fact that melt flow at the flow front is a fountain flow leads to a complex distribution of the shear rate [28]. The cells close to the melt front get stretched by the fountain flow. The cells are deformed before they reach the flow front. The fountain flow brings them to the cavity wall where they get further stretched by the high shear stress here. Minor shear fields result in ellipsoidal shaped cells, while for pronounced shear fields the shape changes into long and thin cells [28]. The cells may break up and get split into several smaller cells [28]. But, orientation and deformation of cells also depends on viscosity of melt, surface tension and the cells' size [28]. As a consequence of the aforementioned mechanism, the cells at the melt front are stretched, cold shifted or may break open during their

flow from the center to the much colder cavity surface, resulting in silver streaks or swirls on the parts surface [28]. In terms of processing, variotherm mold temperature control can effectively counteract these effects. Here, a significantly increased temperature at the cavity surface reduces the temperature difference of melt and mold and may allow a compensation of this effect. However, this topic is not in scope of the thesis and is discussed elsewhere: [123–128] as well has been demonstrated by the author’s work: [86, 129, 130].

During filling process, generally ellipsoidal cells are created [131]. Shearing and stretching support deformation and coalescence of growing cells [84]. Cells of a spherical shape are attributed to be created after stop of injection [131]. In literature, this is also described as “foaming during filling” and “foaming after filling” [131]. During filling the cavity pressure behind the flow front may increase to a level below solubility pressure, resulting in a decrease of cell sizes and a re-dissolution of gas into the melt. The unfoamed compact skin layer is created by two effects: One effect is the re-dissolution of gas into the melt, the other effect is a suppression of foaming by high pressure [28]. The temperatures difference of mold and melt result in a quick freezing of the unfoamed melt. Figure 20 depicts the mechanism of structure formation during filling in dependency of cavity pressure and shear strain for different filling levels.

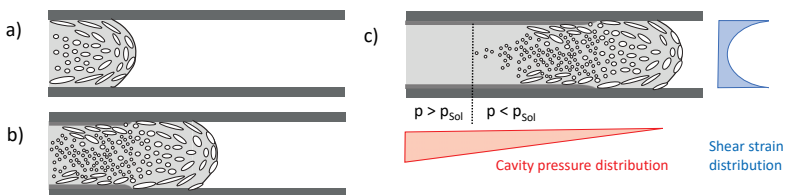


Figure 20: Schematic depiction of cell formation during filling for different filling levels according to [28]; p_{sol} = solubility pressure

A lot of investigation on cell formation behavior during filling as well the consequences of filling rates on final structures has been worked out elsewhere: [11, 84, 131, 132]. Here, also a scientific review on the effects associated with RHCP process [133] as well a deep review on cell deformation and collapsing phenomena at the flow front was done by Zhang et. al. [133, 134]. As distinctiveness, besides the melt and the blowing agent they also considered air inside the cavity as a third phase in the filling process [134].

5 Low-pressure / conventional foam injection molding procedure

There is no general classification for low or high-pressure procedure in literature and definition often is not clear. While a procedure with a cavity pressure < 100 bar is referred to low-pressure procedure [1], the distinction may also be made by the shot size in which a non-volumetrically mold filling (short-shot) is referred to low-pressure procedure while a volumetrically injection of melt (full-shot) is referred to high-pressure procedure [21]. However, in this thesis the distinction should be made by process sequence. For low-pressure procedure (LP-FIM), filling volume is smaller than cavity volume and no packing pressure is applied. This is the procedure used for most current applications and thus also referred as conventional foam injection molding.

In low-pressure or conventional foam injection molding process, in general conventional injection molds are used. However, special design rules for foam, i.e. suitable gate design and geometric restrictions should be respected [44]. The cavity is only filled to a predefined volume. By stop of injection, a pressure drop is on hand allowing the gas to expand and the gas-melt mixture to swell into the unfilled cavity volume. Packing pressure is not applied, to not reduce the available space for foam expansion and to not destroy the growing cells. The injection volume defines the density reduction, which is around 5 % to 20 % for typical applications [80]. Figure 21 summarizes the procedure and depicts important process parameters for cell formation, grouped in parameter defined by the injection molding machine ("imm parameter") and parameter defined by the mold ("mold parameter").

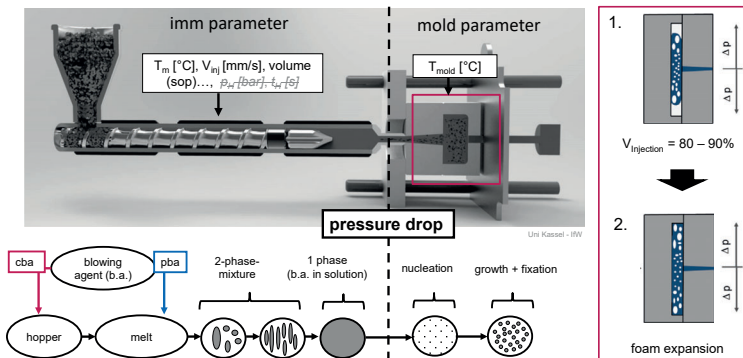


Figure 21: Low-pressure / conventional foam injection molding procedure (LP-FIM) – cell formation during procedure and highlighted processing parameter (T_m = melt temperature, V_{inj} = injection speed, T_{mold} = mold temperature, volume (sop) = filling volume)

Figure 22 illustrates the process sequence and Figure 23 compares typical cavity pressure curves recorded for compact injection molding and low-pressure foam injection molding. Switching over to packing phase and applying packing pressure in compact injection molding leads to an increasing pressure as well a higher cavity pressure level. In low-pressure foam injection molding by stop of injection the cavity pressure doesn't increase that much compared to compact molding. Due to the fact that the mold is not filled volumetrically, and no packing pressure is applied, the cavity pressure decreases immediately after stop of injection.



Figure 22: Process sequence for low-pressure foam injection molding procedure (LP-FIM); (start of cycle -> closing mold -> open nozzle mold -> open nozzle plasticizing unit -> injection -> no packing pressure -> close nozzle plasticizing unit -> close nozzle mold -> cooling – parallel: dosing material and injection of gas -> opening of mold and ejection -> end of cycle

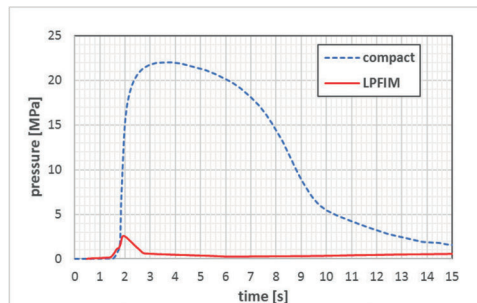


Figure 23: Experimental cavity pressure curves: compact molding and low-pressure foam injection molding (LP-FIM); stop of injection / switch-over point (sop) for LP-FIM = 85 %

5.1 Phases of cell formation in low-pressure procedure

As already mentioned, all mechanism associated with solubility of gas and evolution of cells mainly depend on pressure and temperature conditions, changing during process. In the following, the different process phases and their role or influence of structure formation are described. For low-pressure procedure the cell formation

mechanism can be classified into three phases, depicted in Figure 24. Additionally, the phase-relevant cell formation mechanism and process parameters are depicted.

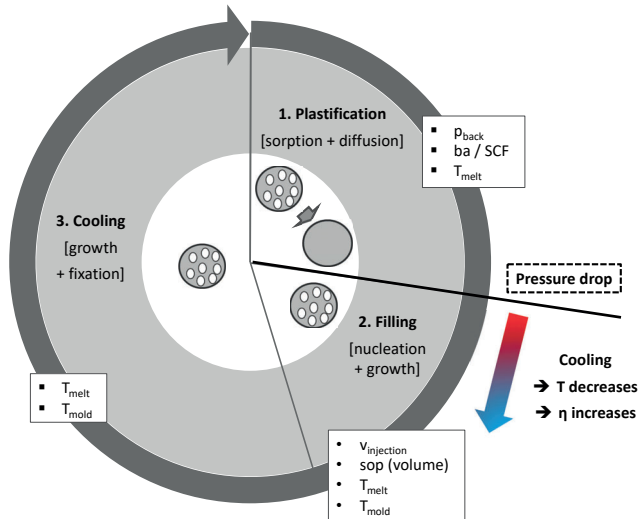


Figure 24: Cell formation mechanism in low-pressure / conventional foam injection molding procedure (p_{back} = back pressure, ba / SCF = concentration of blowing agent / content of supercritical fluid, T_{melt} = melt temperature, $V_{injection}$ = injection speed, sop (volume) = switch over point (injected volume), T_{mold} = mold temperature, T = temperature, η = dynamic viscosity)

1. Plasticizing

In the plasticizing phase, sorption and diffusion processes are the driving forces to achieve a single-phase solution. Polymer and gaseous phases are mixed and by the help of pressure and temperature the gas is forced into solution. Here, a suitable temperature control, a reproducible gas insertion as well a sufficient back pressure is necessary to prevent gas from escaping and enable sorption and diffusion processes. As already mentioned, this phase is not in focus of this thesis. A single-phase mixture (polymer melt supersaturated with gas) is presumed to be provided prior to injection. However, details on this phase are given in chapter 4.1. The main influencing process parameters are back pressure (pressure by screw), melt temperature and blowing agent concentration.

2. Injection / Filling

Inside plasticizing unit, the melt-gas mixture is pressurized to ensure a single-phase mixture. By leaving the nozzle and entering the mold, a pressure drop occurs which leads to thermodynamic instability and building of nucleus. Parallel to mold filling more nucleus are built and cells start to grow. The melt flow inside the cavity shifts the flow front, thus a flow path dependent pressure gradient with increasing pressure near the gate occurs. Details on this phase are given in chapter 4.2. At the point in time, the injection is stopped, most of the melt is still supersaturated with gas. The sudden pressure drop initiates nucleation and cell growth. Expanding cells lead to swelling of melt volume and volumetrically filling of the mold. The gas expansion depends on the local pressure and temperature conditions and is mainly defined by mold geometry and filling volume. Important process parameters are injection speed, injection volume (switch over point), as well melt and mold temperature. In low-pressure foam injection molding, filling and formation of cellular structure occur simultaneously, thus can only be controlled to a limited extend.

3. Cooling phase

The cooling phase as it is defined by injection molding machine, specifies the time between end of filling (and packing phase) to opening of the mold. Within this time, cells can grow to an equilibrium size and structure is solidified. However, in low-pressure foam injection molding, cell growth and fixation already start by start of injection. Cooling effects occur simultaneously to injection and affect the mechanism. By entering the mold, melt temperature decreases and thus also viscosity increases. Due to the temperature difference of mold and melt, the skin layers quickly solidify and a temperature gradient in the cross section of the component results. Shrinkage effects during cooling phase also unblock new free volume, supporting further cell growth [19, 31]. Since this happens slowly, cell growth dominates instead of nucleation [19]. Cell growth stops by achieving an equilibrium of forces of gas inside the cells and resistance by melt in cell walls. This status can either occur by an increasing viscosity due to cooling or by growth of neighboring cells and is limited by the expandable volume.

5.2 Evolution of cells in low-pressure procedure

As already mentioned, cell formation is mainly defined by the given pressure and temperature conditions. The pressure during mold filling mainly defines the nucleation and cell growth process. Cells can be created if pressure is lower than the saturation pressure of the blowing agent. This pressure is inter alia a function of shear viscosity, time, position and blowing agent content. Pressure drop defines nucleation and cell growth. The resulting melt temperature, mainly affected by set melt and set mold temperature, shearing effects as well cooling conditions, define the materials' resistance in cell formation process. Besides local differences in temperatures by varying wall thicknesses or different cooling conditions, a gradient in temperature in thickness direction occurs in processing, affecting the cell formation process.

To make the conditions inside the mold and the cell formation mechanism during filling phase more transparent, commercially available flow simulation software (Moldex3D) was used. The correlations of pressure and temperature in terms of cell size and the non-homogeneity or gradient in cell size resulting in low-pressure foam injection molding should be pointed out. A rectangular plate (120 x 80 x 3 mm) with a fan gate, shown in Figure 18, was simulated (the same geometry was used for experiments shown in chapter 5.3). Injection was stopped at 85 % of filling volume (switch over point), no packing pressure was applied. A PC/N₂ - mixture (Makrolon 2405, Covestro, Germany) was chosen. It should be noted again that boundary conditions in real parts may be different from idealized simulation results; especially different part geometries can result in different cell size distributions.

Pressure vs. cell formation

Cavity pressure is one of the main influencing parameters on cell formation mechanism. Pressure is locally different and depends apart from process parameter settings on parts' geometry (flow length, thickness of flow path).

To observe the conditions inside the part and not on its surface, the results for the core or mid layer of the part - which is half the part's thickness – are displayed in the following. Figure 25 highlights the definition of this layer and the positions of three selected analysis points (sensor nodes) used in further analysis. The sensor nodes are

represent different positions in flow length: near gate (“ng”), middle of low length (“m”) and away from gate (“afg”)

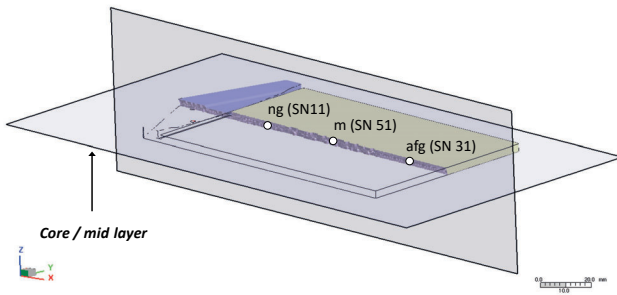


Figure 25: Definition of cutting planes and analysis points (sensornodes) - near gate (SN11), middle of flow path (SN 51) and away from gate (SN31) in the mid layer representing half of the parts thickness.

Figure 26 depicts the simulation results for pressure and cell size at different points in time. Here, also the gate is excluded to focus on the conditions inside the part. As can be seen, distribution of pressure and cell size change by time and filling rate. During injection, pressure is higher and cell size is lower near the gate. After stop of injection (*sop*), pressure decreases rapidly, and main cell growth starts. Cell growth is flow path dependent and main growth occurs in the unfilled cavity volume, starting from the flow front. Here, only pressure of air is on hand while cell growth near the gate is affected by higher pressures.

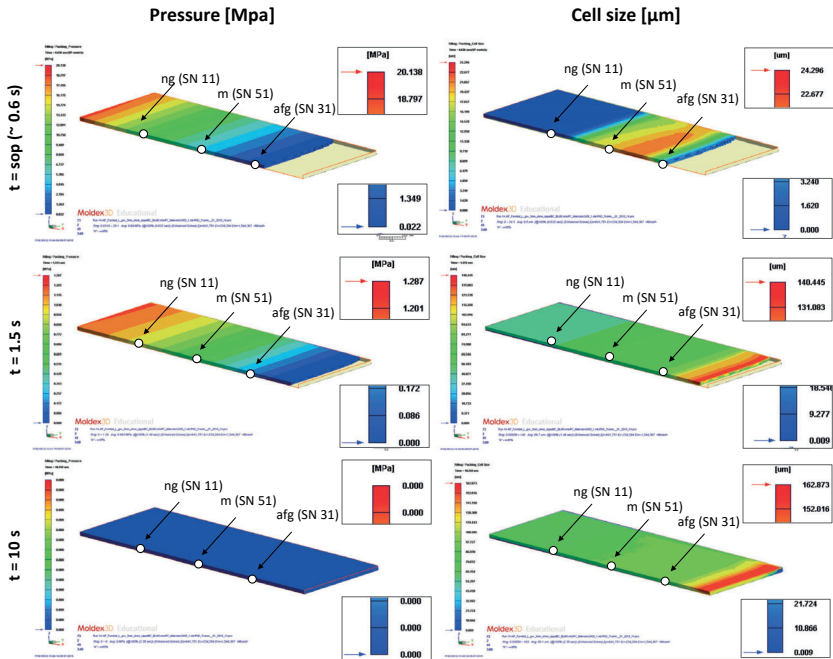


Figure 26: Simulation results for low-pressure foam injection molding; cross sectional cut through the core layer of the part - pressure (left) and cell size (right) at different points in time and highlighted positions of sensor nodes for further analysis

Figure 27 shows the simulation results for pressure and cell size of the sensor nodes highlighted in Figure 25 and Figure 26. Cavity pressure curves (red) and resulting cell sizes (blue) in the core layer of the part are displayed. Results are shown for positions near the gate “ng” (SN11), middle of flow path “m” (SN51) and away from gate “afg” (SN31), from start of injection up to a point in time where cell size reached a constant value (around 10 s). Figure 28 points out a detail of Figure 27 and highlights just the start of injection (0 s to 1.7 s). It should be noted, that there are some discontinuities in the calculation results. After stop of injection, pressure calculation is not smooth and affects the calculation of cell size. However, the general trends for evolution of cells during procedure can be shown by these simulation results.

During injection phase the pressure inside the cavity increases by an increasing filling rate. Near the gate (ng) pressure reaches a higher level compared to the middle of flow path (m). At the position evaluated away from gate (afg), for the chosen injection

volume of 85 % the pressure is nearly uninfluenced by injection and remains close to 0 MPa. Cells start to grow during injection caused by the huge pressure drop in the melt by entering the mold. Near the gate and in the middle of the flow path, cell size decreases by an increasing pressure (> 2.8 MPa) during injection. Here, from a distinct pressure (~ 11 MPa) cell size is $0 \mu\text{m}$, thus cells are forced back into solution. For the other two positions cells created during injection phase remained in the melt. Right after stop of injection, cells grow again until an equilibrium of forces (melt resistance vs. pressure inside cells) is achieved. This process is supported by a decreasing cavity temperature. Cell size attains a constant value while the structure solidifies.

⇒ Finally, a significant gradient of cell size depending on position is on hand. An increase of cell size by an increasing flow length can be observed – cell size near the gate ($74,2 \mu\text{m}$) < cell size in middle of flow path ($97,5 \mu\text{m}$) < cell size away from gate ($105,6 \mu\text{m}$).

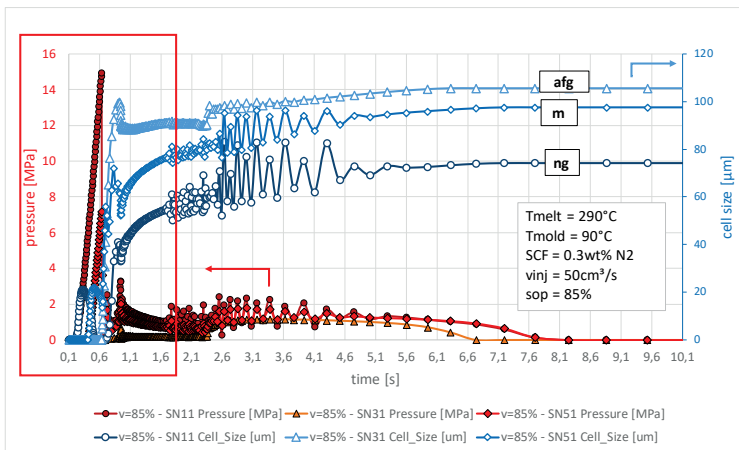


Figure 27: Simulation results for cavity pressure (red) and cell size (blue) in low-pressure foam injection molding at 3 different positions in core-layer of the part; sop = 85 % filling volume [discontinuities in calculation between ~ 1.6 s and ~ 5 s are a problem given by the simulation software used and should not be judged; instead the general trends is intended to be highlighted here]

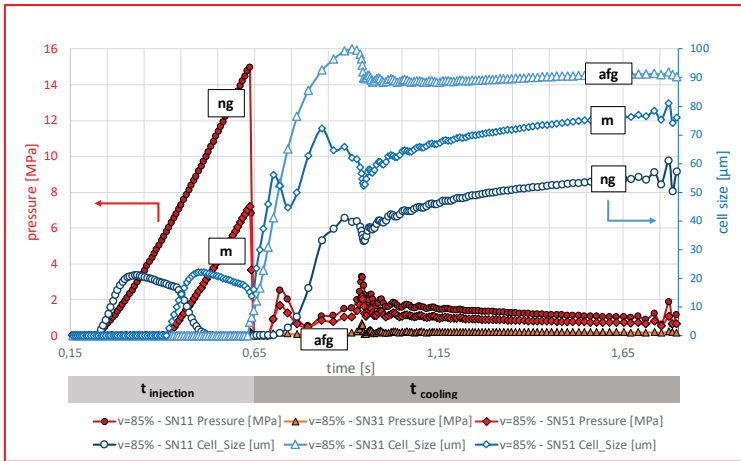


Figure 28: Detail of Figure 27 – time = 0 – 1.7 s

In literature often cell density is used as a measure for cell structure characteristics. As described in chapter 3.3 for an ideal cell structure, cell size and cell density are linked in an inverse proportional way. The higher cell density, the smaller the cells are. Simulation results for cell density are omitted here and can be found in the appendix (chapter 11.5.2).

Temperature vs. cell formation

Besides cavity pressure, temperature is also one of the main influencing parameters on cell formation mechanism. Temperature is rated here as a “*process factor*” which is mainly a consequence of melt and mold temperature. However, temperature also has a huge influence on viscosity. Due to the huge difference in temperature between mold and melt, the fact that cooling is conducted by the mold and the low thermal conductivity of polymers, a gradient in temperature is especially observed over the cross-section of the part. While Figure 26 to Figure 28 refer to the middle layer in parts’ thickness, in the following the cell formation by cross section should be discussed.

Due to the cooling of the mold, temperature decreases continuously. By a decreasing temperature, viscosity also decreases. The material solidifies by achieving the freezing temperature (here: $T_{\text{freeze}} = 170 \text{ }^{\circ}\text{C}$), preventing any more cell growth. Both

effects mentioned, solidification and equilibrium of forces lead to slow down and stop of cell growth. Figure 29 displays simulation results for three sensor nodes representing positions in the cross section of the part – skin layer “skin”, core layer “core” and intermediate layer “int. layer” from start of injection up a point in time where cell size reached a constant value (around 10 s).

For the intermediate and the core area, cell size increases continuously until slowly reaching a balanced level. Cell growth is slowed down the closer the melt temperature is to freezing temperature, but finally stops by achieving this temperature. For the cells at and close to the parts surface cell formation quickly stops due to quick solidification of melt.

⇒ The difference in temperature initiated by the cooled mold leads to a gradient in cell size over cross section.

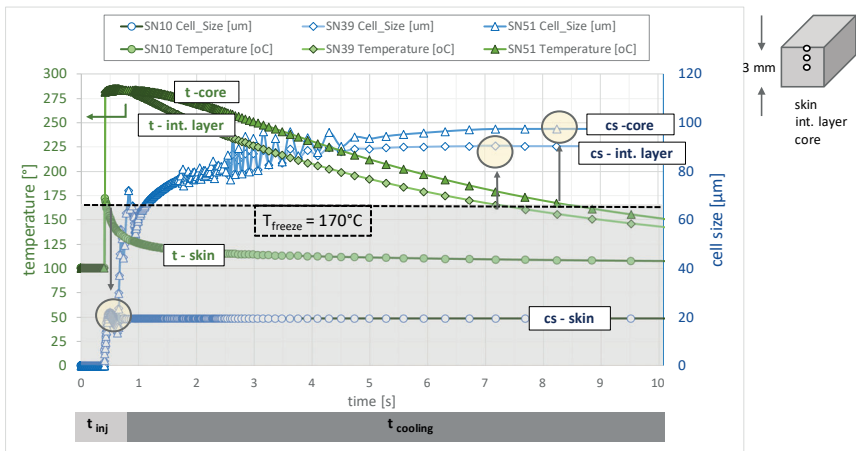


Figure 29: Simulation results for temperature (green) and cell size (blue) in low-pressure foam injection molding at three different positions over cross-section of the part: skin layer “skin”, intermediate layer “int.” and core layer “core”; sop = 85 % filling volume; T = temperature, cs = cell size

5.3 Final cell structure in low-pressure procedure

In LP-FIM the structure is often characterized by coalescence, highly deformed cells and a structural non-uniformity [83]. All these characteristics are attributed to the coupling of mold-filling and foaming [30]. Thus, boundary conditions for cell formation differ by position. The effect of the previous discussed local differences in pressure and temperature on the parts' final cell structure is discussed in this chapter.

Figure 30 depicts simulation results for the final characteristics of the structure. Final cell size and material's density (time = End Of Cooling) for the convenient simulated process is compared. As can be seen, cell characteristics and density are flow path dependent. For the region at the end of the flow path, cell size is bigger, and density is lower compared to gate or middle region. It should be noted, that density is a function of cell size and cell density. Thus, structures can exhibit same density consisting of a huge number of small cells or just a few big ones. Two main effects may lead to an in parts huge deviation of cellular characteristics in dependency of the flow path: Free foaming at flow front and local different nucleation [19].

Near the gate, a higher pressure by constant melt flow during filling results in less cell formation and a higher local density. For positions of higher pressure gradient (end of the flow path) often more silver streaks as well an increase in surface roughness is observed. Due to the pressure drop, initiated by stop of injection, the main gas expansion is initiated. However, the expansion is affected by the free volume and a gradient in structure can occur in direction to the unfilled volume. Thus, cell size is bigger, and density is lower in the core region at the end of the flow path. Besides the geometrical and cooling conditions defined by the mold, both effects depend on filling volume, filling speed and viscosity. Thus, they can be affected by process parameter definition. The influence of process parameters will be discussed in chapter 8.1.

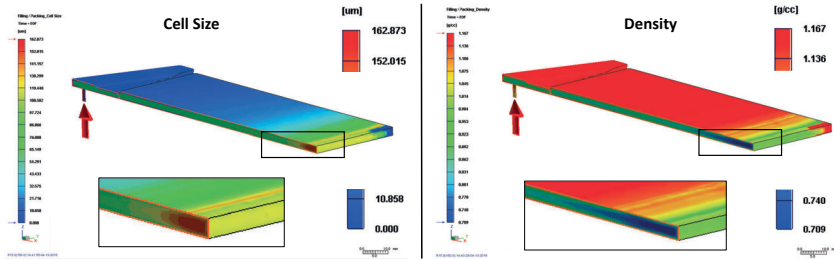


Figure 30: Final structure characteristics for low-pressure / conventional foam injection molding process ($sop = 85\%$) - left: cell size distribution, right: density distribution; time = End of Cooling

⇒ The results may be different by using another part geometry, gate situation, switch over point or different process settings. However, a structural non-uniformity is inevitable in Low-pressure foam injection molding.

In his experiments, Cramer [19] also investigated the cell size for different positions of the flow path, also using a rectangular plate filled by a central cold runner gate. He found a significant difference in structures by using two different types of polycarbonate. For the higher viscosity material (Makrolon 2405) he found the biggest cells near the gate, smaller ones in the middle of the flow path and again bigger ones away from gate. He assumed that near the gate cells started to grow due to a slow pressure drop by shrinkage during solidification phase, resulting in a growth of a few big cells (less nucleation). The different gate situation of his part geometry compared to the part used for experiments and simulation within this thesis, may be the reason for the differences in cell size (ng) in his experiments compared to the simulation results shown in Figure 27 and Figure 28. For the lower viscosity material (Makrolon 2005) he found the smallest cells away from gate while near gate and in the middle of the flow path comparable sizes (but smaller ones compared to Makrolon 2405) occurred. He assumed the in general smaller cells for this material affected by a faster supersaturation near gate during filling phase promoted by the lower materials viscosity. He assumed that high pressure drop rates away from gate at the point in time injection was stopped, lead to high nucleation rates resulting in smallest cells here [19]. These results show the complexity of interactions of process and material and underline the difficulty of general statements.

Within this thesis, in addition to the simulation of procedure, also foam injection molded samples of same part geometry were produced under comparable conditions to simulation settings. In contrast to simulation, in experiments the switch-over point, thus the amount of injected material could be reduced to a greater extent. In experiments, the switch-over point was adjusted to the minimum setting unless the parts were filled by foaming process to achieve the maximum foaming ratio. Here, switch-over point was set to 70 % while in simulation for this setting a short shot, thus an insufficient filling occurred. The parts were cut and analyzed by light-microscope (RLM) as well by μ CT. Figure 31 shows a scheme of these parts and highlights the positions for sample preparation.

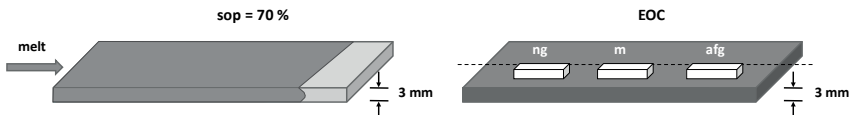


Figure 31: Scheme of low-pressure foam injection molded sample ($sop = 70\%$); sample preparation near gate (*ng*), middle of flow (*m*) and away from gate (*afg*)

Figure 32 shows microscopic pictures of three different samples (length ~ 15 mm), cut at the positions highlighted in Figure 31. Large samples in direction of melt flow were prepared in order to get a representative result for analysis. By the help of image analysis software (Adobe Photoshop) the cross section of these samples has been divided in 20 slices (height of each slice 0.15 mm) and pictures have been switched into black and white by applying a high contrast. Thus, cells remained black while the polymer matrix is white. Afterwards, the gray values of each slide over the whole sample length has been measured and correlated with the materials' density. The measurement position has been plotted over the calculated density values to achieve a density distribution over cross section of the samples. A similar approach for description of density over cross section was used in [1] and [19].

As can be seen, cellular structure changes by flow length. The structure becomes more inhomogeneous and coarse-celled by an increasing flow length. Near the gate a structure exhibiting round cells in the core area and sheared cells in the transition zone to compact skin layer is observed. A clearly separated compact skin layer is on hand. In the middle of the flow path, structure is more inhomogeneous. Big sheared cells can be seen in the core layer while smaller, sheared cells are on hand in the transition zone. A separated compact skin layer can still be seen. Away from gate, big

voids and a mixture of small and medium sized cells is observed in the core layer. Transition zone and compact skin layer are not clearly defined anymore, and small cells can also be found in the skin layer. The pronounced flow-dependent characteristic as they are often described in literature cannot adequately be observed by the light-microscopic pictures due the coalescences and non-uniformity of structure.

The overall density (including the skin layers) is slightly increasing by an increasing flow length. Near the gate, the structure shows a clear separation of compact skin layer and a sharp transition to the lower-density cellular core representing $\sim 2/3^{\text{rd}}$ of sample thickness can be observed. At the middle of the flow path and away from gate, density distribution changes and a continuous transition zone with lowest density in the center is on hand. The simulation of the procedure showed bigger cells and lower density in the core area at the end of the flow path.

⇒ The accordance to the simulation and the experimental results cannot clearly be judged due to the inhomogeneity in real structures. However, a significant change in structure and in density distribution by position is on hand.

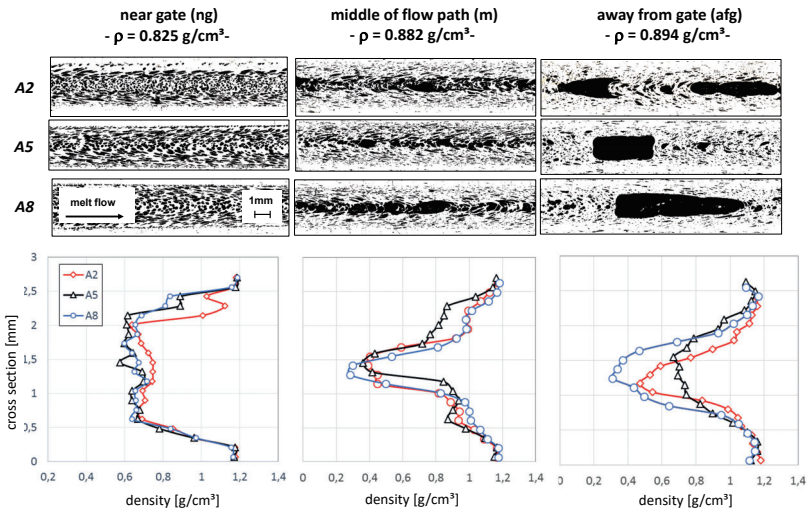


Figure 32: Cross sectional cuts of low-pressure foam injection molded samples ($sop = 70\%$) for different positions over flow path (upper) and grey-scale based density distribution (lower) [Results based on [97]]

In accordance to the depicted results, in literature also a huge variation of density in thickness [19] as well flow direction [18, 19] is described. The general observation of the structure to be flow path dependent and in parts very inhomogeneous [28, 32, 84, 131] as well to dramatically change and get coarser by increasing flow path, is already described and shown in results reported in [1, 19, 131].

To get more information on cell characteristics and shape of cells (also in direction transversal to melt flow), μ CT images of the same parts near the gate and away from gate were taken. Figure 33 shows the three-dimensional reconstruction of all cells between the compact skin layers (a) as well of a quarter-piece cut of this volume (b). In addition to the information that a coarser structure and bigger cells are on hand away from gate, a pronounced elongation of cells close to the compact skin layer can be observed. While in the core area cells exhibit a round shape, especially near the gate the cells are elongated and got fixed in this shape. In literature this effect is described to be a consequence of the frontal flow. During filling, different flow velocities over the flow channel thickness occur, leading to a stretching of the melt [19]. Cell growth is overlaid by stretching and shearing effects causing deformation of cells. The stretching effect induced by the frontal flow and higher shear rates near the skin layer results in a higher orientation. In the transient layer shearing decreases, resulting in less orientation and elongation of cells [19, 84, 135]. This aspect has already been discussed in chapter 4.2. As already mentioned, for LP-FIM, Wang et al. [28] divided the foaming process in “*foaming during filling*” and “*foaming during cooling phase*” [28]. While during filling, procedure-related orientation and deformation of cells occur, in cooling phase spherical or polygonal cells are created [28]. This is attributed to the fact that during filling, nucleation and cell growth happen under dynamic condition while in cooling phase a more static condition is on hand [84]. An orientation of cells may cause anisotropic mechanical behavior [19, 84].

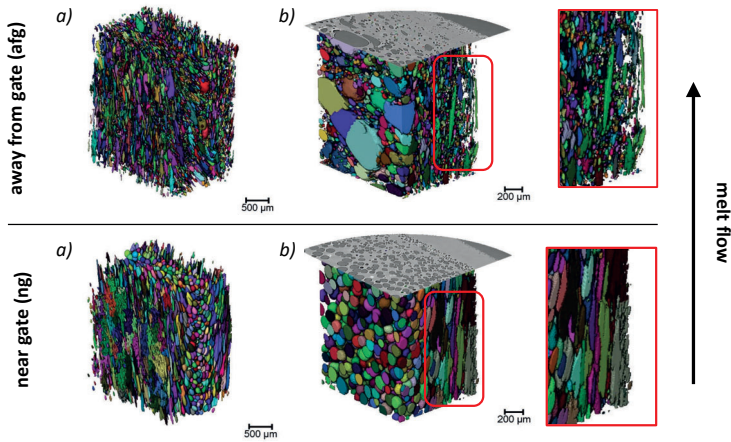


Figure 33: 3D reconstruction of cell volumes (based on [97]): a) all cells between compact skin layers, b) quarter-piece cut of a) near the gate and away from gate (sample B5)

- ⇒ The results given by the μ CT analysis demonstrate the characteristics for LP-FIM structures in an excellent way and confirm the results described in literature.
- ⇒ The differences of uniformity in dependency of flow path as well an increasing orientation of cells from core to skin could be observed.

5.4 Potential and restrictions of low-pressure procedure

As already mentioned in chapter 3.1, low-pressure / conventional foam injection molding can provide several advantages for products and processing (also see [80]). In products, especially the elimination of sink marks and reduction of warpage caused by internal pressure of cells instead of applying packing pressure as well material savings and increasing materials viscosity are the main advantages. In terms of process, the use of roughly conventional mold design and the use of less clamping forces due to low pressure should be mentioned. These points are the motivation and legitimation for most common applications.

However, as can be seen in the aforementioned remarks, cell formation in low-pressure foam injection molding is a complex phenomenon and depends on several effects. Filling and formation of cellular structure occur simultaneously. The process

cannot be controlled adequately to control structure formation as well materials and density reduction is limited. Thus, cell formation can only be controlled indirectly and in a restricted range which restricts the light-weight potential of this procedure. The following restrictions are on hand:

- **Limited density reduction:** The switch over point (sop), defining the filling volume cannot be set to every optional level. The maximum reduction is defined by geometrical conditions like thickness of flow path and processing conditions like amount of blowing agent and temperatures. If sop is set too early, the free foaming flow front will not reach the end of the flow path and short shot will occur for final part. Thus, in technical injection molding applications density reduction is typically limited to 15 – 20 % [1].
- **Geometrical restrictions:** The cell formation depends on geometrical boundary conditions. The longer the flow path, the higher the necessary filling pressure. This can eliminate cells or lead to inhomogeneous structures. Changes in wall thickness also have to be viewed critical. By changing wall thicknesses the pressure profile in flow front is influenced during filling, thus often non-uniform structures, coalescences or problems in shaping accuracy result here [44].
- **Unreliable mechanical properties:** As a result of the locally differing boundary conditions (pressure, temperature, shearing stress), often non-uniform structures occur. Besides cell size or cell density, also thickness of compact skin layer is affected. Thus, mechanical properties are affected and also change by flow length. Inhomogeneities or big coalescences may cause potential fault locations (see [1, 15, 84]).
- **Insufficient surface quality:** A general drawback of foam injection molding is the low quality of the surface finish, which often prevents its use in visible parts. Due to the pressure drop during cavity filling, cells are created at the flow front. The frontal flow causes these cells to become extended and sheared. Finally, some burst open and are transported to the cavity surface. Due to the big difference in temperature, of mold wall and melt, the burst cells rapidly freeze. This can lead to increased surface roughness and to optically visible effects, such as silver streaks or so-called tiger-stripes. Application examples from the past few years have shown that this effect can be counteracted by variotherm mold temperature control, enabling high surface qualities to be achieved [123–127]. However, for

low-pressure foam injection molding only a low level of pressure is available for reproducing the surface. Especially at the end of the flow path the pressure is often too low for appropriate surface reproduction and the effect of variotherm temperature control is limited.

6 High-pressure foam injection molding procedure with mold volume expansion

High-pressure foam injection molding itself is mentioned as the typical injection molding procedure – filling, packing, cooling phase - using melt containing blowing agent. Thus, the cavity is filled volumetrically, and packing pressure is applied. During cavity filling, foam formation occurs due to the pressure drop during injection. But, when the filling is done volumetrically, the pressure inside the mold is generally higher than the solubility pressure and the expanded gas may be re-dissolved. If this procedure is used with standard molds, the foam can expand again by the free volume given by material shrinkage during solidification. But, the typical way to use this procedure in application - and like is often guessed when talking about high-pressure foam injection molding – is to additionally use molds with expandable cavity volumes (high-pressure volume expansion foaming: HP-VE-FIM). In doing so, the cavity is filled volumetrically with melt containing blowing agent, followed by packing pressure or a pressure-less delay time. Afterwards, the cavity volume is extended. This initiates a second pressure drop which leads to cell nucleation and growth and offers the possibility to decouple filling and foaming. Generally, the foaming process takes place in the whole component and the result is a component with a compact skin layer and a foamed core area with closed cells.

In doing so, filling and foaming may be decoupled and a significantly higher ratio of foaming, a less flow path dependent and more uniform distribution of the density as well improved surface quality can be achieved in comparison to conventional foam injection molding.

Figure 34 summarizes the procedure in the same way the low-pressure procedure has been depicted (Figure 21). Procedure specific process parameters, important for cell development, are highlighted and the parameter are summarized in injection molding machine defined “*imm parameter*” and parameter defined by the mold “*mold parameter*”. Figure 35 illustrates the process sequence.

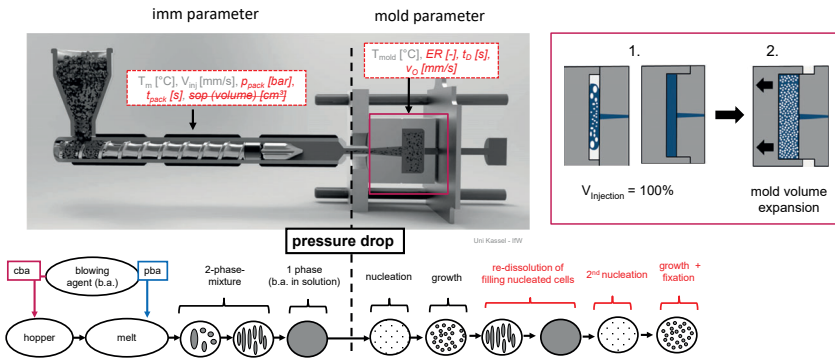


Figure 34: High-pressure foam injection molding with volume expandable molds (HP-VE-FIM) – cell formation during procedure; procedure-specific process parameter are highlighted (T_m = melt temperature, V_{inj} = injection speed, p_{pack} = packing pressure, t_{pack} = packing time, sop = switch-over point, T_{mold} = mold temperature, ER = expansion ratio; t_0 = delay time, v_0 = opening speed)

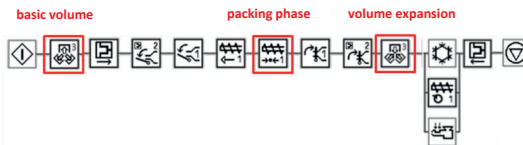


Figure 35: Process sequence for high-pressure foam injection molding with volume-expandable molds (start of cycle -> core moving out -> closing mold -> open nozzle mold -> open nozzle plasticizing unit -> injection -> packing pressure -> close nozzle plasticizing unit -> close nozzle mold -> core moving in -> cooling – parallel: dosing material and injection of gas -> opening of mold and ejection -> end of cycle)

Figure 36 shows cavity pressure curves recorded in high-pressure foam injection molding process with cavity volume expansion compared to compact molding and low-pressure foam injection molding. Here, a packing phase of 2 s was applied, followed by expansion operation executed by a moving core inside the closed mold. Due to the volumetrically mold filling, the cavity pressure increases up to a level like in compact injection molding. Switching over to packing phase and applying packing pressure keeps the pressure at a high level. Right after packing pressure is stopped, cavity pressure decreases rapidly. The expansion operation leads to a sharp pressure drop.

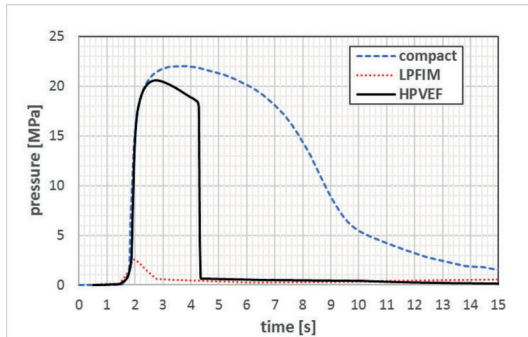


Figure 36: Experimental cavity pressure curves - comparison of high-pressure volume-expansion foaming (HP-VE-FIM) with compact molding (compact) and low-pressure foam injection molding (LP-FIM)

The general technology of expandable molds was even mentioned in a publication of H. MacMillan in 1979 [49]. The procedure was developed to improve surface quality [1, 19, 136]. Meanwhile in research, several institutes do investigations with this mold technology, however it is not widely used in industry. Due to its light weight potential, the technology was already adapted to alumina foam casting [137] and magnesium foam casting [138].

High-pressure foam injection molding with volume-expandable molds is an effective way to achieve high expansion ratios or density reductions and uniform cell structures. Another motivation is to use this procedure to increase stiffness by variation of geometry. While foaming decreases the mechanical properties, the volume expansion can lead to an increasing moment of inertia which finally can increase bending stiffness. However, the foaming mechanism are similar to batch foaming processes, thus the procedure exhibits the potential to produce bimodal, open and nanofoam structures as it is realized in batch foaming [36].

In high-pressure foam injection molding with mold volume expansion (HP-VE-FIM), The cavity volume can either be enlarged via a movable core inside the closed mold or via an opening stroke, conducted by the injection molding machine. For both variants, the same principle applies: an expansion of cavity volume leads to a controlled pressure drop resulting in nucleation and cell formation. The difference is the technological implementation and hereby also the flexibility in geometry. In this thesis the definition of procedures should be done as following:

- ***High-pressure mold opening foam injection molding (HP-MO-FIM):***

The mold volume expansion is conducted by an opening stroke of the mold due to the clamping unit of the injection molding machine. The expanded area is usually defined by the parting plane of the mold.

- ***High-pressure core-back foam injection molding (HP-CB-FIM):***

The mold remains closed during the procedure and cores inside the mold are moved. This movement is usually done by a separate drive (e.g. a hydraulic cylinder), not directly by the clamping unit of the machine. More geometrical flexibility is given, the expanded areas are not restricted to the mold parting line.

There are only some applications where this special mold technology is used at present. For application, mostly molds with shearing edges are used to clearly define the expansion volume and accurately shape the part's geometry. Chapter 6.4 and 6.5 classify the mold concepts and give a short (not complete) overview of different concepts and a short review of existing molds.

6.1 Phases of cell formation in high-pressure procedure with mold volume expansion

As it was done in chapter 5.1 for low-pressure procedure, in the following, the different process phases and their role or influence on cell formation process (sorption, diffusion, nucleation, growth and fixation) are summarized. In low-pressure foam injection molding the foam expansion or free foam phenomena is limited by flow resistance and geometrical boundary conditions. Furthermore, during filling shear flow effects are dominant which counteract the expansion mechanism [15]. For high-pressure procedure in combination with mold-volume expansion, the cell formation mechanism may be decoupled from filling, thus the procedure can be classified into five process phases, depicted in Figure 37.

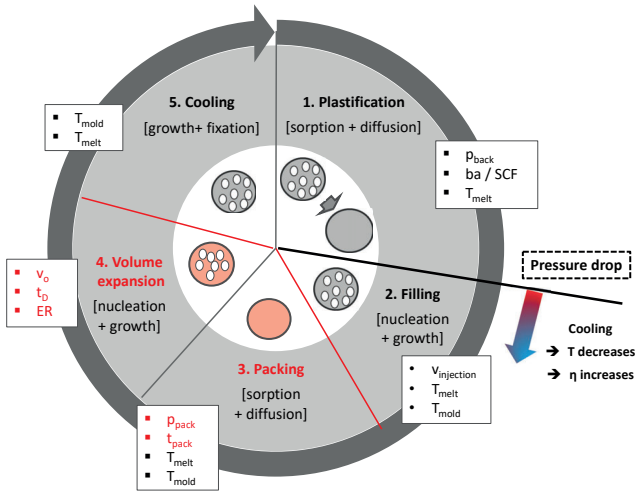


Figure 37: Cell formation mechanism in high-pressure foam injection molding with mold-volume expansion (p_{back} = back pressure, ba / SCF = blowing agent content / concentration of supercritical fluid, T_{melt} = melt temperature, $V_{injection}$ = injection speed, T_{mold} = mold temperature; p_{pack} = packing pressure t_{pack} = packing time, v_o = opening speed; t_D = delay time, ER = expansion ratio, T = temperature, η = dynamic viscosity))

1. Plasticizing

In plasticizing phase there is no difference in processing compared to low-pressure procedure. Sorption and diffusion processes are the driving forces to achieve a single-phase solution and a single-phase melt-gas mixture is provided before injection. The mechanisms happening here are not in focus of this thesis, a pressurized single-phase mixture before injection is presupposed.

2. Injection

Also, during injection the mechanisms are the same compared with low-pressure procedure. The melt-gas mixture expands by leaving the nozzle and entering the mold due to the pressure drop. Nucleation and cell growth effects take place. The gas starts to expand parallel to mold filling, while the melt flow inside the cavity shifts the flow front and thus the main pressure drop. In distinction to the low-pressure procedure, injection is not stopped early. At a filling volume of 95 – 98 % as it is usually done in compact injection molding, process control switches from the

velocity-controlled injection phase to pressure-controlled packing phase. Filling phase is mainly defined by injection speed, melt and mold temperature.

3. Packing phase

The cavity pressure increases the closer to filling is to 100 %. Packing pressure fills the mold volumetrically and ensures a high-pressure level. It is immediately applied without pressure drop; thus free foaming of melt front can only occur during injection phase. Packing phase keeps the cavity pressure at a high level. The pressure pushes the melt at the cavity surface, enabling to balance surface defects occurred by cell formation during filling as well may decrease cell size again. If sufficient packing pressure is applied for a sufficient time, gas can be forced back into solution and again a single-phase mixture inside the cavity is achieved. Thus, filling phase and cell formation can be decoupled from one another. Packing pressure level and packing time are the significant process parameters here. The level of pressure and the time needed mainly depend on the amount and type of gas in the mixture and temperature conditions. The role of packing phase is deeply discussed in chapter 8.4.

Using an active packing phase followed by mold volume expansion may decouple filling and foam formation phase. Thus, foam formation can actively be controlled.

4. Core-back operation

The mold opening or core back operation initiates an active pressure drop inside the cavity, which induces thermally instability and nucleation. The level of cavity pressure before expansion, expansion speed and expansion ratio (ratio of final volume to initial volume) affect the pressure drop rate (PDR). Both competing mechanism, nucleation and cell growth can actively be influenced by expansion speed. A higher expansion speed supports nucleation mechanism by higher pressure drop rates (PDR) while slow expansion speeds lead to less nucleation allowing more cell growth.

Simultaneous cell nucleation resulting in a more uniform cellular structure may occur since pressure drop is initiated contemporaneous within the whole part (not in dependency of the filling conditions).

This process phase has a major influence on final cell structure and may shift the mechanism of cell growth to nucleation or the other way around.

5. Cooling phase

The cooling phase is defined by the injection molding machine. For high-pressure procedure it specifies the time between end of packing phase and mold opening. As it is the same in low-pressure procedure, cooling effects occur simultaneously to injection, thus filling and packing phase and affect the cell formation mechanism. By entering the mold, melt temperature decreases and thus also viscosity starts to increase. The skin layers quickly freeze at the cooler mold wall and a temperature gradient in the cross section of the component is on hand. Core-back operation may affect the temperature conditions in the core area of the part by phase transformation (from single-phase mixture into two phases - gas and melt). In contrast to low-pressure procedure, final cell growth starts after core-back operation, thus within the machine-defined cooling phase. By achieving an equilibrium of forces inside the cells and forces of the melt, mainly defined by viscosity, thus by temperature conditions, structure solidifies. Apart from cooling time, no special process parameter in HP-VE-FIM is set here to actively influence cell formation mechanism.

6.2 Evolution of cells in high-pressure procedure with mold volume expansion

Pressure vs. cell formation

In the following, the correlations of pressure and cell size as well cell density are worked out in the same way as it was done for low-pressure procedure in chapter 5.2. The same part geometry and similar boundary conditions were used for simulation. Switch over point was set to 98 % filling volume, followed by a packing pressure of 80 / 60 MPa (linear profile) for 2 s, followed by mold volume expansion in part's thickness direction. These settings are similar to the molding experiments described later. Figure 38 shows the cavity at initial volume (Figure 38 a)) and after mold volume expansion (Figure 38 b)). Figure 39 depicts simulation results for pressure and cell size at different points in time. Here, switch over point (~ 0.7 s = 98 % filling volume), end of packing phase (~ 2.7 s) and results for 10 s after start of injection are depicted.

As it is observed for low-pressure procedure, during injection, a gradient in cavity pressure from gate to flow front can be seen, resulting in an inverse gradient in cell size. Applying packing pressure leads to an increase of cavity pressure, resulting in a high balanced level, independent of flow length. The pre-created cells (in literature also mentioned as “*gate-nucleated cells*” [30]) cannot be observed anymore at the end of packing phase. Afterwards, cavity volume expansion initiates a pressure drop, resulting in an ambient pressure level at every location inside the part. As a consequence of pressure drop, cell size increases again. Due to the fact, that the pressure drop is initiated within the whole expanded volume at the same time, numerous cells are nucleated and can grow simultaneously, resulting in a uniform, flow path independent cell structure.

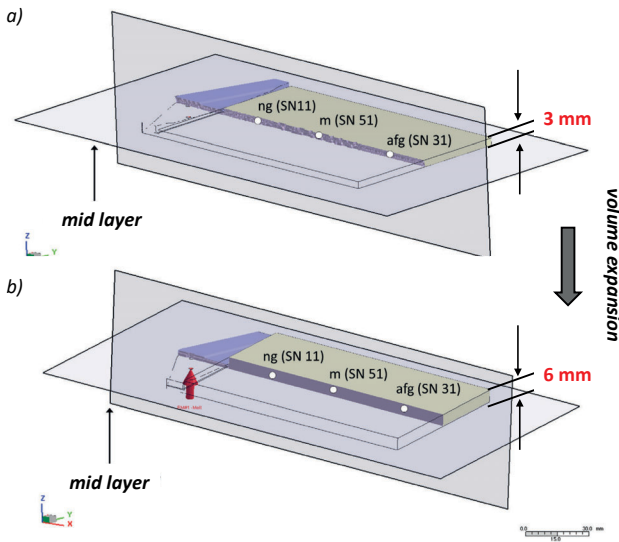


Figure 38: Definition of cutting planes and analysis points (sensornodes) - near gate (SN11), middle (SN 51) and away from gate (SN31) in the mid layer representing half of the parts thickness: a) cavity volume during filling and packing phase, b) cavity volume after volume expansion by mold opening

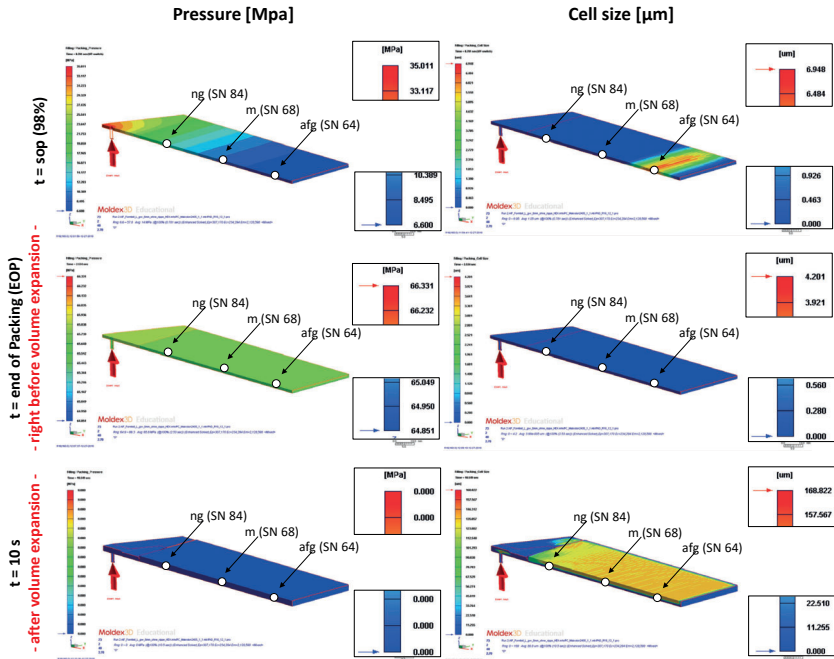


Figure 39: Simulation results for high-pressure foam injection molding with mold volume expansion (HP-VE-FIM) - cross sectional cut through the part: pressure (left) and cell size (right) at different points in time and highlighted sensor nodes for further analysis (core-layer); $p_{pack} = 2s$ @60/80 MPa

Figure 40 shows the corresponding cavity pressure curves (red) and resulting cell sizes (blue) for different positions of the part, highlighted in Figure 39 – near the gate “ng” (SN84), middle of flow path “m” (SN68) and away from gate “afg” (SN64), from start of injection up to a point in time where cell size reached a constant value (around 10 s). Figure 41 points out a detail of this figure and highlights the time from start of injection up to 1.2 s.

The cavity pressure in filling and packing phase is similar compared to compact injection molding. By increasing filling volume, cavity pressure increases. However, close to switch over point, pressure level gets equal for all positions and increases heavily by volumetrically filling and application of packing pressure. As it could be observed for low-pressure procedure, cells start growing during injection caused by the pressure drop by leaving the nozzle and entering the mold. For all positions, cell size decreases by increasing pressure during injection. Cell size drops first near gate,

followed by the middle of the flow path and away from gate. This is due to the fact that pressure increase is time-shifted for these positions. From a distinct pressure, cell size decreases and drops to $0 \mu\text{m}$ for all positions. Cell size remains at $0 \mu\text{m}$ during whole packing phase and cells grow again after core back operation. At every position, cells start to grow at the same point in time and under similar pressure conditions (0 MPa) now.

Cells grow until the given mold volume is filled, finally reaching similar cell sizes. Cells attain a constant value while the structure solidifies. Concerning the final cell density (see appendix, chapter 11.5.2), a difference by position is observable. Near the gate cell density is higher than away from gate, indicating smaller cell sizes near the gate. However, the difference is much lower compared to the low-pressure procedure and affect cell sizes in a minor way.

⇒ For high-pressure volume expansion foam injection molding, the final cell size shows a negligible flow path dependent difference, indicating a uniform cell structure within the expanded volume.

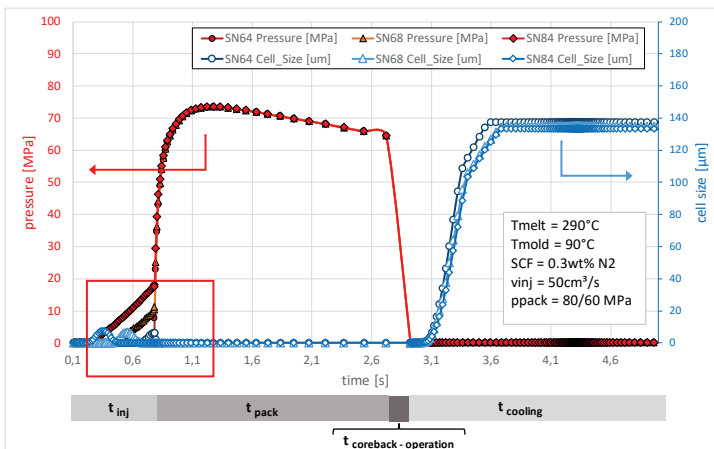


Figure 40: Simulation results for cavity pressure (red) and cell size (blue) in high-pressure foam injection molding at 3 different positions in core-layer of the part, $p_{pack} = 2 \text{ s}$ @ $60/80 \text{ MPa}$

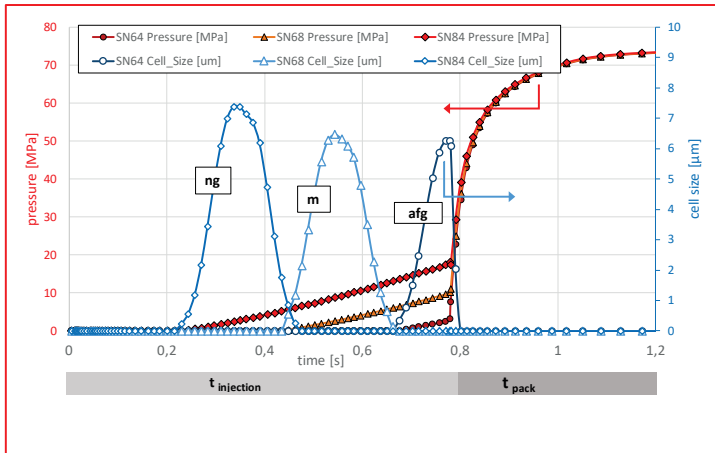


Figure 41: Detail of Figure 40 - time = 0 – 1.5 s

Temperature vs. cell size

While Figure 40 to Figure 41 referred to the core layer, in the following the cell formation in cross section should be discussed. In high-pressure procedure with volume-expandable molds, the gradient in temperature over the cross-section of the part may be different from low-pressure procedure. The delay time before mold volume expansion may lead to an increase in compact skin layer thickness. In combination with high expansion a different temperature profile with sharper transitions may occur.

Figure 42 displays simulation results for temperature and cell size of three sensor nodes representing different positions in the cross section of the part – skin layer “s”, core layer “c” and intermediate layer “im” from start of injection up a point in time where cell size and temperature reached a constant value (around 10 s). Due to the huge temperature difference of melt and mold, the skin layer freeze immediately and no cells are able to grow. The temperatures in the intermediate and the core layer are affected by the mold volume expansion. The temperature drops by volume expansion simultaneously to cell growth. In the simulation of the low-pressure procedure, cell size slowly grows until freezing temperature is achieved.

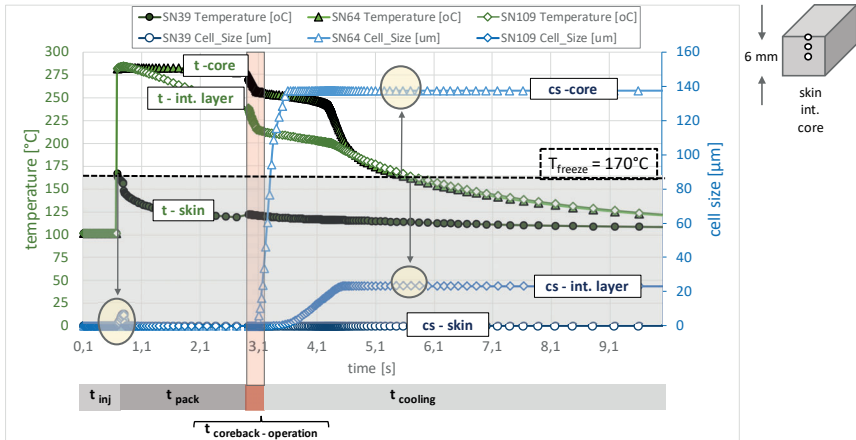


Figure 42: Simulation results for temperature (green) and cell size (blue) in high-pressure foam injection molding with mold volume expansion at 3 different positions over cross-section of the part – skin layer “skin”, intermediate layer “int.” and core layer “core”; packing time = 2 s

- ⇒ In the core layer the cell size quickly reaches a constant level. In the intermediate layer cell growth can be observed. However, for both layers, cell growth stops a long time before melt is solidified.
- ⇒ It may be concluded that the balance of cell size seems to be mainly affected by pressure drop here (a high number of cells is developed at the same time) and not by temperature conditions as it has been observed in low-pressure procedure.

6.2.1 Re-diffusion of early nucleated cells

Formation of cells depend on pressure, temperature and time. As already described, in foam injection molding, several process parameters affect these process values in a complex way. Cavity pressure is not isobar and temperature not isothermal; both are time dependent. Furthermore, the type of gas and its content play an essential role. Thus, theoretical calculated pressure and diffusion time may not lead to a correct result. Besides simulation, molds with visualization systems can help to get a better insight here and clarify which status of the polymer-gas mixture is on hand – single-phase or two-phase mixture – at given process conditions. Details on visualization experiments in foam injection molding are given in chapter 3.4.1.

The phase status of the polymer-gas mixture before cavity expansion is quite important in terms of final cell structure. A higher packing pressure and time is reported to support uniformity of cellular structure [58]. An increase of the cell radius smaller than its critical value results in a collapse and the cell's gas diffuses back into the melt [104]. If the packing conditions are insufficient to re-dissolve the gate-nucleated cells, a two phases mixture is on hand before cavity expansion, resulting in a structure characterized by two cell types: large and fine cells [58]. The large cells are attributed to the undissolved cells remaining in the mixture prior to cavity expansion while the fine cells are attributed to new cells nucleated by the pressure drop [58]. Furthermore, the presence of remaining cells in the melt reduces the available gas for nucleation [58, 59] as well increase melt compressibility [58]. The latter results in a slower pressure drop rate [58]. The final shape is also affected by the condition of the melt prior to cavity expansion. While for experiments with remaining cells elongated or spherical cells were found, in contrast for experiments with complete dissolution, spherical cells with an improved structural uniformity across samples' thickness are reported [58].

Concerning the re-diffusion processes, even in visualization experiments by Villamizar and Han [22] in 1978 the collapse of cells by applying packing pressure had been observed. The level of packing pressure defined the time until cells collapsed or could not be detected anymore. The authors observed a non-symmetrical shape before collapsing and assumed a non-symmetrical stress induced by the packing pressure [22]. Mahmoodi et al. [29] did experimental investigations as well modelling of cell dynamics in foam injection molding with focus on cell collapse phenomena under pressure (their setup could detect cells $> 400 \mu\text{m}$). By applying a full shot and packing pressure they first observed a "*growth stage*" during filling, a "*collapse stage*" during packing phase and "*re-growth stage*" after pressure release. It is assumed that collapse depends on packing pressure level and initial cell size before packing pressure phase [29].

At Kyoto University and University of Toronto several studies on mold opening and core-back process were conducted by using molds with visualization systems. In [34] for a PP/1.68wt%CO₂ mixture it was experimentally demonstrated that cells created during filling process disappeared during packing phase prior to mold volume expansion. For a CO₂-content of 1.42 %, a quick increase in pressure (without actively applying packing pressure) with a peak of $\sim 8.5 \text{ MPa}$ for a time $< 0.5 \text{ s}$ was sufficient

to disappear cells or no more cells could be observed [34]. Disappearing of cells inside the cavity was also investigated for a PP/0.5wt%N₂ mixture [35, 36]. The authors report that the cavity pressure resulting due to volumetrically mold filling was sufficient to disappear the early nucleated cells or to make them too small to observe by their visualization system [35]. Shaayegan et. al. [33] reports a presumed dissolution of cells in a PS/3wt%CO₂ mixture for a packing pressure of 24 MPa applied for 8 s.

It needs to be noted that the aforementioned values are only valid for the investigated systems and their boundary conditions, e.g. type of polymer, blowing agent, blowing agent content, temperature, mold geometry, etc. They are mentioned as an indication for successful visualization experiments in foam injection molding.

6.2.2 Pressure drop rate / Comparison with batch foaming

Batch foaming is a process where gas is dissolved in a solid polymer matrix by the help of temperature and high pressure. After saturation of gas in the polymer, either the pressure is released, or the temperature is increased to initiate thermodynamic instability and initiate the foaming process. The process is often used to investigate the foaming mechanism and foaming behavior of materials and blend systems with CO₂ or N₂. The batch foaming process is a free foaming process, expansion is typically not limited by a mold. In terms of the pressure based variant, pressure drop rate (PDR) is one of the control factors in terms of number density of cells and cell growth rate [68]. For high-pressure foam injection molding with expandable cavity volumes, many aspects of cell formation are rated to be based on similar mechanism observed in batch foaming processes. The pressure drop initiated due cavity volume expansion is similar to pressure quench in batch foaming process. The principle of foaming behavior is the same, thus knowledge of batch-foaming behavior can be used to analyze and explain cell formation in foam injection molding process [34, 36].

In core-back experiments by Ishikawa and Ohshima [35, 36] PP/N₂ and PP/CO₂ (with sorbitol gelling agent) were used and results were compared with the foaming behavior in pressure quench batch foaming process. As similarities the authors pointed out that an increasing pressure drop leads to an increasing number of cells as well a decrease in cell size and unfoamed skin layer thickness [36]. As differences they found out that a higher specificity of cell size distribution is on hand in foam

injection molding [36]. This effect is more pronounced for higher expansion ratios [36]. Furthermore, they observed a different effect by using different types of blowing agents [36]. While in their core-back experiments N_2 lead to a much finer cell structure, defined by smaller cells and a higher number of cells, in batch foaming experiments CO_2 lead to larger number and higher cell growth rates [35]. As an explanation the authors mentioned that the initial gas concentration and saturation pressures are different for both processes. In contrast to foam injection molding, in batch foaming process, pressure drop rate and gas saturation pressure cannot be set independently. The batch foaming experiments started from an equilibrium concentration of gasses at high pressure levels (11 MPa) [35]. Although, the degree of supersaturation was the same for both gasses, due to higher solubility, the initial concentration of CO_2 was much higher than the initial concentration of N_2 [35]. In foam injection molding inside the plasticizing unit no equilibrium concentration of gas is on hand. If the concentration of both gasses is the same, the saturation pressure of N_2 is higher than for CO_2 . Thus, also the resulting degree of supersaturation of N_2 during core-back operation is higher than for CO_2 , resulting in an increasing number of cells and decreasing cell size [35]. However, in their experiments, Ishikawa and Ohshima [35] showed that the classical nucleation and cell growth models valid for batch foaming can also be used to simulate the core-back process [35].

In experiments of Taki [68] (PP/ CO_2) for PDR's between 1 – 1.81 MPa/s and in experiments of Tamaro et. al. [139] (PS/ CO_2) for PDR's of 50 to 500 MPa/s, it could be shown that the amount of nucleated cells increased linear as function of PDR in a bi-logarithmic scale, independently of temperature [139]. The PDR is involved in the competition of nucleation and cell growth mechanism [139]. By an increasing PDR, nucleation is favored. The number of stable nuclei is increased and in general smaller cells occur due to the consumption of available gas diffusing into a higher amount of cells [139]. An increasing PDR also leads to a faster cell growth due to a shortening of diffusion paths by higher number of cells [139]. The effect of the gas concentration on diffusion is less important here [139].

Besides the PDR also its level plays an important role, both affect the thermodynamic instability induced in the polymer-gas solution [139]. Based on modelling of the effect of PDR on nucleation a threshold for density of nucleated cells exists of around 10 GPa/s (as reported and cross-referenced in [139]). However, Tamaro et. al. [139]

notes, that the correlation of nucleation and PDR for high pressures and the existence of a threshold are not well understood now [139]. Within his batch foaming experiments no gradient in cell size could be observed [139]. He assumed the result to be a reason of the small sample size inhibiting just a negligible temperature gradient [139]. For real polymer foaming processes a gradient in temperature exists, leading to a gradient in cell size [139].

⇒ For high-pressure foam injection molding with expandable cavity volumes, the mold technology can be used to actively shift mechanism between nucleation and cell growth. Pressure level before volume expansion and the expansion speed, defining the pressure drop rate, are the significant factors to actively influence cell formation mechanism.

6.3 Final cell structure in high-pressure procedure with mold volume expansion

Accordingly, to the previous discussed results, in the following final cell structure is shown in Figure 43. Here, cell size and material's density (time = End Of Cooling) for the convenient simulated process are compared. In contrast to low-pressure foam injection molding, cell characteristics and density just slightly differ by position. Thus, a homogeneous, not flow-path dependent cell structure with equal cell size and density distribution is achieved. The packing pressure decoupled filling and foam formation as it created, more equal starting conditions in the melt before volume expansion. Core-back operation initiates the pressure drop everywhere in the part at the same time. Consequently, simultaneous nucleation may take place everywhere in the part leading to a balanced number of cells and cell growth (for equal boundary conditions). However, it should be noted that for real processes, complex geometries or long flow paths, packing pressure may not be able to achieve balanced conditions at every point. Thus, core-back operation initiates pressure drop and simultaneous nucleation everywhere at the same time, but the starting conditions may be different. Consequently, a local difference in structure may occur in reality.

The qualitative influence of process parameters will be discussed in chapter 8.1.

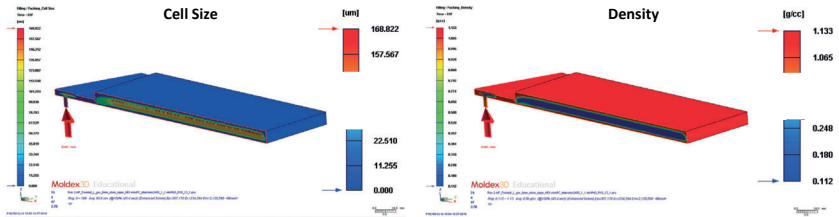


Figure 43: Simulation results for high-pressure foam injection molding with core-back - final structure characteristics: cell size distribution (left) and density distribution (right); $t = \text{End of Cooling}$

High-pressure mold-opening foam injection molded samples (HP-MO-FIM) of the same part geometry were produced under similar conditions as used in simulation. At a filling volume of 98 % procedure switched over to packing phase and a graded pressure of 80 / 60 MPa was applied for 2 s. Afterwards cavity volume was expanded by mold opening operation in direction of parts' thickness. An expansion ratio of 2 was executed by an expansion speed of 20 mm/s. The parts were cut and analyzed by light-microscope as well μCT . Figure 44 shows one of these parts and highlights the positions for sample preparation.

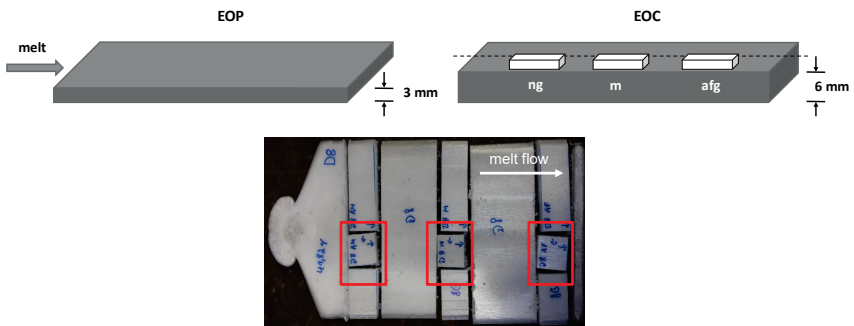


Figure 44: Scheme of high-pressure mold-opening sample preparation (upper) and picture of high-pressure mold opening molding sample (lower); sample preparation near gate (ng), middle of flow (m) and away from gate (afg); PC/N₂ (0.3 wt%), ER = 2 (lower); EOP = end of packing (before volume expansion, EOC = end of cooling

Figure 45 shows microscopic pictures of three different samples, cut at the positions highlighted in Figure 44. Preparation and analysis were done in the same way as described in chapter 5.3. The overall density (including skin layers) slightly increases by increasing flow length. However, cellular structure is quite uniform, independent

of flow path. This observation is also reported and shown in similar investigations in literature [1, 18].

- ⇒ The structure shows a clearly separated unfoamed skin layer and a sharp transition to the lower-density cellular core representing $\sim 2/3^{\text{rd}}$ of sample thickness.
- ⇒ The density of the core area is at a comparable nearly constant level, independent of flow length.
- ⇒ Homogeneity of cell size, independent of flow length and density distribution over parts thickness show a good accordance to the simulation of the procedure.

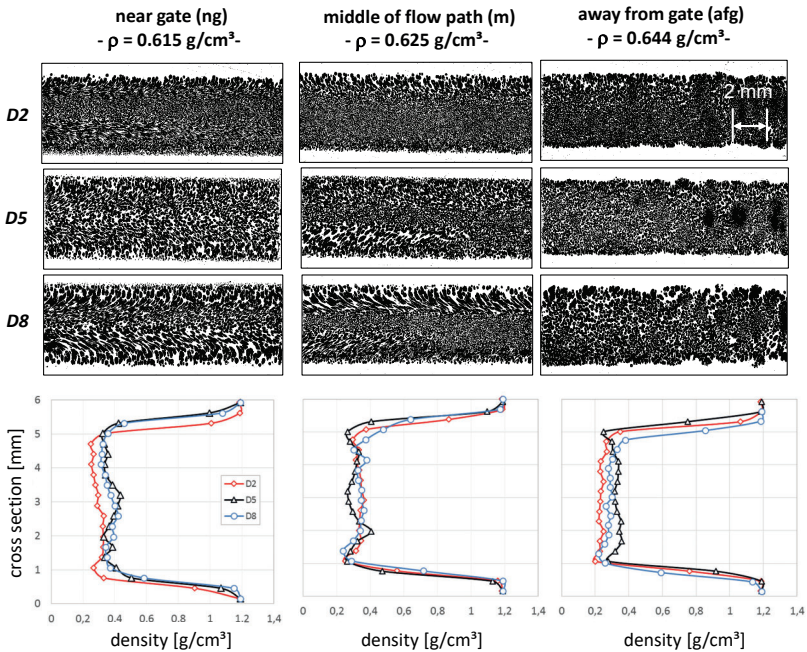


Figure 45: Cross sectional cuts of high-pressure and mold-opening foam injection molded samples for different positions over flow path (upper) and grey-scale based density distribution (lower); results based on [97]

As it was done for the low-pressure foam injection molded samples, μCT images near the gate and away from gate of the same parts as shown in Figure 45 were taken.

Figure 46 shows the three-dimensional reconstruction of all cells between the compact skin layers (a) as well of a quarter-piece cut of this volume (b). A difference in structure for both positions can also be observed for this samples.

Cell size in the center is similar near and away from gate. However, an elongation of cells or sheared cells can be seen near the gate. Close to the skin layer cells are oriented in direction of volume expansion. For the transition zone, orientation changes slightly into a flow-induced orientation as could be observed for the low-pressure procedure. The closer the cells are located to the center, the smaller and less oriented they are. Cells in the core area exhibit a round shape (planar view). Away from gate no obvious orientation is on hand. In their HP-MO-FIM experiments [84] also report little deformation of cells, however they were found to be nearly equally shaped in flow direction and perpendicular to melt flow [84]. During filling, nucleation and cell growth happen under dynamic condition [84]. LP-FIM stops here and skin-close cells exhibit a flow-induced elongation and orientation in direction of melt flow.

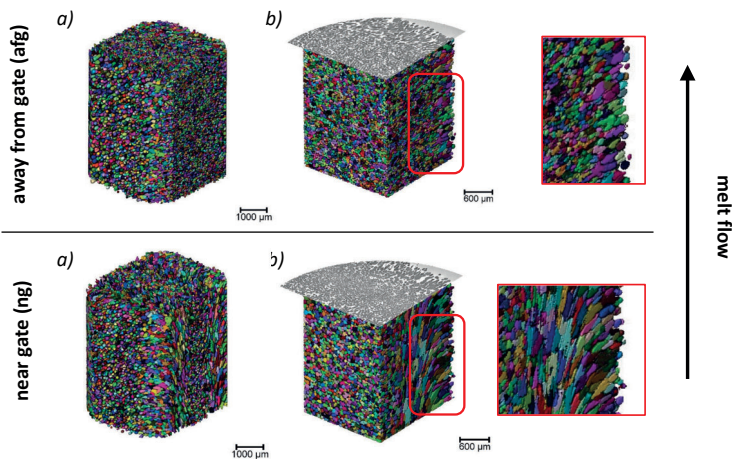


Figure 46: 3D reconstruction of cell volumes (based on [97]): a) all cells between compact skin layers, b) quarter-piece cut of a) near the gate and away from gate (sample D2)

⇒ The in general less orientation of cells in HP-VE-FIM compared to LP-FIM may be explained by the fact that cells nucleate again and grow again by a relatively static condition if re-dissolution has been occurred successfully [84].

6.4 Mold concepts for mold opening

As defined earlier, in this subchapter mold concepts are listed where additional mold volume is provided by an opening stroke of the clamping unit of the injection molding machine. For this, the injection molding machine must be equipped with a mold-opening option. Here, depending on the type of machine, parameters like opening distance, opening speed and in some cases an opening profile can be set. The expansion geometry in this concept is usually restricted to the mold parting line. As the simplest design, a conventional mold can be used which is opened to a predefined extend. Here, typically some delay time is set to prevent the melt of flowing in between the parting line after conducting the core-back expansion. This can lead to an insufficient shaping of the mold geometry at the outer faces of the product. To work against this issue and allow accurately shaped mold geometries, molds with shearing edges can be used. Here, melt cannot flow into the parting line and the expansion volume is clearly defined. This mold concept is in principle simple and easy to use, because no additional equipment is necessary. Furthermore, the options defining the expansion are still integrated within the process sequence of the injection molding machine. However, by realizing the mold volume expansion by the injection molding machine, a precise control of speed and distance is often not realizable. Opening the clamping unit to a precise defined distance within parts of a second is often not possible for standard machine control. To ensure a precise opening operation, for hydraulic machines mechanical blockings or pressure pads are available by some machine producers [44]. For electrical machines a more precise positioning is on hand by the servomotors used here [44].

In the following, some mold concepts used in research and industry are summarized. For details on construction and parts please see appendix (“ Mold concepts for mold opening”).

At the University of Toronto, a conventional mold (containing a glass-window for visualization experiments and gas-counter-pressure option) was used for experiments with mold opening, while the mold was opened to a predefined extend (see Figure 142) [33]. The mold did not exhibit vertical flash faces / shearing edges. Also, a simple mold (without visualization window) not specifically designed for foaming applications was used for mold-opening experiments in [140]. In the investigations of

[15], [34, 35, 141] and [142] molds with shearing edges were used. Thus, the expanded volume and parts' geometry is clearly defined after expansion. The mold volume expansion is also operated via the clamping unit of the injection molding machine. The mold used by Spörrer [15] is equipped with many special features like gas-counter pressure and a conformal oil cooling / heating system which also allows conducting an isothermal process. This is a unique feature which allows to control the process independently of cooling phenomena which is normally an unavoidable co-variant in injection molding procedure (see Figure 143). A special feature of the mold used in [34, 35, 141] is also a visualization window to monitor the cell formation process (see Figure 144 in the appendix).

Besides the aforementioned molds for research, also some examples of applied research and industrial application are given in [126, 142–145]. By using a mold with shearing edges, at the Fraunhofer ICT fiber-reinforced, back injection sheet sandwich panels were produced [142, 143] (see Figure 145 in the appendix). BMW invented a mold for producing foamed car dashboards for the BMW 1 and BMW 3 Series together with Kraus Maffei and named the procedure (by using a chemical blowing) “SGI – process” (see Figure 146 in the appendix) [144]. Here, a slightly opened cavity was partly filled with melt. Afterwards a compression stroke distributed the melt, followed by cavity expansion. All operations were realized by the injection molding machine. Another current application is the mass production of big planar sandwich panels (up to 2500 mm x 1500 mm x 6 to 21 mm), with density reductions of 40 – 60 % named as “VarioLine” [145]. They are produced via mold opening (mold with shearing edges) in combination with gas-counter pressure, blown by a cba. The applications here are mainly in the field of underfloor and back wall plates, doors, housings, etc. in automotive trailers, caravans and boats [145].

6.5 Mold concepts for core-back

The use of standard core-back molds is often associated with geometrical restrictions. Mold expansion is carried out in one direction, usually referred to mold opening direction. Thus, light-weight potential is restricted for geometrical complex parts [15]. In literature, an overview of first patents referring to foam injection processes as well mold technologies are given by Throne [46]. Here, also a patent including molds with movable parts, patented in 1972 by Kritsis et al. is mentioned.

In this patent a movement of cores inside the closed mold, also locally, is described: *“another object of the invention is to provide such a method in which the foaming process is readily reversible so that an object may be molded partly foamed and partly solid.”* [146] as well *“The mold assembly ... may be opened and closed by any known mechanism, such as a hydraulic cylinder which may be operable to move one of the mold members ... whereby to expand the mold cavity ... after the injection of mixture thereinto”* [146].

In the following, mold concepts with externally control of mold volume expansion – not done by the clamping unit of the injection molding machine are listed. This principle is also known to uncover undercuts or provide additional space in multi-component or gas-assisted technologies. Mostly, an additional hydraulic cylinder is mounted on the mold, enabling the providing of additional volume inside the closed mold. Typically, the core-puller system of the injection molding machine is used to provide hydraulic pressure for the cylinder. For this, the control options are not that extensive compared to mold opening options. The point in time to provide and stop pressure supply can easily be set for a distinct time in procedure. But, in regard to speed and position control, there are some limitations. Mostly, the speed can only be defined by the flow rate of the oil and the position of the core is mostly defined by mechanical blocks. If the pressure supply for the cylinder is provided by the injection molding machine, the maximum available pressure must be considered. It must be ensured that the core does not move by the melt pressure during injection and packing phase. This can be secured by choosing a sufficient size of the cylinder and the pressure supply or by an additional mechanical blocking during injection phase. As in the case of molds with shearing edges, the mold volume after expansion is clearly defined, thus a clear shape of the product can be realized - presupposed an accurate melt temperature is on hand allowing an expansion of the foam into the new volume. Depending on the construction, the expanded volume is not limited to the mold parting line, it can be conducted locally or via different cores. By the knowledge of the author, currently not realized, but also possible are special core-constructions like folding cores. The construction and the know-how by the mold maker are essential in terms of this point.

As it was done in the last subchapter, known mold concepts for core-back are described shortly in the following. For details on mold construction and produced parts please see appendix (“ Mold concepts for core-back”).

In the PhD thesis of Müller [14], two different molds were used. One mold was used to produce chemical blown samples. On top of this mold a hydraulic cylinder was mounted which moved a partly sloped plate into the mold. This plate pushed a spring-loaded surface area into the mold to provide expansion volume. The whole mold volume is expanded, producing a rectangular plate filled by a film gate. The expansion ratio can be set by changing spacers (see Figure 147 – left). A second mold was used to produce physically blown samples (see Figure 147 - right). Unfortunately, it is not clear which technology was used to expand the mold volume here.

In the PhD thesis of Flórez Sastre [1] and Cramer [19] a core-back mold in which the core was moved via a wedge element driven by an external motor has been used (see Figure 148). By this mold a simple plate with central cold runner was produced. The thickness of the part could continuously be set between 0 and 8 mm. For investigations by Kirschling [16] and Rohleder [18] a core-back mold producing a rectangular plate (see Figure 149) was used. The core movement is done via a triangle ramp driven by a hydraulic cylinder (oil supply by machine) and allows to increase the initial plate's thickness stepwise up to 4 mm by the help of mechanical blocks. Furthermore, the mold is equipped with pressure sensors near and far from gate as well valves for gas-counter pressure. It has a film gate realized as cold runner as well a hot runner option by a second gating plate.

In the field of high-pressure foam casting of aluminum, Wiehler [137] adapted the core-back technology from polymer foams processing to produce integral aluminum foams. By the help of a hydraulic cylinder a ramp was moved into and out of the mold, to move a core. A rectangular plate was casted, and the full volume of the plate was expanded (see Figure 150).

A current approach to use the lightweight potential of core-back procedure is reported in [147]. Here, sandwich panels are produced by overmolding of glass-fiber reinforced PP sheets, followed by core-back foaming.

7 Local core-back procedure

According to the definition of this thesis (see chapter 6), in core-back technology, inside the closed mold cores are moved to expand the cavity volume. The expanded area and the expansion direction are defined by the core geometry. For most examples given in chapter 6.5, the whole cavity volume is expanded in thickness direction. In the conclusion of his PhD thesis, Spörrer [15] mentions, that geometrical freedom for mold opening or core-back parts is restricted and volume expansion is only realized in direction of mold opening [15]. Thus, mainly plane parts and no complex parts are manufactured by this procedure and the light-weight potential of highly-expanded integral foams cannot be exploit completely in geometrical complex parts [15]. However, the core-back procedure can also be restricted to partitions of the cavity. This may be realized by moving cores to locally expand cavity volume, like it is done in multi-component technologies to provide additional space for a second component. In the following, this process variation is named as local core-back procedure.

The special procedure of local core-back was firstly scientifically investigated and published by the Institute of Materials Engineering – Polymer Technology at the University of Kassel: [41, 96, 111, 129, 130, 148–152]. Here, the procedure was also named as *“pull and foam”* process. This procedure skips the aforementioned restrictions of mold opening or standard core-back procedure. The freedom of design for foam injection molded parts is significantly extended and parts with locally tailored properties may be manufactured.

Within this thesis, two local core-back molds have been used for experiments and simulation. With an existing mold, essential experiments have been conducted. Based on the findings by using this mold, an improved mold has been designed, built and brought into service. Thus, the results shown in the next chapters refer to both molds and part geometries.

Figure 47 describes the procedure based on the part geometry molded with the first simple mold concept (more details on the mold are given in chapter 7.1.1). The procedure is basically the same as it is used in standard core-back or mold opening. Melt, containing blowing agent, is volumetrically injected into the cavity, followed by a short packing phase. But, in difference, only selected areas within the cavity are

expanded. Thus, the cavity volume is only expanded locally, and the foam mainly expands in these areas. Typically, additional melt volume is supplied here prior to expansion to provide sufficient melt for foam formation. By this procedure, various formations and movement directions of cores can be realized. As a result, parts with locally foamed structures can be manufactured while adjacent areas may remain compact or less foamed.

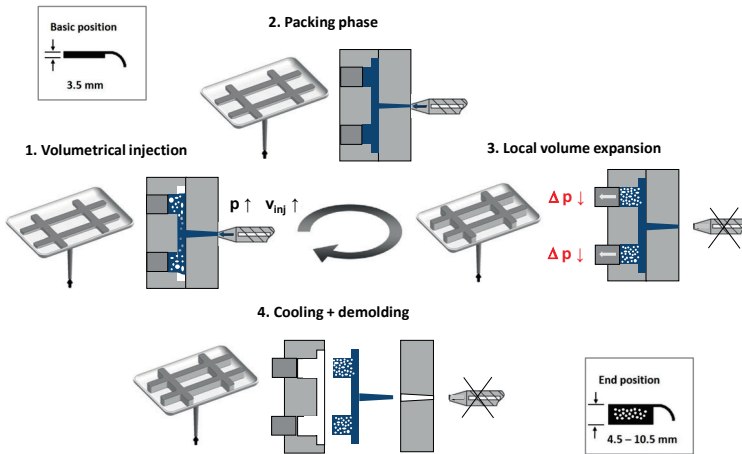


Figure 47: Local core-back procedure depicted by the first (already existing) core-back mold (results also published in [41])

By using this procedure, the geometrical and thermal boundary conditions play an essential role in context to the local foam structure in the parts. They define the amount of material which is on hand when the core-back operation is done, thus the local cell formation, local morphology and local density. Figure 48 shows prototype parts, manufactured with different materials and types of blowing agents. Depending on local temperature conditions and blowing agent pressure, foam formation may be restricted to the expanded areas (Figure 48 a) if the adjacent non-expanded areas are already frozen or cooled down to point where the resistance of melt higher than the pressure of the blowing agent. Otherwise, the local pressure drop also affects the non-solidified melt volume next to the expanded areas and cell formation and growth can also occur here (Figure 48 b)).

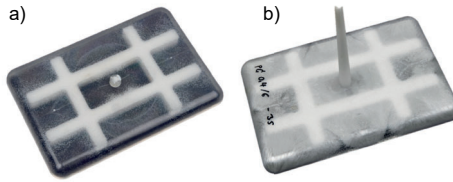


Figure 48: Prototype parts with locally foamed sections; a) PS/cba – foam formation is restricted to the expanded area, b) PC/pba – foaming also occurred in the non-expanded areas

Figure 49 show simulation results for cell formation at different points in time during procedure, allowing a qualitative insight into cell formation. As already discussed in chapter 5.2 and shown for standard core-back or mold-opening in chapter 6.2, during injection cells are created at the shifting flow front. Packing pressure forces the cells back into solution, thus no more cells are on hand before core-back operation. The local volume expansion (for expanded volumes typically more melt is provided for basic position) leads to local cell formation in the expanded areas. In the adjacent non-expanded areas, no cells are observable for the final structure due to the fact that melt is already frozen here at the point in time the expansion is initiated.

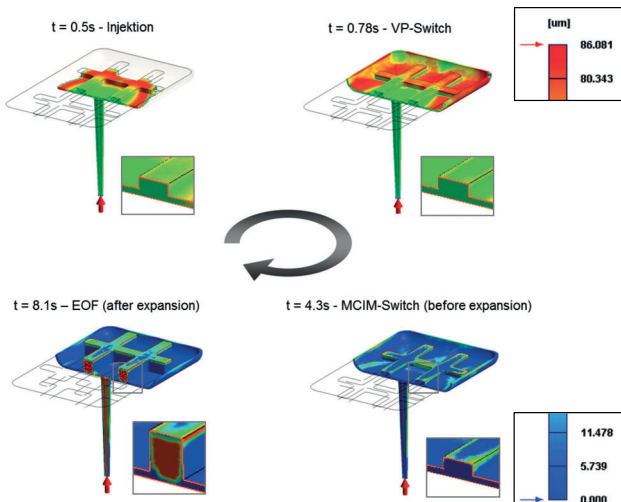


Figure 49: Simulation result for cell size at different points in procedure - timesteps: during injection phase (0.5 s) / switch over point (0.78 s) / before local core-back operation (4.3 s) / and after local core-back operation (8.1 s); material = PP/N₂ ($\rho = 0.905 \text{ g/cm}^3$)

Figure 50 depicts the resulting density. As an inverse result to the cell formation, density is low at the shifting flow front during filling. The increase in packing pressure increases the density to a barely balanced level before volume expansion. As a consequence of cell formation, after core-back operation, density is low in the expanded areas while in the non-expanded areas density is close to the density of the compact material.

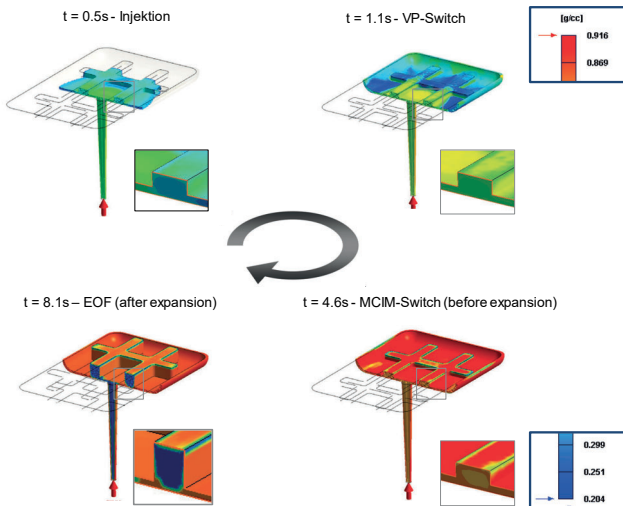


Figure 50: Simulation result for density at different points in procedure - timesteps: during injection phase (0.5 s) / switch over point (0.78 s) / before local core-back operation (4.3 s) / and after local core-back operation (8.1 s); material = PP/N₂ ($\rho = 0.905 \text{ g/cm}^3$)

Figure 51 depicts pressure and cell size development according to this simulation for two sensor nodes, one located in the expanded area “A” and one in the non-expanded area “B”. During injection phase pressure increases, especially at the end of filling when switched over to packing phase. A short packing pressure followed a short delay time without additional packing pressure was applied. Afterwards, core-back operation was done and the pressure for both locations decreased rapidly. Regarding the cell size, for both locations a cell formation during injection can be seen because of the high pressure drop by entering the mold. When the injection pressure reaches $\sim 10 \text{ MPa}$, cell size decreases sharply, and the cells are re-dissolved by the high-pressure until mold volume expansion is done. The pressure-drop leads to a second cell-growth in the highly expanded area “A”. No more cell growth can be seen for the

7.1.1 First simple mold

In the first simple mold core-movement is conducted via a triangle ramp driven by the hydraulic cylinder on top of the mold. Here, only a part of the cavity volume is moved. The part is 120 x 80 mm and has a basic wall thickness of 1.5 mm, the expanded cross-ribbed section (8 mm width) located at the back / ejection side of the part can continuously set from 0 mm to 10 mm. Basic and end position are blocked via distortion-locked screws. This mold was built to show the general feasibility of the local core-back procedure.

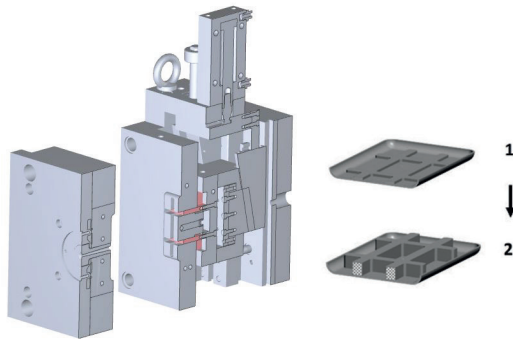


Figure 52: Existing first simple core-back mold with local mold volume expansion (Institute of materials engineering University of Kassel); movable insert highlighted in red

7.1.2 Improved mold

The existing core-back mold used by Kirschling [16] and Rohleder [18] as well the first simple local core-back mold at the Institute of Materials Engineering, University of Kassel (see chapter 6.5 and 7.1.1) have some conceptual and constructive restrictions which do not allow a precise variation of the core-back parameter or just allow a variation in a restricted manner. The core-back operation of both molds is done by the core-pulling program of injection molding machine. This does not allow a precise control of expansion speed, only by adjusting the flow rate of oil. The basic and end position of the core-back mold used in [16] and [18] (rectangular plate) can only be set stepwise by mechanical blocks up to a max. expansion ratio of 2 (200%). For the first local core-back mold these positions can be set continuously, but the

position may shift by time because the fixation of position by distortion-locked screws is self-releasing by time. Furthermore, for both molds, the volume expansion cannot be done by applying high packing pressures or high temperatures. For these conditions the ramp sticks and the core doesn't move anymore. Also, if high pressure is applied, a positional shift of the core could be seen for some cases because the cylinders are too small to handle the high pressures. Some of these restrictions also apply for similar molds, shown in chapter 6. Especially a precise and wide range setting of opening speed, thus, an active control on pressure drop cannot be done in most cases.

Within this thesis a new powerful core-back mold was designed, built and brought into service to counteract the mentioned restrictions and allow a precise control of the core-back parameter. The cavity volume expansion is conducted and controlled via an external device. It is set independently from injection molding machine, thus, totally freedom of core movement is given. This enables a precise control of core-back operation to actively influence mechanism in cell formation process. The key features of the mold are:

- An externally controllable hydraulic cylinder, enabling a precise definition of speed, pressure and movement profile. The cylinder is driven by an electrohydraulic valve, supplied by the oil reservoir of the injection molding machine. It is equipped with pressure sensors and a positioning system. The signals are processed by an electrohydraulic control unit (Compax3F, Parker Hannifin GmbH, Germany). Several positions and speeds can be set to define a movement profile. These parameters, as well the basic and final position of the cylinder can be changed continuously shot by shot. The maximum core-back distance is 28 mm. The movement can be done in both directions (compression or expansion), switched over by position or pressure. To synchronize this externally device with the injection molding cycle, 24 V signals of the injection molding machine are used.
- A hot runner system with two injection points allows to fill the mold lengthwise or transverse realized by a film gate. To switch the injection point, just the front / sprue plate needs to be changed.
- A changeable core-back insert allows using different core-back geometries by changing the insert plates mounted on the cylinder. The part design was chosen to be flexible and realize different width to height ratios to correlate geometry and

expansion ratios. The original insert molds a rectangular plate with the dimensions 120 x 80 mm. The core-back geometry molds 4 rectangular ribs of different widths (4/ 6/ 8/ 10 mm). The basic wall thickness of this part can be set between 0.7 and 3.0 mm by simply changing mechanical spacers. The height of the ribs is continuously adjustable from 0 to 28 mm.

- A variotherm mold temperature control via rapid heating ceramic inserts is implemented to achieve high surface qualities. Two independently controllable ceramic elements with a conformal cooling are built as a thermally insulated mold insert (built by gwk GmbH, Germany). The temperature is controlled by an external control device, also synchronized with the injection molding cycle by using 24 V signals. However, the effect of variotherm process control is not in focus of this thesis. Exemplarily results are shown in the appendix (see chapter 11.9).

Figure 53 depicts the key features of the improved local core-back mold and details on the part geometry molded by the standard core-back insert.

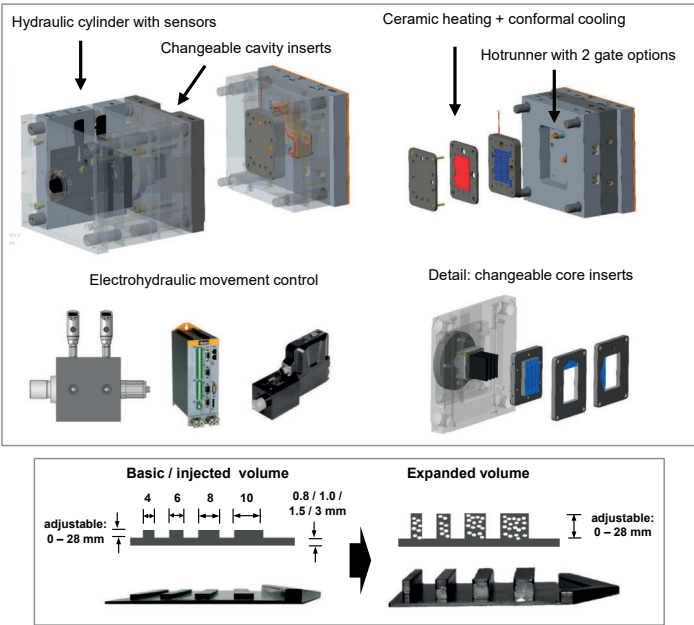


Figure 53: Construction details and key features of new core-back mold (upper) and geometrical details on part design (lower)

The variotherm mold temperature control and the core-back operation are operated independently from injection molding machine. The implementation of these components as well the synchronization with the injection molding cycle no adequate machine interfaces (e.g. “Varan” or bus systems) have been available. Thus, finally synchronization with the injection molding sequence is realized via 24 V signals defined in the process sequence, depicted in Figure 54.

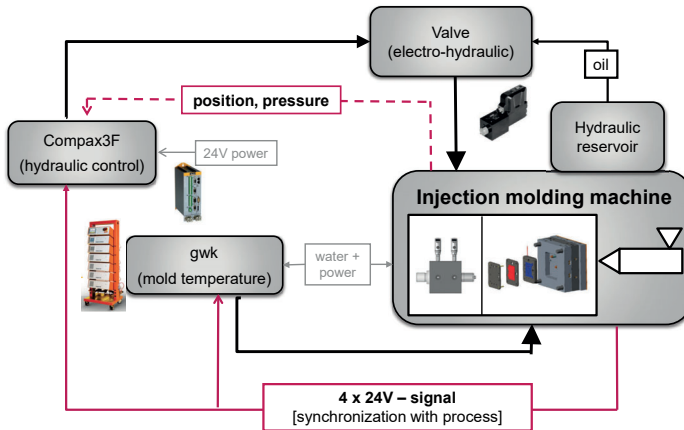


Figure 54: Synchronization of injection molding machine and external control units for variotherm process control and core-back operation

The variotherm insert is controlled by an external temperature control unit (gwk). Heating up the cavity is started by closing an electrical contact at the beginning of each cycle. To make sure that the set temperature is achieved, closing of the mold is delayed. After packing phase, the electrical contact is opened, and the external temperature control unit switches to mold cooling.

The core-back operation is controlled via a system consisting of a hydraulic control unit (Compax3F), an electro-hydraulic valve and a 2-way hydraulic cylinder equipped with a position and pressure sensors. The point of origin, the start and end positions, as well the movement profile of the cylinder or the core is edited by a special software and uploaded into the hydraulic control unit. It is operated by switch signals of the injection molding machine, receives pressure and position signals from the hydraulic cylinder and sends signals to the valve which controls the oil flow to set the cylinders' position.

Several switch signals are used to synchronize the variotherm control unit as well the hydraulic control unit with the process sequence. The modified process sequence is shown in Figure 55. As can be seen, at the beginning of each cycle, hydraulic pressure is applied, followed by several switch-signals to let the cylinder move to its basic position. Afterwards, the injection process is started (opening of nozzles, injection, packing pressure, closing of nozzles). The cavity volume expansion is set via switch signals to operate the hydraulic cylinder and make it move its pre-programmed profile. Alternatively, here also mold opening, set by the injection molding machine can be used to expand the whole cavity volume. After cooling and opening of the mold, the part is ejected by the help of the hydraulic cylinder, also controlled via switch signals.

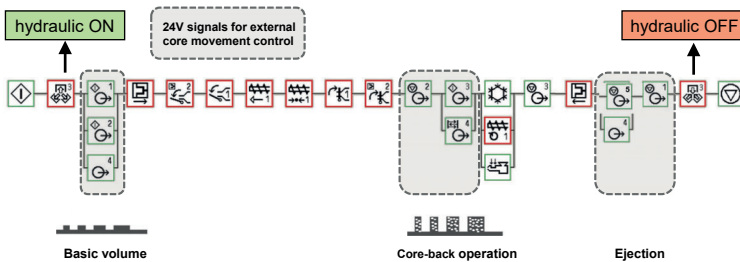


Figure 55: Process sequence including the external core movement control (hydraulic cylinder movement), synchronized with the injection molding cycle

To monitor pressure conditions during procedure, a pressure sensor is implemented in the moving core area, located in the 10 mm rib.

More details on the mold, the rapid heat cooling (variotherm) insert and the core movement control are given in the appendix (see chapters 11.8 and 11.9).

7.2 Density distribution

This chapter focusses on the formation of density in local core-back technology. Since the geometrical boundary conditions of the expanded areas change during cavity enlargement, the surface to volume ratio may locally change significantly during procedure, affecting the local cell formation and local density. This point is negligible in conventional mold opening where the whole cavity volume is expanded, and the

surface area just changes slightly. Here, cell formation is induced for larger areas and density reduction occurs within the whole part.

As already mentioned, the core-back operation mainly affects the expanded volume area. However, depending on the process parameter settings, geometry and temperature conditions, adjacent areas may also be affected, and cell formation and density reduction may occur here. The local melt temperature at the point in time the core-back operation is done defines the amount of melting core available to take part in cell formation.

It became evident that for the first as well the improved local core-back mold parts with local foamed sections and adjacent compact areas could be produced. The key factors here are packing pressure, blowing agent power and the remaining melting core at the moment the cavity expansion is executed. The experimental results confirm the simulation results for this procedure shown in Figure 49 to Figure 51.

Parts produced by the first local core-back mold

To quantify the effect of local cell formation, density measurements were taken by using the Archimedes principle according to DIN EN 1183. Figure 56 shows a prototype part, produced with the first simple core-back mold. The expansion ratio in the volume-expanded area “A” can directly set by the core movement distance. For the adjacent non-expanded area “B”, cell formation cannot be influenced directly.

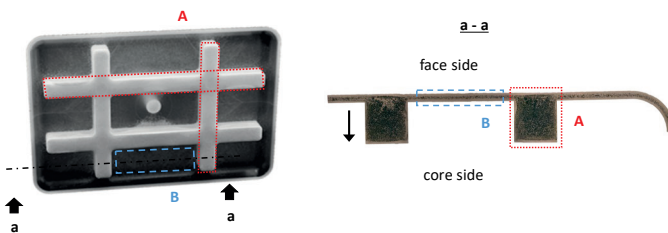


Figure 56: Prototype part produced by local core-back procedure (PS/cba) - demarcation of investigated areas for density measurements; volume-expanded area “A” and non-expanded area “B” (results also published in [148])

Figure 57 shows a scatterplot of the relative density, which is density of the foamed material related to the density of the unfoamed compact material ($\rho_{\text{foam}} / \rho_{\text{solid}}$) plotted over expansion ratio (final position foamed rib / basic position compact rib) for a PC-ABS blend. The mean values of each parameter setting are connected by regression lines. The parts were produced by different process settings (variation of SCF-content and delay time).

As expected, an increasing expansion ratio results in a decrease in density within the expanded area (A). For the maximum expansion ratio (here: 2.71), a density reduction of approximately 50 % results for this material. However, the density in the non-expanded areas (B) is also affected. An increasing expansion ratio in the expanded area (A) correlates with a decreasing density in the non-expanded area (B). The fact that cells are also created here, leads to the conclusion that still a melting core exists at the point in time the volume expansion is executed, thus the pressure drop can also take effect in these areas. The density reduction for maximum expansion ratio in the non-expanded area (B) are approx. 20 – 30 %. Due to this effect, the density in the expanded areas (A) does not decrease linear with the expansion ratio as it would be the case by expanding the whole cavity volume. A higher density in the non-expanded area (B) leads to a lower density in the expanded area (A). This effect can actively be influenced by the delay time. The longer the delay time, the less melting core before volume expansion is available in the thin-walled area (B) and a higher density reduction is on hand in the expanded area (A). This effect can clearly be observed, although the variation of delay time was just 1 s (due to the restricted process window by this mold). The effect increases in correlation with an increasing expansion ratio. The effect of blowing agent content is negligible here. For more results please refer to [152] and [148].

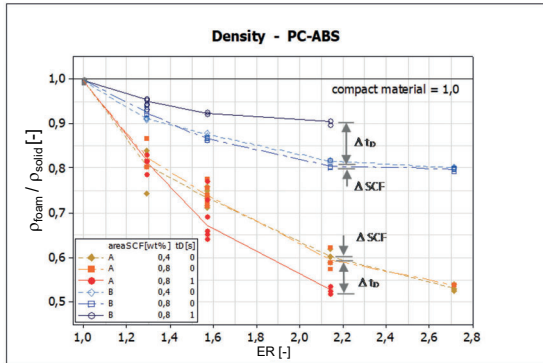


Figure 57: Density for volume-expanded area "A" and non-expanded area "B" for different process settings (SCF = supercritical fluid content, t_D = delay time, ER = expansion ratio); material = PC-ABS/N₂ (results also published in [148])

To get a deeper insight in boundary conditions inside the mold during procedure, two pressure sensors were implemented in the cavity. One is located in the moving core (A), the other one in the non-expanded area (B). Cavity pressure was recorded simultaneously for both areas (see Figure 58). It became evident, that the pressure drop is not restricted to the expanded area (A). Pressure drops simultaneously in both areas by volume expansion. Thus, pressure drop is equal for both positions and does not contribute to the differences observed for cell or density formation.

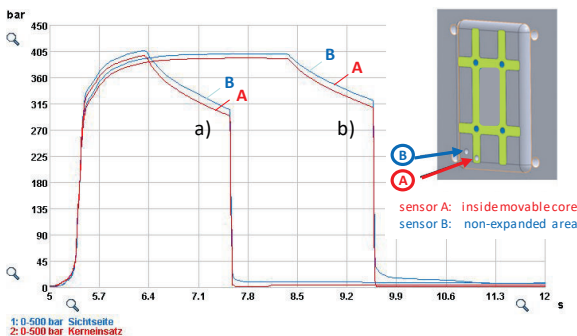


Figure 58: Screenshot of recorded cavity pressure for two different process settings at different locations; A = sensor located in the moving core, B = sensor located in the non-expanded area (results also published in [41])

Parts produced by the improved local core-back mold

For the parts produced by the improved mold no extensive density measurements were taken. Depending on the process settings (longer delay times by applying packing pressure), also a clear separation of foamed and adjacent non-foamed areas could be achieved (see Figure 59).

For accurately shaped parts, density reductions around 50 % could be attained. Although, some coalescences or holes could be observed in the microstructure (Figure 60). Also, parts with an expansion ratio up to 12 (see chapter 7.4) could successfully be molded. Here, density reductions up to 70 % for the 10 mm width rib section have been measured; however, the narrow ribs were molded incompletely. Pictures of these parts are shown in chapter 7.4.

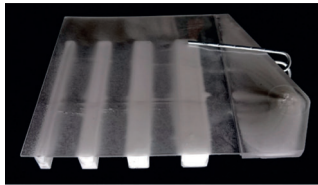


Figure 59: Local core-back parts produced with the new core-back mold: PC/N₂ with clear separation of foamed and non-foamed areas

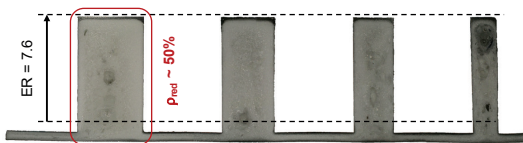


Figure 60: Cross-sectional cut of a PA6-GF30/0.5wt%N₂ part produced with an expansion ratio of 7.6 (basic thickness of plate = 1.5 mm)

7.3 Focusing temperature conditions

Injection molding is a non-isothermal process. Once the melt entered the mold and got into contact with the mold wall, the cooling process starts and melt temperature must be rated as a co-variant for all parameters affecting the cycle time. The melt temperature inside the mold can only be influenced indirectly. It is mainly defined by

melt and mold temperature as well the wall thickness of the part. Due to wall thickness variations and non-uniformity of mold cooling, temperature differs locally in processing. As already mentioned, the temperature is very important to the structure formation. For amorphous materials, the temperature difference of melt to glass transition temperature ($T_{\text{melt}} - T_G$) and for semi-crystalline materials the difference of melt to crystallization temperature ($T_{\text{melt}} - T_C$) defies the time to solidification, thus affects cell growth dynamics and stabilization effects [42].

In injection molding process, the melt cools from the outside to the core by the cooler mold wall and the active cooling of the mold. Due to the low thermal conductivity of polymer melts, cooling time approximately increases to the power of 2 by its wall thickness. To highlight the influence of wall thickness, Figure 61 show the temperature distribution over parts' cross section for two different wall thicknesses (1 mm and 3 mm) at different points in time. The results are based on simulation of a compact molded part (based on part design and cooling design of improved prototype part). The depicted times refer to the start of injection. As can be seen, for the 1 mm thick part melt freezes quickly while for a time ~ 2 s no more melting core is on hand, while for the 3 mm thick part even for a time of 10 s still molten material in the core area existent.

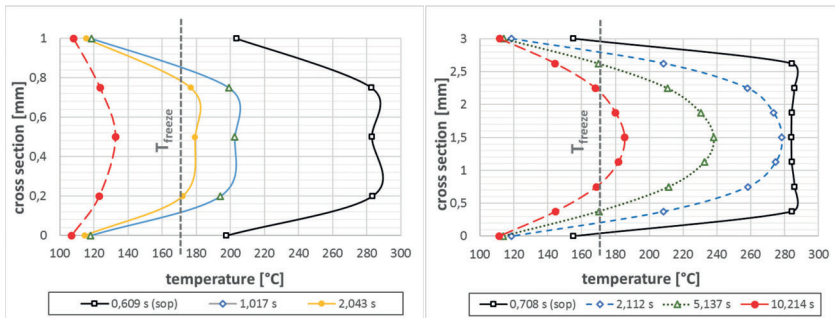


Figure 61: Simulation of temperature profiles in dependency of time (compact molding); cross-section of a 1 mm thick part (left) and cross-section of a 3 mm thick part (right); material = PC, $T_{\text{melt}} = 280^\circ\text{C}$, $T_{\text{mold}} = 90^\circ\text{C}$, $T_{\text{freeze}} = 170^\circ\text{C}$

Core-back procedure

To control cell nucleation and growth, the knowledge of temperature conditions inside the mold are of high importance in mold-opening technology [153].

For the expanded areas usually a reservoir of melt is supplied to enable cell formation here (basic volume). In the non-expanded areas, usually less amount of melting core is on hand and the molten volume available for cell formation is limited here. The volume of melting core and the temperature of the melt at the point in time the volume expansion is initiated, define the boundary conditions for the foam formation process. The temperature affects solidification and foamability, respectively the maximum expansion ratio, the structural parameters, as well the homogeneity of the structure. The temperature, as a function of time, is in core-back procedure additionally affected by process parameters like delay time, packing time and expansion speed. These parameters extend the cooling and solidification of melt. This aspect has to be considered by designing or using core-back molds, especially when small volume areas should be expanded.

A high temperature gradient may lead to delamination of the core due to the reason that the core layer exhibits the lowest viscosity while the outer layers are already frozen. This aspect is discussed in the investigations of [15]. Here, a special core-back mold was designed allowing to conduct an isothermal process at high mold temperatures. Thus, it was possible to highly foam thin-walled parts without delamination effects (delamination is normally caused by the temperature gradient in cross section). Before core-back operation, here a delay time was set to balance the temperature for the whole part [15].

Local core-back

Some details and consequences in context with temperature boundary conditions in local core-back have already been discussed in chapter 7. In terms of the special core-back mold, described in chapter 7.1.2, partially foamed components with different wall thicknesses are produced. Figure 62 highlights the geometrical boundary conditions. As can be seen, for this part geometry, expansion volume is defined by a fixed width of the rib sections as well an adjustable basic height. Thus, the ratio of expansion volume to (cooled) surface differs by each rib. As a consequence, the

temperature conditions inside the mold differ locally and are not easy to predict without software tools.

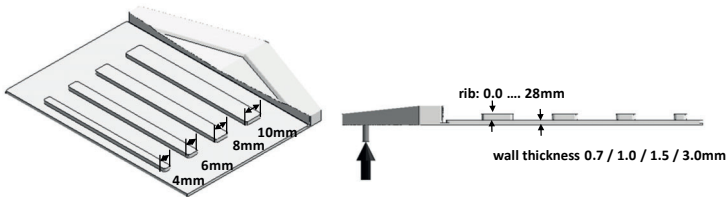


Figure 62: Geometrical boundary conditions of the improved local core-back part

Simulation software is an established tool to predict temperature conditions in injection molding procedure. In terms of foam injection molding it was used in the PhD thesis of Cramer [19] and Spörrer [15] to predict the temperature conditions in the compact material (simulation of foam injection molding was not available at this time).

In the following, here also simulation software is used to describe the local melt temperature conditions before core-back operation qualitatively. For this example, a PC-ABS blend with a melting temperature of 290 °C and a constant mold temperature of 90 °C, according to the injection molding experiments (shown in chapter 8.3.2) was used for simulation. An indicator to predict foamability and achievable expansion ratio by the given expansion volumes may be the result “*melting core*”. It visualizes the molten volume available to attend at the cell formation process. Simulation software may help to analyze the resulting amount for different times.

By the help of image editing software, the simulation results were analyzed, and the amount of melting core was measured. Figure 63 describes the decrease of the melting core over time and highlights the amount of melting core in total as well details for the 2 mm and for the 8 mm rib (cross sectional cuts). By the help of this results, temperature can be analyzed more detailed by a direct visualization of the molten volume. All ribs exhibit the same height, but differ in width, thus the basic volume available for expansion differs.

From the time step of 5 s, the melting core is restricted to the rib section of the part and no more melting core is on hand for the thin-walled sections. Also, at this point in time no more connection of melt to the gate can be seen. Thus, also packing

pressure may not have any more influence. The rib with 2 mm width is completely frozen after 13 s, the rib with 10 mm width after 18 s (not displayed here). However, the basic position (here: 2 mm) may be adjusted to a higher / lower value to provide more / less molten material for expansion, shifting the process window.

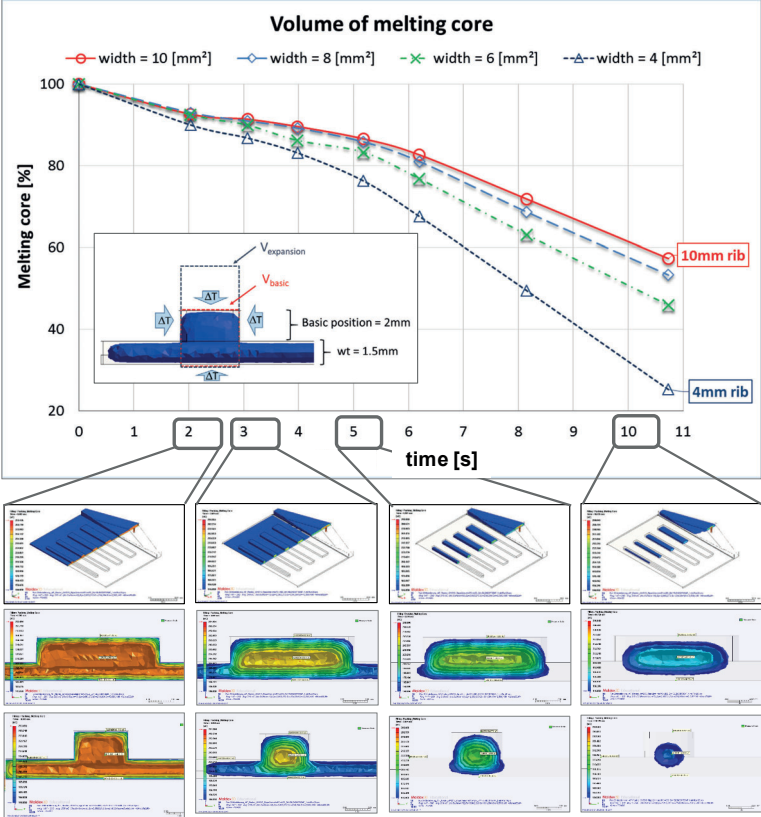


Figure 63: Improved local core-back mold– volume of melting core available at different delay times (upper) and melting core visualizations for total melting core, for the biggest volume rib (10 mm width) and the smallest volume rib (4 mm width)

By the knowledge of the remaining amount of melting core, the optimal time for core-back operation or the optimal basic volume to provide prior to expansion may be calculated to achieve a desired expansion ratio or desired density. If the optimal viscosity for foaming is known, simulation software can also point out the local viscosity by processing time, helping to make a forecast of the resulting structure.

These results help to better understand the foam formation and the final foam structure. Furthermore, they may allow a prediction of foamability as well transferability or tailored demarcation of foamed and non-foamed sections for different part geometries e.g. for snapping hooks or mounting elements.

7.4 Geometrical boundary conditions

Formation of compact skin layer

In contrast to low pressure foam injection molding, for high-pressure procedure with mold volume expansion, cellular structure is not covered completely by a compact skin layer. Here, the expansion operation affects skin layer formation for the surfaces not being initially in contact to the cooled mold wall. Figure 64 shows cross-sectional cuts of two parts manufactured with different expansion ratios. An unfoamed compact skin layer is created at all surfaces being in contact to the cooled mold wall for the initial part geometry (before volume expansion). The volume expanded areas do not exhibit a compact skin layer. Here, cells can be observed also at the surface. The cells are created simultaneously to volume expansion and thus can also nucleate and grow in the outer layers.

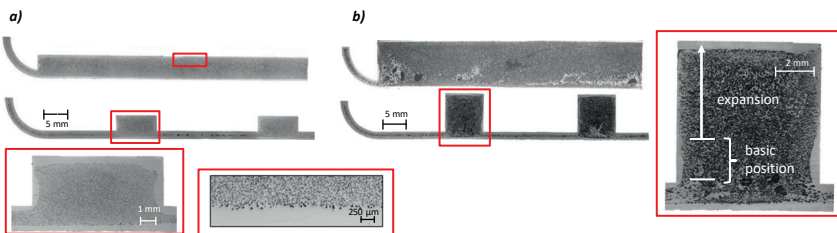


Figure 64: Morphology of PC-ABS/N₂ manufactured with local core-back – general overview and details for different expansion ratios (results also published in [148])

Accuracy of geometry

The maximum expansion ratio and thus also the accuracy of geometry strongly depend on the material and the type of blowing agent.

An insufficient molding of the cavity has been observed for some experiments with high expansion ratios using cba. This finding is also described in [154], even by using high amounts of cba. It is assumed to be attributed to the limited cba power. Here, the pressure of blowing agent is lower than the pressure of pba's. Even by using higher amounts than suggested by the ba supplier, ba power is insufficient to achieve accurate and sharp-countered molding of geometry. Thus, forces or resistance of melt is higher than expansion forces inside the growing cells. This effect is more pronounced using higher delay times, accompanying with longer cooling time and consequently less melting core being available. The materials' viscosity may be too high to allow accurate molding. Figure 65 shows the morphology of a chemically blown PP at high expansion ratio and long delay time.



Figure 65: Morphology of a PP/cba part, with high expansion ratio and long delay times (results also published in [152])

For physically blown parts a different effect for high expansion ratios has been observed. Here, sink marks at the backside of the expanded areas and rupture effects in the flanks of the expanded areas have occurred. It is assumed, that pba provides enough power for expansion, but the available melt is stretched too high and is already frozen. Possibly, a vacuum-like effect by the moving core may support this fining. This phenomenon also raises by higher delay times. Figure 66 highlights the effect of sink marks and rupture for the first prototype part produced with pba. Figure 67 (PC-ABS/N₂) and Figure 68 (PA6-GF30/N₂) highlight different expansion ratios for the second prototype part produced with pba. Here, the effect of insufficient molding in dependency of the width of the rib can be seen. The more volume provided before expansion, the lower the possible expansion ratio and the more rupture and sink mark effects occur.

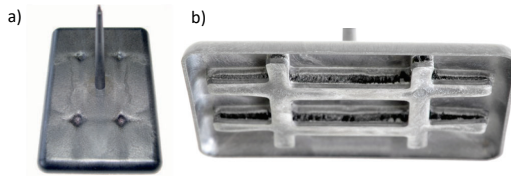


Figure 66: Sink marks at the parts surface (a) and rupture effect at flanks of core-back geometry (b) for a physically foamed part (PC-ABS/N₂) with high expansion ratio and long delay times

The maximum expansion ratio significantly depends on the material used. While for PC-ABS/N₂ up to an expansion ratio of 3 all ribs are molded accurate, for higher expansion ratios, rupture effects take place for some ribs and from an expansion ratio > 5 the whole expanded structure breaks open. An insufficient molding of the thinner ribs may be attributed to the low amount of melting core available before volume expansion. This point has already been discussed in chapter 7.3.

However, for PA6-GF30/N₂ a much higher expansion ratio could be observed. Up to an ER of 5.4 a geometrical adequate shape and a homogeneous structure is observed. For this material even for an ER of 12 (maximum core-back distance of the improved mold) the ribs of 10 mm and 8 mm width exhibit an accurate shape, exhibiting local density reduction of 70 %.

Figure 69 shows parts produced with PA66-GF/N₂ by using the maximum available core-back distance of the mold. Here, the basic thickness was set to 3 mm and no initial rib volume had been provided before volume expansion (ribs were foamed directly from the plate). For higher expansion ratios a further decrease of density is assumed for this material.

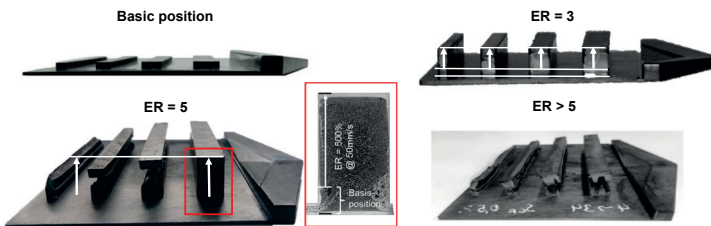


Figure 67: PC-ABS/0.5wt%N₂ parts produced by different expansion ratios (constant part weight)

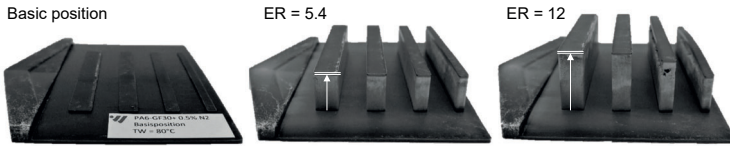


Figure 68: PA6-GF30/0.5wt%N₂ parts with different expansion ratios (constant part weight)

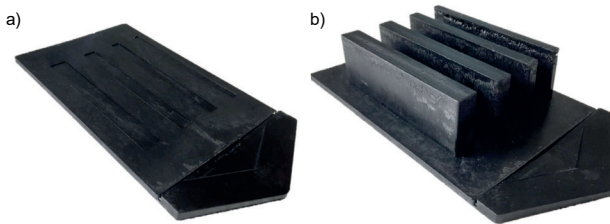


Figure 69: PA66-GF/0.5wt%N₂ parts produced with an expansion ratio of 12 (basic thickness of plate = 3 mm): a) basic geometry (before expansion), b) geometry after volume expansion

7.5 Freedom of design and geometrical transferability

Designing ribbed parts

Tick-walled areas and wall-thickness variations are often critical in compact injection molding. Due to differences in shrinkage, sink marks may occur. This effect is often visible on surfaces of thin-walled parts with ribs at their backside. Thus, guidelines exist to design the width and height of ribs in dependency of the parts' wall thickness. For compact molded ribs a thickness of ribs $\leq 0.5 - 0.7$ times of basic wall thickness is recommended to prevent sink marks [155]. In terms of stiffness, rib height is much more influential than the number of ribs (e.g. $10 \times \text{height} = 40 \times \text{stiffness}$, but $10 \times \text{number} = 3 \times \text{stiffness}$) [155]. However, in terms of rib height, a limitation of 5 to 10 times of basic wall thickness is supposed to prevent buckling [155]. Furthermore, the thickness of ribs also affects the cooling time (an increase of thickness from 0.5 to 1 time of wall thickness leads to an increase of cooling time of around 40 %) [155].

Foam injection molding may widen these restrictions and increases freedom of design. Foaming may work against the sink marks by acting like an inner packing pressure. Wall thickness variations and thick-walled areas are less critical than for compact molding [44]. However, for low-pressure foam injection molding, also

several construction and design restrictions are on hand. For example, for parts with wall thickness variations, the gate should be located in the thick-walled region, enabling the foam to expand also in the thin-walled sections. In regards of rib constructions, also the ratio of parts' wall thickness in regards to width and height of the ribs has to be adjusted [44]. Furthermore, a radius in the basis and a draft angle is recommended [44] and the height of ribs is limited by the foamability. An insufficient foaming may affect the stiffening effect. The thickness of ribs is recommended to be equal to the basic wall thickness [44]. Thus, an equal foaming of all regions is achieved. Ribs should be arranged in flow direction to achieve a complete molding and an accurate shape. Snapping hooks, screw bosses or mounting elements should be arranged close to the gate to exclude them from foaming [44]. Figure 70 highlights some design guidelines and geometrical restrictions for compact and foam injection molded ribs.

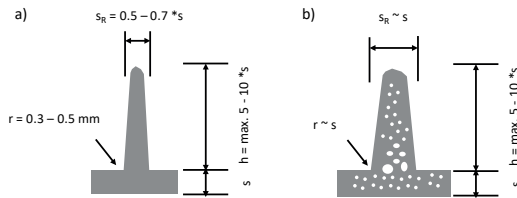


Figure 70: Design guidelines and restrictions for rib constructions in compact injection molding (a) and foam injection molding (b) according to [44]

In core-back procedure, the aforementioned restrictions may be annulled. The molded parts, already shown in this chapter show the difference and potential. Neither a radius has to be arranged in the basis of a rib, nor any ratio of basic wall thickness to width or height of ribs has to be respected. Also, huge wall thickness variations can easily be molded, and gate position can be located anywhere.

- ⇒ Decoupling of filling and foaming allows designing parts like compact molded parts with the additional advantage of reduction or elimination of sink marks due foam formation.
- ⇒ Gate location and wall thickness variation do not affect the final foam structure in a big extend because the final structure is developed after cavity filling.

Geometrical transferability

In terms of geometrical transferability, experiments with different materials and expansion ratios have been conducted with the improved core back mold. In experiments, expansion ratio was stepwise adjusted, and accuracy of molding was evaluated. Figure 71 shows the maximum expansion ratios observed for PC-ABS/N₂ (criteria: geometrical accurately shaped rib) and the simulation data for melting core in dependency to the basic area (before expansion). It became evident that the volume of molten material provided prior to expansion defines the maximum expansion ratio. The more volume provided, the higher the maximum achievable expansion ratio. The simulation data is based on process simulations already shown in Figure 63. The area of melting core was measured for the expanded areas at the point in time, the core-back operation was initiated (after 3 s of packing pressure). For every rib (width: 4 mm to 10 mm by initial height of 3.5 mm → 14 to 35 mm²) the simulated melting core was measured to be around 90 %. Thus, the calculations of maximum ER based on the experiments and the maximum ER based on the simulation of the melting core show the same trend. However, it should be noted that these results also depend on material, blowing agent type, content as well temperature conditions.

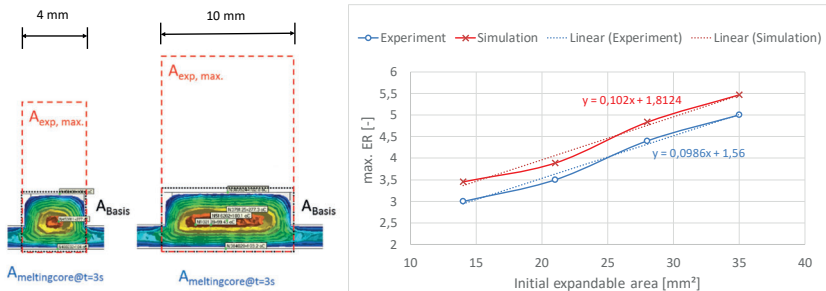


Figure 71: Maximum expansion ratios in dependency of basic geometries calculated on basis of experimental data and on basis of numerical simulation of melting core; material: PC-ABS/N₂

The results exemplarily show the correlation of basic volume (before expansion) and the achievable expansion ratio and may be used to judge the geometrical transferability to predict expansion ratios for non-experimentally investigated geometries.

⇒ Thus, the simulation of melting cores allows a prediction of non-experimentally investigated geometries.

8 Process – structure relationship

This chapter focusses on the influences of process parameters on the resulting cellular structure. It is subclassified in general process parameters and process parameters defined by the process variants - low-pressure procedure and high-pressure procedure. All experimental results shown were conducted by using nitrogen as a physical blowing agent (pba), induced by the MuCell system. Chemical blowing agents (cba) have also been processed successfully, but often include nucleation additives and are coated on polymers which are not the same type as the matrix polymer. Thus, the influence of process on nucleation may be overlaid and is expected to be more process-dependent for physical blowing agents.

8.1 Process parameter independent of process variant

The following process parameters are set independently of the process variant. Their effects have been well discussed in literature. However, due to their high influence on cell formation they are mentioned here shortly.

8.1.1 Blowing agent content

In terms of cell formation, blowing agent (ba) content is of a high significance. However, the effect may differ by material. An increasing ba content leads to an increase in nucleus, thus an increase in number of cells and decreasing cell size [34]. More cells are created simultaneously, resulting in a finer-celled structure due to two reasons. First, the available gas is consumed by more cells growing at the same time. Thus, less gas is available for each cell. Second, cells cannot grow independently within the free volume due to the existence of neighboring cells. Furthermore, the homogeneity of structure is supported by increasing ba content. In general, less coarsening phenomena occurs due to less growth of cells (by increasing nucleation).

In the following, two exemplarily structures are shown to highlight the effect of ba content. Here, microscopic pictures of cross-sectional cut parts, produced by high-pressure core-back foaming (local core-back procedure) are shown. The results

illustrate the general trend and are also valid for the low-pressure procedure. Figure 72 shows physically blown PP parts at 2 different ba contents produced at same processing conditions. It is observed that a low ba content lead to a coarse and inhomogeneous structure (Figure 72 a)). Furthermore, some big cells can be observed which partly are grown to the parts' surface and skin layer formation is negligible. For the high ba content, a much finer cell structure is created (Figure 72 b)). A clear separated compact skin layer is observable for the regions being in touch with the cooled cavity surface before expansion. For this example, the formation of the compact skin layer is procedure-dependent.

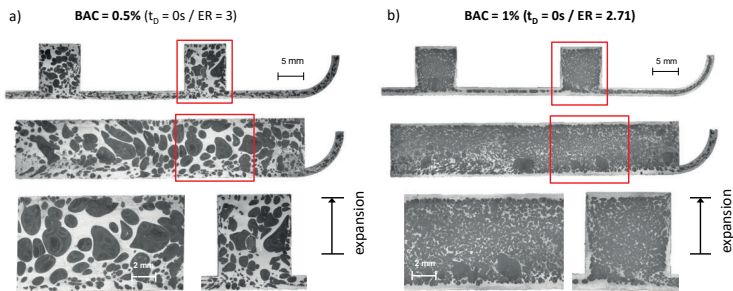


Figure 72: Morphology of PP at different blowing agent contents: a) SCF = 0.5 wt%, b) SCF = 1.0 wt% (results also published in [156])

8.1.2 Melt and mold temperature

The set melt temperature is controlled by the injection molding machine and defines the melt temperature at the start of injection. The set mold temperature defines the temperature difference of cavity wall and injected melt and thus also the speed of cooling and the solidification time. The resulting, time-dependent melt temperature in the cavity during process is mainly affected by these two parameters. Further aspects like shear-induced temperature increase may also take effect here. Temperature variations have not been in focus of this thesis and have not been experimentally investigated; thus, its influence is described by observations described in literature.

A higher temperature results in a lower materials viscosity. For low-pressure procedure, this leads to a faster pressure decrease when the injection is stopped and a faster balancing of pressure at different positions in the cavity takes place. Thus, a more uniform cell formation and a more homogeneous density distribution may result [19]. The same effect has been observed for two different viscosity materials processed at the same conditions in low-pressure foam injection molding. The lower viscosity material exhibited a faster pressure drop after stop of injection, shifting the mechanism to nucleation, resulting in a finer-celled structure [19]. A low temperature resulted in a higher gradient in cell size over the parts' cross section [19]. This effect is explained by the faster pressure release due to a decreasing melt viscosity for increasing temperatures, finally supporting nucleation [19]. Another effect observed for low melt temperatures is the development of bigger cells, exhibiting an orientation in flow direction [19].

For high-pressure procedure, mechanism may be different due to decoupling of filling and final cell formation. Here, the thermal boundary conditions, defining the melting core and thus foamability are already discussed in chapter 7.3. For high-pressure mold opening experiments, in literature a decreasing circularity of cells for increasing mold temperatures is reported [140]. It is assumed that a faster cooling prevents cell wall rupture as well limits growth deformation, thus maintains cell's circular shape [140].

A point to mention is, that temperature also defines the solubility of the ba's and the level of saturation (see chapter 3.2.1). This may also affect cell formation mechanism.

8.2 Process parameter influences for low-pressure procedure

In literature, for low-pressure foam injection molding a big influence on cell formation is described for the already discussed process parameters melt and mold temperature, blowing agent content and injection speed [1, 19, 44, 157]. These parameters may have a huge influence on cell size. For example, in the experiments of Flórez Sastre [1] a mean cell diameter from 10 to 200 μm has been achieved by parameter variation [1, 19]. However, the process parameters set by the injection molding machine and the resulting physical values during procedure may have complex interactions. The main process parameters directly or indirectly affect

pressure, temperature and viscosity. Thus, they define the boundary conditions for the cell formation mechanism – sorption, diffusion, nucleation, cell growth and fixation. These finally define the cell structure characteristics like cell size, cell density, homogeneity, etc. Figure 73 depicts the complex correlations and groups into “*process parameters*” which are user defined by machine and mold settings, “*process values*” which are resulting physical values, defining the boundary conditions and “*resulting characteristics*”, representing the final cellular structure.

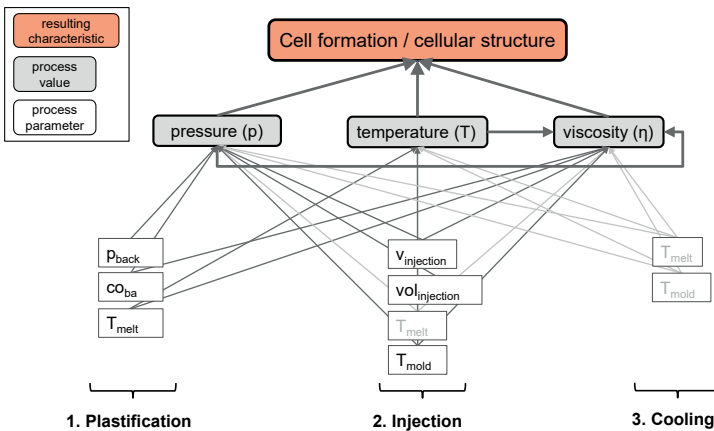


Figure 73: Correlations of process parameter, process values and resulting cellular structure in low-pressure foam injection molding

Also, some of these correlations are mentioned in literature. For example, Cramer [19] also mentions that injection speed, injection volume (sop) and mold temperature (in Figure 73 classified as injection parameter) as well melt temperature and blowing agent content (in Figure 73 classified as injection parameter) affect cell formation due to the fact that they affect cavity pressure [19].

Since the process parameter effects for the blowing agent content as well melt and mold temperature have already been discussed, in the following subchapters the two remaining, procedure-specific process parameters filling volume (sop) and injection speed are discussed.

8.2.1 Injection volume (switch over point)

The switch-over point (sop), defined by the injected volume defines the amount of expandable volume and affects the pressure conditions inside the cavity. If sop is set too early, expanding melt may not reach the end of the flow front and short shot occurs. If sop is set late, cell formation and density reduction is limited. The later the sop is defined, the higher the resulting cavity pressure and the more the pressure drop is shifted to the end of the flow path. As a consequence, it may affect cell size and its distribution.

A qualitative comparison of the influence of sop on cell size is given in Figure 74. Here, cell size at switch over point and resulting cell size is shown for two different sops. It can be seen that the shift in flow front lead to a difference in final cell size distribution and final cell size values.

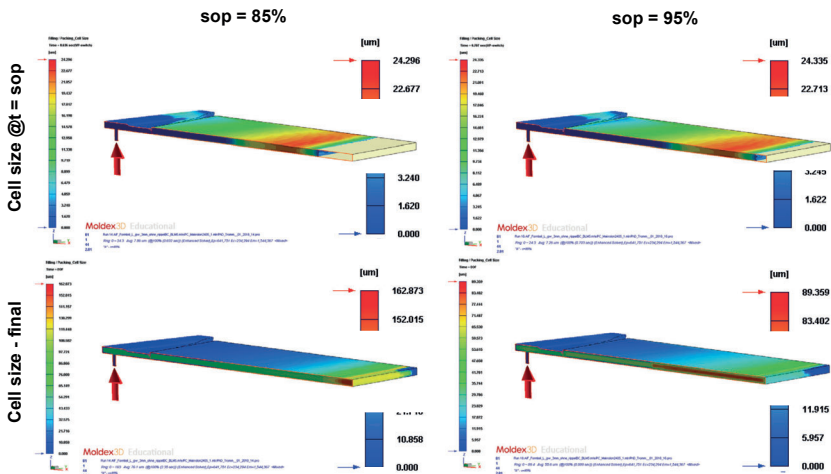


Figure 74: Effect of switch over point (sop) / filling volume on cell size; left: $v = 85\%$; right: 95%

Figure 75 depicts the evaluation of pressure and cell sizes simulated for sop of 85 %, 90 % and 95 % near gate (ng) and away from gate (afg). Near the gate sop = 85 % and sop = 90 % exhibit the same cell size while sop = 95 % leads to a smaller cell size here. Away from gate, there is a more pronounced difference in pressure and cell size for all sop. The later the sop is set which means more volume injected, the higher the pressure and the smaller the cells are.

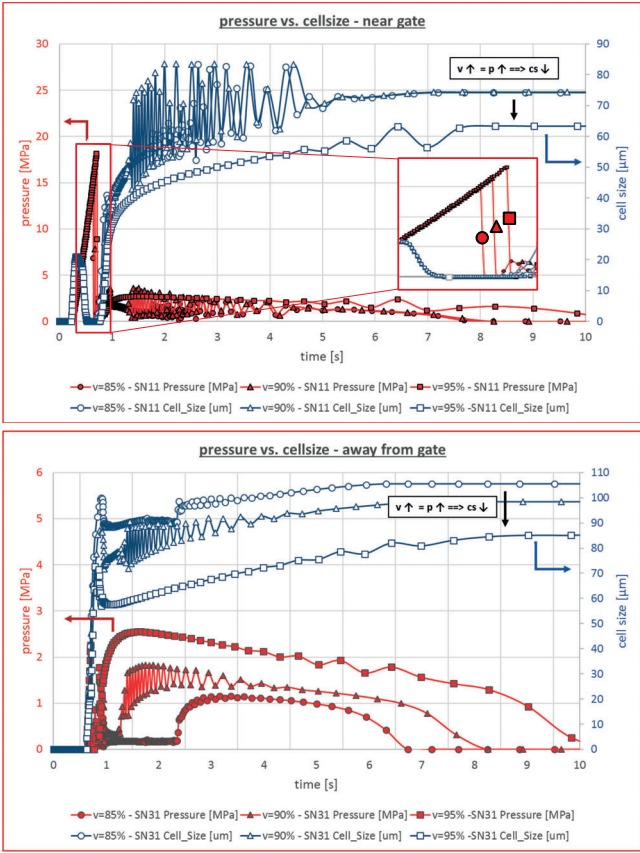


Figure 75: Pressure and cell size in low-pressure foam injection molding for different filling volumes / switch over points – v = 85 %, v = 90 % and v = 95 % - near the gate (upper) and away from gate (lower) [discontinuities in calculation between ~ 1.2 s and ~ 3 s are a problem given by the simulation software used and should not be judged; instead the general trends should be highlighted here]

Figure 76 summarizes the aforementioned results and depicts the gradient in cell size (difference afg to ng) over the flow length in dependency of filling volume. As can be observed, the filling volume of 95 % exhibits a lower gradient in cell size than the lower filling volume of 85 %.

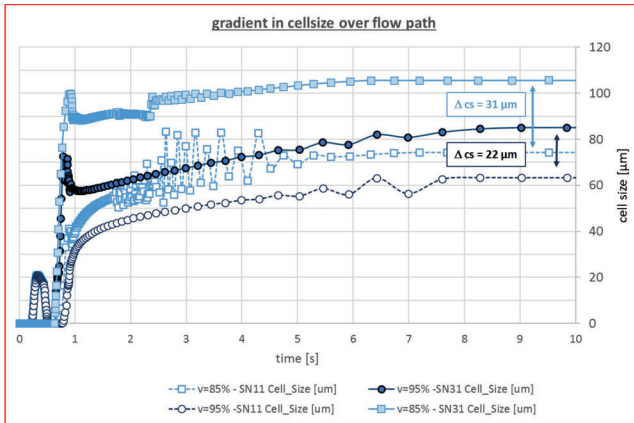


Figure 76: Gradient of cell size by flow position (near gate vs. away from gate) in low-pressure foam injection molding; comparison of two different filling volumes / switch-over points

Deformation of cells and cell density are not worked out here. In literature, besides the gradient in cell size, also an effect of sop on the elongation of cells is described [28, 84]. An increase in shot size was reported to shift elongated cells into a more spherical shape [84]. Furthermore, a decrease of cell density is reported for an increasing sop [28].

8.2.2 Injection speed

In foam injection molding, besides melt temperature, injection speed is rated as the most influential parameter [44]. In general, a higher injection speed is suggested to achieve a more uniform structure. For low-pressure procedure, injection speed mainly defines the resulting pressure and pressure drop inside the cavity [19, 28, 44]. Thus, this is a parameter rated to be able to actively shift effects to nucleation or cell growth. In Ishikawa and Ohshima [34] injection speed is reported to be a key factor for uniform cell development. A higher injection speed results in a higher-pressure gradient inside the cavity. Thus, less amount of melt exhibits a pressure level lower than partial pressure of the blowing agent [19]. Consequently, less cells are created behind the flow front and the loss of gas by collapsing cells at the flow front is reduced [1, 19]. Furthermore, the higher pressure level results in a higher pressure drop rate after stop of injection, supporting nucleation, thus finer-celled structures [19].

Additionally, less time is available for diffusion of available gas into the already created cells. Consequently, nucleation dominates, and structure may become more uniform [1]. Also, a more uniform structure with less deformation of cells by using higher injection speeds is described by [84]. The faster the mold filling is done, the less difference in nucleation times and temperature history from gate to end of flow path is on hand. Hence, a high injection speed may support uniformity [84]. The level of effect also depends on the materials' viscosity, shown in experiments by [19].

Also, the skin layer thickness is influenced by the injection speed. For higher injection speeds, thinner skin layers have been observed as reported by Cramer [19]. Based on his experiments, Cramer [19] states the influence of injection speed to significantly affect the uniformity of skin layer thickness in the way that a higher injection speed leads to more uniformity of skin layer thickness by flow length.

Density distribution

Figure 77 and Figure 78 compare the morphology and resulting density distribution for two different injection speeds: 50 cm³/s and 200 cm³/s (for details on process parameters see Figure 124 in the appendix). For both speeds, morphology and distribution of density change by position. The structure is getting coarser by increasing flow length. A more uniform structure for high injection speeds, as reported in literature and shown by own simulation results, is not directly obvious here. The structures exhibit some coarse regions which do not allow a quantitative cell size measurement. For the position near the gate, the density change from skin layer to core is sharper for the low injection speed. The high injection speed samples exhibit a more continuous transition. For the middle of the flow path and away from gate, no pronounced difference in density distribution comparing both injection speeds is on hand. The overall density (whole sample including skin layer) increases by flow length but is similar for both injection speed settings. The deviation of density (afg vs. ng) by flow length is 8.4 % (50 cm³/s) and 11.9 % (200 cm³/s).

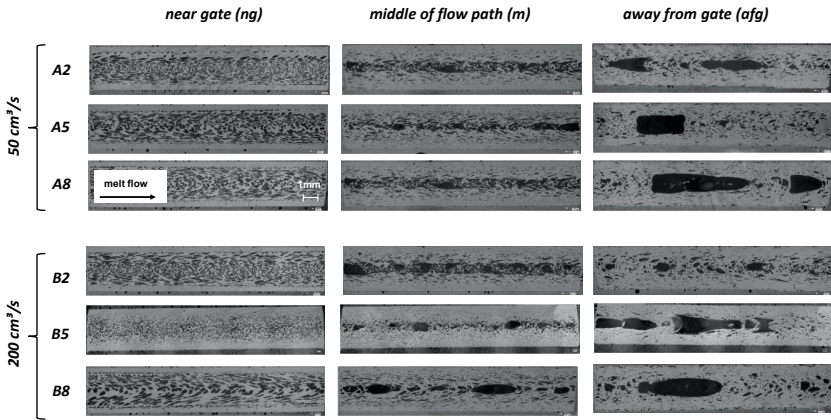


Figure 77: Morphology of low-pressure foam injection molded samples (material = PC/N₂, sop = 70 %) for different positions, manufactured by variation of injection speed

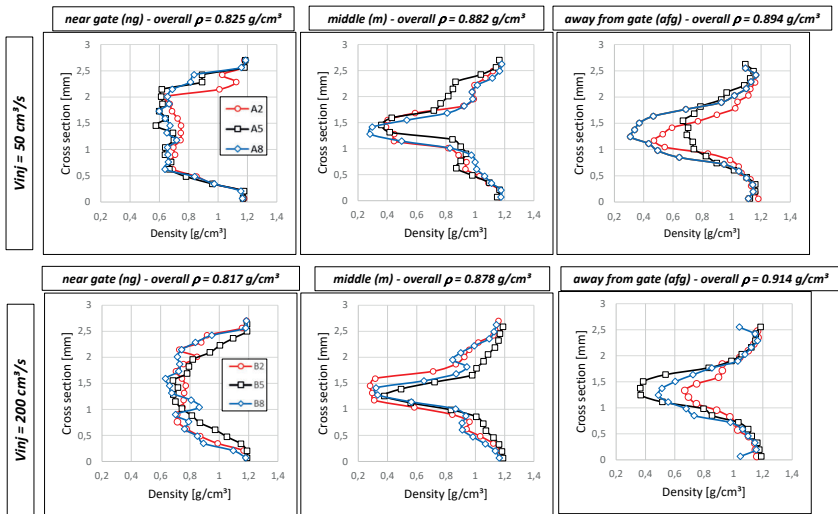


Figure 78: Density profiles of low-pressure foam injection molded samples (material = PC/N₂, sop = 70 %); upper: $V_{inj} = 50 \text{ cm}^3/\text{s}$, lower: $V_{inj} = 200 \text{ cm}^3/\text{s}$

Cellular structure and cell size

Figure 79 compares the 3D reconstruction of the low-pressure samples produced at different injection speeds. Here, for reconstruction of the μ CT scan the BVC filter (exclusion of cells which are cut by the borders of the analyzed volumes) was used and a quarter-piece cut of the structures is shown. Independent of injection speed, some general effects can be observed. As already shown in the microscopic pictures, away from gate structure is coarser. An orientation or elongation of cells in direction of melt flow close to the compact skin layer is much more pronounced near the gate compared to the position away from gate. Comparing the injection speeds, a more pronounced elongation of these cells is on hand for the high injection speed sample; cells seem to be thinner and more stretched here.

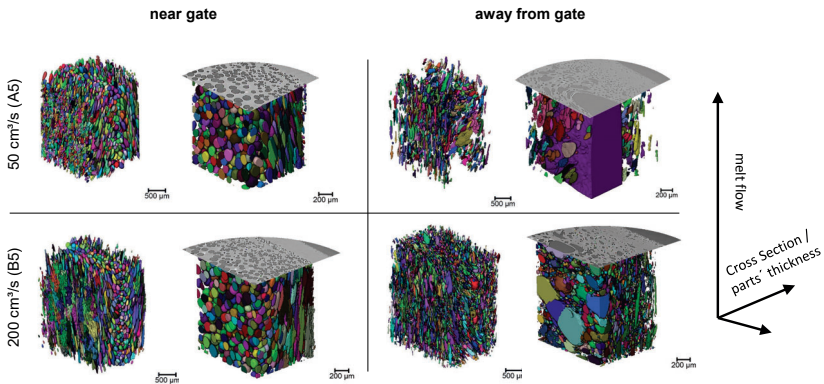


Figure 79: 3D reconstruction of cell volumes for low-pressure foam injection molded samples (material = PC/N₂, sop = 70 %): near gate (ng) and away from gate (afg) for two different injection speeds

Figure 80 depicts the 3D cell volumes in dependency of the position of their barycenter in direction of parts' thickness. For the lower injection speed, cell volumes near the gate exhibit a homogeneous distribution. Away from gate, a distribution by trend of bigger volumes to be located in the core area is observed. For the high injection speed, near the gate, the distribution of cell volumes is less homogeneous compared to low injection speed. Noticably, big cell volumes are observable near the compact skin layers, while remarkably small volume cells are located in the core. This observation may be explained by the cells elongated in melt flow direction. These cells exhibit a small diameter if measured rectangular to flow direction in 2D, but

exhibit big volumes due to their elongation in flow direction. Away from gate, cell volume distribution is very pronounced by big cells to be located in the core. Thus, more scattering of cell volume is on hand for the higher injection speed setting. Near the gate cell size and number of cells is quite similar for both injection speeds while away from gate a significant increase of cells' number is on hand. However, due to the inhomogeneity of structure, the trends in distribution should be in focus and a quantitative comparison of cell sizes is omitted here.

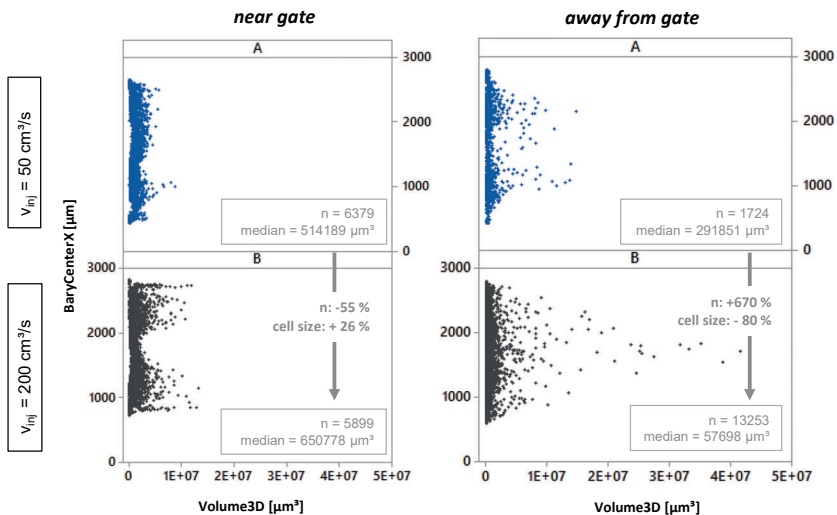


Figure 80: Position of cells' barycenter plotted over 3D cell volume for low-pressure foam injection molded samples (material = PC/N₂, sop = 70 %) in dependency of injection speed - data: full cell volume with BVC filter (exclusion of cells which are cut by the borders of the analyzed volumes)

Shape of cells

To judge the shape of cells, the *Aspect Ratio 3D* (proportion of max. width to max. length) is used as an indicator. *Aspect Ratio 3D* and *Sphericity* show the same trend. However, the effect of cell elongation is more pronounced using this value compared to *Sphericity*. A low aspect ratio is representative for elongated cells. The closer this value is to 1, the higher cells' roundness is. In analogy to the *Volume 3D*, Figure 81 depicts the *Aspect Ratio 3D* in dependency of the position of cell's barycenter. A very

noticeable trend of cell's shape is observed to strongly depend on its position. For both injection speed settings, near the gate the distribution may be described as an epsilon shape. Aspect ratios from low to high are observed near the compact skin layers. In the transition zone, low aspect ratios are on hand, corresponding with a strong elongation. The closer cells' position is to the core, the higher the aspect ratios are. The highest values for aspect ratio are observed in the core area. Away from gate, also a characteristic of changing aspect ratio from areas next to skin layer, intermediate and core layer are noted. Especially, for the high injection speed setting, aspect ratio, thus, roundness is more pronounced in the core.

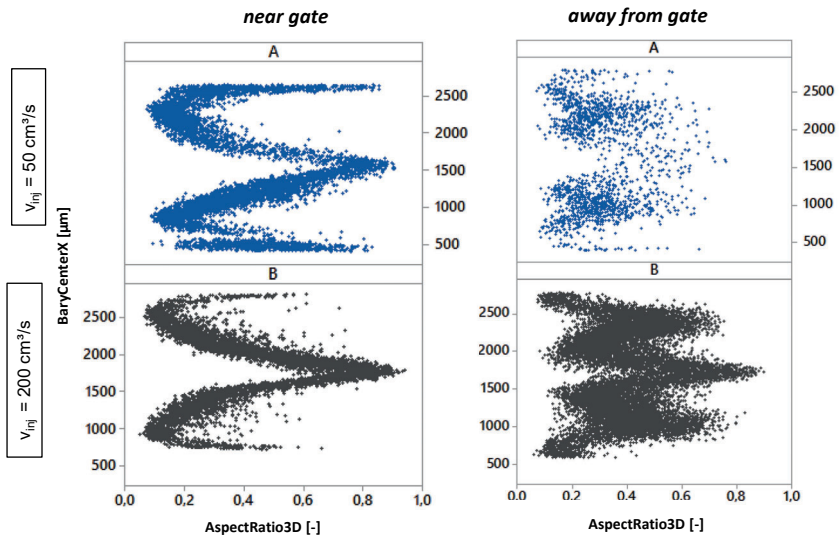


Figure 81: Position of cells' barycenter plotted over Aspect Ratio 3D of low-pressure foam injection molded samples (material = PC/N₂, sop = 70 %) in dependency of injection speed; data: full cell volume with BVC filter (exclusion of cells which are cut by the borders of the analyzed volumes)

⇒ Independent of injection speed, morphology and distribution of density change by position. The structure is getting coarser by increasing flow length. Near the gate, a more pronounced change in density from skin to core is observed for the low injection speed while for the high injection speed samples a more continuous transition is seen. For the other positions, no pronounced difference in density

distribution comparing both injection speeds is on hand. An orientation or elongation of cells in direction of melt flow close to the compact skin layer is observed, being more pronounced for the high injection speed sample. For the high injection speed, near the gate, the distribution of cell volumes is less homogeneous compared to low injection speed. More scattering of cell volume is on hand for the higher injection speed setting. The shape of cells strongly depends on position. A trend of a continuous, pronounced change in aspect ratio from skin to core is observable. As a tendency, aspect ratio is high, thus, roundness is more pronounced in the core area.

8.3 Process parameter influences for high-pressure procedure with mold volume expansion

As it was stated for low-pressure procedure, the main process parameters directly or indirectly affect pressure, temperature and viscosity. Thus, they define the boundary conditions for the cell formation mechanism – sorption, diffusion, nucleation, cell growth and fixation and the final cell structure characteristics. However, in high-pressure procedure due to the additional process phases, additional “process parameters” are on hand, influencing the “process values”. Thus, an active control of structure development is given in high-pressure procedure with volume expandable molds, while structure may not be varied systematically using the low-pressure procedure [1].

Figure 73 depicts the complex correlations and groups into “*process parameters*” - user defined parameters by machine and mold settings, “*process values*” – resulting physical values as well “*resulting characteristics*” – final cellular structure. As can be seen, in comparison to low-pressure procedure, much more correlations are on hand during procedure.

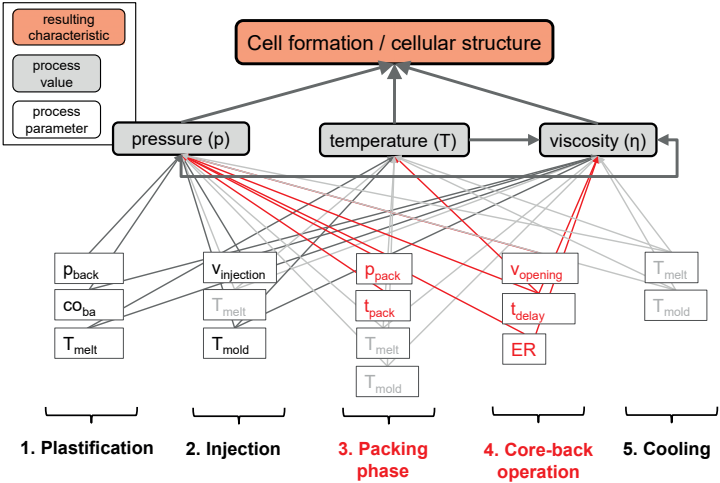


Figure 82: Correlations of process parameters, process values and resulting cellular structure in high-pressure foam injection molding with expandable molds

In the following chapters, the influence of the core-back specific parameters will be discussed. Especially the effect of packing pressure and its effect on homogeneity of structure is in focus. This point is only rarely discussed in literature. Here, levels for packing pressure and time are often unknown, thus it is not clear if cells may be forced back into solution before volume expansion and if this point is relevant to structure characteristics.

8.3.1 Procedure specific parameters

In the following the procedure specific parameters expansion ratio, delay time and expansion speed are explained and discussed individually. To rate their significance and possible interactions, these parameters are included in a DoE, described in chapter 8.3.2. The effect of injection speed is separately worked out and discussed in chapter 8.3.3.

8.3.1.1 Expansion ratio

In contrast to low-pressure foam injection molding, in core-back procedure, expansion can directly be set by the core-back distance, defining the expansion ratio. In terms of maximum expansion ratio and formation of structure, rheological aspects (mainly defined by materials' properties and temperature) play an essential role. The relationship of viscosity to melt strength is important here. For Polypropylene especially long-chain branches types are favorable [44]. Also, fillers and additives may affect the melt strength and thus the expansion ratio.

Expansion ratio (ER) is defined as ratio of basic volume (initial volume in injection phase) to expanded volume (volume after core-back operation) of the core-back area. Typically, the basic volume in the expanded areas is set to a larger volume to provide an extra amount of melt for expansion. The basic volume defines the amount of melt available for expansion, consequently, defines the max. expansion ratio. For the experiments within this thesis, the basic volume was usually set by the part's basic wall thickness and additionally 2mm initial height of core-back volume (first and second prototype part). Figure 83 illustrates the basic and end position of the core used for the experiments with the first mold, defining the height of the ribbed section before (a)) and after expansion (b)).

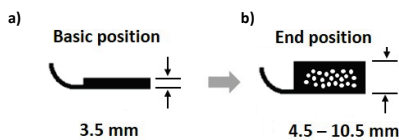


Figure 83: Schematic cut of prototype part 1 - height of core-back area: a) basic position (injection phase), b) end position (after core-back operation) (results also published in [148])

Figure 84 shows cross-sectional cuts of expanded volume areas, produced with by the first mold (PC/ABS). For low expansion ratios, a fine-celled, homogeneous structure is observed. Higher expansion ratios lead to bigger cells and the structure gets more inhomogeneous. Furthermore, big cells or rupture effects can be seen for this material (PC/ABS). These effects are mainly observable near the compact skin layers at the fixed side of the mold.

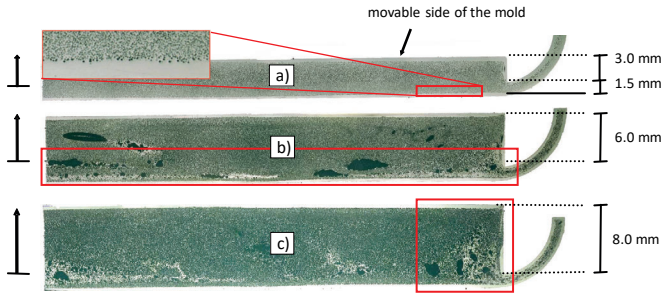


Figure 84: Morphology of PC/ABS at different expansion ratios: a) $ER = 1.29$, b) $ER = 2.14$, c) $ER = 2.71$ (results also published in [156])

Figure 85 shows results for parts of PP, produced with a low amount of blowing agent. An increasing cell size, coalescence effects and an elongation of cells in direction of core movement by increasing expansion ratio can be observed.

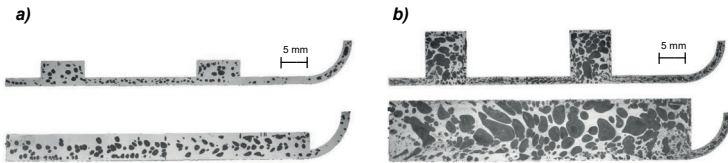


Figure 85: Morphology of PP at different expansion ratios ($SCF = 0.5$ wt%, $tD = 0$ s): a) $ER = 1.29$, b) $ER = 2.71$ (results also published in [148])

Figure 86 shows the results of cell size measurements in terms of boxplots. Cell size is plotted over of expansion ratio. By the example of PA6-GF15/N₂, the general trend of an increasing cell size (median value) and increasing inhomogeneity of structure (range of box and outliers) correlating with an increasing expansion ratio is depicted.

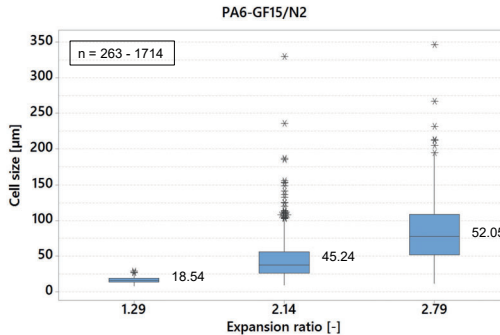


Figure 86: Boxplots of cell size for different expansion ratios of PA6-GF15/0.3 wt%N₂ (the boxes depict 50 % of the measurement values; the horizontal lines within each box mark the median value; the vertical lines highlight the maximum and minimum deviation, and the stars depict statistically calculated outliers)

The observation on cell size to increase and core density to decrease is confirmed by several investigations [15, 36]. In his experiments Spörrer [15] investigated bigger cells by an increasing expansion ratio and mentions delamination effects in the foam core for high expansion ratios [15]. Based on a constant cell nucleation density, he also calculated the resulting cell size for different expansion ratios and theoretically depicted the increase in cell size [15]. For local core-back procedure, cell formation also occurs in the non-expanded areas. Thus, the correlations of expansion ratio, density reduction and resulting cell sizes is more complex and may differ.

Delamination effects for high expansion ratios are also described in literature [15]. This effect is attributed to the presence of a significant temperature gradient within the cross section [15]. The melting core exhibits the lowest viscosity, thus is and is “weakest point” [15].

A pronounced elongation of cells with fibril-like, unidirectional structures in core-back direction is described by Ohshima [36]. These structures were achieved by using Polypropylene with sorbitol gelling agent executing high expansion ratios [36].

In terms of density, in her experiments, Flórez Sastre [1] observed a gradually change in density over cross-section for low expansion ratios while for high expansion ratios a pronounced or sharp change of density between skin and core occurred [1].

Another limiting factor for expansion ratio may be the power of the blowing agent. Especially cba is usually processed with lower concentrations and releases CO₂ which limits the achievable foam expansion [57]. This aspect is already mentioned and shown in chapter 7.4.

⇒ The trend of an increasing cell size and increasing non-uniformity of structure is also obvious in the results of the DoE, presented in chapter 8.3.2.

8.3.1.2 Delay time (pressure-less)

If the process is conducted by applying packing pressure, time between injection phase and expansion operation is delayed by packing time. The effect of an actively applied packing phase, accompanying with a delay time under pressure is separately discussed in chapter 8.4.

However, process may also be performed without an active packing pressure but using a delay time e.g. for skin layer formation. Any delay time, applied with or without pressure, affects the temperature and viscosity. A higher delay time leads to a smaller amount of melting core and may increase the thickness of compact skin layer [1]. The remaining melting core is expanded to a higher extend, thus the density of the foamed core region is lower, and cells may become bigger.

In the following, results according to the first prototype mold are shown. Here, the use of packing pressure is restricted due to constructive reasons of the mold. By applying packing pressure, the core sticks and does not move anymore to expand the volume. Thus, parts were produced without an active pressure phase. Figure 87 and Figure 88 show exemplarily results for PC-ABS and for PP. For both materials an increase in delay time also leads to a much coarser structure. In combination with a high expansion ratio, for PC-ABS an incomplete molding can occur. Sink marks and the rupture of the expanded areas can be observed (compare chapter 7.4). It is assumed that melt is too cold at the moment the core is moved. For PP, a dramatic increase in cell size can be seen and just a negligible skin layer is created for the higher delay time. It is assumed that cell growth occurred during delay time due to the non-

existing packing pressure. Similar effects were found by processing aluminum foams in core-back procedure by Wiehler [137] (see Figure 150 in the appendix).

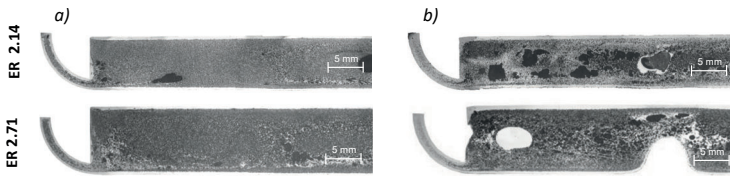


Figure 87: Morphology of PC-ABS/N₂ at two different expansion ratios in combination with different delay times: a) $t_D = 0$ s, b) $t_D = 1$ s (results also published in [156])

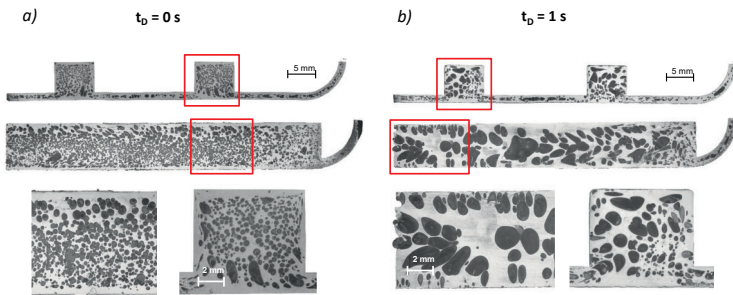


Figure 88: Morphology of PP/N₂ at different delay times: a) $t_D = 0$ s, b) $t_D = 1$ s (results also published in [152])

⇒ Cell formation is assumed to be dominated by growth instead of nucleation if expansion is delayed without applying packing pressure (or insufficient packing pressure).

⇒ In order to achieve small cell sizes and a uniform structure it is not recommended to perform the procedure without active packing pressure

8.3.1.3 Expansion speed

Nucleation and cell growth are competing mechanisms occurring during cell formation process. The pressure drop rate (PDR) has a major effect on nucleation and may shift mechanism to nucleation or growth. If pressure drop is high, nucleation is the dominant effect. For low pressure drop rates, nucleation and cell growth occur simultaneously. To achieve homogeneous structures with small cells, the mechanism of nucleation should be the dominant one. This general effect has already been discussed in chapter 6.2.2. In mold opening or core-back foam injection molding, expansion speed (also mentioned as core-back speed or opening speed) directly affects the PDR, thus cell formation mechanism.

To achieve microcellular foams ($< 50 \mu\text{m}$) by homogeneous nucleation in foam injection molding, according to [158] a PDR of $> 20.000 \text{ bar/s}$ (2000 MPa/s) is needed and needs to take effect within the relevant pressure range of a pressure level $< 150 \text{ bar}$ (15 MPa) [158]. In Altstädt and Mantey [44] it is mentioned, that in experiments with a core-back mold a PDR of 3300 bar/s (330 MPa/s) was achieved which must be insufficient to achieve homogeneous nucleation of microcellular foams, defined to be smaller than $10 \mu\text{m}$ [44]. Fillers and additives may help to achieve finer-celled structures due to heterogeneous nucleation.

In her experiments, Flórez Sastre [1] used three levels of expansion speed. She observed a high number of small cells for high expansion speeds and a low number of big cells for slow expansion speeds [1]. For slow speeds it is assumed that nucleation is not favored, and the available blowing agent diffuses into the early formed cells. Although, the levels used (0.2 to 0.8 mm/s) were very slow compared to the range of levels in other investigations and author's own experiments.

In [35, 36] the effect of expansion speed is investigated by visualization experiments. Here, an increasing expansion speed leads to a faster depressurization rate, consequently to a decreasing cell size and an increasing number of cells for CO_2 and N_2 [34, 36]. A variation of core-back speed in the range of 1 mm/s to 10 mm/s was executed

and observed that an increase in expansion speed lead to an earlier start of growth and faster growth rates [34–36].

Wu et. al. [154] did also variations of the core-back speed in the range of 1 to 9 mm/s and found an insufficient accuracy replication of the shape of the mold for low core-back speeds (here: less than 7 mm/s) [154].

In Xi et. al. [159] a variation of expansion speed was done in the range of 80 to 150 mm/s. No active packing phase was used and mold-opening was initiated right after cavity filling. The expansion was initiated via a hydraulic cylinder moving wedges to expand the cavity volume. However, the indicated resulting pressure drop rates only ranged from 0.5 to 1.15 MPa/s [159]. These values seem to be very low compared to the pressure drop rates based on measurements within this thesis. Moreover, by processing PLA and PLA composites a finer cell structure is stated to result for lower expansion speeds [159]. These results do not match with the aforementioned trends described in literature and the results of this thesis.

The improved mold used in this thesis, allows a variation of expansion speed in a wide range. The levels of speed can be set between 0 and 100 mm/s. Figure 89 shows resulting cavity pressure profiles recorded for different core-back speeds from 1 mm/s up to 50 mm/s (cavity pressure sensor implemented in the 10 mm rib). The core-back operation was initiated from a pressure level of 30 to 35 MPa. For higher pressure levels a higher pressure drop rate is obvious (see chapter 8.4.3). Table 1 depicts the pressure drop rates during core-back operation, calculated from the cavity pressure curves.

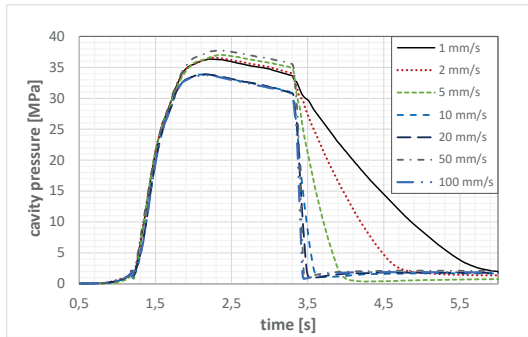


Figure 89: Experimental pressure profiles recorded with the improved core-back mold for different core-back speeds: 1 / 2 / 5 / 10 / 20 / 50 mm/s; $p_{pack} = 40$ MPa bar for 2 s

Table 1: Resulting pressure drop rates for set core-back speeds according to the experimental recorded cavity pressures depicted in Figure 89

Set core-back speed [mm/s]	dp/dt [MPa/s]
1	11.5
2	20.4
5	53.6
10	104.1
20	155.4
50	244.4
100	306.6

⇒ An increasing expansion speed results in higher pressure drop rates, thus supports finer-celled structures. This effect is also obvious in the results of the DoE, presented in chapter 8.3.2.

8.3.2 Significance and effective direction of process parameters

In many experiments process parameters are investigated individually and variation is done one factor at a time (OFAT). By this, the significance of parameters amongst each other is hidden and it is not clear if interactions, which is the influence of a parameter's level on the effect of another parameter, exist. An example may be the effect of injection speed on cell structure formation. In low-pressure procedure it is rated as a major influence. But, by applying packing pressure, its influence is expected

to be overlaid and to be much smaller / negligible (see chapters 8.2.2 and 8.3.3) due to decoupling of filling and foaming. By variation of one effect after another, the effect of packing pressure level on the effect of injection speed may not be respected and interactions may not be quantified.

An experiment using the improved mold was designed to judge the influence of core-back parameters by simultaneous variation of process parameters by using PC-ABS/N₂. Design of experiments (DoE) was used to allow a statistical analysis of the correlations and interactions. Based on pre-experiments, a full-factorial design including 4 factors at 2 levels, including a center point was set up. A geometry exhibiting an initial wall thickness of 1.5 mm and additionally 2 mm of initial rib height was set as basic position. The core-back operation has been executed by the mold; thus, the rib section has been expanded. After the first analysis of the DoE, non-linearity of effects have been observed and the experimental design has been extended by adding face-centered star points to be able to describe the non-linearity of effects. Thus, in total 18 experiments (runs) have been performed. Table 2 depicts the parameter and their settings (the resulting runs are listed in Figure 126 in the appendix).

Table 2: Parameter settings used for experiments (DoE); material: PC-ABS/N₂

Parameter	Abbreviation	Setting (min -/ max)
injection speed [cm ³ /s]	v _{inj}	200
packing pressure [MPa]	p _{pack}	900
melt temperature [°C]	T _{melt}	290
mold temperature [°C]	T _{mold}	90
expansion ratio [%]	ER	200 / 300
expansion / opening speed [mm/s]	v _o	10 / 100
packing time [s]	t _{pack}	1 / 3
blowing agent content [wt% N ₂]	bac / SCF*	0.2 / 0.5

*SCF = Supercritical fluid = amount of physical blowing agent

To reduce to number of experiments, packing pressure and injection speed have been set to constant values here. The effect of packing pressure is worked out separately by experiments done with a visualization mold, conducted at the University of Toronto and in an additional pressure study; both results are discussed in chapter 8.4. Injection speed is not respected here, because in HP-VE-FIM pre-

experiments it just showed a negligible effect on structure in HP-VE-FIM (analyzed by light microscopy). However, this parameter is discussed separately in chapter 8.3.3.

The parts have been cut, and final structure of the 10 mm rib was analyzed by SEM and light-microscopy. For evaluation, cell sizes in the core area were measured. Figure 90 shows cell sizes for selected settings, depicted as boxplots. Each individual boxplot contains the results of 140 to 300 cells, evaluated at three different parts. The range of the boxes and the vertical lines are an indicator for deviation of values. Small boxes and short lines demark a narrow distribution of cell sizes, while a big range represents a wide distribution. Significant differences between the parameter settings can be seen. The biggest cells (median $\sim 160 \mu\text{m}$) with a huge deviation are observed for setting “A2” while the smallest cells (median $\sim 15 \mu\text{m}$) with the smallest deviation are observed for “B1”. Thus, the parameter variations resulted in a variation of cell size by the factor of 10.

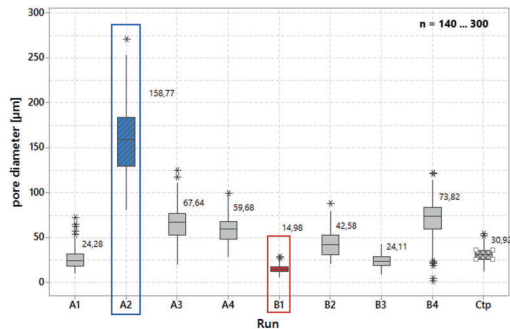


Figure 90: Cell size in the core-region of the 10 mm rib, results for selected parameter settings; (the boxes depict 50 % of the measurement values; the horizontal lines within each box mark the median value; the vertical lines highlight the maximum and minimum deviation, and the stars depict statistically calculated outliers) (results also published in [129, 130])

In the statistical analysis it became evident that all investigated process parameters are rated to be significant in term of the result “cell size”. However, a in parts strong non-linearity is on hand displayed by the central point being located far away from linear regression line.

Figure 91 summarizes the results in terms of response surface plots. The scale of cell size is the same for all plots; thus, the height of effects may be compared. While blowing agent content (SCF) and packing time (t_{pack}) exhibit a linear influence,

opening speed (v_o) and the expansion ratio (ER) show a non-linear effect. Expansion ratio, opening speed and blowing agent content are the most significant parameters for cell size (chronological order). An increase in blowing agent content or opening speed leads to a reduced cell size while an increase in expansion ratio affect the cell size contrary. Packing time is also a significant effect, but for the set level of packing pressure affects the cell size in a minor way.

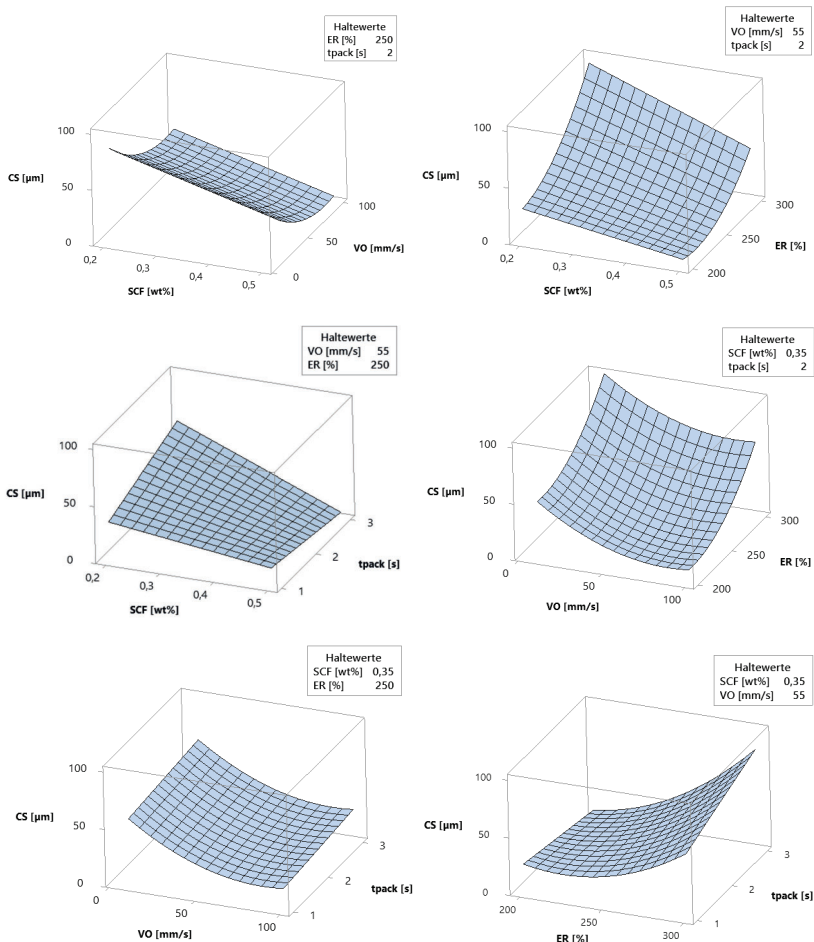


Figure 91: Response surface plots for cell size in the core region of the 10 mm rib; CS = cell size, v_o = opening speed, ER = expansion ratio, tpack = packing time

Figure 92 displays the statistically significant interactions. In principle these results may also be seen in the response surface plots, however, the effect of one parameter’s level on the result of another parameter variation can be seen more clearly here. For the interaction of blowing agent content and expansion ratio mainly the level of cell size is shifted by the expansion ratio. The effective direction is equal, and the rating is similar. For low expansion ratios expansion volume is limited, thus lower cell sizes result for lower levels. In terms of the interactions of packing time with blowing agent content or expansion ratio, a slightly change of effective direction of these parameters in dependency of the level of packing time is observed. A higher packing time supports the decreasing cell size for a high blowing agent content. However, for low blowing agent content, the assessment is contrary. For the expansion ratio – packing time interaction, also a change of assessment can be seen within the investigated process window (around ER 225 %). These results highlight the complex interaction of process parameters.

It should be noted here that the set process parameter levels (set melt and set mold temperature, set packing pressure) and resulting process values (viscosity, melt temperature and pressure) are not constant during procedure. With exception of viscosity they decrease by time. Thus, they are rated to be a co-variant of packing time.

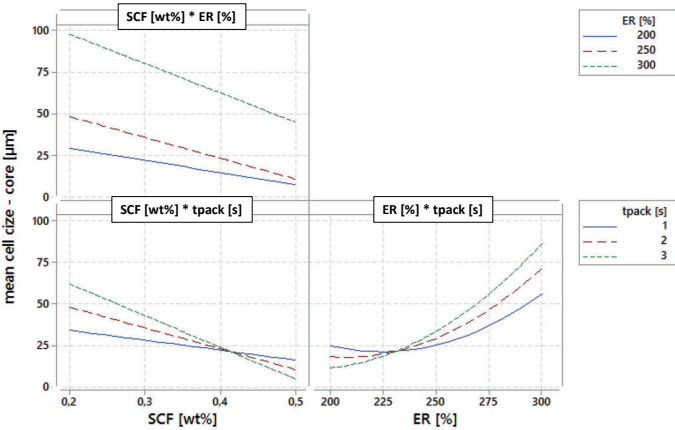


Figure 92: Interaction plot for mean cell size (fitted means) based on cell size measurements in the core area of the 10 mm rib

8.3.3 Significance of injection speed

This chapter deals with the significance of injection speed in terms of final structure formation in high-pressure procedure with mold volume expansion. As already mentioned, the effect of injection speed on the final foam structure is expected to be different in low- and high-pressure procedure. Injection speed is a major process parameter defining the cavity pressure and pressure drop rate. In HP-VE-FIM the procedure and cavity pressure is different by using a later sop and by the use of a packing phase. Thus, effect of injection speed may be overlaid by procedure-specific parameter effects.

While the effect of injection speed on the final foam structure in low-pressure procedure is well discussed in literature (see chapter 8.2.2), it's influence in high-pressure procedure is only minor discussed. To the author's hypothesis, the effect of injection speed may negligible if filling and foaming are decoupled by using an adequate packing pressure phase.

In his investigations with core-back (precision mold opening), Rohleder [18] claims that injection speed influences the gradient of morphology along the flow path [18]. By using core-back procedure, he mentions a wider process window as well a more uniform density distribution but concludes its influence on process-property-relationship as low (see [18] p. 164). For an increasing injection speed, he found an increasing cell size as well a gradient of cell size and skin layer thickness which both decrease by increasing injection speed [18]. However, it is not clear which processing parameters he exactly used and if packing pressure has been applied. Shaayegan did high-pressure foam injection molding experiments without mold opening [21]. He used a PS/3wt%CO₂ and a packing pressure of 8 MPa for 1 s. For a position near the gate he observed re-dissolving of gate-nucleated cells before shrinkage effects took place and evolution of cells started. He found that a variation of injection speed (25 to 50 cm³/s) did not affect the overall cell density, but cell growth rate [21]. However, this result cannot directly be transferred to high-pressure procedure in combination with mold opening. While high-pressure procedure without cavity volume expansion is driven by cell growth due to slow pressure drop, high-pressure procedure with cavity volume expansion is driven by nucleation due high pressure drop rate.

Density distribution

According to the experiments on the influence of injection speed in low-pressure procedure, also high-pressure experiments with variation of injection speed have been conducted. For the experiments, shown in this chapter, samples were produced by mold opening, instead of core back. Initial part thickness (cross section) was expanded from 3 mm to 6 mm by an opening stroke of the mold at an expansion speed of 20 mm/s, conducted via the injection molding machine. Thus, the full part volume (excluding fan gate) was expanded by $ER = 2$. Packing pressure was set to 80/60 MPa for 2 s, while injection speed was set to 50, 125 and 200 cm^3/s (for details on process parameters see Figure 124) in the appendix. Figure 93 and Figure 94 compare the morphologies and resulting density profiles based on three morphologies manufactured with minimum (50 cm^3/s) and maximum (200 cm^3/s) injection speed settings. A uniform cell structure with a sharp transition of compact skin layer to the foamed core region can be observed. The overall density (including skin layer) slightly increases by flow length and exhibits a deviation of 4.5 % (50 cm^3/s) to 8.0 % (200 cm^3/s). Except of a slight difference in density values near the gate, the overall densities are similar for both injection speed settings.

- ⇒ As already show in chapter 6.3, in contrast to low-pressure procedure, the overall morphology and density distribution is not affected by position.
- ⇒ No significant effect of injection speed on density profile can be observed.

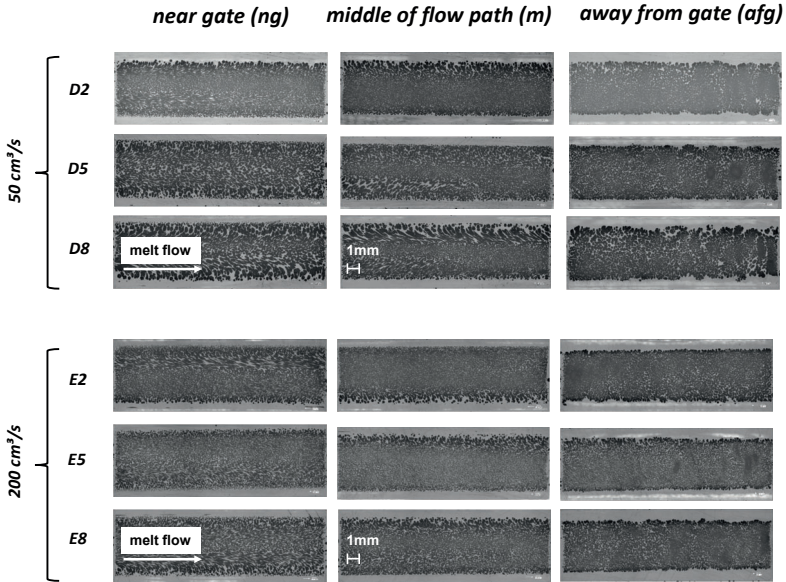


Figure 93: Morphology of high-pressure mold-opening molded samples (material = PC/N₂, $\rho_{pack} = 2 \text{ s}$ @ 80 / 60 MPa); upper: $V_{inj} = 50 \text{ cm}^3/\text{s}$, lower: $V_{inj} = 200 \text{ cm}^3/\text{s}$

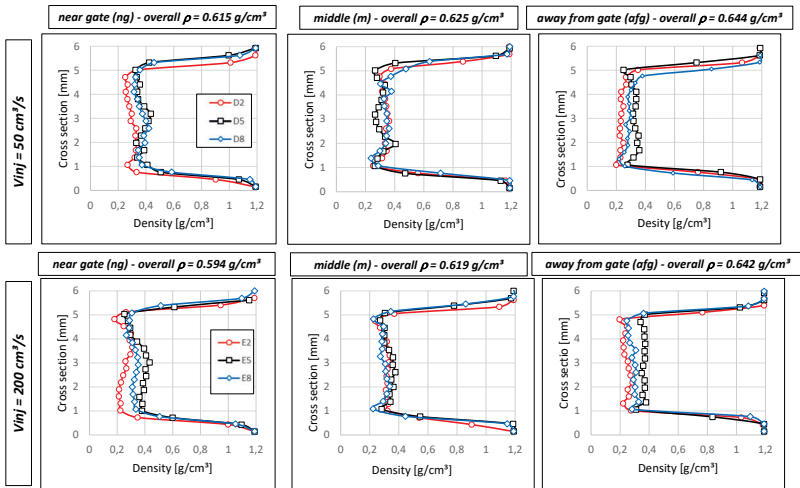


Figure 94: Density profiles of high-pressure mold-opening molded samples (material = PC/N₂, $\rho_{pack} = 2 \text{ s}$ @ 80 / 60 MPa); upper: $V_{inj} = 50 \text{ cm}^3/\text{s}$, lower: $V_{inj} = 200 \text{ cm}^3/\text{s}$

Cellular structure and cell size

Figure 95 compares the 3D reconstruction of the core-back samples produced at different injection speeds. For the low injection speed an orientation or elongation of cells close to the compact skin in direction of melt flow and expansion direction is on hand (this point has even been mentioned in chapter 6.3). However, for the high injection speed this effect cannot be seen anymore.

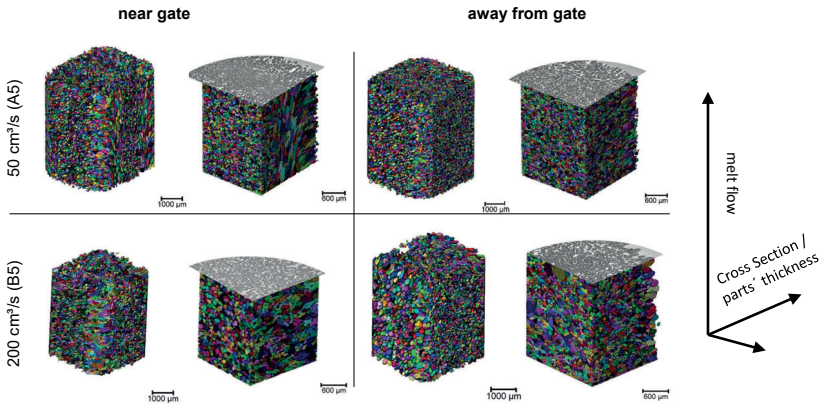


Figure 95: 3D reconstruction of cell volumes of high-pressure mold-opening molded samples (material = PC/N₂, $p_{pack} = 2 \text{ s @ } 80 / 60 \text{ MPa}$): near gate (ng) and away from gate (afg) for two different injection speeds

- ⇒ Independent of injection speed, cell structure is homogeneous and similar for both positions.
- ⇒ In comparison to the low-pressure foam injection molded structures a much more uniform structure with smaller cell sizes can be observed.

Figure 96 depicts the 3D cell volumes in dependency of the position of their barycenter in direction of parts' thickness which corresponds to mold-opening direction. Apart from some bigger cells away from gate at high injection speed, distribution of cell size is very equal for both speed levels. The smallest cells are located in the core region. A sharp transition of size distribution is more pronounced away from gate. However, the low injection speed leads to a higher number of cells and a smaller median cell size compared to the high speed level.

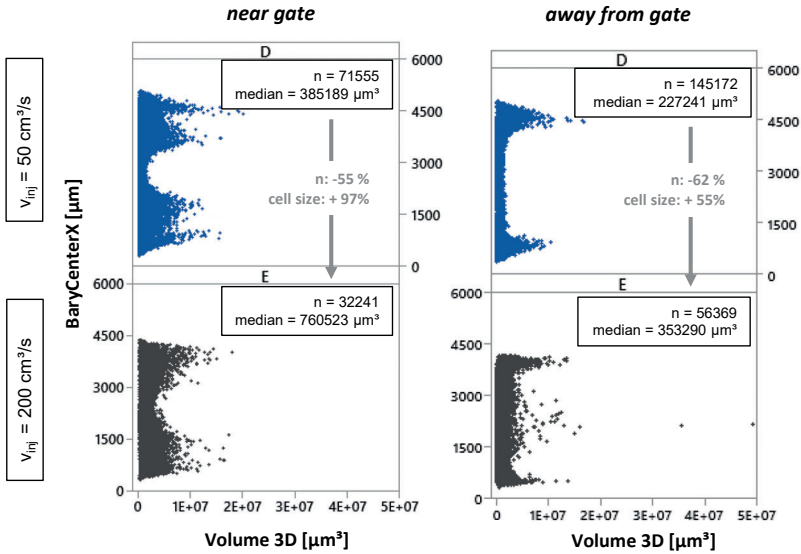


Figure 96: Position of cells' barycenter plotted over 3D cell volume of high-pressure mold-opening molded samples (material = PC/N₂, $p_{pack} = 2 \text{ s @ } 80 / 60 \text{ MPa}$) in dependency of injection speed – data: full cell volume with BVC filter (exclusion of cells which are cut by the borders of the analyzed volumes)

- ⇒ The distribution of cell sizes over parts cross section is quite similar for both speed levels.
- ⇒ Independent of injection speed, more cells and smaller cells (median μm value) are observed away from gate.

Shape of cells

Figure 97 depicts the *Aspect Ratio 3D* in dependency of the position of cell's barycenter. Near the gate, a noticeable trend of cell's shape is observed to correlate on its position. Here, especially for the low speed sample, a wide range of aspect ratios is on hand for the cells close to the skin layer. In the transition zone cells exhibit a higher aspect ratio the closer they are located to the core. This trend is not that pronounced for the high injection speed. Here, a trend of low aspect ratio cells near the skin layer, corresponding with elongated cells (in volume expansion direction), and a wider distribution of values in the transition zone is observed. In the core, for

both speeds, and additionally close to the skin layer for the low injection speed, aspect ratio is maximum, corresponding with a high roundness of cells. Away from gate a similar distribution of values can be seen for both settings. A trend of aspect ratio to increase in direction to the core can be seen. However, a wide distribution of values is on hand for all positions.

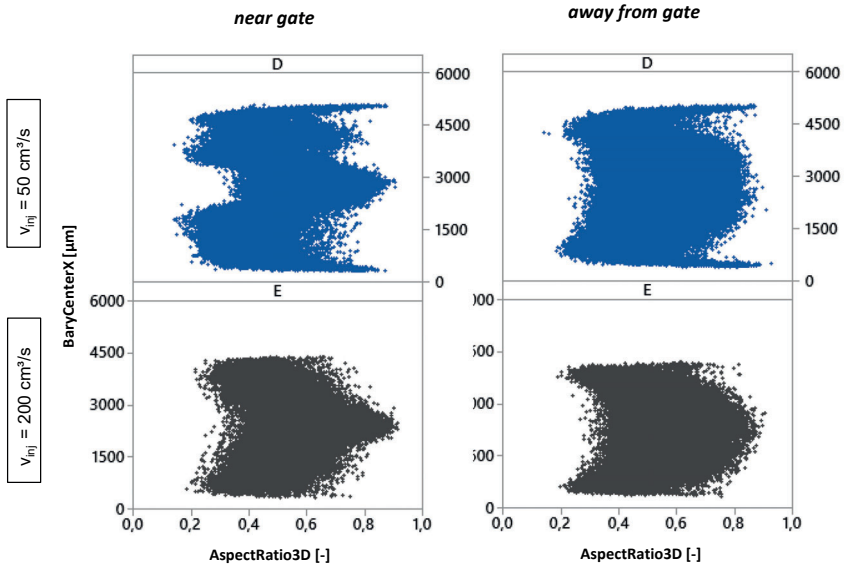


Figure 97: Position of cells' barycenter plotted over Aspect Ratio 3D of high-pressure / mold-opening molded samples (material = PC/N₂, $p_{pack} = 2 \text{ s}$ @ 80 / 60 MPa) in dependency of injection speed; data: full cell volume with BVC filter (exclusion of cells which are cut by the borders of the analyzed volumes)

⇒ The results of this chapter show, that cellular structure in high-pressure / mold opening or core-back procedure is more homogeneous over parts' cross section and less flow-path dependent compared to low-pressure procedure. However, it is affected by the injection phase. This leads to the conclusion that either packing pressure setting was insufficient to completely decouple filling and foaming or once created nucleus are not possible to be „reset“ by packing phase. The latter would lead to two nucleation phases – one during injection and second by pressure drop initiated by cavity expansion. This interpretation is supported by the pseudo-classical nucleation theory, reported in chapter 3.2.3.

Similar results are reported by Flórez Sastre [1]. In these studies a delay time before volume expansion was used, but no uniform density over the flow path could be observed [1]. Instead, density variations of up to 19% from gate to the end of flow path are reported [1]. Nevertheless, it is concluded that compared with foam morphologies produced in low-pressure foam injection molding, core-back molded structures are highly uniform and reproducible [1].

8.4 The role of packing phase in high pressure procedure with mold volume expansion

The effect of packing phase on cell size, cell density and homogeneity of structure is widely unknown. Within the plasticizing process, dissolution of gas in polymer melt is supported by stretching and shearing elements, leading to a reduction of diffusion path (see [51]). Instead, inside an injection mold, dissolution of cells can only be accomplished by pressure.

In high-pressure foam injection molding with volume expansion (HP-VE-FIM) experiments described in literature, it is often not clearly defined if packing pressure was applied or not. Sometimes, delay time before mold volume expansion is mentioned without making a statement if this was done pressure-less or by applying packing pressure. By applying packing pressure, it is investigated that the expanded gas may be forced back into solution, as discussed in chapter 6.2.1. If this was successfully done, a “reset” of injection-defined cell formation is supposed. This may lead to a more uniform structure within the final part.

As already discussed in chapter 6.2.1, in the last years only a few investigations dealt with the effect of packing phase in terms of re-diffusion of early nucleated cells. However, it is unknown which conditions are necessary to force early nucleated cells back into solution for a non-investigated injection mold. The geometrical conditions and process parameter define the resulting physical values inside the mold. The amount of gas defines the solubility pressure level, needed for re-diffusion of gas and the material defines the diffusion rate. Besides the unknown dissolution times, it is not known if the same status of melt-gas mixture may be achieved like it is on hand within the plasticizing unit. Furthermore, it is not clear how big the influence on final

structure is, if cells are completely dissolved or not and which role is played by the initial level of cavity pressure before volume expansion operation.

The content of the following chapter is based on collaborative HP-MO-FIM experiments using a visualization mold (chapter 8.4.1 and chapter 8.4.2) and HP-CB-FIM experiments using the new core-back mold (chapter 8.4.3 and chapter 8.4.4) built and introduced in this thesis.

The visualization experiments were executed at the Microcellular Plastics Manufacturing Laboratory (MPML), University of Toronto conducted by the author of this thesis and Dr. Shaayegan (MPML). The final cellular structures were analyzed via SEM (MPML) and exactly the same samples were also analyzed with μ CT (at the Institute of Materials Engineering, Polymer Technology, University of Kassel). The results of this collaboration are already published in the Journal Polymer ([83]). Chapter 8.4.1 and chapter 8.4.2 are in principle a summary of the findings.

8.4.1 Evolution of cells during filling and packing phase

The following subchapter is based on results worked out in the own publication: [83].

A Polystyrene-blowing agent mixture (MuCell© technology) has been processed in HP-MO-FIM experiments within two individual experimental series, using 3 wt%CO₂ as well 0.3 wt%N₂. The mold opening operation has been realized by the clamping unit of the injection molding machine and in-situ visualization technique was used to monitor and study the formation and evolution of cells during the mold-filling and melt-packing phases. The mold was equipped with a prism insert and a high-speed camera. The cavity was filled via a fan gate and molds a rectangular plate with dimensions 135 mm x 111 mm and an initial thickness of 3.2 mm. The mold opening distance was set to 3 mm, resulting in a final part thickness of 6.2 mm at an expansion speed of 20 mm/s. However, the mold has not been equipped with shearing edges, thus after cavity expansion melt was able to flow into the mold parting line, resulting in not accurately shaped cavity dimensions. More details on the visualization mold appear elsewhere [160] and in the appendix (Figure 142).

Based on preliminary experiments, a DoE (full factorial design) with 3 factors at 2 levels, a central point, and 6 face-centered points has been designed (16 runs including a repetition of the central point). A variation of melt temperature, packing pressure level and packing time has been executed. The cavity was filled volumetrically, followed by packing phase and mold opening operation. For more details on the individual process parameter settings please refer to Figure 127 in the appendix.

Figure 98 depicts cavity pressure profiles of the experimental trials recorded for PS/CO₂. The minimum, medium, and maximum packing pressures and packing time conditions used within the experiments are highlighted here. While for the strongest packing condition the cavity pressure before mold opening maintained well above the solubility pressure of the dissolved CO₂, for the other packing conditions cavity pressures were either lower or close about the solubility pressure of the PS/CO₂ mixture.

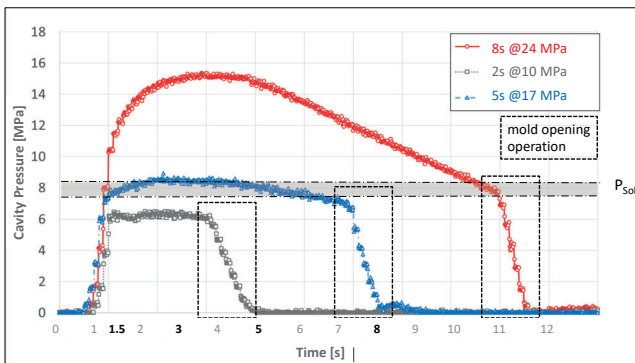


Figure 98: Cavity pressure profiles at the middle of the mold cavity for various packing conditions (PS/3wt% CO₂, $T_{melt} = 220$ °C; dynamic solubility pressure of CO₂ in PS (p_{Sol}) was estimated $\sim 7.8 - 8.4$ MPa; “MO” denotes “mold opening” in the figure) (results also published in [83])

The videos were taken at the middle of flow path and recorded the whole cycle from start of injection up to mold opening operation. Thus, the melt flow and formation of cells could be observed for this time. By mold opening operation, immediately a huge number of cells have been nucleated simultaneously and quickly reached a balanced cell size at the glass window. Thus, any further analysis on the evolution of cells inside the part has been prevented. Visualization snapshots were extracted from the videos (Image J) and tracked cells were analyzed in terms of its characteristics (Adobe Photoshop®). Here, two characteristics have been measured: *Cell area* as an indicator

for cell size and *Circularity* as an indicator for cells' deformation. *Cell area* refers to the area inside a selected cell, while *Circularity* is defined the following: $Circularity = \frac{4 * \pi * Cell Area}{(Cell Perimeter)^2}$, thus that an ideal circular cell exhibits the maximum value of 1.

Video analysis

Figure 99 shows visualization snapshots of high-pressure foam injection molding experiment with a) low (10 MPa) and b) high (24 MPa) packing pressure, applied for 8 s, followed by mold opening for a PS/3wt%CO₂- mixture. For the low-pressure level, cells remained undissolved in the system during packing phase. For the high-pressure level, no more cells could be observed in the system before mold opening. The size and the shape of the cells, which had been created during the mold-filling phase, changed by time. This was confirmed by tracking cells which remained within the visualization area during their deformation. This general trend has been observed in most trials within the experiment.

⇒ The video analysis in general showed that an increase in packing pressure and packing time resulted in smaller cell sizes and larger deformed cells. Sufficient packing conditions removed all cells (not visible anymore in the videos) and may have re-dissolved them back into the melt before mold opening operation.

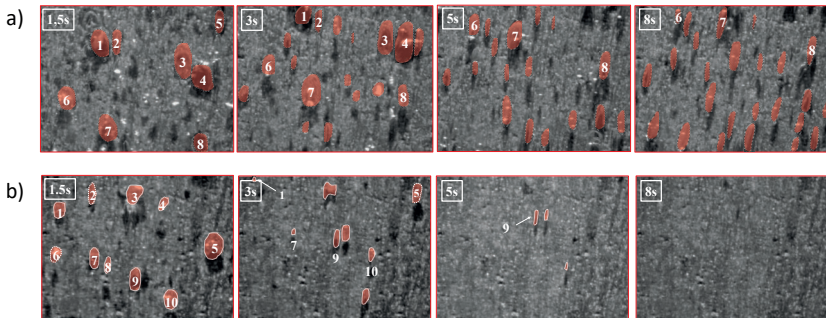


Figure 99: Visualization snapshots with highlighted cells from HP-MO-FIM of PS/CO₂ during the mold filling and packing at T_{melt} : 230 °C: a) packing: 10 MPa for 8 s, b) packing 24 MPa for 8 s; the time reference is the moment melt/gas mixture entered the mold cavity; the cells are highlighted with red color for clarity (results also published in [83])

Cell Area and shape of cells

A general decrease in Cell area by time could be detected for the most trials. However, for some settings their size remained constant from a packing time of 5 s. Figure 100 shows measurement results for Cell area over time for experiments conducted with a packing time of 8 s at various packing pressure levels. For packing pressures of 17 and 24 MPa, the cell size was reduced. However, for 10 MPa, the reduction in cell size is not that pronounced. No more cells have been observed in the trials using 24 MPa packing pressure for 8 s, indicating that packing pressure level and time were sufficient to re-dissolve all cells (as shown in Figure 99 b)). For the other runs, the cell area was reduced, but nucleated cells could sustain the cavity pressure and could be tracked until the mold-opening operation.

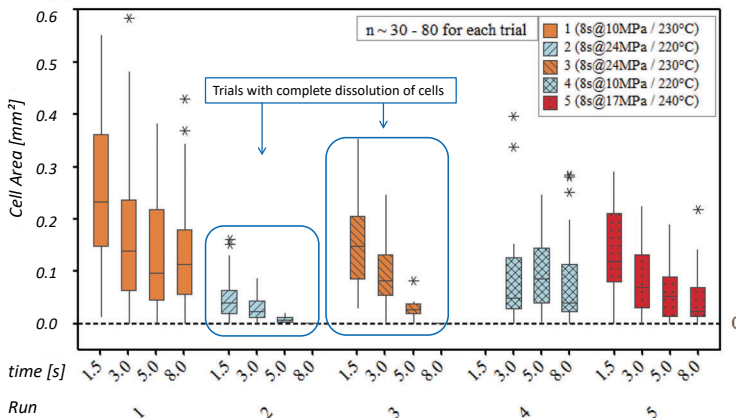


Figure 100: Boxplot of Cell area at different time steps for all experiments with $t_{\text{pack}} = 8$ s (n is the number of cells investigated for each condition); (the boxes depict 50 % of the measurement values; the horizontal lines within each box mark the median value; the vertical lines highlight the maximum and minimum deviation, and the stars depict statistically calculated outliers) (results also published in [83])

The statistical analysis of the DoE (including all 16 runs) in terms of response surface plots for Cell area is shown in Figure 101. This type of figure displays the synergistic influences of the process parameter settings on the measured response. It can be seen that cells' size was reduced by using a higher packing pressure (p_{pack}) or by using a longer packing time (t_{pack}). For higher melt temperatures, however, a smaller

reduction in cell size is identified. This effect may be caused due to the fact that an increasing melt temperature leads to a decrease of CO₂'s solubility in the polymer melt (see [57]). Thus, the applied packing pressure is supposed not to be as effective in dissolving cells inside the melt as it is using a lower melt temperature.

⇒ The results also show that the packing pressure level is rated as the most significant effect on the cell size, compared with packing time and melt temperature.

⇒ No significant interaction was evaluated between the parameter settings.

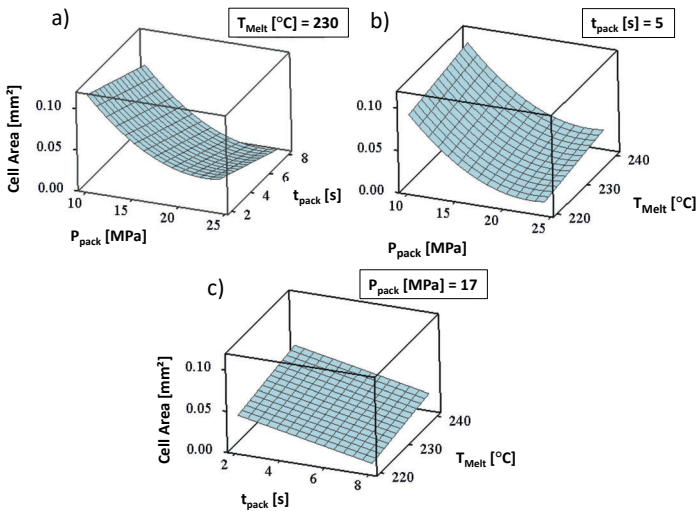


Figure 101: Response Surface Plots (full quadratic analysis): Effects of processing parameters on the cell area: a) synergistic effects of packing pressure and packing time, b) synergistic effects of packing pressure and melt temperature, c) synergistic effects of packing time and melt temperature; (The cell area measurement was done at the end of the packing phase, right before the mold opening. The quality of regression model: $R^2 = 90.88\%$.) (results also published in [83])

The in-situ visualization results show that the majority of cells have continuously been elongated in direction of melt flow during filling and packing phase. To quantify this effect, Circularity value has been analyzed in the same way as it has been done for the Cell area. Figures for this result are omitted here and can be found elsewhere: [83]. It became evident, that the effects of the packing pressure and the packing time were highly non-linear, displaying a peak value. The non-linearity is expected to be attributed to the complicated cell deformation and cell dissolution phenomena in the

melt/gas mixture at various packing conditions. It needs to be noted that cavity pressure constantly changed during the packing phase, despite packing pressure was set as a constant value by the machine. This fact might be the reason why the constant shape of the cells could be observed between 5 s and 8 s of packing in some experimental trials and may explain the considerably non-linearity of effects.

Cell decrease rate

Based on the measured Cell area for the video snapshots before mold opening (individual time for the different packing times) and the measured Cell area 1.5 s after start of injection, a Cell decrease rate as an indicator of dissolution speed has been calculated and statistically analyzed. Figure 102 shows the main effect plot for the cell decrease rate. All parameters show the same effective direction, namely the higher the parameter setting, the faster the decrease of the cells is. Packing pressure is rated to be the most significant effect on cell decrease indicating that it is the most significant factor for the re-diffusion process. This result is supported by the statement given in [58] of a short packing time at high pressure levels to support the dissolution of gas due to higher gas permeability.

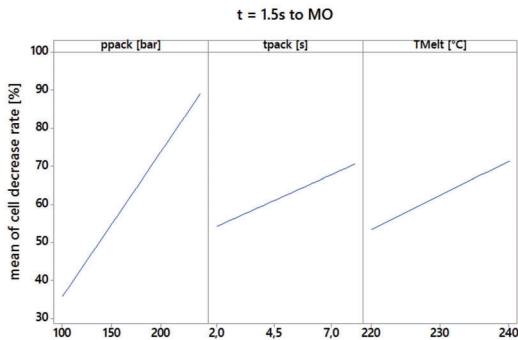


Figure 102: Main effect plot for cell decrease rate calculated for the time between 1.5 s after start of filling and the timestep before mold opening operation

But also, interactions exist, meaning the setting of one parameter influences the result of another parameters' setting (Figure 103). In detail, the magnitude of effect by the packing pressure depends on the melt temperature. The higher the melt

temperature, the smaller the effect of the packing pressure on the cell decrease rate. This may also be attributed to the aforementioned fact of a decreasing solubility of CO₂ for increasing melt temperatures (see [57]). However, it is still unknown or not investigated if a high pressure applied for a short time may be equal in its result compared to a lower pressure applied for a longer time. Maybe the “executed work” of pressure, described by the integral value below the cavity pressure curve is the value to be crucial here (equal integral value = equal work).

⇒ It has been shown that an increase of packing pressure, packing time and melt temperature supports re-diffusion process

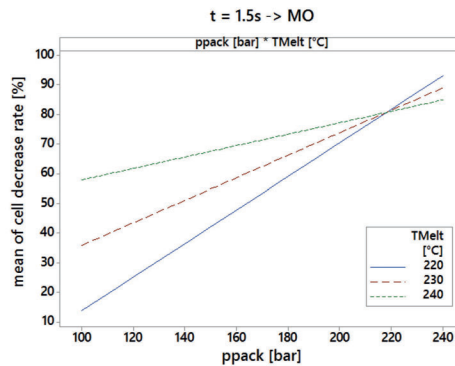


Figure 103: Interaction plot for cell decrease rate calculated for the time between 1.5 s after start of filling and the timestep before mold opening operation; an interaction of packing pressure and melt temperature exists, meaning that the level of melt temperature affects the effect of packing pressure

8.4.2 Effect of packing pressure on final cell structure

The following subchapter is based on results worked out in the own publication: [83].

For the analysis of the final cell structure three runs were chosen which cover the range of the designed experiment: (a) $p_{\text{pack}} = 10$ MPa for 2 s; (b) $p_{\text{pack}} = 17$ MPa for 5 s, and (c) $p_{\text{pack}} = 24$ MPa for 8 s. These runs represented the minimum, the medium, and the maximum packing condition used in the PS/CO₂ experiment (see Figure 98). The analysis was conducted by both, SEM and μ CT.

For the setting of 10 MPa packing pressure applied for 2 s, large voids and cavities could be observed in the SEM images. This structure consisted of the cells that nucleated during the mold filling and remained in the system as well the cells that were nucleated through the pressure drop induced by mold opening. Here, undissolved cells have been observed by visualization. It is assumed that these cells coalesced and deformed during mold opening, resulting in the formation of large voids and cavities (Figure 104 a). For the setting of 24 MPa packing pressure applied for 8 s, a uniform and fine-celled structure is on hand (Figure 104 c)). Here, the visualization results verified that most of the nucleated cells had been removed prior to mold opening. The cavity expansion induced a second pressure drop enabling a simultaneous cell growth, resulting in smaller cells and a higher cell density. In addition to the different conditions in the melt before mold opening, the pressure drop rates for both settings are different. An analysis of the cavity pressure profiles (see Figure 98) showed the fastest pressure drop (~ 13 MPa/s) for the strongest packing condition (compared to ~ 7 MPa for the weakest condition). This may also support nucleation mechanism for the strong packing condition.

But it should be noted that the melt temperature was different at the point in time of mold opening when using 2 s or 8 s melt packing. Thus, the melt was at a higher temperature after 2 s of packing compared to 8 s of packing. This may also have supported the coalescence in structure shown in Figure 104 a).

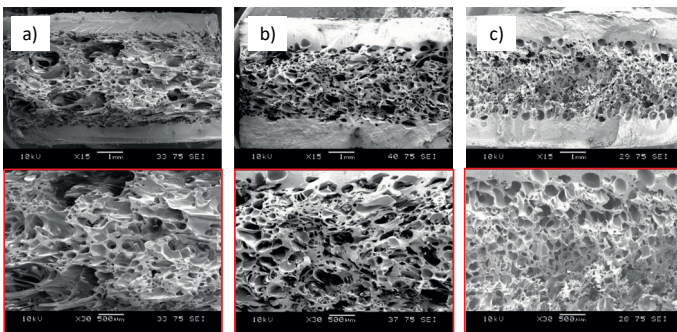


Figure 104: SEM micrographs for HP-MO-FIM of PS/CO₂: a) packing: 10 MPa for 2 s: cell density: 2.5×10^5 (#/cm³), b) packing: 17 MPa for 5 s: cell density: 6.8×10^5 (#/cm³), c) packing: 24 MPa for 8 s: cell density: 1×10^6 (#/cm³) (Injection rate: 80 cm³/s; CO₂: 3wt%; T_{melt}: 220 °C; The samples were cut from the middle of mold cavity) (results also published in [83])

For the μ CT analysis, exactly the same samples that are shown in Figure 104 were used for evaluation. Figure 105 shows the 3D reconstruction of the cell volumes based on the tomographical data. The skin-close cells for a low packing pressure of 10 MPa for 2 s and 17 MPa for 5 s (Figure 105 a) and b)) were in parts elongated and exhibited a sheared structure in direction of melt flow. This effect could not be observed to be pronounced for cells that were generated using a high packing pressure of 24 MPa applied for 8 s (Figure 105 c).

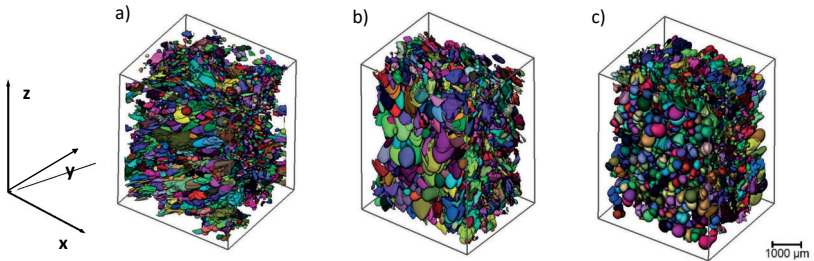


Figure 105: 3D reconstruction of μ CT-data of HP-MO-FIM of PS/CO₂, segmentation of full-cell volume between compact skin layers by using BVC filter to exclude cell fragments: a) packing pressure of 10 MPa for 2 s, b) packing pressure of 17 MPa for 5 s and, c) packing pressure of 24 MPa for 8 s (Injection rate: 80 cm³/s; CO₂: 3wt%; T_{melt}: 220 °C; Y: mold-opening direction; Z: melt-flow direction) (results also published in [83])

In order to achieve a more detailed description of structures, the cell volumes (of each individual cell) have been plotted over its barycenter position in the “y direction”, representing the specimen’s cross section corresponding to the mold-opening direction. As it was depicted for the similar analysis shown before, the depiction includes the unfoamed skin layers.

Figure 106 shows the scatterplots for the three investigated runs. For the sample produced with a low packing pressure of 10 MPa for 2 s (Figure 106 a)), the majority of the cells exhibit a small volume, but also an immense cell volume scattering by trend of bigger cells located in the core area is observed. This indicates the presence of an inhomogeneous structure with some larger voids. For the samples produced with a higher packing pressure and a longer packing time, less scattering in cell volume values is on hand, indicating a more uniform structure. For the strongest packing condition of 24 MPa for 8 s (Figure 106 c), just a few large cells could be observed. The distribution of cell sizes is very equal over the part’s thickness,

indicating a negligible gradient in cell size by cross section. These results show a good agreement to the SEM observations shown in Figure 103.

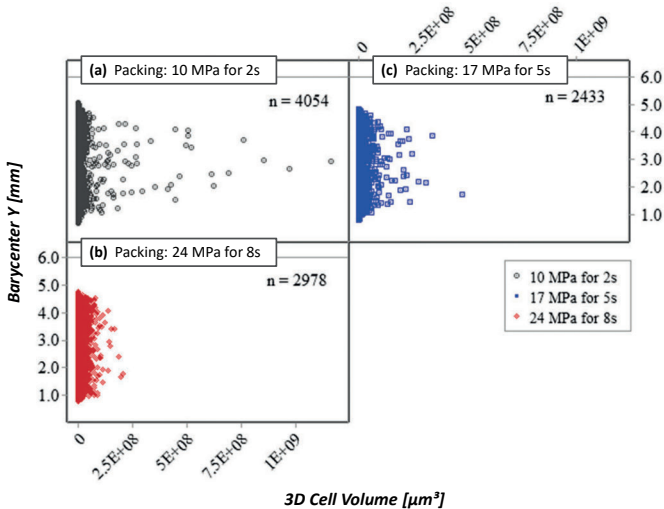


Figure 106: Scatterplot of cell volumes for HP-MO-FIM of PS/CO₂ in dependency of cells' barycenter in "y" direction (mold-opening direction) according to Figure 105 for: a) packing: 10 MPa for 2 s, b) packing: 17 MPa for 5 s, c) packing: 24 MPa for 8 s (results also published in [83])

Similar experiments have been conducted by using a PS/0.5wt%N₂ mixture. By the higher solubility pressure of N₂ in PS compared to that of CO₂, a higher packing pressure combined with a longer packing time may be required to re-dissolve nucleated cells back into the melt. In analogy to the experiments with PS/CO₂, in the following also three experimental settings are discussed, representing the minimum, medium and maximum packing condition. A re-dissolution of nucleated cells before mold opening occurred for the maximum packing condition, ensured by visualization of the experiments. In general, the cellular structure was much finer compared to the PS/CO₂ samples. This is attributed to the higher nucleating efficiency of N₂ as blowing agent, than that of CO₂.

The weakest setting of 20 MPa for 4 s produced a non-uniform cellular structure with large voids and cavities (Figure 107 a)). Applying 30 MPa for 6 s resulted in a finer-celled structure with less voids, however cells are still on hand (Figure 107 b)). The strongest packing condition of 40 MPa for 8 s resulted in a more uniform cellular structure with smaller and fewer cavity voids (Figure 107 c)). For the settings not

displayed here, it can be summarized that a longer packing time even for low packing pressures improved the cellular structure's uniformity and removed big cavities.

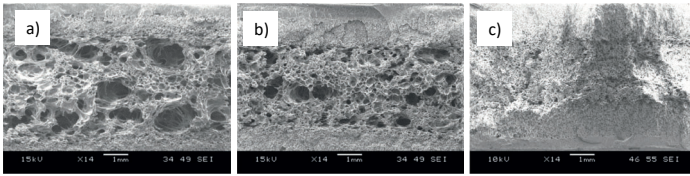


Figure 107: SEM micrographs for HP-MO-FIM of PS/N₂: a) packing: 20 MPa for 4 s, b) packing: 30 MPa for 6 s, c) packing: 40 MPa for 8 s (here, all nucleated cells disappeared during the mold filling); (Injection rate: 80 cm³/s; N₂: 0.5wt%; T_{melt}: 240 °C) (results also published in [83])

Also, for the PS/N₂ experiment, exactly the same shown in Figure 107 were analyzed by μ CT. Figure 108 displays the 3D reconstruction of the tomographical data in analogy to the previous depictions within this chapter and Figure 109 shows the corresponding scatterplots.

A packing pressure of 20 MPa applied for 2 s (Figure 108 a)) lead to a structure with an immense scattering of cell volume, indicating an inhomogeneous structure with large voids. Applying a higher packing for a longer time, less scattering can be seen in the cell volume values. The strongest packing condition of 40 MPa for 8 s (Figure 108 a)), resulted in a structure of very equal cell volumes. This indicates a more homogeneous structure over the part's thickness, with a negligible cell size distribution. As it has been shown in the analysis of the PS/CO₂ experiments, these results also confirm the observation of the SEM images shown in Figure 107. In analogy to the results of the PS/CO₂ system (Figure 106), the same trend, which is the formation of a more homogeneous cell size distribution over the parts' thickness by using a proper packing pressure/packing time combination also became evident. However, the trend was much sharper in the PS/N₂ system (Figure 109). A pronounced elongation of skin-close cells in direction of melt flow for weaker packing settings cannot be detected for the PS/N₂ system.

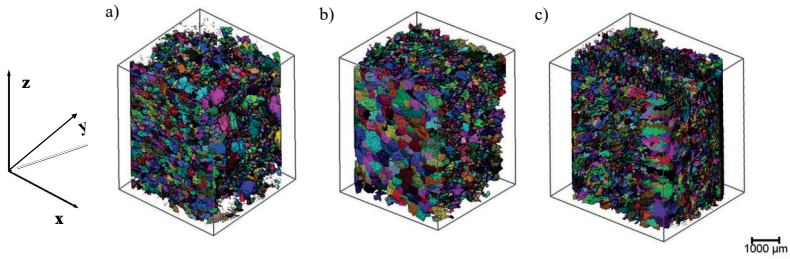


Figure 108: 3D reconstruction of μ CT-data for HP-MO-FIM of PS/ N_2 , segmentation of full-cell volume between compact skin layers by using BVC filter to exclude cell fragments: a) packing pressure of 20 MPa for 4 s, b) packing pressure of 30 MPa for 6 s and c) packing pressure of 40 MPa for 8 s (Injection speed: 80 cm³/s; N_2 : 0.5%; T_{melt} : 240 °C; y: Mold-opening direction; Z: Melt-flow direction) (results also published in [83])

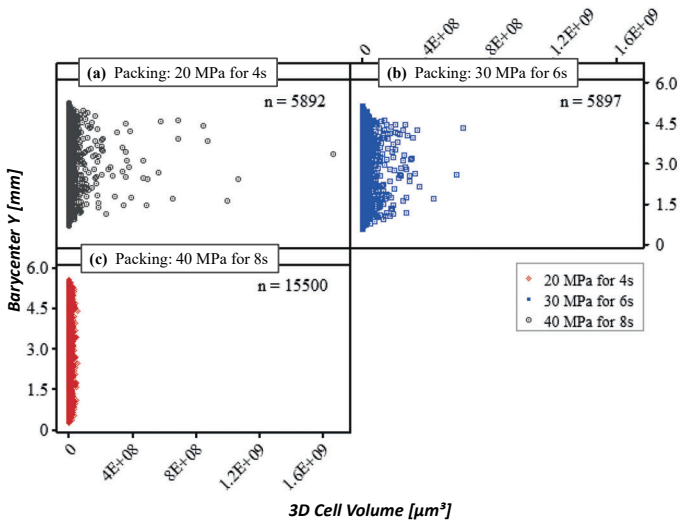


Figure 109: Scatterplot of cell volumes for HP-MO-FIM of PS/ N_2 in dependency of its barycenter position in “y” direction (mold-opening direction) according to Figure 108: a) packing: 20 MPa for 4 s, b) packing: 30 MPa for 6 s, c) packing: 40 MPa for 8 s (results also published in [83])

⇒ To summarize the findings of this subchapter it became evident that a complete dissolution of the gate-nucleated cells resulted in a more uniform and finer cellular structure after mold opening compared to settings where cells have not been re-dissolved for both the PS/ CO_2 and PS/ N_2 system.

8.4.3 The effect of pressure level

The effect of packing pressure level on final cell structure in core-back foam injection molding is rarely discussed in literature. An influence of increasing packing pressure on a refinement of structure and a more homogeneous density in the core area are also reported in [1] for injection molded foams with a constant density reduction of 20 %; however, packing conditions and further details are not clearly mentioned here.

As mentioned in chapter 6.2.1 an increase in packing pressure level and time is reported to support homogeneity of cellular structure. The presence of remaining cells in the melt prior to cavity expansion resulted in a non-uniform structure, characterized by a mix of bigger and smaller cells [58]. Also, cells were found not to be spherical for this case [58]. An expanded structure based on a single-phase mixture resulted in both, an increased uniformity of small cells and spherical shaped cells [58]. However, a threshold value is reported to exist for the positive effect of packing pressure level [58]. In his experiments with PS/5wt%CO₂ Shaayegan et. al. [58] found an increased cell density up to a pressure of 14 MPa, while higher pressure levels just lead to a negligible effect.

On the one hand, from a distinct pressure level, which is sufficient to force the gate-nucleated cells back into solution, a higher level may not have any more effect on the second cell growth after volume expansion. Cell growth can take effect again when pressure drops below the solubility pressure of the given system, independent of the initial pressure level. On the other hand, it is not clear if cells may be forced back into solution completely or if they just may be shrunked to a size which cannot be detected anymore by the camera systems used within the corresponding investigations. Thus, length and level of pressure to again achieve a single-phase solution is unknown. Furthermore, a higher pressure level may possibly also compress the melt, resulting in a higher PDR by volume expansion / core-back operation.

To investigate the influence of packing pressure level on final cell structure, high-pressure experiments with different levels of packing pressure, followed by mold opening were conducted. The improved injection mold was used to mold a simple rectangular plate (without ribs). After injection and packing phase, the full cavity volume was expanded by $ER = 2$. The Initial part thickness was expanded from 3 mm to 6 mm by an opening stroke of the mold at a speed of 20 mm/s, conducted via the

injection molding machine (for more details on the process settings refer to Figure 125). PC/N2 was used to be able to visually observe the influence of packing phase for the final parts.

To get knowledge about the cell evolution before mold opening, pre-experiments were done without cavity expansion. The parts were produced by variation of packing time and packing pressure, followed by a pressure-less cooling phase. By the help of the variotherm mold temperature control, the surface of the cavity was heated up to 160°C prior to injection. Thus, a silver streaks free surface was created, allowing an easy visual observation on cell formation inside the final parts. If cell formation has been prevented, only some surface defects at the non-heated side could be detected, covering the otherwise transparent PC parts. If cells are on hand, the PC is not transparent anymore. Figure 110 depicts an excerpt of results of this study. For 2 s of packing time (results omitted here) for pressure levels of 20 to 50 MPa parts were not transparent which means that cells are on hand. From a pressure of 60 MPa, PC started to become clear, indicating a re-dissolution of cells during procedure. However, even for 80 MPa still some cells could be observed inside the part. For 4 s of packing time up to 30 MPa, a lot of cells were on hand, the amorphous PC was not clear. Starting from a pressure of 40 MPa the majority of cells was re-dissolved. For 50 MPa a few big cells could be observed maybe occurred by free volume given by shrinkage effects during cooling phase. From 60 MPa the material was clear, and no more cells were observable. For 8 s of packing time, cells were completely re-dissolved for pressure levels higher than 40 MPa.

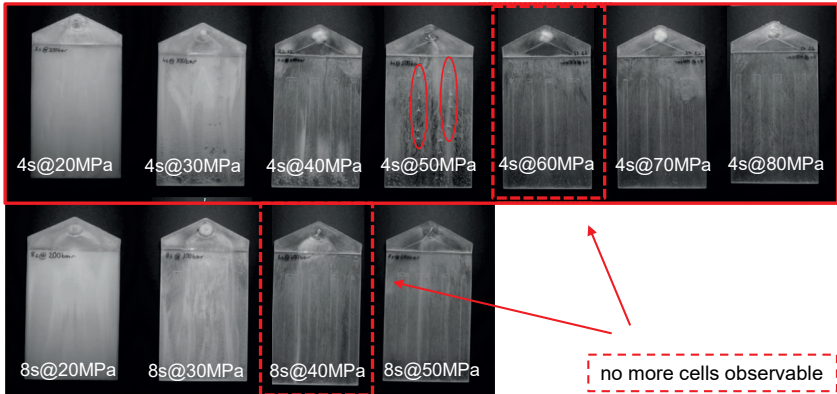


Figure 110: Study on re-diffusion of cells in high-pressure procedure without mold volume expansion; variation of packing pressure level for packing time of 4 s and 8 s; PC/0.3wt%N₂-mixture

Based on this observation, in the mold opening experiments a fixed packing time of 4 s was set and packing time has been varied from 10 to 80 MPa, immediately followed by mold opening operation. However, it should be mentioned that the cavity pressure conditions of the mold-opening experiments do not match the conditions of the pre-experiments. Figure 111 shows recorded cavity pressure data for selected trials of the pre-experiments and the finally chosen settings for the mold opening experiments. Despite packing pressure has also been stopped after the set packing time in the pre-experiments, resulting cavity pressure did not decrease immediately to zero. Instead, a distinct pressure level has been observed until the end of procedure (opening the mold for ejection). Thus, the packing time – packing pressure combinations to force cells back into solution are different and are to be judged as indicative values. Thus, it is not clear if cells were also forced back into solution within the mold-opening experiments.

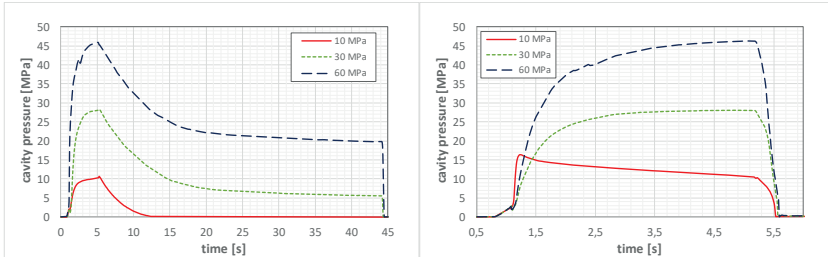


Figure 111: Cavity pressure profiles for chosen trials of pre-experiments (left) and mold-opening experiments with 4 s of packing pressure, expansion speed = 20 mm/s (right) at 10, 30 and 60 MPa

Cellular structure over parts' cross section

The samples were prepared and cut in the middle of the flow path. The whole cross-sectional structure (including the unfoamed skin layers) has been analyzed by μ CT. Figure 112 to Figure 114 show the morphologies (3D reconstructions and SEM) as well the distribution of cell size, represented by *Volume 3D* and *Aspect Ratio 3D* over the parts' cross section.

A trend of cell size to decrease by increasing packing pressure can be observed. Furthermore, the distribution of cell volumes over the cross-section changes by packing pressure level. For low-pressure levels, big cells are located in the core, as it is known from typical low-pressure molded samples with integral structures. From a packing pressure of 30 MPa, a significant change of structure can be seen. The deviation of cell size is much smaller, indicating a much more homogeneous structure. Here, the cell size distribution is inverse and instead of biggest cells in the center (observed for lower pressure levels), now smallest cells can be observed here. This trend is observable up to the highest investigated pressure level of 80 MPa.

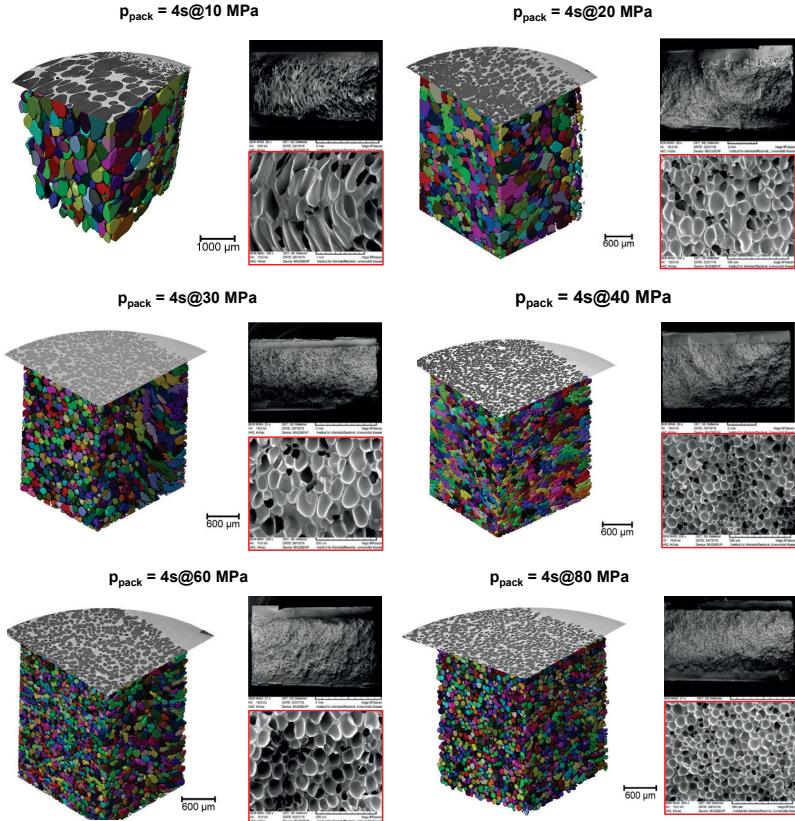


Figure 112: Cellular structure of HP-MO-FIM experiments produced by a packing phase of 4 s and a packing pressure level of 10 to 80 MPa; reconstruction of μCT data and SEM pictures

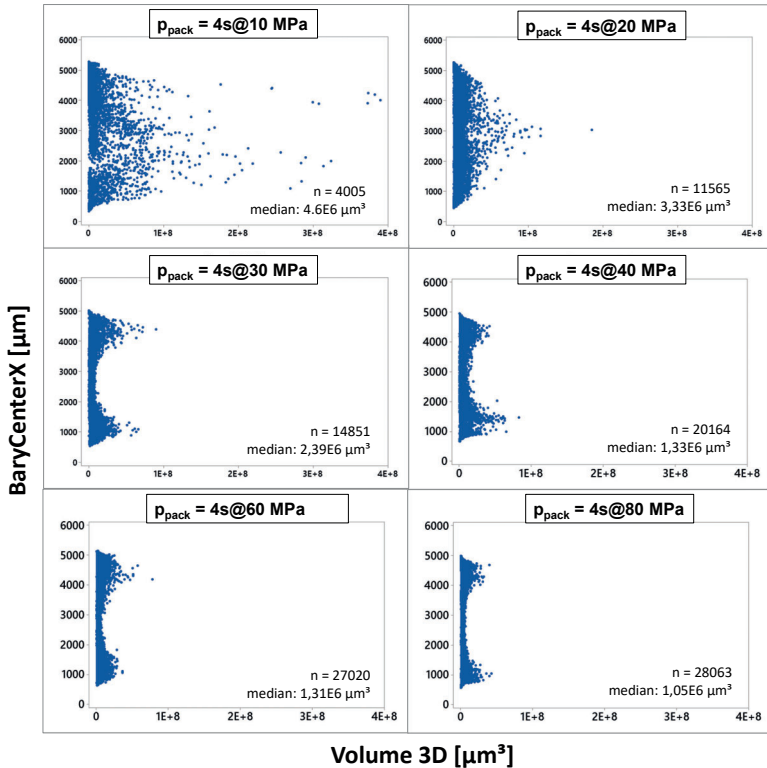


Figure 113: Scatterplots of cell volumes (Volume 3D) plotted over cross section (BaryCenterX) = mold opening direction according to the structures shown in Figure 112

The Aspect Ratio, as an indicator for cells' shape and elongation of cells, also changes by pressure level. Also, starting from a pressure level of 30 MPa, a pronounced trend of cells located in the center to exhibit a high roundness is obvious. For this pressure level a threshold seems to be on hand, significantly affecting the final structure for the investigated system.

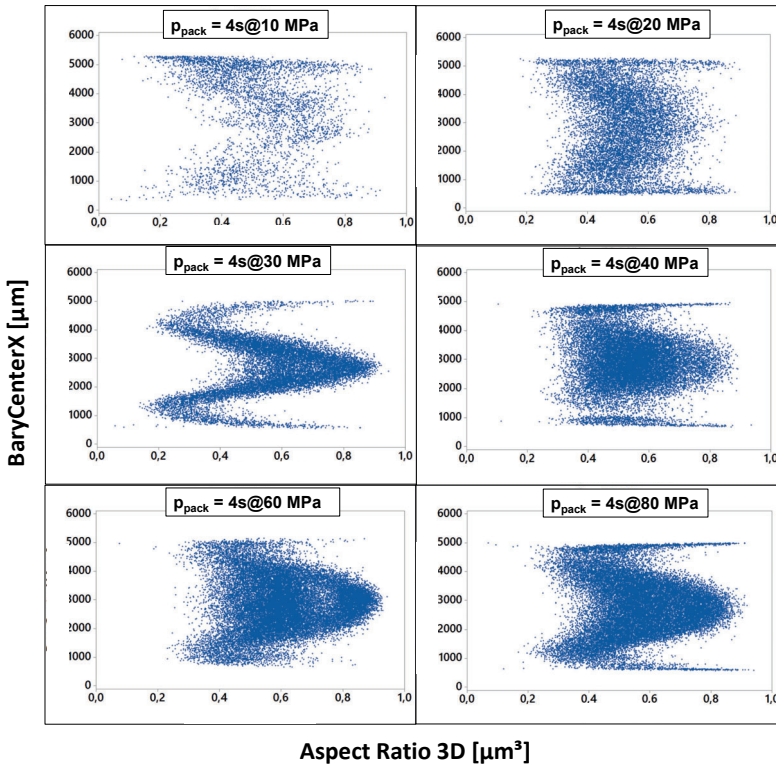


Figure 114: Scatterplots of aspect ratio (Aspect Ratio 3D) plotted over cross section (BaryCenterX) = mold opening direction according to the structures shown in Figure 112

Cavity pressure / Pressure drop rates

It became evident that a higher pressure drop rate (PDR) results for higher levels of packing pressure. This effect is highlighted in Figure 115 and Figure 116. Figure 115 highlights two chosen cavity pressure curves for local core-back experiments (volume expansion induced by external core movement control) while Figure 116 depicts the cavity pressure curves recorded during the mold opening experiments shown in Figure 112 to Figure 114 (volume expansion induced by clamping unit of injection molding machine). The higher PDR leads to a higher nucleation efficiency, consequently a more uniform structure with smaller cells. This effect can clearly be seen in the according structures shown in Figure 112 to Figure 114.

Besides the pressure level, the pressure drop rate is affected by the expansion speed. While for the core-back experiments (shown in Figure 115) an expansion speed of 100 mm/s from a packing pressure level of 10 MPa resulted in a PDR of ~ 130 MPa/s, a comparable value has been calculated for an expansion speed of 20 mm/s from a packing pressure level of 80 MPa within the mold-opening experiments (see Figure 116). The highest pressure drop rates, thus the highest nucleation efficiency can be achieved for a high expansion speed in combination with a high packing pressure level.

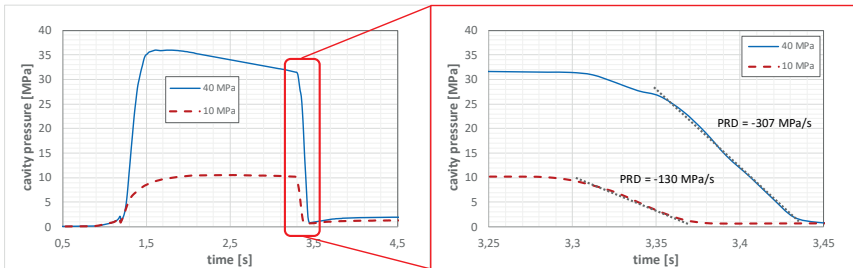


Figure 115: Experimental cavity pressure curves and pressure drop rates in dependency of pressure level before volume expansion; core-back experiments (cavity expansion initiated by external core movement control); expansion speed = 100 mm/s

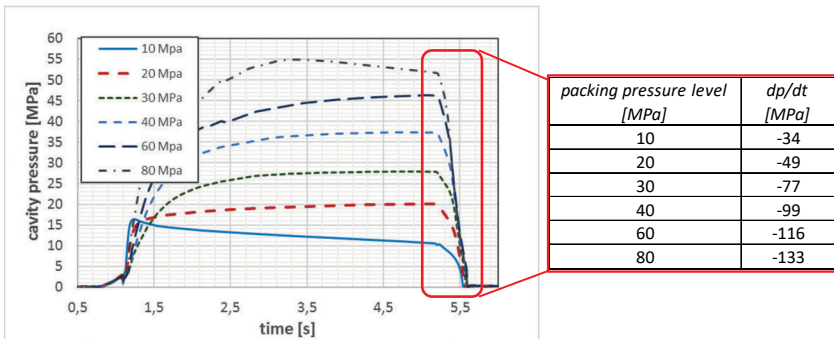


Figure 116: Experimental cavity pressure curves and pressure drop rates in dependency of pressure level before volume expansion; mold-opening experiments – according to Figure 112 to Figure 114 - (cavity expansion initiated by clamping unit of injection molding machine); expansion speed = 20 mm/s

Bai et. al. [84] did injection compression molding experiments combined with core-back and found a similar trend. They used compression pressures from 10 MPa up to 30 MPa for 5 s, however core-back speed was limited here (2 mm/s). For 10 MPa they found deformed cells, while here starting from 20 MPa most of the deformed cells had gone (re-dissolution of filling-induced cells is assumed) [84]. For 30 MPa new spherical cells could be observed, assuming a complete re-dissolution of cells [84].

Figure 117 shows the mean and median 3D cell volumes of the own experiments. As can be seen, from a packing pressure of 30 – 40 MPa just slight change of cell volumes can be observed. Higher pressure levels just affect the cell size slightly (difference in values for 10 MPa due to big inhomogeneity in structure). These results confirm the assumption of a threshold of packing pressure level mentioned in [58] to affect the final structure in terms of cell size and uniformity.

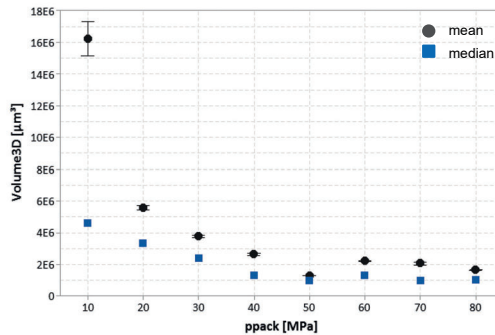


Figure 117: Mean and median cell volumes (*Volume3D*) of the mold-opening experiments

Cellular structure by parts' flow length

To get an information on the effect of packing pressure in dependency of the parts flow length, morphology has been investigated at different positions (near gate “ng”, middle “m” and away from gate “afg”). Figure 118 compares these positions for a part manufactured at low (Figure 118 a)), a part manufactured at medium (Figure 118 b)) and a part manufactured at high packing pressure (Figure 118 c)). Obviously, the structure manufactured with medium and high packing pressure exhibits a more homogeneous structure by the flow length. However, even for the highest level of

packing pressure of 80 MPa for 4 s (Figure 118 c)), still a gradient in cells structure exists.

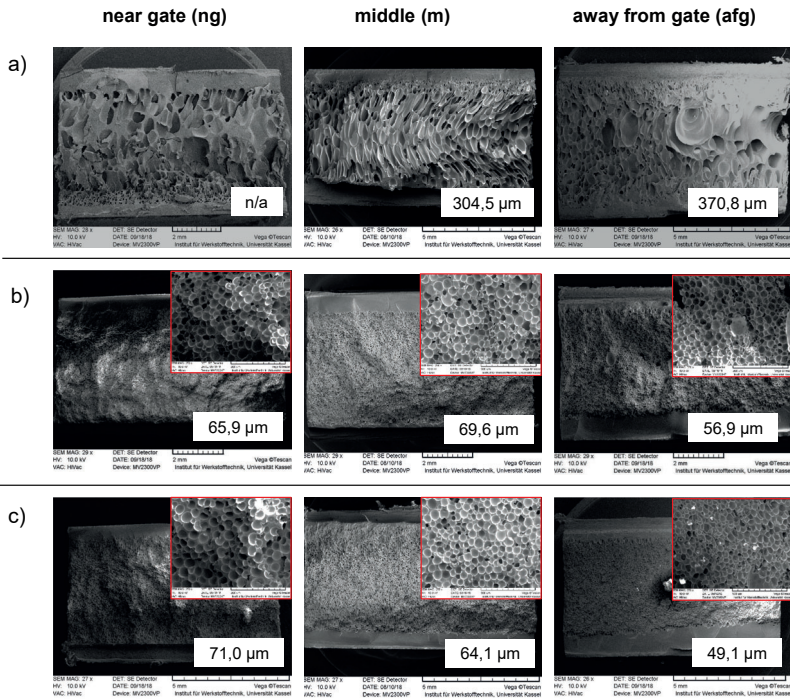


Figure 118: Morphology at different flow positions: near gate (ng) / middle of the flow path (m) / away from gate (afg) for a sample manufactured with a) $p_{pack} = 10$ MPa and b) $p_{pack} = 40$ MPa and c) $p_{pack} = 80$ MPa ($t_{pack} = 4$ s for all); the highlighted values in the lower right corners depict the median cell size

The following may be concluded to summarize the findings for the effect of pressure level:

- ⇒ The cavity pressure measurements have shown that packing pressure level affects the pressure drop rate. For higher pressure levels higher pressure drop rates have been observed, supporting nucleation.
- ⇒ Pressure drop rate is a consequence of pressure level and expansion speed. The highest pressure drop rates are achieved for a high expansion speed from a high packing pressure level.

- ⇒ From a packing pressure of 30 MPa, a significant change of structure for the investigated system can be seen. The structure is more uniform and exhibits a sharp transition from skin to core with smallest cells in the core region. Also, a pronounced trend of cells located in the center to exhibit a high roundness is obvious from this pressure level.
- ⇒ The uniformity of structure by flow length also is supported by higher pressure levels. However, even for the highest level still a gradient is observable. This result might suggest that no complete reset of pre-nucleated cellular structure has been occurred as originally assumed by the author of this thesis. Cells or nucleus once created by the first pressure drop during mold filling seem to still affect the structure even after recompression of melt and initiating a second pressure drop.

8.4.4 Repeated compression and decompression of melt

As mentioned in the last chapter, it is unknown if inside the cavity the same status of melt-gas mixture may be achieved like it is on hand within the plasticizing unit. Also, the results of chapter 8.3.3 show, that structure in high-pressure /mold opening or core-back procedure is still affected by the injection phase, despite an assumed decoupling of filling and foaming by the high pressure. As already mentioned, maybe once created nucleus are not possible to be completely „reset“ by the packing phase.

In foam injection molding investigations by Hopmann et. al. [161] re-pressurization experiments were done by a mold equipped with a movable piston in the cavity. The piston was moved back and forth to decrease and increase the cavity pressure. Two de- and recompression cycles after injection phase were implemented in the process sequence. Using a Polypropylene, it was observed that an increase in cell density and a finer celled structure occurred [161]. They assumed that nucleated cells were mostly re-dissolved in the melt, but some cell nuclei may have been preserved before 2nd decompression, thus a higher number of nuclei has been on hand promoting finer-celled structures [161]. As an outlook they concluded that de- and recompression of melt could be implemented in dosing phase to actively support nucleation [161].

Zhou and Chen [173] also did multiple de-and re-pressurization experiments in foam injection molding in order to investigate the effect on foaming and the mechanical properties. They used a linear PP in combination with a chemical blowing agent conducted by mold-opening procedure and a mold with shearing edges. They found the cell density to be approximately the double by using two mold opening operations compared to samples produced by one mold opening operation [173]. Further opening and closing operations just showed a low effect on the cell density [173]. The repeated mold-opening operation also lead to an improvement of the mechanical properties [173].

The freedom of core-back movement profile variation given by the improved core-back mold, designed and built within this thesis was used to also investigate this phenomenon. Core-back experiments with repeated re- and decompression have been conducted. Figure 119 shows the resulting cavity pressure, for different de-and recompression cycles recorded by a pressure sensor located directly in the moving core. The core-back operation has been conducted up to 5 times, immediately executed one after another to still work in an adequate melt temperature condition.

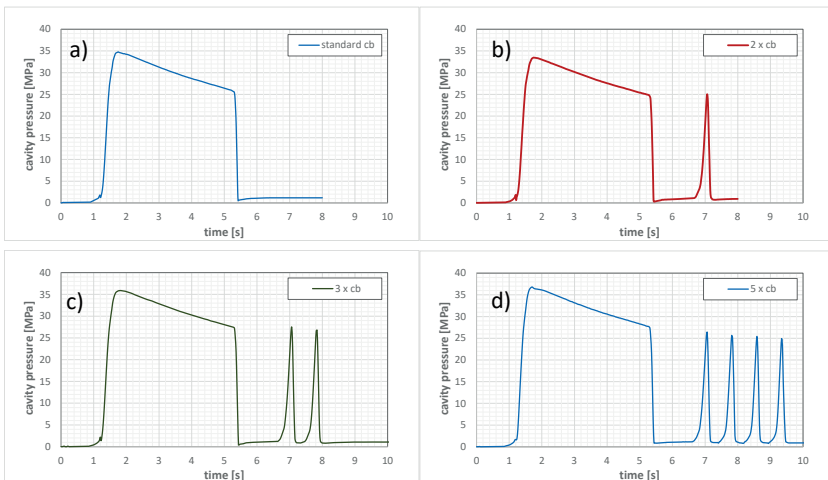


Figure 119: Cavity pressure profiles for a) standard core-back procedure, b) double core-back procedure, c) triple core-back procedure and d) 5-times core-back procedure

Figure 120 shows the resulting morphologies of a standard, a triple and a five times core-back operation experiment, using a PP/0.5wt%N₂ mixture.

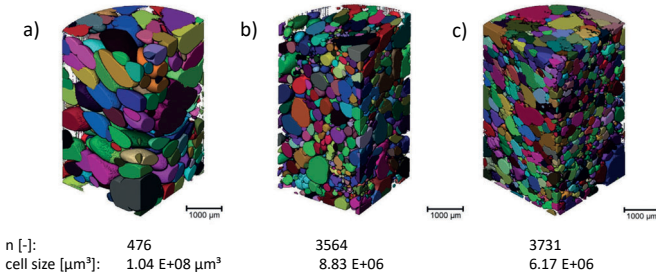


Figure 120: Resulting morphologies in the center of high-pressure foam injection molded sample of PP/0.5wt%N₂; a) standard core-back, b) 2 times core-back, c) 5 times core-back operation

- ⇒ A clear trend of finer-celled structure is observed for increasing repetition of core-back operations. This effect confirms the results of the investigations by [161] and [173].
- ⇒ Although the pressure conditions inside the cavity do not match typical cavity pressure conditions in core-back procedure, the results support the aforementioned findings of chapters 8.3 and 8.4 that the injection-nucleated and created cells may not be “reset” completely by an increasing cavity pressure. Furthermore, (dynamic) solubility and nucleation may be supported by stress-induction during the melt de- and recompression cycles as reported in chapters 3.2.1 and 3.2.3 referring to the investigations of [50, 54].

The effect of structure refinement by cavity pressure increase may also be very interesting for application and should be investigated more deeply. Maybe the same effect could be realized by a graded packing pressure definition, precisely controlled by the injection molding machine e.g. by using a precisely controlled screw position within the packing phase. This may be a simple tool for structure refinement making complex molds unnecessary. However, the pressure-time context, which is the executed work of pressure as well the temperature conditions should be respected.

9 Conclusion

Within the thesis the differences in procedure as well in cell formation of low-pressure foam injection molding (LP-FIM) and high-pressure foam injection molding with volume-expandable molds (HP-VE-FIM) – mold opening (HP-MO-FIM) and core-back (HP-CB-FIM) - have been worked out and the new procedure of local core-back is introduced and investigated. Simulation software and visualization experiments have been used to make cell evolution process during filling and packing phase more transparent and highlight differences in procedures. Experiments were conducted to show the differences in final structure, characterized by 2D analysis (RLM, SEM) and 3D analysis (μ CT) methods. The characterization focused on density, cell size and shape of cells in dependency of flow path and cells' position in parts' cross-section.

Within this thesis a new unique mold for local core-back procedure was designed, constructed, build and brought into service. This mold allows inter alia an active control on cavity pressure and pressure drop rate (PDR), thus an active control on cell formation mechanism. This is realized by an externally controlled hydraulic cylinder with programmable movement profiles. Expansion ratio, expansion speed, direction (expansion or compression) may be set independently of the injection molding process sequence. Furthermore, a changeable core-back insert to allow the foaming of different geometries is implemented.

The influence of process parameters and the specifics for core-back and local core-back procedure have been worked out and statistically described by design of experiments. Here, as a usually non-considered process parameter, the effect of packing pressure on cellular structure has intensively been investigated. This was done by visualization molding experiments conducted to investigate the cell formation inside the mold and by additional experiments with the new core-back-mold in order to work out the effect of pressure level as well multiple de-and recompression cycles (multiple core-back operations).

Comparison of procedures

In LP-FIM, cell formation occurs simultaneously to mold filling, thus structure formation is affected by shearing effects and locally different boundary conditions, resulting in inhomogeneous cell structures and deformed cells. From skin to core the

density changes continuously and at the end of the flow path huge cavities may be on hand. Close to the compact skin layer, sheared cells with a flow-induced elongation can be seen. This flow-path dependent, non-uniform cell structure may lead to non-uniform mechanical properties. The cell formation can only be controlled in a very restricted manner.

In HP-VE-FIM, also cell formation occurs simultaneously to mold filling. But, cells may be re-dissolved back into the melt by applying an active packing phase. A second cell formation occurs due to a controlled mold volume expansion, initiating a second pressure drop. Thus, filling and foaming may be decoupled. The second pressure drop is initiated simultaneously and under more equal conditions for every position of the part, resulting in significantly less filling-induced and much more uniform cell structures. A sharp transition in density from compact skin to low-density core can be observed and cellular structure at the end of the flow path is comparable to the structure close to gate. A negligible elongation of skin-close cells in direction of melt flow has been observed. It became evident that the level of pressure plays an important role in terms of homogeneity of structure and cell size. Higher pressure results in smaller and more uniform cells, however a threshold seems to exist not affecting the structure anymore.

By using the new procedure of local core-back, the foam formation may be limited locally to omit selected areas from foaming. Locally foamed structures with high density reductions have been produced. Thus, part's properties may be tailored and freedom of design (e.g. wall thickness variations) is extended dramatically. The local temperature conditions are essential for demarcation of foamed and non-foamed areas and the achievable expansion ratio.

For both, mold opening and core-back procedure, the essential parameters in terms of cell formation are packing pressure and expansion speed, allowing to decouple filling and foam formation phase. Thus, the mechanism may actively be shifted between nucleation and cell growth. Controlling cavity pressure and pressure drop rate are the key factors to actively control cell formation and to achieve uniform, fine-celled structures.

Hypothesis review

Hypothesis 1: “The influence of machine-defined injection parameter as they are found for low-pressure procedure may be overlaid by specifics of high-pressure procedure with mold volume expansion (difference in process sequence and additional process parameter).” [chapters 8.2 and 8.3]

It became evident that cavity pressure and temperature conditions during procedure are significantly different for LP-FIM and HP-VE-FIM. In LP-FIM the characteristics of structure (e.g. cell size, shape of cells) are defined during mold filling. Here, structure formation is mainly defined by the injection parameters which can only be controlled in a restricted manner. In HP-VE-FIM filling and foaming phase may be decoupled and structure formation mainly occurs after end of filling initiated by volume expansion. Several procedure-specific parameters are on hand to actively affect the structure formation. The results of the DoE have shown that these parameters affect the structure in a significant manner. Thus, an overlay of machine defined parameters by specifics of HP-VE-FIM procedure is on hand. In terms of injection speed, in contrast to LP-FIM, only a negligible effect of speed level has been observed, demonstrating an overlay of effects using a packing phase. However, although by applying high packing pressures, a slight effect of injection speed level could still be observed, indicating that filling and foaming have not been decoupled completely.

Hypothesis 2: “An active packing phase may decouple filling and foaming resulting in significantly different cellular structures for high-pressure foam injection molding with mold volume expansion compared to low-pressure foam injection molding.” [chapter 8.4]

The visualization experiments have shown that sufficient packing conditions may force filling-induced cells back into solution and decouple filling and foaming. By SEM and μ CT analysis, packing pressure has been identified as the most influential parameter in HP-VE-FIM in terms of cell size, shape of cells and uniformity of structure. In LP-FIM an integral structure and an integral density distribution from skin to core as well sheared cells, elongated in flow direction are observed. In contrast, in HP-VE-FIM, applying sufficient packing pressure, a sharp transition of structure and density from skin to core and a negligible flow-induced elongation of skin-close cells is on hand. This finding may be different from investigations in

literature which did not include the packing pressure as a parameter. However, the results show that a complete decoupling of filling-induced structure formation has not been achieved even for the highest packing conditions used (80 MPa for 4 s). It is assumed that nuclei “survived” and different number of nuclei are on hand by inducing the pressure drop. This assumption is supported by “re-compression” experiments (chapter 8.4.4). A repeated compression and decompression results in finer-celled structures. Here, pseudo-classical nucleation may have occurred, and re-compression may have activated additional nuclei.

Hypothesis 3: *“Increased packing conditions support fine-celled structures and overall uniformity in high-pressure foam injection molding with mold volume expansion.”* [chapter 8.4]

A decrease of cell size and a more spherical shape of cells, resulting in an improved overall uniformity of structure has been found to be achieved for higher packing conditions, which is increasing packing pressure level and increasing packing time. Packing pressure level is rated to be more influential than packing time. An increase of packing level has been investigated to result in a finer-celled, spherical and more uniform structure. Furthermore, the experimentally recorded pressure drop rates have shown that an increase in packing level also increases pressure drop rate, thus supports nucleation. However, a threshold seems to exist in terms of packing level to affect the cells’ size and shape. Re-pressurization followed by repeated application of pressure has been investigated to also support nucleation efficiency, resulting in finer-celled structures.

Lightweight and application potential

Using HP-VE-FIM, the conventional design rules may largely be annulled. Decoupling of filling and foaming allows to design parts and gate locations like compact molded parts with the additional advantage of foaming. Wall thickness variations are typically critical areas. While in compact molding wall thickness variations may lead to sink marks and unsymmetrical shrinkage, in LP-FIM the foam structure changes by changing the wall thickness and an incomplete molding may occur. If thick-walled areas are created by mold volume expansion after complete mold filling, these drawbacks may be waived. The part design of the new local core-back mold built

within this thesis has clearly demonstrated that wall thickness variations are not critical in terms of sink marks or shaping. Ribs neither need a radius or any ratio of basic wall thickness to width or height of ribs must be respected nor ribs have to be arranged in flow direction if they are molded by a moving core. Furthermore, the local core back procedure enables the production of parts, with clearly separated foamed and non-foamed areas. Thus, critical areas like assembly areas or snap-fits may be excluded from foaming and customized parts with tailored mechanical properties may be molded in one process step.

With the new local core-back mold built within this thesis, accurately shaped parts with local expansion ratios up to 12 (limited by mold design) and affiliated density reductions of up to 70 % have been achieved. Comparable values are usually reported by using different processing technologies like foam extrusion, batch foaming or processing polyurethane foams. The produced sandwich-like structures with compact skin layers and a highly expanded core produced in one processing step, offer a tremendous light-weight potential due high bending stiffnesses at low part weight (additional information is given in the appendix).

Experiments with the new core-back mold which are not referred within this thesis have shown that the limitations in surface quality usually been on hand for foam injection molded parts may be avoided by using variotherm mold temperature control (an excerpt of these results is shown in the appendix). Especially for amorphous materials the results were better than expected. Reproduction of the cavity surface and the positive effect of the hot mold surface is supported by the packing phase used in HP-VE-FIM. Thus, also good surface qualities may be achieved for high expansion ratios or density reductions even away from gate.

In terms of application, the procedure may be implemented in a mold in a simple and cheap way. Thus, just a hydraulic cylinder controlled by the core-pulling program of the injection molding machine and the additional use of mechanical blocks for positioning is needed.

The basic mechanism in HP-VE-FIM are very similar to quench batch foaming, thus also potential to produce bimodal, open or nano-cell structure as it is realized in batch foaming is given [36]. A trend of highly expanded core-back foams is recently reported in literature, mentioned to be used for future applications in the fields of

absorption, damping, filters or membranes as well heat insulation applications. A huge potential in terms of insulation and mechanical properties is reported to be on hand for nano-cellular foams [36, 162, 163]. Often, special materials or blends are used to exploit the limitations and to achieve high expansion ratios. For example, by using a pre-isothermal treatment process, an expansion ratio up to 17.7 has been achieved for a PLA core-back foam [164]. Fibril-like structures with an expansion ratio up to 18 have been reported by processing an-isotactic PP / cellulose nanofiber nanocomposite in core-back procedure [165]. Also fibril-like structures prepared by core-back molding of an isotactic PP (i-PP) and crystal nucleating agents, resulted in open-celled nano-cellular foams (expansion ratios up to 5) [162]. These foams may be characterized by hierarchical structures with open-cells in the cell walls and fibril like structures in core-back direction. Another interesting approach is the use of conductive polymer composites in foam injection molding. During foam formation, the fibers are elongated tangential to the growing cells. As a consequence, a conductive network with enhanced fiber inter-connectivity has been achieved [166–168]. Here, also further potential is seen by using core-back technology.

All these investigations underline the research interest and the enormous potential of HP-VE-FIM procedure for future applications.

Forecast / Future work

Further investigations on de- and re-compression should be conducted to clarify the observations described in chapter 8.4.4. The refinement of cellular structure by repeated core-back operations should be confirmed for several materials. It might be included into the machine control in a simple way e.g. by using a precisely controlled, screw position within the packing phase.

Several investigations have shown that cellular characteristics must be considered to predict the mechanical properties of foam injection molded structures. However, the cellular characteristics may differ a lot within a complex shaped part and are inadequately described by density, skin layer thickness and amount of foamed core. Thus, an approximation by simple equations is not purposeful to predict mechanical properties. A promising approach is to perform an accurate simulation and transfer local cellular characteristics into a FEM software. A first successful attempt has been made within an internal study [169]. Here, the numerical simulation results of cellular

structures for local core-back parts have been exported from Moldex3D (Core Tech Systems) and successfully transferred via the materials modeling software Digimat (MSC Software) into a FEM software. However, a lot of software-specific expertise was needed. Once, this integrated approach is implemented and an easy workflow is available, foam injection molding, both LP-FIM and HP-VE-FIM procedures are expected to be much better accepted and used in industry.

To the author's opinion, high-pressure foam injection molding with volume-expandable molds is one of the key technologies, for serial production of light-weight constructions, offering a tremendous potential also for geometrical complex parts.

“Ever tried. Ever failed. No matter. Try again. Fail again. Fail better.”

SAMUEL BECKETT, *Worstward Ho!*

10 References

- [1] Flórez Sastre, L. F. 2011. *Einfluss der Schaummorphologie auf die mechanischen Eigenschaften von Kunststoffstrukturschäumen. / Influence of the foam morphology on the mechanical properties of structural polymer foams*. PhD thesis, University of Aachen, Germany.
- [2] Barzegari, M. R. and Rodrigue, D. 2009. The effect of injection molding conditions on the morphology of polymer structural foams. *Polym. Eng. Sci.* 49, 5, 949–959.
- [3] Rodrigue, D., Leduc, S., Tovar-Cisneros, C., and Gonzalez-Nunez, R. The effect of mould temperature on morphology of injection moulded HDPE structural foams. In *Blowing Agents and Foaming Processes 2007, 22-23 May, Frankfurt/Main, Germany*, 1-11 (paper 11).
- [4] Müller, N. and Ehrenstein, G. W. 2004. Evaluation and Modeling of Injection-Molded Rigid Polypropylene Integral Foam. *Journal of Cellular Plastics* 40, 1 (Jan. 2004), 45–59.
- [5] Spörrer, A. N. J. and Altstädt, V. 2007. Controlling Morphology of Injection Molded Structural Foams by Mold Design and Processing Parameters. *Journal of Cellular Plastics* 43, 4-5, 313–330.
- [6] Spörrer, A. N. J. The challenge of foam Injection-Moulding -Possibilities to improve surface appearance, foam morphology and mechanical properties. In *Blowing Agent and Foaming Processes, 22-23 May 2007, Frankfurt/Main, Germany*, 1–12.
- [7] Michaeli, W., Florez, L., Obeloer, D., and Brinkmann, M. 2009. Analysis of the Impact Properties of Structural Foams. *Journal of Cellular Plastics* 45, 4, 321–351.
- [8] Michaeli, W., Florez, L., and Obeloer, D. 2009. Schaumdesign - Anwendungsgerechte Auslegung von Thermoplastschäumen / Foam design - Application oriented design of thermoplastic foams. *Plastverarbeiter*, 80–82.
- [9] Lee, John W. S., Wang, J., Yoon, J. D., and Park, C. B. 2008. Strategies to Achieve a Uniform Cell Structure with a High Void Fraction in Advanced Structural Foam Molding. *Ind. Eng. Chem. Res.* 47, 23, 9457–9464.

- [10] Xu, X., Park, C. B., Lee, John W. S., and Zhu, X. 2008. Advanced structural foam molding using a continuous polymer/gas melt flow stream. *J. Appl. Polym. Sci.* 109, 5, 2855–2861.
- [11] Wang, G., Mark, L. H., Shaayegan, V., and Park, C. B. 2015. Foaming behavior and control of polypropylene/nitrogen system in microcellular foam injection molding. In *Antec 2015*.
- [12] Bledzki, A. K. and Faruk, O. 2005. Effects of the Chemical Foaming Agents, Injection Parameters, and Melt-Flow Index on Microstructure and Mechanical Properties of Microcellular Injection Molded Wood-Fiber/Polypropylene Composites. *Journal of Applied Polymer Science*, 97, 1090–1096.
- [13] Bledzki, A. K., Rohleder, M., Kirschling, H., and Chate, A. 2012. Correlation between injection moulding processing parameters and mechanical properties of microcellular polycarbonate. *Journal of Cellular Plastics* 48, 4, 301–340.
- [14] Müller, N. 2006. *Spritzgegossene Integralschaumstrukturen mit ausgeprägter Dichtereduktion / Foam injection molded integral foam structures with pronounced density reduction*. PhD thesis, University of Erlangen-Nürnberg, Germany.
- [15] Spörrer, A. 2010. *Leichte Integralschäume durch Schaumspritzgießen mit optimierten Werkstoffen und variothermen Werkzeugen / Lightweight integral foams by foam injection molding with optimized materials and variothermal tools*. PhD thesis, University of Bayreuth, Germany.
- [16] Kirschling, H. M. M. 2009. *Mikroschäume aus Polycarbonat / Microcellular foams of polycarbonate*. PhD thesis, University of Kassel, Germany.
- [17] Kühn-Gajdzik, J. 2011. *Amorphe und teilkristalline Mikroschäume im Spritzgießverfahren / Amorphous and semi-crystalline microcellular foams by foam injection molding*. PhD thesis, University of Kassel, Germany.
- [18] Rohleder, M. 2014. *Dynamisches Lastverhalten von mikrozellularen Polycarbonatschäumen / Dynamic load behaviour of microcellular polycarbonate foams. Morphologie, Energieabsorption und Temperatureinfluss*. PhD thesis, University of Kassel, Germany.

- [19] Cramer, A. 2008. *Analyse und Optimierung der Bauteileigenschaften beim Thermoplast-Schaumspritzgießen. / Analysis and optimization of component properties in thermoplastic foam injection molding*. PhD thesis, University of Aachen, Germany.
- [20] Bledzki, A. K., Kirschling, H., Rohleder, M., and Chate, A. 2012. Correlation between injection moulding processing parameters and mechanical properties of microcellular polycarbonate. *Journal of Cellular Plastics* 48, 4, 301–340.
- [21] Shaayegan, V., Wang, G., and Park, C. B. 2016. Effect of foam processing parameters on bubble nucleation and growth dynamics in high-pressure foam injection molding. *Chemical Engineering Science* 155, 27–37.
- [22] Villamizar, C. A. and Han, C. D. 1978. Studies on structural foam processing II. Bubble dynamics in foam injection molding. *Polym Eng Sci* 18, 9, 699–710.
- [23] Han, C. D. and Yoo, H. J. 1981. Studies on structural foam processing. IV. Bubble growth during mold filling. *Polymer Engineering & Science* 21, 9, 518–533.
- [24] Ahmadzai, A., Behraves, A. H., Sarabi, M. T., and Shahi, P. 2014. Visualization of foaming phenomena in thermoplastic injection molding process. *Journal of Cellular Plastics* 50, 3, 279–300.
- [25] Chen, S.-C., Liao, W.-H., and Chien, R.-D. 2012. Structure and mechanical properties of polystyrene foams made through microcellular injection molding via control mechanisms of gas counter pressure and mold temperature. *International Communications in Heat and Mass Transfer* 39, 8, 1125–1131.
- [26] Dong, G., Zhao, G., Guan, Y., Wang, G., and Wang, X. 2014. The cell forming process of microcellular injection-molded parts. *J. Appl. Polym. Sci.* 131, 12, 40365 (1-11).
- [27] Dong, G., Zhao, G., Guan, Y., Li, S., and Wang, X. 2015. Formation mechanism and structural characteristics of unfoamed skin layer in microcellular injection-molded parts. *Journal of Cellular Plastics*, 52 (4), 419–439.
- [28] Wang, G.-l., Zhao, G.-q., Wang, J.-c., and Zhang, L. 2015. Research on formation mechanisms and control of external and inner bubble morphology in microcellular injection molding. *Polymer Engineering & Science* 55, 4, 807–835.

- [29] Mahmoodi, M., Behraves, A. H., Rezavand, S. A. M., and Golzar, M. 2010. Theoretical and visual study of bubble dynamics in foam injection molding. *Polym. Eng. Sci.* 50, 3, 561–569.
- [30] Shaayegan, V., Wang, G., and Park, C. B. 2016. Study of the bubble nucleation and growth mechanisms in high-pressure foam injection molding through in-situ visualization. *European Polymer Journal* 76, 2–13.
- [31] Shaayegan, V., Wang, G., Reghem, E., Boisson, M., and Park, C. B. Mechanism of Bubble Nucleation and Growth in High-Pressure Foam Injection Molding Using Gas-Counter Pressure. In *SPE ANTEC 2015, Orlando (FL)*, 23.-25-05.2015.
- [32] Shaayegan, V., Wang, G., Mark, L. H., and Park, C. B. 2016. Identification of Cell-Nucleation Mechanism in Foam Injection Molding with Gas-counter Pressure via Mold Visualization. *AIChE J.*, 62 (11), 4035–4046.
- [33] Shaayegan, V., Wang, C., Costa, F., Han, S., and Park, C. B. 2017. Effect of the Melt Compressibility and the Pressure Drop Rate on the Cell-Nucleation Behavior in Foam Injection Molding with Mold Opening. *European Polymer Journal*, 92, 314–325.
- [34] Ishikawa, T. and Ohshima, M. 2011. Visual observation and numerical studies of polymer foaming behavior of polypropylene/carbon dioxide system in a core-back injection molding process. *Polym. Eng. Sci.* 51, 8, 1617–1625.
- [35] Ishikawa, T., Taki, K., and Ohshima, M. 2012. Visual observation and numerical studies of N₂ vs. CO₂ foaming behavior in core-back foam injection molding. *Polymer Engineering & Science* 52, 4, 875–883.
- [36] Ohshima, M. Controllability of Cellular Structure of Polypropylene Foams by Core-Back Foam Injection Molding. In *SPE Polyolefins Conference 2013, Huston (TX), USA*, 24.-27.02.2013.
- [37] Chen, S.-C., Lee, K.-H., Lin, Y.-W., Shiu, T.-Y., Chang, C.-W., and Chien, J. C. Numerical Verification of Rheological Characterization of Polystyrene During Microcellular Injection Molding. In *SPE ANTEC 2012, Orlando (FL)*, 02.-04.04.2012.

- [38] Shiu, T.-Y., Chang, Y.-J., Huang, C.-T., Hsu, D., and Chang, R.-Y. Dynamic behavior and experimental validation of cell nucleation and growing mechanism in microcellular injection molding process. In *SPE ANTEC 2012, Orlando (FL), 02.-04.04.2012*.
- [39] N.N. 2014. *Accurate Simulation Results on MuCell Technology Enables Adoption of Moldex3D Solution. Case Study / report; Proplast Italy, CoreTech System Co., Ltd.*
- [40] N.N. 2016. *Kyoto University Successfully Utilized Moldex3D to Validate New MuCell® Process; CoreTech Systems Co., Ltd., Taiwan.*
- [41] Heim, H.-P. and Tromm, M. 2016. High-pressure foam injection molding with local core-back method - simulation approach. In *SPE FOAMS 2016 14.09.16 - 15.09.16, Seattle, WA, USA*.
- [42] Di Maio, E. and Kiran, E. 2018. Foaming of polymers with supercritical fluids and perspectives on the current knowledge gaps and challenges. *The Journal of Supercritical Fluids*, 134, 157-166.
- [43] Meyer, W. 1979. New Structural Foam Developments in Europe. *Journal of Cellular Plastics* 15, 2, 91–98.
- [44] Altstädt, V. and Mantey, A. 2010. *Thermoplast-Schaumspritzgießen / Thermoplastic foam injection molding*. Carl Hanser Verlag GmbH & CO. KG.
- [45] Throne, J. L. 1976. Structural Foam Molding Parameters. *Journal of Cellular Plastics* 12, 3, 161–176.
- [46] Throne, J. L. 1976. The Newer Structural Foam Techniques. *Journal of Cellular Plastics* 12, 5, 264–283.
- [47] Hendry, J. 1979. Structural Foam Processing and Applications / Yesterday, Today and Tomorrow. *Journal of Cellular Plastics*, 220–222.
- [48] H. Eckardt. 1981. Structural and coinjection foam molding. *Advances in Plastics Technology*, 04/19811 (2), 40–49.
- [49] MacMillan, H. 1979. High Pressure Structural Foam. *Journal of Cellular Plastics* 15, 4, 223–226.
- [50] Chul B. Park and S. T. Lee, Eds. 2014. *Foam Extrusion*. Polymeric Foams. Taylor & Francis Inc, Bosa Roca.

- [51] Suh, N. P. 2003. Impact of microcellular plastics on industrial practice and academic research. *Macromol. Symp.* 201, 1, 187–202.
- [52] Stadlbauer, M. 2005. Rheologische Aspekte beim Schäumen von Polymeren / Rheological aspects in foaming of polymers. In *Fachtagung Polymerschäume, SKZ / Conference Polymer Foams, SKZ, Würzburg, Germany*, 1–12.
- [53] Siu N. Leung. 2009. *Mechanism of cell nucleation, growth, and coarsening in plastic foaming: theory, simulation, and experiment*. PhD thesis, University of Toronto, Canada.
- [54] Wong, A. 2012. *In Situ Observation of Plastic Foaming under Static Condition, Extensional Flow and Shear Flow*. PhD thesis, University of Toronto, Canada.
- [55] Stange, J. 2006. *Einfluss rheologischer Eigenschaften auf das Schäumverhalten von Polypropylenen unterschiedlicher molekularer Struktur. / Influence of rheological properties on the foaming behavior of polypropylenes of different molecular structure*. PhD thesis, University of Erlangen-Nürnberg, Germany.
- [56] Throne, J. L. 2004. *Thermoplastic foam extrusion. An introduction*. C. Hanser; Hanser Gardner, München, Cincinnati.
- [57] Sato, Y., Fujiwara, K., Takikawa, T., Sumarno, Takishima, S., and Masuoka, H. 1999. Solubilities and diffusion coefficients of carbon dioxide and nitrogen in polypropylene, high-density polyethylene, and polystyrene under high pressures and temperatures. *Fluid Phase Equilibria* 162, 1, 261–276.
- [58] Shaayegan, V., Wang, C., Costa, F., Han, S., and Park, C. B. 2017. Effect of the melt compressibility and the pressure drop rate on the cell-nucleation behavior in foam injection molding with mold opening. *European Polymer Journal* 92, Supplement C, 314–325.
- [59] Shaayegan, V., Wang, C., Park, C. B., Costa, F., and Han, S. Mechanism of Cell Nucleation in High-Pressure Foam Injection Molding Followed by Precise Mold-Opening. In *SPE ANTEC 2016 23.-25.05.2016*, 1199–1203.
- [60] Kastner, C. and Steinbichler, G. Development of measurement method for determination of dynamic solubility limits in injection foam molding. In *PPS-34, Taipei, Taiwan, 21.05.-25.05.2018*, 30048. DOI=10.1063/1.5088306.

-
- [61] G. Becker, D. Brown, H. Gausepohl, R., Ed. 1997. *Polystyrol. Kunststoff Handbuch / Polystyrene. Polymer Handbook* 48. Carl Hanser Verlag, München, Wien.
- [62] Elliott, J. 2004. *Diffusion in Polymers, Permeation and diffusion of solvents into amorphous polymers*. Course M6 - Lecture 6.
- [63] Heinrich, H., Jaeger, P., and Eggers, R. 2009. Diffusion von Gasen und Gasgemischen in Polymere unter hohen Drücken / Diffusion of gasses and gas mixtures in polymers for high pressures. *Chemie Ingenieur Technik* 81, 10, 1607–1611.
- [64] Wang, G., Wang, C., Zhao, J., Wang, G., Park, C. B., and Zhao, G. 2017. Modelling of thermal transport through a nanocellular polymer foam. Toward the generation of a new superinsulating material. *Nanoscale* 9, 18, 5996–6009.
- [65] Vachaparambil, K. J. and Einarsrud, K. E. 2018. Explanation of Bubble Nucleation Mechanisms. A Gradient Theory Approach. *J. Electrochem. Soc.* 165, 10, E504-E512.
- [66] A. Wong, C. P. 2014. Fundamental Mechanisms of Cell Nucleation in Plastic Foam Processing. In *Foam Extrusion*, Chul B. Park and S. T. Lee, Eds. Polymeric Foams. Taylor & Francis Inc, Boca Roca.
- [67] Feng, J. J. and Bertelo, C. A. 2004. Prediction of bubble growth and size distribution in polymer foaming based on a new heterogeneous nucleation model. *Journal of Rheology* 48, 2, 439–462.
- [68] Taki, K. 2008. Experimental and numerical studies on the effects of pressure release rate on number density of bubbles and bubble growth in a polymeric foaming process. *Chemical Engineering Science* 63, 14, 3643–3653.
- [69] Heim, H.-P. 2016. *Specialized injection molding techniques*. PDL handbook series. William Andrew is an imprint of Elsevier, Oxford, UK.
- [70] Udadyay, R. K. 1985. Study of Bubble Growth in Foam Injection Molding. *Advances in Polymer Technology*, Vol. 5, No. 1, 55–64.
- [71] Ataei, M., Shaayegan, V., Wang, C., Costa, F., Han, S., Park Chul B, Bussmann, M. 2019. Numerical analysis of the effect of the local variation of viscosity on

- bubble growth and deformation in polymer foaming. *Journal of Rheology*, 63, 895–903.
- [72] N.S. Ramesh. 2014. Foam Growth in Polymers. In *Foam Extrusion*, Chul B. Park and S. T. Lee, Eds. Polymeric Foams. Taylor & Francis Inc, Boca Roca, 213–236.
- [73] Tamaro, D., D’Avino, G., Di Maio, E., Pasquino, R., Villone, M. M., Gonzales, D., Groombridge, M., Grizzuti, N., and Maffettone, P. L. 2016. Validated modeling of bubble growth, impingement and retraction to predict cell-opening in thermoplastic foaming. *Chemical Engineering Journal* 287, 492–502.
- [74] Gomez-Gomez, F. J., Arencon, D., Sanchez-Soto, M. A., and Martinez, A. B. 2012. Influence of the injection moulding parameters on the microstructure and thermal properties of microcellular polyethylene terephthalate glycol foams. *Journal of Cellular Plastics* 49, 1, 47–63.
- [75] Liao, R., Yu, W., and Zhou, C. 2010. Rheological control in foaming polymeric materials: I. Amorphous polymers. *Polymer* 51, 2, 568–580.
- [76] Liao, R., Yu, W., and Zhou, C. 2010. *Rheological control in foaming polymeric materials: II. Semi-crystalline polymers* 51.
- [77] Spörrer, A. N. J. and Altstädt, V. The Challenge of foam injection-moulding-possibilities to improve surface appearance, foam morphology and mechanical properties. In *Blowing Agent and Foaming Processes 2007; 22-23 May Frankfurt/Main, Germany*, 1–12 (paper 16).
- [78] Wang, L., Ishihara, S., Ando, M., Minato, A., Hikima, Y., and Ohshima, M. 2016. Fabrication of High Expansion Microcellular Injection-Molded Polypropylene Foams by Adding Long-Chain Branches. *Ind. Eng. Chem. Res.* 55, 46, 11970–11982.
- [79] Mills, N. J. 2007. *Polymer foams handbook. Engineering and biomechanics applications and design guide*. Butterworth Heinemann, Amsterdam.
- [80] Wong, A., Guo, H., Kumar, V., Park, C. B., and Suh, N. 2016. Microcellular Plastics. *Encyclopedia of Polymer Science and Technology*.
- [81] Pinto, J., Solórzano, E., Rodriguez-Perez, M. A., and Saja, J. A. d. 2013. Characterization of the cellular structure based on user-interactive image analysis procedures. *Journal of Cellular Plastics* 49, 6, 555–575.

- [82] Buahom, P. and Areerat, S. 2011. The estimation of cell density in isotropic microcellular polymeric foams using the critical bubble lattice. *Journal of Cellular Plastics* 47, 2, 133–152.
- [83] Tromm, M., Shaayegan, V., Wang, C., Heim, H.-P., and Park, C. B. 2019. Investigation of the mold-filling phenomenon in high-pressure foam injection molding and its effects on the cellular structure in expanded foams. *Polymer* 160, 43–52.
- [84] Bai, T., Dong, B., Xiao, M., Liu, H., Wang, N., Wang, Y., Wang, C., Liu, C., Cao, W., Zhang, J., Ma, Y., and Guo, Z. 2018. Polystyrene Foam with High Cell Density and Small Cell Size by Compression-Injection Molding and Core Back Foaming Technique: Evolution of Cells in Cavity. *Macromolecular Materials and Engineering*, 1800110 (1 of 11).
- [85] Peters, R. 2003. *Schaumstrukturanalyse mit digitalen Bildverarbeitungsmethoden / Analysis of foam structures with digital imaging techniques*. PhD thesis, University of Aachen, Germany.
- [86] Tromm, M. and Heim, H.-P. Controlling cellular structure and surface quality in foam injection molding –innovative core-back mold for research. (Poster). In *SPE Foams 2017, Bayreuth, Germany, 11.-12.10.2017*.
- [87] Volpe, V., Lanzillo, S., Affinita, G., Villacci, B., Macchiarolo, I., and Pantani, R. 2019. Lightweight High-Performance Polymer Composite for Automotive Applications. *Polymers* 11, 326.
- [88] Rizvi, S., Alaei, M., Yadav, A., and Bhatnagar, N. 2014. Quantitative analysis of cell distribution in injection molded microcellular foam. *Journal of Cellular Plastics* 50, 3, 199–219.
- [89] Barzegari, M. R. and Rodrigue, D. 2007. The effect of density profile on the flexural properties of structural foams. *Polym Eng Sci* 47, 9, 1459–1468.
- [90] Rodrigue, D. 2008. Using Density Profiles to Predict the Flexural Modulus of Structural Polymer Foams. *Journal of Cellular Plastics* 44, 5, 381–389.
- [91] Elmoutaouakkil, A., Salvo, L., Maire, E., and Peix, G. 2002. 2D and 3D Characterization of Metal Foams Using X-ray Tomography. *Adv. Eng. Mater.* 4, 10, 803–807.

- [92] G. van Dalen, M.W. Koster. 2012. 2D & 3D particle size analysis of micro-CT images. In *Bruker-microCT UserMeeting 2012, Brussels, Belgium*, 157–171.
- [93] S. Pérez-Tamarit, E. Solórzano, A. Hilger, I. Manke, and M.A. Rodríguez-Pérez. 2018. Multi-scale tomographic analysis of polymeric foams_ A detailed study of the cellular structure. *European Polymer Journal* 109, 169–178.
- [94] Bacaicoa, I., Lütje, M., Sälzer, P., Umbach, C., Brückner-Foit, A., Heim, H.-P., Middendorf, B. 2017. Comparative investigation of two-dimensional imaging methods and X-ray tomography in the characterization of microstructure. *Materials Testing* 59, 10, 1–8.
- [95] Pérez-Tamarit, S., Solórzano, E., Hilger, A., Manke, I., and Rodríguez-Pérez, M. A. 2018. Multi-scale tomographic analysis of polymeric foams: A detailed study of the cellular structure. *European Polymer Journal* 109, 169–178.
- [96] Heim, H.-P. and Tromm, M. 2014. Formation of morphology as a function of process control by foam injection molding of a functionally graded component. In *SPE ANTEC 2014, Las Vegas (NV), USA, 28.-30.04.2014*, 1551–1556.
- [97] Mihailovic, J. 2019. *Zellstrukturcharakterisierung mittels dreidimensionaler Bildgebungsverfahren / Characterisation of cellular structures with threedimensional imaging techniques*. Masterthesis (supervisor: M. Tromm), University of Kassel, Germany.
- [98] Taki, K., Yanagimoto, T., Funami, E., Okamoto, M., and Ohshima, M. 2004. Visual observation of CO₂ foaming of polypropylene-clay nanocomposites. *Polymer Engineering and science* 44, 6, 1004–1011.
- [99] Wong, A., Park, C. B. 2012. A visualization system for observing plastic foaming processes under shear stress. *Polymer Testing* 31, 3, 417–424.
- [100] Leung, S. N., Wong, A., Wang, L. C., and Park, C. B. 2012. Mechanism of extensional stress-induced cell formation in polymeric foaming processes with the presence of nucleating agents. *The Journal of Supercritical Fluids* 63, 187–198.
- [101] Tamaro, D. 2016. *Fundamentals of cell opening in polymer foaming*. PhD thesis, University of Naples, Italy.
- [102] Han, C. D. and Villamizar, C. A. 1978. Studies on structural foam processing I. The rheology of foam extrusion. *Polym. Eng. Sci.* 18, 9, 687–698.

- [103] Yoo, H. J. and Han, C. D. 1981. Studies on structural foam processing. III. Bubble dynamics in foam extrusion through a converging die. *Polym. Eng. Sci.* 21, 2, 69–75.
- [104] Huang, H.-X., Tian, J.-D., and Guan, W.-S. 2014. Microcellular injection-compression molding (micm): A novel technology for effectively improving cellular structure of polystyrene foams. *Polym. Eng. Sci.* 54, 2, 327–335.
- [105] Gómez-Monterde, J., Sánchez-Soto, M., and Maspoch, M. L. 2018. Microcellular PP/GF composites: Morphological, mechanical and fracture characterization. *Composites Part A: Applied Science and Manufacturing* 104, 1–13.
- [106] Tai-Yi Shiu, Yuan-Jung Chang, Chao-Tsai Huang, David Hsu, Rong-Yu Chang. 2012. Dynamic behavior and experimental validation of cell nucleation and growing mechanism in microcellular injection molding process. In *SPE ANTEC 2012, Orlando (FL), 02.-04.04.2012*.
- [107] M. Ataei, V. Shaayegan, F. Costa, S. Han, C. B. Park, M. Bussmann. Simulation of Polymer Foaming using the Lattice Boltzmann Method. *Journal of Computational Physics*, Preprint submitted on August 13, 2019.
- [108] Hopmann, C. and Sander, D. 2015. Charakterisierung des Materialverhaltens treibfluidbeladener Kunststoffschmelze zur verbesserten Füllsimulation des Schaumspritzgießprozesses / Characterization of material behaviour of blowing agent loaded polymer melt for improvement of filling simulation of foam injection molding process. *GAK* 68, 9, 618–623.
- [109] Wang, C., Shaayegan, V., Ataei, M., Costa, F., Han, S., Bussmann, M., and Park, C. B. 2019. Accurate Theoretical Modeling of Cell Growth by Comparing with Visualized Data in High-Pressure Foam Injection Molding. *European Polymer Journal* 119.
- [110] N.N. 2012. *Understanding Microcellular Foaming Injection (MuCell) Technology with CAE Application. Moldex3D*. Presentation on Mucell AddOn, EN 2012.05.30, 1–118.
- [111] Tromm, M. 2016. “Simulation of High Pressure Foam Injection Molding with Local Core-back”. *Moldex3D Global Innovation Talent Award #Moldex3DStory Contest- 2nd price EMEA Region, 30.09.2016*, Hsinchu, Taiwan.

- [112] Rosskothén, K. 2014. Elastische Leichtgewichte erzeugen / Create elastic lightweight parts. *Kunststoffe*, 2, 68–71.
- [113] Baumgart, C., Hübner, F., and Altstädt, V. 2015. Kleine Lücken zum leichteren Drücken - Mikrosphären in Flüssigsilikonem schäumen / Foaming of microspheres in liquid silicone rubber. *Kunststoffe*, 11, 84–87.
- [114] J. Peng, E. Yu, X. Sun, L.-S. Turng, X.-F. Peng. 2011. Study of Microcellular Injection Molding with Expandable Thermoplastic Microsphere. *Intern. Polymer Processing XXVI*, 3, 249–255.
- [115] Wang, L., Hikima, Y., Ohshima, M., Yusa, A., Yamamoto, S., and Goto, H. 2018. Unusual Fabrication of Lightweight Injection-Molded Polypropylene Foams by Using Air as the Novel Foaming Agent. *Ind. Eng. Chem. Res.*, 57 (10), 3800–3804.
- [116] Yusa, A., Yamamoto, S., Goto, H., Uezono, H., Asaoka, F., Wang, L., Ando, M., Ishihara, S., and Ohshima, M. 2017. A new microcellular foam injection-molding technology using non-supercritical fluid physical blowing agents. *Polym Eng Sci* 57, 1, 105–113.
- [117] Szych, P., Kürten, A. 2017. Die neue leichte Art zu schäumen / The new easy way of foaming. *Kunststoffe*, 09, 46–50.
- [118] Gómez-Monterde, J., Hain, J., Sánchez-Soto, M., and Maspoch, M. L. 2019. Microcellular injection moulding: A comparison between MuCell process and the novel micro-foaming technology IQ Foam. *Journal of Materials Processing Technology* 268, 162–170.
- [119] Sun, X. and Turng, L.-S. 2012. A novel foaming injection molding process using gas-laden pellets. In *SPE FOAMS 2012, Barcelona, Spain, 12.-13.09.2012*.
- [120] Sun, X., Kharbas, H., and Turng, L.-S. 2014. Enhancing cell nucleation for a novel microcellular injection molding process using gas-laden-pellets. In *SPE ANTEC 2014, Las Vegas (NV), USA, 28.-30.04.2014*, 1540–1545.
- [121] Peng, J., Sun, X., Srithep, Y., Peng, X.-F., and Turng, L.-S. 2014. Vapor-foamed injection molding of polycarbonate using sodium chloride and active carbon as nucleating agents. In *SPE ANTEC 2014, Las Vegas (NV), USA, 28.-30.04.2014*, 1726–1731.

- [122] J. L. Throne. 1976. Structural Foam Molding Parameters. *Journal of Cellular Plastics*, May/June, 161–176.
- [123] Michaeli, W. and Cramer, A. 2006. Bessere Oberflächen beim Schaumspritzgießen / Improved surface qualities in foam injection molding. *Kunststoffe*, 12, 21–27.
- [124] Müller, N. 2014. Leichte und schlierenfreie Sichtbauteile / Lightweight and swirl-free components for visible application. *Kunststoffe*, 2, 42–43.
- [125] Bauer, R. 2014. Schaumspritzgießen 2.0 / Foam injection molding 2.0. Wittmann Battenfeld und Schaumform entwickeln neue Anwendungen für geschäumte Spritzgussteile. *Kunststoffe*, 12, 18–24.
- [126] Endlweber, R. and Gießauf, J. 2014. Darf's etwas mehr sein? Verfahrenskombination öffnen dem Schaumspritzgießen neue Horizonte / Combination of procedures open up new horizons in foam injection molding. *Kunststoffe*, 12, 30–34.
- [127] Doriat, C. 2015. Vorübergehend heiß. Wechseltemperierung als Problemlöser in der Kunststoffverarbeitung. *Kunststoffe*, 1, 23–28.
- [128] C. Hopmann, N. Lammert, Y. Zhang. 2016. Schaumspritzgießen dynamisch temperiert / Dynamic mold temperature control in foam injection molding. *Kunststoffe*, 8, 61–65.
- [129] Heim, H.-P. and Tromm, M. 2017. *Schlussbericht zu IGF-Vorhaben Nr. 18254 N/1 / Final report IGF-Project Nr. 18254 N/1. Thermoplast-Schaumspritzgießverfahren pull and foam / Thermoplastic foam injection technique pull and foam*, University of Kassel, Germany.
- [130] Tromm, M. and Heim, H.-P. Customized foam. Process variant of foam injection molding opens up new lightweight construction potential. *Kunststoffe International* 2018, 01/02, 24–28.
- [131] Dong, G., Zhao, G., Guan, Y., Wang, G., and Wang, X. 2014. The cell forming process of microcellular injection-molded parts. *J. Appl. Polym. Sci.* 131, 12, n/a-n/a.

- [132] Zhang, L., Zhao, G., and Wang, G. 2017. Formation mechanism of porous structure in plastic parts injected by microcellular injection molding technology with variable mold temperature. *Applied Thermal Engineering* 114, 484–497.
- [133] Zhang, L., Zhao, G., Wang, G., Dong, G., and Wu, H. 2017. Investigation on bubble morphological evolution and plastic part surface quality of microcellular injection molding process based on a multiphase-solid coupled heat transfer model. *International Journal of Heat and Mass Transfer* 104, 1246–1258.
- [134] Zhang, L., Zhao, G., Dong, G., Li, S., and Wang, G. 2015. Bubble morphological evolution and surface defect formation mechanism in the microcellular foam injection molding process. *RSC Adv* 5, 86, 70032–70050.
- [135] Anfu, G., Yang, Mao, Meng, Hua, and He. 2019. A Combined In-Mold Decoration and Microcellular Injection Molding Method for Preparing Foamed Products with Improved Surface Appearance. *Polymers* 11, 778.
- [136] Eckardt, H. 2003. Thermoplastic Structural Foam - A well known and new process. In *Blowing Agents and Foaming Processes 2003, Munich, Germany, 19.-20.05.2003*. RAPRA Technology, Shawbury, 65–76.
- [137] Wiehler, H. 2010. *Prozessentwicklung des Hochdruckintegralschaumgießens von Aluminium / Process development of high-pressure integral foam casting of alumina*. PhD thesis, University of Erlangen-Nürnberg.
- [138] Hirschmann, M. 2007. *Herstellung und Eigenschaften von spritzgegossenen Magnesium-Integralschäumen / Manufacturing and properties of injection molded integral foams of magnesia*. PhD thesis, University of Erlangen-Nürnberg, Germany.
- [139] Tamarro, D., Iannace, S., and Di Maio, E. 2017. Insight into bubble nucleation at high-pressure drop rate. *Journal of Cellular Plastics* 53, 5, 551–560.
- [140] Kastner, C., Steinbichler, G., Kahlen, S., Jerabek, M. 2019. Influence of process parameters on mechanical properties of physically foamed, fiber reinforced polypropylene parts. *Journal of Applied Polymer Science*, 47275 (1-11).
- [141] Ohshima, M. and Ishikawa, T. 2011. *Visual Observation and Numerical Analysis for a Core-back mode Foam Injection Molding*. Industrial workshop on polymer foams, Bayreuth.

- [142] Roch, A., Menrath, A., and Huber, T. 2013. Faserverstärkte Thermoplaste in Sandwichbauweise / Fiber reinforced thermoplastics in sandwich constructions. *Kunststoffe*, 10, 183–189.
- [143] A. Roch, , A. Menrath, T. Huber, F. Henning, P. Elsner 2013. Lightweight potential of fibre-reinforced foams.
- [144] Reisch, T. 2012. Cockpitkonzept der Zukunft am Beispiel der BMW 1-er und 3-er Reihe / Future cockpit concept by the example of BMW series 1 and 3. In *Schriftenreihe Kunststofftechnik VDI 2012*.
- [145] Doriat, C. 2006. Platten in Perfektion / Sheets in perpection. *Kunststoffe*, 2, 22–26.
- [146] Kyritsis et al. and USM Corporation, Boston, Mass. 1970. *United States Patent*, 1498389029947316359-03697204.
- [147] Kasemphaibulsuk, P., Holzner, M., Kuboki, T., and Hrymak, A. 2017. Foam injection molding of glass fiber reinforced polypropylene composites with laminate skins. *Polym. Compos.* 45, 1408.
- [148] Heim, H.-P. and Tromm, M. 2016. Injection molded components with functionally graded foam structures - Procedure and essential results. *Journal of Cellular Plastics* 2016, 52(3), 299–319.
- [149] Heim, H.-P. and Tromm, M. Pull and foam - method: Partially foamed components - first investigations with chemical and physical blowing agents. Barcelona, Spain. In *SPE FOAMS 2012, Barcelona, Spain 12.-13.09.2012*.
- [150] Heim, H.-P., Bledzki, A., Rohleder, M., and Tromm, M. 2012. Formation of foam structures and influence of processing procedure in foam injection moulding of thermoplastic materials. In *CELLMAT 2012, Dresden, Germany, 07.-09.09.2012*.
- [151] Heim, H.-P., Tromm, M., Jarka, S., Schnieders, J., and Gövert, S. 2012. Pull and Foam-Injection moulding method. Foamed ribs for stiffening plane components. In *SPE ANTEC 2012, Orlando (FL), 02.-04.04.2012*.
- [152] Heim, H.-P. and Tromm, M. 2015. General aspects of foam injection molding using local precision mold opening technology. *Polymer* 56, 111–118.

- [153] Chu, Raymond K. M., Mark, L. H., Jahani, D., and Park, C. B. 2015. Estimation of the foaming temperature of mold-opening foam injection molding process. *Journal of Cellular Plastics*, 0(0), 1–23.
- [154] Wu et al. 2019. Effects of process parameters on core-back foam injection molding process. *eXPRESS Polymer Letters* Vol 13, 4, 390–405.
- [155] Ehrenstein, G. W. 2007. *Mit Kunststoffen konstruieren / Construction with plastics*. Hanser, München.
- [156] Heim, H.-P. and Tromm, M. 2012. Pull and Foam - Method: First Investigations with chemical and physical blowing agents. In *FOAMS 2012, Barcelona, Spain, 12.-13.09.2012*.
- [157] Barzegari, M. R. and Rodrigue, D. 2009. The effect of injection molding conditions on the morphology of polymer structural foams. *Polym Eng Sci* 49, 5, 949–959.
- [158] Suh, N. P. 2003. Impact of microcellular plastics on industrial practice and academic research. *Macromol. Symp.* 201, 1, 187–202.
- [159] Xie, P., Wu, G., Cao, Z., Han, Z., Zhang, Y., An, Y., and Yang, W. 2018. Effect of Mold Opening Process on Microporous Structure and Properties of Microcellular Polylactide–Polylactide Nanocomposites. *Polymers* 10, 554.
- [160] V. Shaayegan, L. H. Mark, A. Tabatabaei, C. B. Park*. 2016. A new insight into foaming mechanisms in injection A new insight into foaming mechanisms in injection molding via a novel visualization mold. *eXPRESS Polymer Letters*, 10 (6), 462–469.
- [161] Hopmann, C., Theunissen, M., Sander, D., and Zhang, Y. Investigation of the nucleation process and its effects on the foam structure in foam injection molding. In *SPE FOAMS 2017, Bayreuth, Germany, 11.-12.10.2017*.
- [162] Miyamoto, R., Yasuhara, S., Shikuma, H., and Ohshima, M. 2014. Preparation of micro/nanocellular polypropylene foam with crystal nucleating agents. *Polym Eng Sci* 54, 9, 2075–2085.
- [163] Jin, Zhao, and Park. 2019. Recent Trends of Foaming in Polymer Processing: A Review. *Polymers* 11, 953, 1–24.

- [164] Li, B., Zhao, G., Wang, G., Zhang, L., and Gong, J. 2018. Fabrication of high-expansion microcellular PLA foams based on pre-isothermal cold crystallization and supercritical CO₂ foaming. *Polymer Degradation and Stability* 156, 75–88.
- [165] Wang, L., Ishihara, S., Hikima, Y., Ohshima, M., Sekiguchi, T., Sato, A., and Yano, H. 2017. Unprecedented Development of Ultrahigh Expansion Injection-Molded Polypropylene Foams by Introducing Hydrophobic-Modified Cellulose Nanofibers. *ACS Appl. Mater. Interfaces* 9, 11, 9250–9254.
- [166] Ameli, A., Nofar, M., Wang, S., and Park, C. B. 2014. Lightweight Polypropylene/Stainless-Steel Fiber Composite Foams with Low Percolation for Efficient Electromagnetic Interference Shielding. *ACS Applied Materials & Interfaces* 6, 14, 11091–11100.
- [167] Ameli, A., Jung, P. U., and Park, C. B. 2013. Through-plane electrical conductivity of injection-molded polypropylene/carbon-fiber composite foams. *Composites Science and Technology* 76, 37–44.
- [168] Ameli, A., Shaayegan, V., and Park, C. B. Visualization of Cell-Growth Induced Fiber Orientation in Polymer Composite Foams.
- [169] Schäfer, T. 2017. *Kopplung von Spritzguss- und FE-Simulation unter Zuhilfenahme der Materialmodellierungssoftware Digimat / Connection of injection molding - and fe-simulation by the help of the materials modelling software Digimat*. Master thesis (supervisor: M. Tromm), University of Kassel, Germany.
- [170] Heim, H.-P. and Tromm, M. 2016. Injection molded components with functionally graded foam structures - Procedure and essential results. *Journal of Cellular Plastics* 52, 3, 299–319.
- [171] Ohshima, M. 2011. *Visual Observation and Numerical Analysis for a Core-back mode Foam Injection Molding*. Industrial workshop on polymer foams, 09.09.2011. Industrial workshop on polymer foams, Bayreuth.
- [172] Hohmann, C. 2015. *Konzeptionierung eines Spritzgießwerkzeuges für das Schaumspritzgießsondervverfahren „Pull and Foam“ / Mold concept for the special foam injection molding technique "pull and foam"*. Diploma thesis (supervisor: M. Tromm), University of Kassel, Germany.

- [173] Zhou, Y.-G. and Chen, T.-Y.: Combining foam injection molding with batch foaming to improve cell density and control cellular orientation via multiple gas dissolution and desorption processes. *Polym Adv Technol.* 2020;1–16

List of author's publications / contributions

Journal papers (peer-reviewed)

- Tromm, M., Shaayegan, V., Wang, C., Heim, H.-P., Park, C. B.: Investigation of the mold-filling phenomenon in high-pressure foam injection molding and its effects on the cellular structure in expanded foams. *Polymer* 160 (2019) 43–52
- H.-P. Heim, M. Tromm: Injection molded components with functionally graded foam structures – Procedure and essential results. *Journal of Cellular Plastics* 52 (2015) 3: 299-319.
- H.-P. Heim, M. Tromm: General aspects of foam injection molding using local precision mold opening technology. *Polymer* 56 (2015) 111-118.

Book chapters

- F. Mieth, M. Tromm: Multicomponent Technologies. In: *Specialized Injection molding Techniques* (Edited by H.-P. Heim). Elsevier 2016, S.1-51. ISBN: 978-0-323-34100-4

Conference paper (peer-reviewed)

- M. Tromm, H.-P. Heim: High-Pressure Foam Injection Molding With Local Core-Back Method – Simulation Approach. In: *FOAMS 2016 (SPE)*. Seattle, WA, USA, 14.09.2016.
- H.-P. Heim, M. Tromm: Formation of morphology as a function of process control by foam injection molding of a functionally graded component. In: *ANTEC 2014 (SPE)*, Las Vegas NV, US, 28-30 April 2014, pp.1551–1556.
- H.-P. Heim, M. Tromm: Pull and Foam – Method: First Investigations with chemical and physical blowing agents. In: *FOAMS 2012 (SPE)*, Barcelona, Spain, 12-13 September 2012.

- H.-P. Heim, M. Tromm, S. Jarka, J. Schnieders & S. Gövert (2012): Pull and Foam-Injection moulding method: Foamed ribs for stiffening plane components. In: ANTEC 2012 (SPE), Orlando, USA, 02-04. April 2012.

Articles / reports / presentations

- M. Tromm: Process variants in foam injection molding - Potentials of special mold technologies. Presentation, ENGEL foammelt 2019, Schwertberg – 20.11.2019
- M. Tromm: „pull and foam“ - Hochaufgeschäumte spritzgegossene Strukturen / Leichtbaupotential durch Schaumspritzgießen mit lokaler Kavitätserweiterung. / pull and foam“ - Highly foamed injection molded structures, lightweight potential by foam injection molding with local cavity enlargement. Presentation, PIAE Europe 2018 (Plastics in Automotive Engineering), Mannheim, VDI-Spezialtag „Kunststoffschäume im Fahrzeug“ / VDI-special „Polymeric foams in automotive applications“, 13.03.2018.
- M. Tromm, H.-P. Heim: Customized foam. Kunststoffe International 01-02/2018, p. 24-28.
- H.-P. Heim, M. Tromm: Thermoplast-Schaumspritzgießverfahren pull and foam / Thermoplastic foam injection molding technique pull and foam. Schlussbericht / Final project report, IGF-Vorhaben Nr. 18254 N/1, 2017.
- M. Tromm, H.-P. Heim: Controlling cellular structure and surface quality in foam injection molding – innovative core-back mold for research. Poster. In: SPE Foams 2017, Bayreuth, 09 - 10.10.2017.
- M. Tromm: Beeinflussung der zellularen Struktur und der Oberflächenqualität beim Schaumspritzgießen durch innovative Werkzeugtechnologie / Influence on cellular structure and surface quality in foam injection molding by using innovative mold technologies. Presentation, DGM Werkstoffwoche 2017, Dresden, 28.-30.09.2017.
- M. Tromm: Simulation of Foam Injection Molding - Conventional Procedure, Core-back and Local Core-back Procedure. Presentation, CCMCP Meeting – 04.-05.05.2017, Toronto, Kanada.

- M. Tromm: Controlling cellular structure and surface quality in foam injection molding by an innovative core-back mold. Presentation, Séminaire de recherche, Département de génie chimique, University Laval, 02.06.2017, Quebec City, Kanada.
- M. Tromm: Simulation of High Pressure Foam Injection Molding with Core-back Operation. Presentation, International Moldex3D Usermeeting 2017, Würzburg, 27.-28.03.2017.
- M. Tromm: Simulation of High Pressure Foam Injection Molding with Local Core-back. Press release, Moldex3D Global Innovation Talent Award 2016, #Moldex3DStory Contest- 2nd price EMEA Region, 30.09.2016 <http://www.moldex3d.com/en/2016-moldex3d-global-innovation-talent-award-winners/> (short version).
- M. Tromm: Verification of new simulation approaches in High-Pressure Foam injection molding with local core-back method. Presentation, CellMAT 2016, Dresden, 07.-09.12.2016.
- M. Tromm: Influence of process control on structure formation and mechanical properties by Injection molding of a partial foamed component. Presentation, CellMAT 2014, Dresden, 22.10.-24.10.2014.
- M. Tromm: Erzeugung lokaler Schaumstrukturen im Spritzgießprozess / Creation of local foam structures in injection molding. Presentation, Schaumtagung Cellmould®, Wittmann-Battenfeld, Meinerzhagen 10.04.2014.
- H.-P. Heim, V. Sauer, F. Mieth & M. Tromm (2014) Assessment of the changeability of plastics processing systems. Poster. In: ANTEC (SPE), Las Vegas NV, US, 28 April 2014
- H.-P. Heim, A. K. Bledzki, M. Rohleder & M. Tromm: Thermo-mechanically graded injection moulded microcellular foams/ Thermomechanisch graduierte injektionsgeformte Mikrozellulärschäume, 1st International Conference on Thermo-Mechanically Graded Materials, Proceedings, Kassel, DE, 29-30.10.2012

- H.-P. Heim, A.K. Bledzki, M. Rohleder & M. Tromm: Formation of foam structures and influence of processing procedure in foam injection moulding of thermoplastic materials. In: CELLMAT, Dresden, Deutschland, 07-09.09.2012

Awards

- Moldex3D Global Innovation Talent Award 2016, „#Moldex3D Story Contest“, 2. price EMEA Region („Simulation of High Pressure Foam Injection Molding with Local Core-back“)

Conference organisation

- Co-Chair of CellMAT 2016 Conference, Dresden, 12/2016
- Co-Chair of CellMAT 2018 Conference, Bad Staffelstein, 10/2018

11 Appendix

11.1 General information

Cause and effect diagram for cellular structure development in HP-CB-FIM

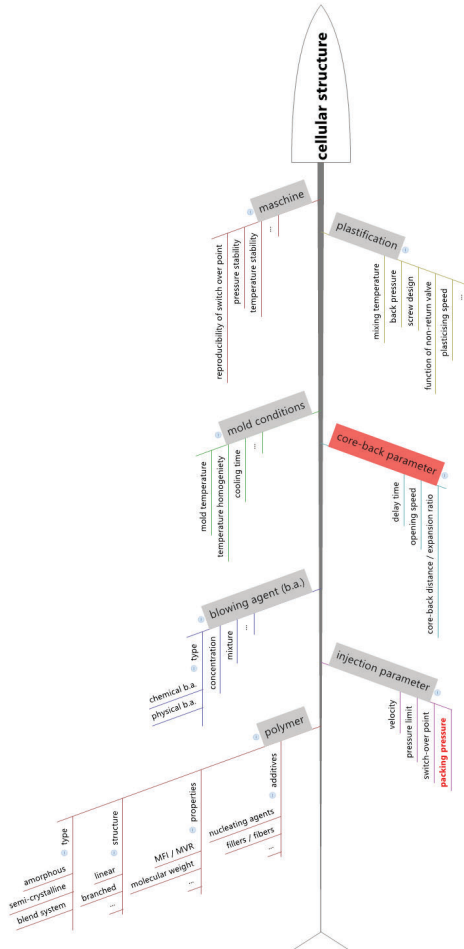


Figure 121: Cause and effect diagram (Ishikawa diagram) for cellular structure development in foam injection molding process; core-back parameters highlighted

11.2 Light-weight potential of High-pressure foam injection molding

Foams are often used to reduce the amount of material and component’s weight. In this regard neat material is substituted by foamed material using similar geometries. However, foams may also be used to enhance component’s stiffness. Foamed material exhibit a lower modulus of elasticity. But, using the materials savings to enhance components thickness, stiffness increases for constant component’s weight. The flexural rigidity is a product of the flexural modulus of elasticity (material resistance) and the moment of inertia (geometrically induced resistance). This value decreases as the density reduction increases. However, the moment of inertia increases disproportionately due to the enlargement of the volume, resulting in an increase of the flexural rigidity at a constant component weight. The flexural modulus does decline by foaming, however, the correlating decrease in stiffness may be overcompensated by the increase of the moment of inertia resulting by the enlargement of the volume. This (sandwich) effect is shown in Figure 122, based by own measurements [129, 152, 170] and also mentioned in literature dealing with HP-VE-FIM [14, 15, 142, 147].

This effect is usually used in sandwich constructions. Foam injection molding and especially the HP-VE-FIM methods, allowing significantly higher expansion ratios, may offer this tremendous potential for lightweight constructions to mass production.

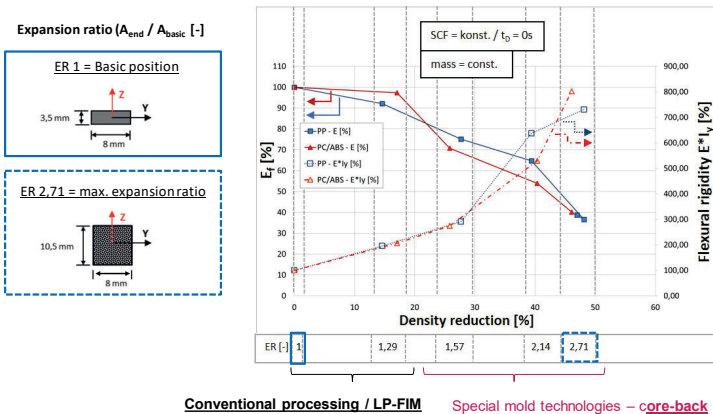


Figure 122: Light-weight potential of foam injection molding: flexural modulus and bending stiffness in dependency of density reduction for PP/ N₂, PC-ABS/ N₂ and PA6-GF15/ N₂ (results also published in [148])

A huge potential of the local core-back technology is seen in the field of foaming rib structures. Thus, theoretical calculations based on measurement data for density and flexural modulus were performed (assuming a linear decrease of flexural modulus and no discussion on ability of demolding). For equal bending stiffness of a foam and a compact rib, significant density reduction have been calculated [129].

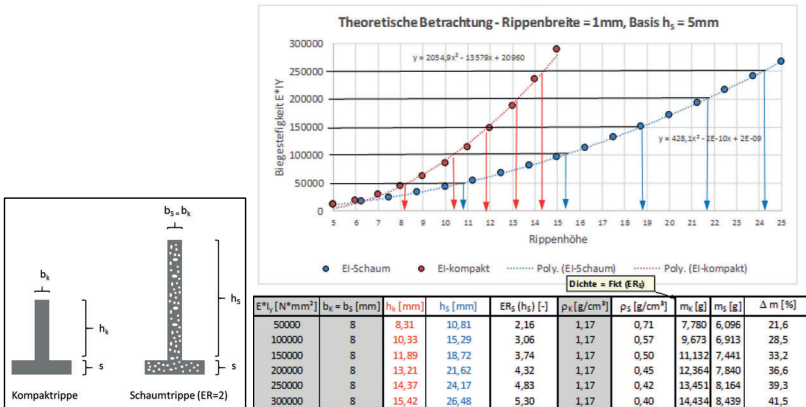


Figure 123: Theoretical bending stiffness of compact and foamed ribs in dependency of rib height (upper); resulting rib heights and mass of ribs for similar stiffness values (lower); index k = compact, index s = foam (results also published in [129])

11.3 Parameter settings

Übersicht der Prozessparameter im Nieder - und Hochdruckverfahren - Schaumspritzgießen -						
veränderte Parameter						
Versuchsreihe	Niederdruck			Hochdruck		
	A	B	C	D	E	F
Temperaturen Aggregat						
- Materialeinzug	50°C	50°C	50°C	50°C	50°C	50°C
- Heizzone 1	260°C	260°C	260°C	260°C	260°C	260°C
- Heizzone 2	265°C	265°C	265°C	265°C	265°C	265°C
- Heizzone 3	270°C	270°C	270°C	270°C	270°C	270°C
- Heizzone 4	275°C	275°C	275°C	275°C	275°C	275°C
- Heizzone 5	280°C	280°C	280°C	280°C	280°C	280°C
Temperaturen Heißkanal						
- Heizzone 1	280°C	280°C	280°C	280°C	280°C	280°C
- Heizzone 2	280°C	280°C	280°C	280°C	280°C	280°C
- Heizzone 3	280°C	280°C	280°C	280°C	280°C	280°C
- Heizzone 4	280°C	280°C	280°C	280°C	280°C	280°C
Dosieren						
- Dosiervolumen	40 cm ³	40 cm ³	40 cm ³	45 cm ³	45 cm ³	45 cm ³
- Schneckengeschwindigkeit	300 mm/s	300 mm/s	300 mm/s	250 mm/s	250 mm/s	250 mm/s
- Staudruck	200 bar	200 bar	200 bar	210 bar	210 bar	210 bar
Einspritzen						
- Einspritzgeschwindigkeit 1	50,00 cm ³ /s	200,00 cm ³ /s	125,00 cm ³ /s	50,00 cm ³ /s	200,00 cm ³ /s	125,00 cm ³ /s
- Einspritzgeschwindigkeit 2	50,00 cm ³ /s	200,00 cm ³ /s	125,00 cm ³ /s	50,00 cm ³ /s	200,00 cm ³ /s	125,00 cm ³ /s
- Einspritzdruck 1	1800 bar	1800 bar	1800 bar	1800 bar	1800 bar	1800 bar
- Einspritzdruck 2	1150 bar	1150 bar	1150 bar	1150 bar	1150 bar	1150 bar
- Massevolumen für Umschaltpunkt 1	16,00 cm ³	16,00 cm ³	16,00 cm ³	10,00 cm ³	10,00 cm ³	10,00 cm ³
- Massevolumen für Umschaltpunkt 2	15,00 cm ³	15,00 cm ³	15,00 cm ³	9,00 cm ³	9,00 cm ³	9,00 cm ³
Nachdruck						
- Nachdruck 1	-	-	-	800 bar	800 bar	800 bar
- Nachdruck 2	-	-	-	600 bar	600 bar	600 bar
- Nachdruckzeit	0 s	0 s	0 s	2 s	2 s	2 s
Kühlen						
- Restkühlzeit	15 s	15 s	15 s	40 s	40 s	40 s
Werkzeug						
- Werkzeugtemperatur	90°C	90°C	90°C	90°C	90°C	90°C
Werkzeug öffnen bis Zwischenstopp						
- Öffnungsgeschwindigkeit	-	-	-	20 mm/s	20 mm/s	20 mm/s
- Öffnungskraft	-	-	-	34 kN	34 kN	34 kN
- Öffnungsweg	-	-	-	3,00 mm	3,00 mm	3,00 mm
- Toleranz Öffnungsweg	-	-	-	0,80 mm	0,80 mm	0,80 mm
MuCell Einheit						
- Gasanteil	0,3wt%	0,3wt%	0,3wt%	0,3wt%	0,3wt%	0,3wt%
- Schussgewicht	40,00 g	40,00 g	40,00 g	40,00 g	40,00 g	40,00 g
- Gas	N ₂	N ₂	N ₂	N ₂	N ₂	N ₂

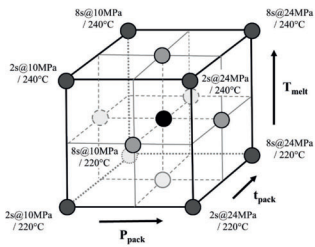
Figure 124: Parameter settings for the HP-MO-FIM experiments with variation of injection speed used for the results shown in chapters 8.2 and 8.3.3

Versuchsreihe	Druckstudie						
Temperaturen Aggregat							
- Materialeinzug	50°C						
- Heizzone 1	260°C						
- Heizzone 2	265°C						
- Heizzone 3	270°C						
- Heizzone 4	275°C						
- Heizzone 5	280°C						
Temperaturen Heißkanal	280°C						
Dosieren							
- Dosiervolumen	45 cm ³						
- Schneckengeschwindigkeit	250 mm/s						
- Staudruck	210 bar						
Einspritzen							
- Einspritzgeschwindigkeit 1	200,00 cm ³ /s						
- Einspritzdruck 1	1800 bar						
Nachdruck							
- Nachdruck	200 bar	300 bar	400 bar	500 bar	600 bar	700 bar	800 bar
- Nachdruckzeit	4 s						
Kühlen	40 s						
Werkzeug							
- Werkzeugtemperatur	90°C						
Werkzeug öffnen bis Zwischenstopp							
- Öffnungsgeschwindigkeit	20 mm/s						
- Öffnungskraft	34 kN						
- Öffnungsweg	3,00 mm						
MuCell Einheit							
- Gasanteil	0,3wt%						
- Schussgewicht	40,00 g						
- Gas	N ₂						

Figure 125: Parameter settings for the HP-MO-FIM experiments with variation of packing pressure level according to chapter 8.4.3

ZtrIPunkt	Blöcke	SCF [wt% N2]	VO [mm/s]	ER [-]	tH [s]	Chargenbez.
1	1	0,50	100	200	1	B1
1	1	0,20	100	200	3	A1
1	1	0,50	100	300	3	B2
1	1	0,20	10	300	3	A2
1	1	0,50	10	200	3	B3
0	1	0,35	55	250	2	CP
1	1	0,20	100	300	1	A3
1	1	0,20	10	200	1	A4
1	1	0,50	10	300	1	B4
-1	2	0,20	55	250	2	S1
-1	2	0,50	55	250	2	S2
-1	2	0,35	10	250	2	S3
-1	2	0,35	100	250	2	S4
-1	2	0,35	55	200	2	S5
-1	2	0,35	55	300	2	S6
-1	2	0,35	55	250	1	S7
-1	2	0,35	55	250	3	S9

Figure 126: Parameter settings according to the DoE performed in chapter 8.3.2



StdOrder	RunOrder	CenterPt	Blocks	ppack [bar]	tpack [s]	TMelt [°C]
1	4	1	1	100	2	220
2	5	1	1	240	8	220
3	2	1	1	240	2	240
4	3	1	1	100	8	240
5	1	0	1	170	5	230
6	10	1	2	240	2	220
7	9	1	2	100	8	220
8	8	1	2	100	2	240
9	7	1	2	240	8	240
10	6	0	2	170	5	230
11	11	-1	3	100	5	230
12	12	-1	3	240	5	230
13	13	-1	3	170	2	230
14	14	-1	3	170	8	230
15	15	-1	3	170	5	220
16	16	-1	3	170	5	240

Figure 127: Experimental design and parameter settings for the experiments according to chapters 8.4.1 and 8.4.2

11.4 Details on μ CT analysis



Figure 128: Sample preparation for structure analysis[97]

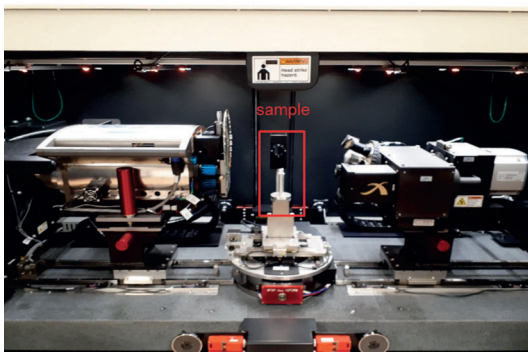


Figure 129: Detail of μ CT device: scanning chamber with mounted sample [97]

	LP-FIM	HP-FIM / pressure study
voltage	80 kV	80 kV
power	6 W	7 W
binning	2	2
exposure time	2	2
projections	1601	1601
resolution	2,94 – 3,37 μm	4,56 – 5,76 μm

Figure 130: μCT device settings used for sample measurement [97]

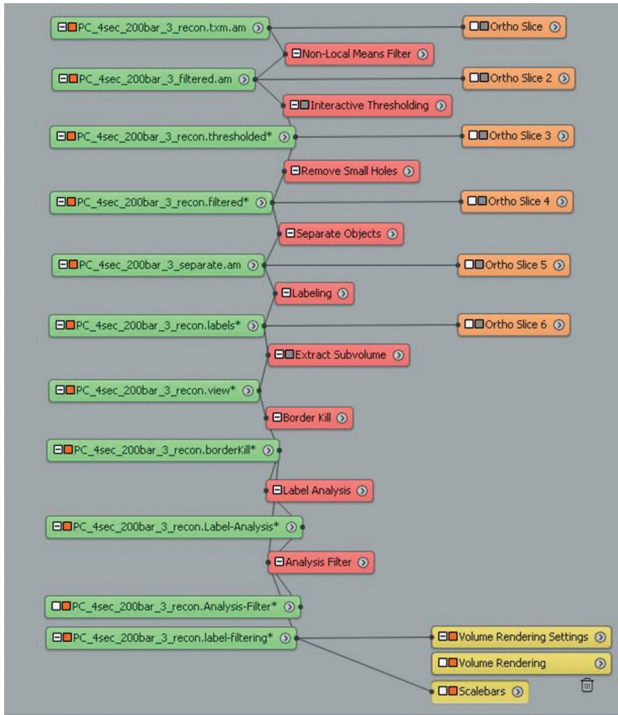


Figure 131: Example for the μCT data reconstruction in AVIZO; order of operations and filters used for reconstruction [97]

11.5 Simulation

11.5.1 Definition of foam injection molding process in Moldex3D

The following screenshots show the options to define the foam injection molding process specifics as well the definitions for the core-back procedure in Moldex3D (R15).

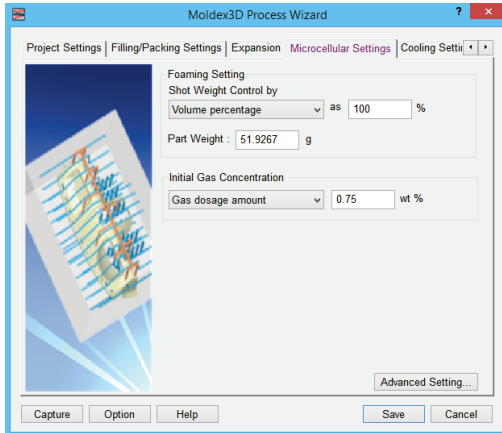


Figure 132: Definition options for sop and blowing agent content in Moldex3D (R15)

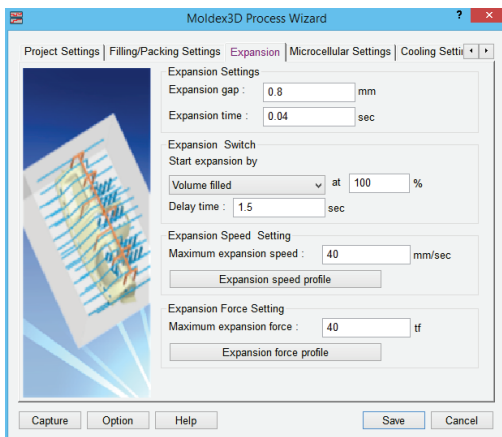


Figure 133: Definition options for expansion settings for mold opening / core-back operation in Moldex3D (R15)

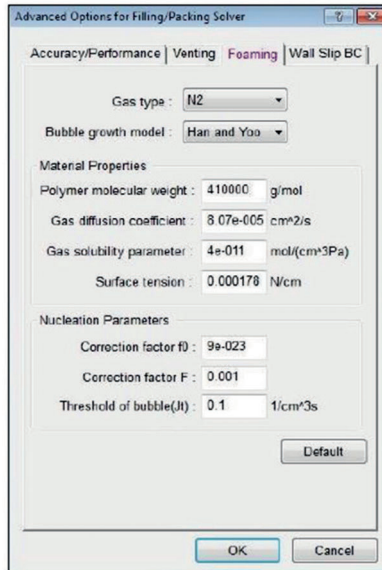


Figure 134: Advanced definition options for calculation of foaming in Moldex3D (R15); choice of gas type (N₂ / CO₂), bubble growth model (Han and Yoo / Shaafi / Payvar) and user-ditable values for foam-related material properties

11.5.2 Results for cell density

Besides cell size also the resulting cell densities are calculated by Moldex3D. In addition to the simulation results shown in chapters 5 and 6, the according results for cell density are depicted in the following, confirming the findings of a more uniform and more flow path independent structure formation in HP-VE-FIM.

Low-pressure procedure

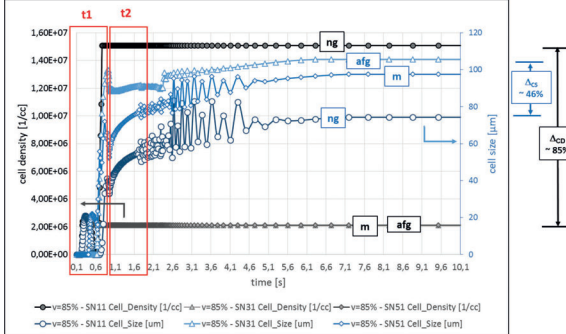


Figure 135: Simulation results for cell density (grey) and cell size (blue) in low-pressure foam injection molding at 3 different positions in the core-layer of the part, sop = 85% filling volume according to Figure 27

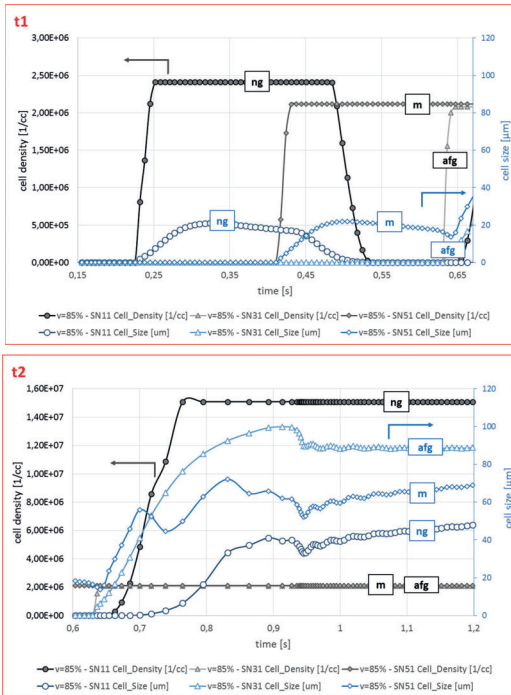


Figure 136: Details of Figure 135 – time = 0 – 1.2 s

High-pressure procedure

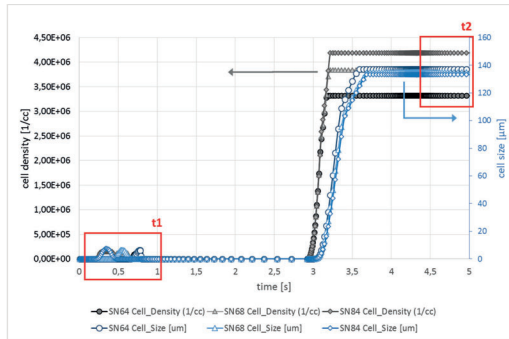


Figure 137: Simulation results for cell density (grey) and cell size (blue) in high-pressure foam injection molding at 3 different positions in core-layer of the part, $p_{pack} = 2 \text{ s}$ @ 60/80 MPa volume according to Figure 40

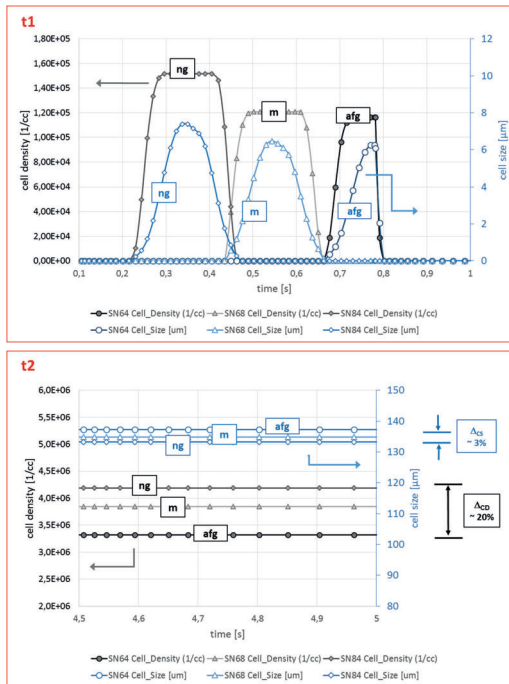


Figure 138: Details of Figure 137 – time = 0 – 1 s and 4.5 – 5 s

11.5.3 Simulation of local core-back procedure

In addition to the simulation results shown before, also further information e.g. indications for compact skin layer thickness and areas of insufficient molding / rupture effects may be predicted by simulation (see Figure 139). Additionally, simulation was used to predict cell structure for a new part geometry. Here, a new mold insert for the improved core-back mold was designed and simulated (see Figure 140).

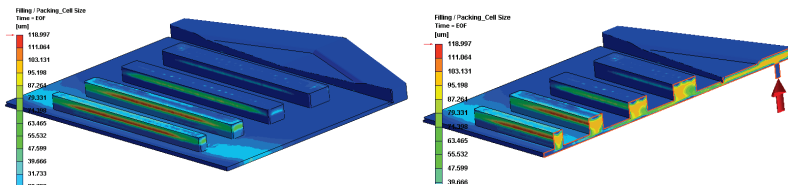


Figure 139: Prediction of compact skin layers and defects / incomplete molding by simulation (rupture of rib flanks)

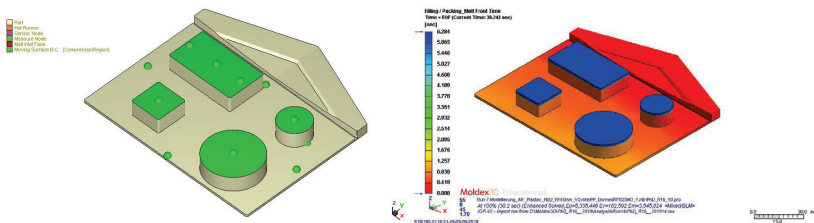


Figure 140: Construction of a new mold insert for the improved local core-back mold (upper: definition of core-back areas and sensor nodes = green; lower: simulation result = filling time)

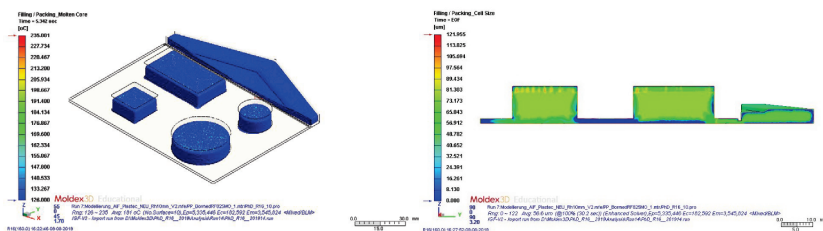


Figure 141: Simulation results for new mold insert for the improved local core-back mold (upper: melting core, middle and lower: final cell size); note: high expansion ratios have not successfully been simulated due to calculation problems in context with the parts' mesh

11.6 Mold concepts for mold opening

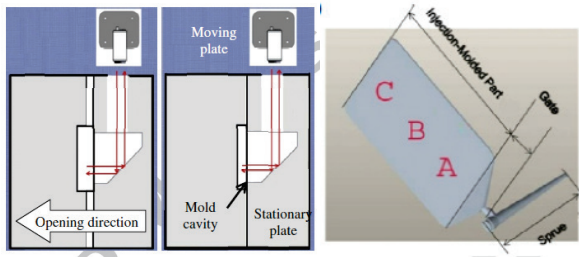


Figure 142. Mold used for foam injection molding experiments at University of Toronto; mold expansion conducted via simple opening stroke [33]; this mold was also used for experiments shown within this thesis reported in chapters 8.4.1 and 8.4.2 (permission to publish by Copyright Clearance Center, License number: 4835480970006; May 24, 2020)

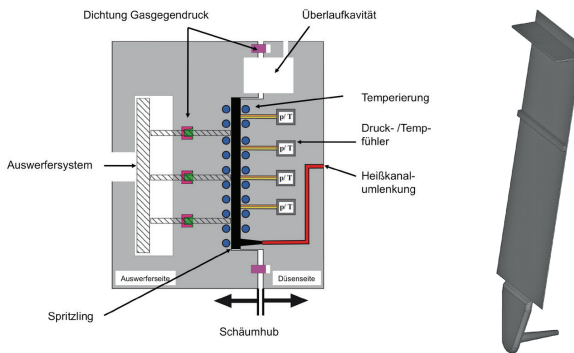


Figure 143: Mold used for investigations at University of Bayreuth, Germany; a special concept of temperature control allows to perform an isothermal process [15] (with kind permission of the author)

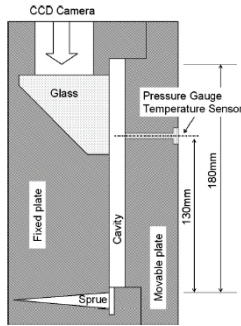
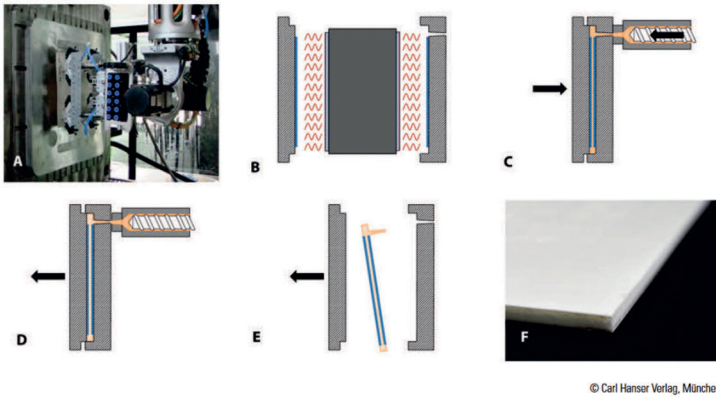


Figure 144: Mold used at the University of Kyoto, Japan [34, 35, 40, 171] permission to publish by Copyright Clearance Center; License number: 4870920204550; Jul 16, 2020)



© Carl Hanser Verlag, München

Figure 145: Mold for applied research studies at Fraunhofer ICT Pfinzta, Germany [142] (with kind permission of Carl Hanser Verlag, Munich)

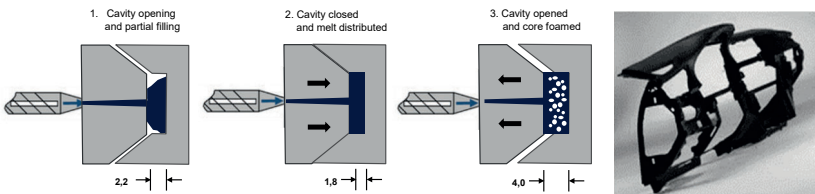


Figure 146: Principle of mold and procedure used to produce foamed dashboards by BMW (according to [144] and product [144] (with kind permission of BMW))

11.7 Mold concepts for core-back

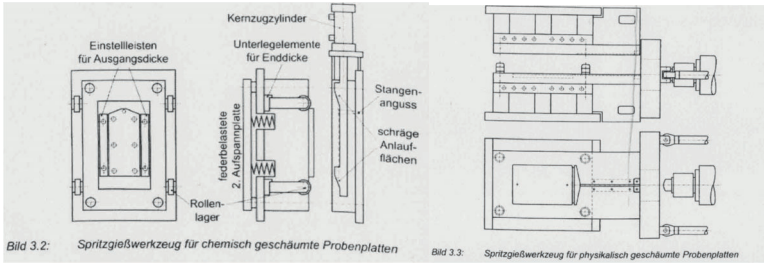


Figure 147: Core-back mold for chemically blown samples (left) and mold for physically blown samples used in studies of [14] (with kind permission of the author) at University of Erlangen-Nürnberg, dimensions of part: 80 x 160 mm

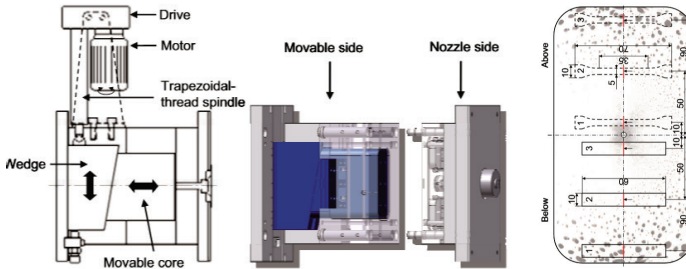


Figure 148: Core-back mold used in studies of [1, 19] (with kind permission of the author) at IKV Aachen, Germany, dimensions of part: 100 x 200 mm

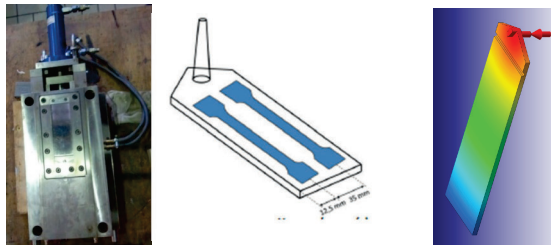


Figure 149: 1. Core-back mold with full expansion of rectangular geometry used in studies of [16] and [18] at Institute of Materials Engineering University of Kassel, Germany; part dimensions 160 x 60 mm, 2 mm initial parts thickness – stepwise expandable up to 4mm; cold and hot runner option

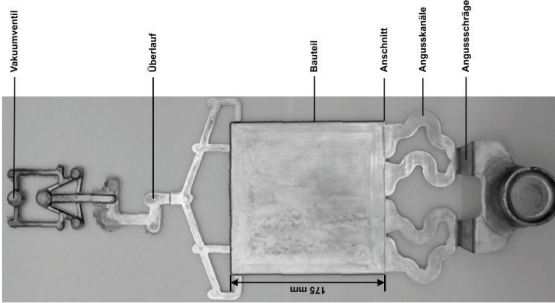
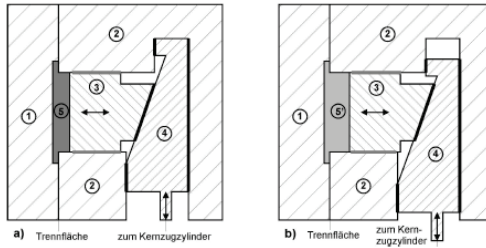
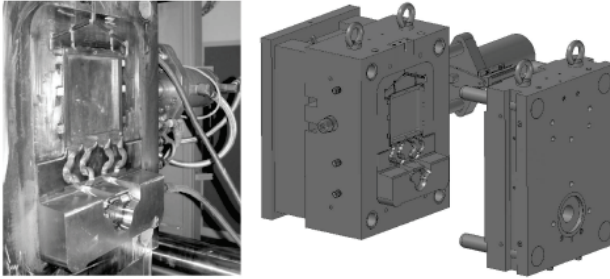


Abbildung 4-2: Gussstückgeometrie des Demonstrationsbauteils „Platte“ mit Anguss und Überlauf.

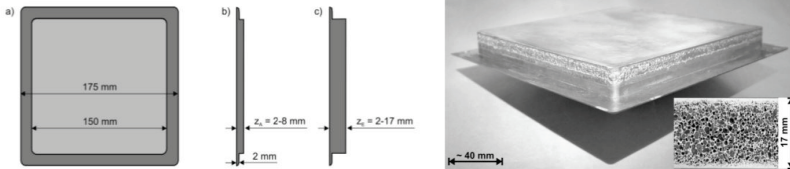
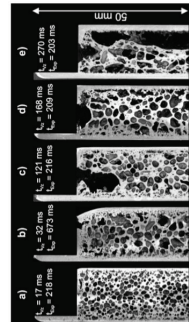


Figure 150: Core-back mold for high-pressure foam casting (upper) of alumina and casted aluminum part (lower) [137] (with kind permission of the author)

11.8 Details on improved mold

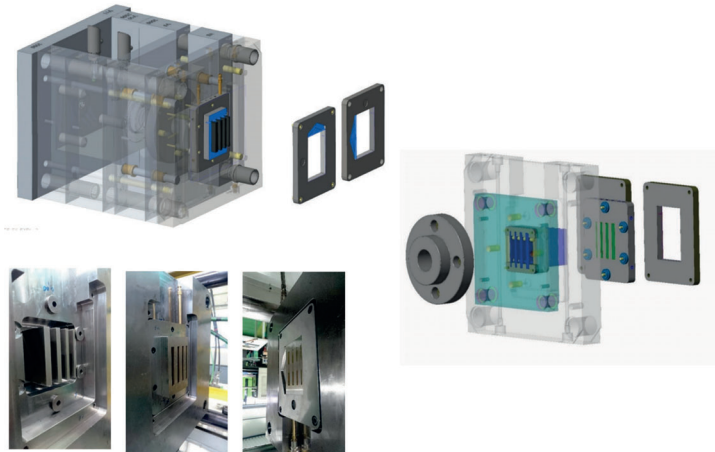


Figure 151: Details on the improved core-back: simple changeability of core-back insert



Figure 152: Improved core-back mold mounted on Arburg 470 machine

Kriterien	Gewicht [%]	Fluidtechnik		Elektromechanik		
		Pneumatisch	Hydraulisch	Zahnstange	Zahnriemen	Gewinde-spindel
Exakte Positionierbarkeit	20	2,0	4,0	4,0	4,0	5,0
Hubgeschwindigkeit	20	1,0	4,0	1,0	1,0	2,0
Axiale Belastbarkeit / Druckkraft	15	1,0	4,0	1,0	1,0	3,0
Integrierbarkeit / geometrische Abmessung	15	3,0	4,0	1,0	1,0	3,0
Kosten (inkl. Wartung)	15	4,0	2,0	3,0	3,0	3,0
Umweltverträglichkeit	5	4,0	2,0	4,0	4,0	4,0
Wirkungsgrad	10	4,0	4,0	3,0	3,0	2,0
Gesamtpunktzahl	100	2,4	3,6	2,3	2,3	3,2

1 = sehr schlecht 3 = neutral 5 = sehr gut

Figure 153: Comparison of different solutions for machine-independent core-movement: pneumatic, hydraulic, linear rack, toothed belt and screw drive (worked out and assessed by [172] (with kind permission of the author))






	Co1 REAL	Co2 REAL	Co3 INT	Co4 INT	Co5 INT	Co6 DINT
Row1	Software Position 1 [mm] Software Geschwindigkeit 1 [mm/s]	Software Geschwindigkeit 1 [mm/s]	Wartezeit 1 [ms]	Software Geschwindigkeit "JOP" [mm/s]	Wartezeit 1 [ms]	Software Beschleunigung [mm/s²]
Row2	Software Position 2 [mm] Software Geschwindigkeit 2 [mm/s]	Software Geschwindigkeit 2 [mm/s]	Wartezeit 2 [ms]		Miner Geschwindigkeit [mm/s]	Software Verzögerung [mm/s]
Row3	Software Position 3 [mm] Software Geschwindigkeit 3 [mm/s]	Software Geschwindigkeit 3 [mm/s]	Wartezeit 3 [ms]	Software Geschwindigkeit "Endlagensposition" [mm/s]	Miner Kraft [N]	Software Ruck-Beschleunigung [mm/s³]
Row4	Software Position 4 [mm] Software Geschwindigkeit 4 [mm/s]	Software Geschwindigkeit 4 [mm/s]	Wartezeit 4 [ms]			Software Gradient Kraftregelung [N/s]
Row5	Software Position 5 [mm] Software Geschwindigkeit 5 [mm/s]	Software Geschwindigkeit 5 [mm/s]	Wartezeit 5 [ms]			
Row6				Software Geschwindigkeit "Endlagensposition 1" [mm/s]		
Row7	Software Position 6 [mm] Software Kraftregelung [N]	Software Geschwindigkeit 6 [mm/s]	Wartezeit 6 [ms]			
Row8	Software Position 7 [mm] Software Kraftregelung [N]	Software Geschwindigkeit 7 [mm/s]	Wartezeit 7 [ms]			
Row9	Software Position 8 [mm] Software Kraftregelung [N]	Software Geschwindigkeit 8 [mm/s]	Wartezeit 8 [ms]			
Row10	Software Position 9 [mm] Software Kraftregelung [N]	Software Geschwindigkeit 9 [mm/s]	Wartezeit 9 [ms]			
Row11	Software Position 10 [mm] Software Kraftregelung [N]	Software Geschwindigkeit 10 [mm/s]	Wartezeit 10 [ms]			
Row12						
Row13	Software Position Software Kraftregelung [N]	Software Geschwindigkeit [mm/s]	Wartezeit Kraftregelung [ms]			
Row14	Software Position Software Kraftregelung [N]	Software Geschwindigkeit [mm/s]	Wartezeit Kraftregelung [ms]			
Row15	Software "Endlagensposition" [mm]					
Row16	Software "Endlagensposition 1" [mm]					

Figure 154: Details and components for the chosen core movement solution: hydraulic control unit with 2-way servo-hydraulic control valve (upper left), software for editing and monitoring the core movement profile (lower left) and recipe table for movement definition (positions, speeds, directions, modus of movement: by position / by pressure)

Kriterien	Gewicht [%]	Konvek-tion	Wärmestrahlung						Wärme-leitung	Induktion	
			Infrarot			Laser					
			Indirekt	Extern Stand-ard	Extern abge-koppelt	Index-platten-werkzeu-g	Intern	Extern			Keramik-heiz-ele-men-te
Funktionalität	Ausreichend hohe Temperatur der Kavitätsoberfläche	20	5	3	4	5	5	5	5	5	5
	Homogene Temperaturverteilung	20	3	2	3	3	3	3	4	3	4
	Hohe Aufheiz-/Abkühlrate	15	3	2	3	4	5	5	4	4	3
Umsetzbarkeit	Integrierbarkeit	20	4	2	2	1	1	1	3	2	1
	Kosten (inkl. Wartung)	15	3	3	3	2	1	1	3	2	2
	Handhabung / Bedienerfreundlichkeit	10	4	3	3	2	3	2	4	2	3
Gesamtpunktzahl		100	3,7	2,5	3,0	2,9	3,0	2,9	3,9	3,1	3,1

1 = sehr schlecht 3 = neutral 5 = sehr gut

Figure 155: Comparison of different solutions for rapid heat and cooling process: convection, infrared, laser, ceramic heat elements, induction (worked out and assessed by [172] (with kind permission of the author))

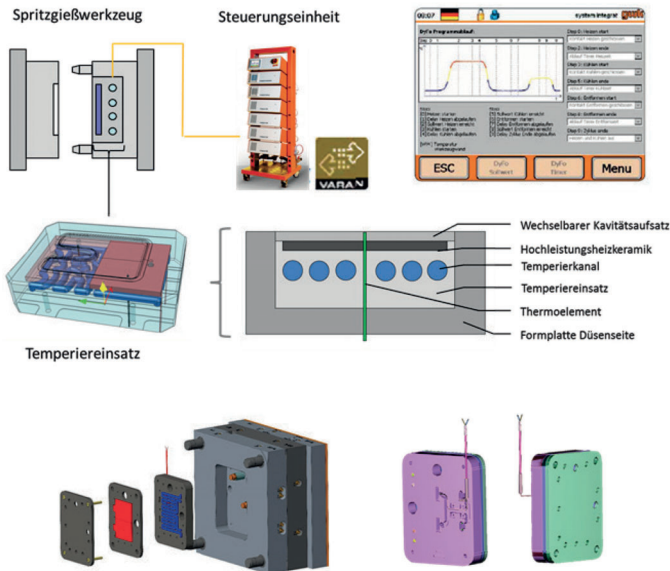


Figure 156: Details on the chosen rapid heat cooling insert: integration and construction details (ceramic insert with conformal cooling designed and built by gwk mbH)

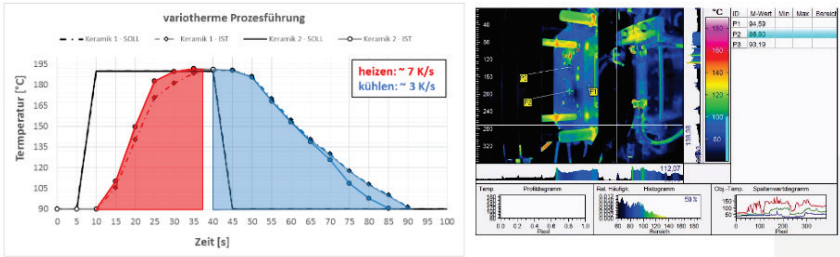


Figure 157: Measurement data for cavity temperature in variotherm process (results also published in [86])

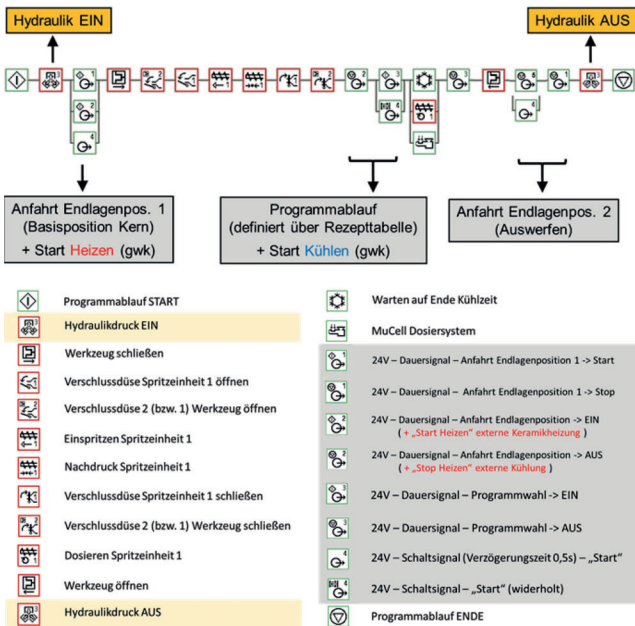


Figure 158: Complete process sequence including 24 V signals for implementing the external driven hydraulic cylinder and the rapid heat cooling insert



Figure 159: Mold and components for external core-movement (upper), initial experiments (middle) and final experimental setup including all electrical devices and computer in an external box (lower)

11.9 Rapid heat cooling process

As already mentioned, a special insert was implemented inside the mold to allow a variotherm process control. This point is not discussed within the thesis to not shift the focus from structure development. The surface side of the cavity may be quickly heated up before injection to achieve an improved surface finish and to eliminate silver streaks. At the beginning the cavity surface was fine-grinded, later a polished surface was used for experiments.

In the experiments using the variotherm process it became evident that the reproduction of the cavity surface / cavity finish is noticeably improved by the high pressure and the active packing phase in high-pressure procedures compared to low-pressure procedure. These experiments may be concluded by the statement that variotherm process in foam injection molding may exploit its advantages only in combination with high-pressure procedures. In the following some exemplarily results are shown.

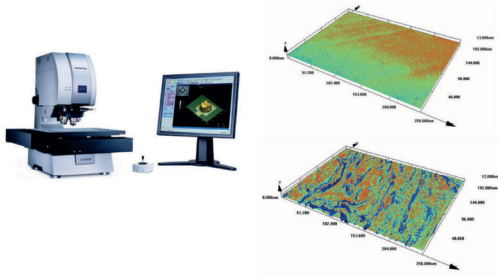


Figure 160: Confocal laser-scanning microscope for quantification of surface reproduction with exemplarily results compact molded surface (upper right) and foam injection molded surface (lower right)

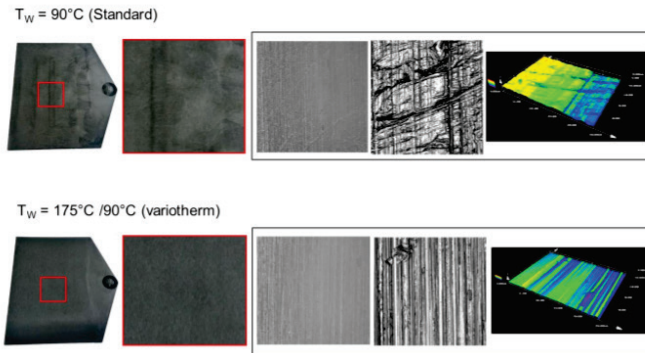


Figure 161: Comparison of surface reproductions (fine-grained cavity surface) – upper: PC-ABS/0.5wt%N₂ @ ER=4.7 (rib region) molded @ $T_{mold}=90^{\circ}\text{C}$; lower: same setting @ $T_{mold}=175^{\circ}\text{C}$

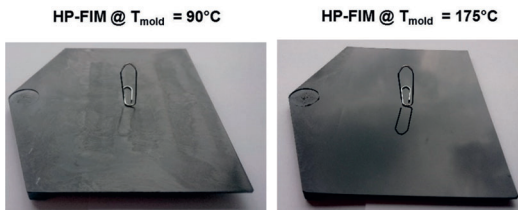


Figure 162: Comparison of surface finish of foam injection molded parts produced by conventional (left) and variotherm process (right) (also published in [86])

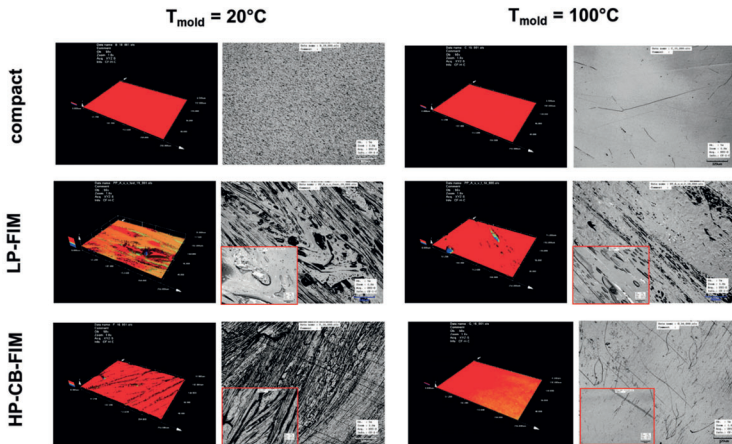


Figure 163: Exemplary result of surface measurements of low-pressure foam injection molded parts - effect of variotherm process on cavity surface reproduction: compact molding (upper), low-pressure procedure (middle), high-pressure core-back procedure (lower); cavity surface is polished

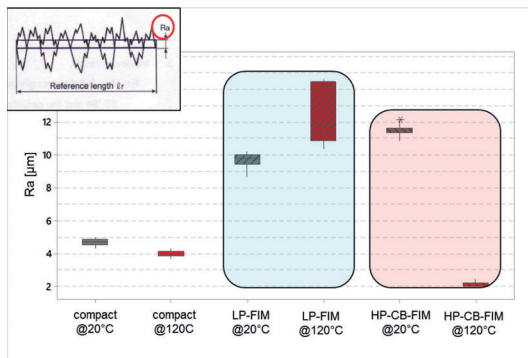


Figure 164: Exemplarily result of surface roughness (R_a) for compact molding ("compact"), low-pressure foam injection molding ("LP-FIM") and high-pressure core-back foam injection molding ("HP-CB-FIM"); standard mold temperature (20°C) compared to variotherm process (100°C)

11.10 Picture Credits

Figure	Source	Approved
9, 149	Kirschling, H. M. M. 2009. Mikroschäume aus Polycarbonat / Microcellular foams of polycarbonate. PhD thesis, University of Kassel, Germany.	Kirschling, H.M.M.; 09.07.2020
16, 32, 33, 46, 128-131	Mihailovic, J. 2019. Zellstrukturcharakterisierung mittels dreidimensionaler Bildgebungsverfahren. / Characterisation of cellular structures with threedimensional imaging techniques. Masterthesis (supervisor: M. Tromm), University of Kassel, Germany.	Mihailovic, J.; 26.05.2020
142	Shaayegan, V., Wang, C., Costa, F., Han, S., and Park, C. B. 2017. Effect of the Melt Compressibility and the Pressure Drop Rate on the Cell-Nucleation Behavior in Foam Injection Molding with Mold Opening. European Polymer Journal, 92, 314–325.	Copyright Clearance Center; License Number: 4835480970006; May 24,2020
143	Spörrer, A. 2010. Leichte Integralschäume durch Schaumspritzgießen mit optimierten Werkstoffen und variothermen Werkzeugen. / Lightweight integral foams by foam injection molding with optimized materials and variothermal tools. PhD thesis, University of Bayreuth, Germany.	Spörrer, A.; 08.07.2020
144	Ishikawa, T. and Ohshima, M. 2011. Visual observation and numerical studies of polymer foaming behavior of polypropylene/carbon dioxide system in a core-back injection molding process. Polym. Eng. Sci. 51, 8, 1617–1625	Copyright Clearance Center; License Number: 4870920204550; Jul 16, 2020
145	Roch, A., Menrath, A., and Huber, T. 2013. Faserverstärkte Thermoplaste in Sandwichbauweise / Fiber reinforced thermoplastics in sandwich constructions. Kunststoffe, 10, 183–189.	Kunststoffe 09.07.2020
146	Reisch, T. 2012. Cockpitkonzept der Zukunft am Beispiel der BMW 1-er und 3-er Reihe / Future cockpit concept by the example of BMW series 1 and 3. In Schriftenreihe Kunststofftechnik VDI 2012	Melzig, J.; 28.07.2020
147	Müller, N. 2006. Spritzgegossene Integralschaumstrukturen mit ausgeprägter Dichtereduktion / Foam injection molded integral foam structures with pronounced density reduction. PhD thesis, University of Erlangen-Nürnberg, Germany.	Müller, N.; 08.07.2020
148	Flórez Sastre, L. F. 2011. Einfluss der Schaummorphologie auf die mechanischen Eigenschaften von Kunststoffstrukturschäumen. / Influence of the foam morphology on the mechanical properties of structural polymer foams. PhD thesis, University of Aachen, Germany.	Flórez, L.F.; 13.07.2020
150	Wiehler, H. 2010. Prozessentwicklung des Hochdruckintegralschaumgießens von Aluminium. / Process development of high-pressure integral foam casting of alumina. PhD thesis, University of Erlangen-Nürnberg.	Wiehler, H.; 14.07.2020

153, 155	Hohmann, C. 2015. Konzeptionierung eines Spritzgießwerkzeuges für das Schaumspritzgießsondervverfahren „Pull and Foam“. / Mold concept for the special foam injection molding technique "pull and foam". Diploma thesis (supervisor: M. Tromm), University of Kassel, Germany.	Hohmann, C.; 02.06.2020
-------------	--	----------------------------

KURZLEBENS LAUF



BERUFSERFAHRUNG

seit 01/2018	Prozessexperte im Technical Competence Center Plastics Processes, B. Braun Melsungen AG
01/2017 - 06/2020	Promotion am Institut für Werkstofftechnik, FG Kunststofftechnik, Universität Kassel
06/2011 - 12/2018	wissenschaftlicher Mitarbeiter am Institut für Werkstofftechnik, FG Kunststofftechnik, Universität Kassel
05-06/2017	Forschungsaufenthalt an der University of Toronto, Mechanical and Industrial Engineering Department, Microcellular Plastics Manufacturing Laboratory (Prof. Chul B Park), Kanada

AUSZEICHNUNGEN / ORGANISATIONEN / VERÖFFENTLICHUNGEN

Auszeichnungen:	Moldex3D Global Innovation Talent Award 2016 , „#Moldex3D Story Contest“, 2. Preis EMEA Region („Simulation of High Pressure Foam Injection Molding with Local Core-back“)
Organisationen:	DGM Fachausschuss „Zellulare Werkstoffe“ (2012 - 2018) Co-Chair der CellMAT 2016 - Konferenz (Dresden, 12/2016), zuständig für die Materialklasse Kunststoffe Co-Chair der CellMAT 2018 - Konferenz (Bad Staffelstein, 10/2018), zuständig für die Materialklasse Kunststoffe
Veröffentlichungen:	3 begutachtete Journalpaper 4 begutachtete Konferenzpaper 1 Buchkapitel div. Fachbeiträge u. Präsentationen